Combustion and Emissions of Alternative Fuels in Gas Turbines

Mohamed Alalim Altaher

Submitted in accordance with the requirements for the degree of Doctor of Philosophy

The University of Leeds

School of Process, Environmental and Material Engineering

Energy Research Institute

August, 2013

The candidate confirms that the work submitted is his own, except where work which has formed part of jointly-authored publications has been included. The contribution of the candidate and the other authors to this work has been explicitly indicated below. The candidate confirms that appropriate credit has been given within the thesis where reference has been made to the work of others.

Chapters 4, 5, 7, 8 and 9 within the thesis have been based on work from jointly authored publications. These jointly authored publications are:

1) Altaher, M. A, G. E. Andrews and H. Li., "PM Characteristics of Low NOx Combustor Burning Biodiesel and its Blends with Kerosene". In Proceedings of ASME Turbo Expo 2013, GT2013-95481.
2) Altaher. M. A, H. Li, C. Wilson, C. Winson, B. Simon and L, Rye., "Hydrocarbon speciation of Exhaust Gases from a Gas Turbine Engine using Conventional and Alternative Aviation Fuels". In proceedings of 6th European Combustion Meeting (ECM 2013), Lund 25-28 June, 2013.
3) Li. H, M.A. Altaher, C. Wilson, C. Winson, B. Simon and L, Rye " Influence of fuel composition, engine power and operation mode on exhaust gas particulate size distribution and gaseous emissions from a gas turbine engine. In Proceedings of ASME Turbo Expo 2013, GT2013-94854.
4) Altaher, M. A, Li. H, C. Wilson, C. Winson, B. Simon., " Particulate emissions and size distributions from renewable fuel blend for gas turbine engine". In 9th Asia-Pacific Conference on Combustion. Gyeongju, South Korea: The Combustion Institute Korean Section, 19-22 May 2013.
5) Li. H, M.A. Altaher, C. Wilson, C. Winson, B. Simon and L, Rye., "Quantification of Aldehydes Emissions in a Gas Turbine Engine using Renewable Aviation Fuels". Submitted to Journal of Atmospheric Environment, May, 2013.
6) Altaher, M.A, G.E. Andrews and H. Li., “Co-firing of Kerosene and Biodiesel with Natural Gas in a Low NOx Radial Swirl Combustor”. In Proceedings of ASME Turbo Expo 2012, GT2012-68597.

7) Andrews, G.E, M.A. Altaher and H. Li., “Hydrogen Combustion at High Combustor Airflow using an Impinging Jet Flame Stabiliser with no Flashback and Low NOx”. In Proceedings of ASME Turbo Expo 2012, GT2012-70046.
8) Li, H., M.A. Altaher, and G.E. Andrews, “Aldehydes Emissions Measurement and OFP assessment of Biodiesel and its Blends with Kerosene using a Low NOx Gas Turbine Combustor”. Proceedings of ASME Turbo Expo 2011, GT2011-45707.
9) Altaher, M.A., H. Li, and G.E. Andrews, “Biodiesel and its Blends with Kerosene as an Alternative Fuel in Low NOx Gas Turbine Combustor”. International Gas Turbine Congress, Osaka, Japan, November 13-18, 2011, IGTC2011-0171.
10) Altaher, M.A., H. Li, and G.E. Andrews, “Effect of Biodiesel and its Blends Co-firing with Natural Gas on Emissions in a Low NOx Gas Turbine Combustor”. International Gas Turbine Congress, Osaka, Japan, November 13-18, 2011. IGTC2011-0101., 2011.
11) Li, H., Altaher, M.A, and Andrews, G.E “Evaluation of combustion and emissions using biodiesel and blends with kerosene in low NOx gas turbine combustor”. Proceedings of ASME Turbo Expo 2010, GT2010-22182.
12) Altaher, M.A., H. Li, and G.E. Andrews. “Effect of Wall Fuel Injection Configuration on Emissions Using Low NOx Radial Swirl Combustor”. In Eighth Asia-Pacific Conference on Combustion. Hyderabad, India: The Combustion Institute Indian Section, 2010.

All work contained within these publications are directly attributable to the candidate while all authors have editing responsibilities.

August, 2013 The University of Leeds Mohamed Alalim Altaher

Acknowledgments

This research has been carried out by a team which has included Prof Gordon E Andrews and Dr Hu Li. My own contributions fully and explicitly indicated in the thesis, have been on everything.

*First of all, I would like to praise and thank **GOD** for helping me to complete this thesis. I wish to express my gratefulness to my supervisors, **Prof. Gordon E Andrews and Dr Hu Li** for their continuous supervision, positive discussions and important ideas through this research work.*

I would like also to thank the staff and friends of the Energy Research Institute (ERI) and Energy and Power Technology limited (EPTeC), special thanks for whom I will never forget go to the following: Bob Boreham, Prof Chris Wilson, Simon Blakey, Winson Chung and Lucas .J. Rye.

*I would like to extend my thanks to the Libyan Government for sponsoring my PhD study, and many thanks for the staff of the Libyan cultural affair in London for their help during my stay in the UK. My deepest thanks, love and gratitude for my parents, brothers, sisters and extraordinary thanks for my wife and my lovely daughter **Fedaa**. This work would not have been completed without their love and continuous support.*

Abstract

Renewable biomass derived fuels are of increasing interest for many applications including industrial and aero gas turbines due to the reduction in fossil fuel CO_2 and the improvement in energy supply security. The first part of this work investigated the performance of biodiesel as a fuel in low NOx combustors of the type used in industrial gas turbines. This work included comparison with kerosene and co-firing with natural gas and blends of kerosene/biodiesel. In the second phase of this work an aircraft gas turbine APU with diffusion combustion. This investigated the gaseous and particulate emissions using kerosene as a base fuel for comparison with several second generation biofuels, which covered a range of H/C and showed that emissions were correlated with the H/C. The third phase of the work was concerned with renewable or clean coal derived hydrogen combustion using a low NOx flame stabilizer for industrial power generation applications.

For the industrial low NOx combustor work a radial swirler flame stabiliser was used. However, the high boiling point of B100 made operation in a premixed vane passage fuel injection mode impossible as ignition could not be achieved. The pilot fuel injector in the centre was the only fuel injection location that B100 would stabilise a flame, due to the central recirculation of burnt gases. A central 8 hole radially outward fuel injector was used as WME (B100) would not operate with radial vane passage fuel injection that is conventionally used for low NOx radial swirlers with natural gas.

In the aero engine phase of the research, nine alternative fuels were tested and compared to conventional JetA1 fuel at idle and full power. The results showed that all fuels produced similar level of NOx compared to JetA1 and a slight reduction in CO. A remarkable reduction in UHC was observed at all conditions for higher H/C fuels. The results also show that there was a good correlation between fuels H/C ratio and particle concentrations, particle size and distributions characteristics. The hot idle

produced ~20% less particles compare to the cold idle. The alternative fuel blends produced fewer particles than JetA1 fuel.

The alternative source of renewable fuels for industrial power generation gas turbines is that of hydrogen derived from renewable or nuclear electricity or from coal or biomass gasification using the water gas shift reaction and CO_2 solvent extraction to leave a pure hydrogen fuel. The key problem are in burning hydrogen in gas turbines is that of the increased NOx formation and the increased risk of flashback into the conventional premixing passages used in natural gas low NOx combustors. This work investigated a novel impinging jet configuration that had previously been used successfully with propane and kerosene fuels. It had no premixing so that there could be no flashback. However, the high reactivity of hydrogen did cause a problem with flame stabilization too close to the jet outlets. This was controlled by reducing the proportion of air added to the initial hydrogen jets. NOx emissions lower than alternative designs were demonstrated at simulated high power conditions. This was a practical combustion technique for high hydrogen content fuels with low NOx emissions and no flashback problems.

Contents

List of Figures

List of Tables

Nomenclature

APU: Auxiliary Power Unit

CBCs: carbonyl compounds.

CFD: computational fluid dynamic

CO: Carbon monoxide.

CO_2: Carbon dioxide.

CTL: coal to liquid fuel

EI: Emission Index.

FID: Flame Ionization Detector.

FAE: Fatty Acid Ester

FT: Fischer Tropsch

FTIR: Fourier Transform Infrared.

FAE: Fatty Acid Ester

FT-SPKs: (FT- Synthetic Paraffinic Kerosene).

ICAO: international civil aviation organization

GMD: Geometric Mean Diameter

GSD: Geometric Standard Deviation

GTL: Gas to Liquid.

NOx: Nitric oxides.

NG: Natural Gas.

NO: Nitrogen Oxide

NO_2: Nitrogen dioxide.

NDIR: Non-Dispersive Infrared.

HEFA : Hydrotreated Ester and Fatty Acid
NDIR: Non-Dispersive Infrared.

NDMA: Nano-Differential Mobility Analyzer

OFP: Ozone Formation Potential.

UHC: Unburned Hydrocarbon.

WME: Waste cooking oil Methyl Ester

PM: Particulate Matter.

SN: Smoke Number

SMPS: Scanning Mobility Particle Size

Chapter 1 : General Introduction

1.1 Gas turbine for electric power generation and low emissions

The gas turbine engine is an example of an internal combustion engine that converts energy stored in the fuel into useable mechanical energy in a rotational power form. Gas turbines are used for electrical power generation, pipeline pumping, ship propulsion and aircraft propulsion. Their major advantages compared with other engine types such as the spark engines are a very high power to weight ratio, which can be about twenty times as powerful as the same size piston engine in terms of floor area required per MW of power. Nowadays, the aerospace and power generation industries rely on gas turbines to power a large variety of machines. These engines initially undergo serious development with shaft power in mind, however attention soon turned to their use for aircraft propulsions[1, 2].

Most aircraft gas turbines operate in a simple cycle configuration since attention must be paid to engine weight and frontal area. However, in industrial gas turbine (IGT) applications, additional equipment can be added to the simple cycle gas turbine, leading to increases in efficiency[1, 3].

1.2 Gas turbine components

Gas turbine engines operate on the Brayton cycle (Fig.1.1) which is also known as an open cycle and the three main components that all gas turbines share are a compressor, combustion chamber and turbine connected together as shown in Fig.1.2[1, 2]. An industrial gas turbine will have a power turbine downstream of the first turbine and this may rotate at the same speed as the main shaft (single shaft power) or at a more optimum speed for the power turbine (dual shaft machine). In an aero engine the power turbine is replaced with a shaft drive to a fan at the engine inlet, which creates most of the thrust. This normally rotates at a different speed to the main gas turbine and all aero gas turbines are at least two shaft machines. For RR aero gas turbines the main turbine has two shafts with the front end of the compressor and rear stages of the turbine being driven at different

speeds. This gives a thermal efficiency advantage at the expense of added complexity. All other aero manufacturers use two shaft machines.

The overall principle is that the air enters through the intake and is compressed before being mixed with the working fluid to provide heat. The working fluid is normally by burning a liquid or gaseous fuel. The burnt gases then expand through the turbine, causing it to rotate and drive the compressor. The exhaust gases are used as the power output source of the engine. In electrical power generation, and other shaft power engines (such as helicopter engines), the flow is used to drive a shaft to turn components such as generators and rotors. For aircraft propulsion, in addition to the fan power, the exhaust gases are expelled from a rear a nozzle to provide a thrust on the aircraft [1-3]. However, in modern aero engines the fan power dominates and pure jet thrust is a low proportion of the total engine thrust. Aero derivative gas turbines take the power drive that is used for fan power to drive a power turbine.

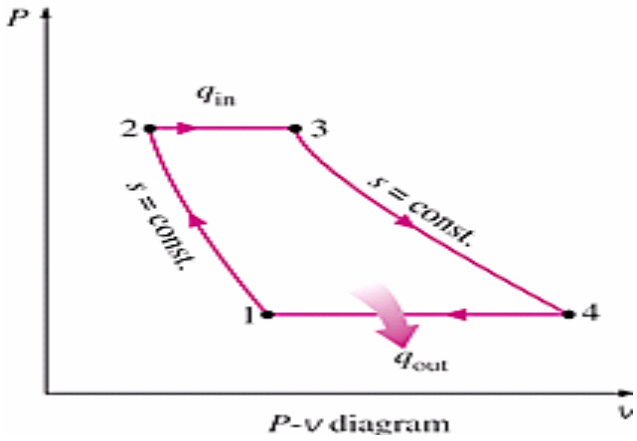

Figure 1.1: The pressure-volume, PV diagram.

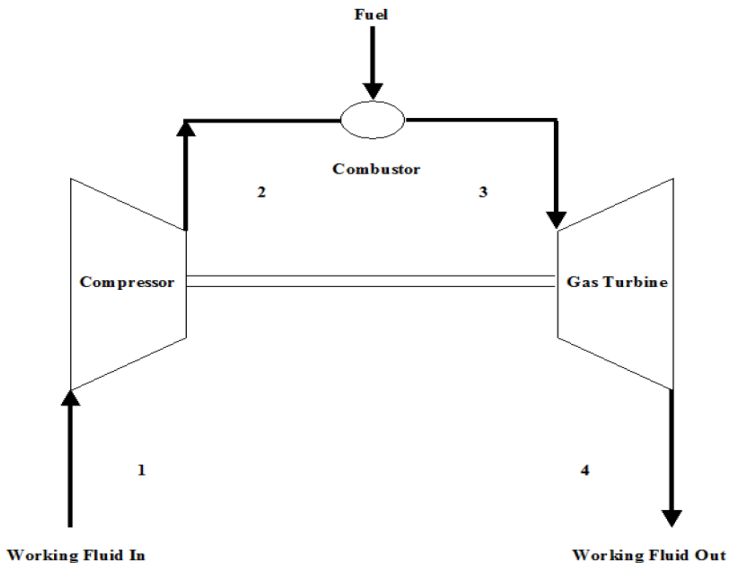

Figure 1.2: Simple gas turbine cycle[3].

In practice, gas turbines are much more complicated than the diagram shown and losses occur in both the compressor and turbine which lower the efficiency of the machine. Thus, the compressor and turbine consist of a set of rotating blades and stationary passages through which the fluid is forced to compress or expand the air or burn the gases. There are two main sources of compressor and turbine inefficiencies: blade tip leakage and blade flow friction. For turbine stages the film cooling required to enable the blade to operate at a lower temperature to the gas, are further causes of flow losses as the film cooling disturbs the boundary layer. Also the film cooling air is taken from the compressor air and does not fully recover its expansion work in the turbine.

The turbine in electrical power generation has two separate and unconnected components, the compressor turbine and the free or power turbine. Each of these has a shaft with the compressor turbine connecting to the compressor and the free turbine connecting to the electrical generator (normally using a gearbox) leading to turboshaft engine[1, 3]. Whereas the gas turbine used for aircraft propulsion can be split into three categories: the turbojet, the turboprop and the turbofan.

Turboprop and turboshaft engines are gas turbine engines used to drive propeller and power helicopters respectively. The output of the power is transmitted by shaft. Turboshafts can also be used to drive generators in

power stations, oil pipelines, natural gas compressors and ship's propellers. Thus, turboprops are lighter than turboshafts of the same size. Turbofan engine is turbojet after improvement of propulsion efficiency by reducing the mean jet velocity by fitting fan at the front of the engine to provide low pressure rise with a large amount of air. The turbofan gives about twice as much thrust for the same fuel consumption as turbojet of the same core size. In general, turbojet engines use only energy from the expanding exhaust stream for propulsion, whereas turbofan and turboprop engines use energy from the turbine to drive a fan or propeller for propulsion [1, 3].

1.3 Types of main Combustion System

The combustion type is determined by many factors include cost, weight, volume, emissions and other specific design or operational issues. There are three basic types of combustor, tubular, annular and tubo-annular (can-annular) as shown in Fig.1.3. All these configurations use a multiple combustors to inject the fuel. In a tubular combustor the flame tube takes the form of a cylindrical can and it is sometimes called can-combustor [1-3]. Each can has its own liner which is also cylindrical in shape and fits around the circumference. In a tubo- annular combustor the flame tubes are cylindrical and arranged in a ring formation the same as tubular setup. Theses cans are however placed inside an annular outer casing and share the same cooling air compartment.

However, industrial engines are much larger than aero-engines and require ease of access for overhaul and repair, therefore a tubular or tubo-annular combustor is a much better choice. In annular combustor two rings are placed inside one another concentrically to form a ring, which forms the outer liner of the main combustor. This ring is then normally split into segments, each with its own fuel injector. The aero-engines (such as the GE CF6, CF6, P&W JT9D and RR RB211 and Trent) need to be light, making an annular combustor firmly as the natural choice [1-3].

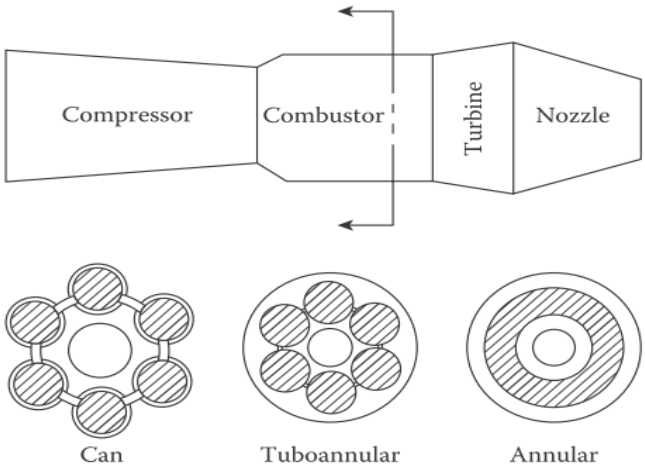

Figure 1.3: main combustor types [2].

Modern Aero engines use annular combustors as they are lighter weight with lower aerodynamic losses between the compressor and turbine. All current aero combustors for large civil jets are of this type and have been since about 1970 when the RB211, GE-CF6 and P&W JT9D engines were developed. However, in large industrial engines can-annular combustors are still common, particularly in reverse flow combustors. In the large CCGT of 400MW combined power generation there are four companies who are in the market, two use annular combustors (Siemens and Alstom) and two can-annular (GE and MHI). For smaller industrial gas turbines, not derived from the aero sector all the manufacturers use reverse flow can-annular combustion: Solar, Siemens Industrial Turbomachinery, Toshiba, Hitachi, KHI, Flex Energy, MAN, etc. The reason for this is the ease of access to the combustor for fuel injector repair and maintenance and for taking out the combustor for repair. To take an annular combustor out requires a full split down of the engine to take out the drive shaft. For aero –derivative small gas turbines (all<50MW) the combustors retain the annular form, although RR went from annular to reverse flow can-annular in the RB211 and Trent industrial versions. GE retained the annular combustor form for their aero-derivatives, but has always used the can-annular in their large industrial GTs [4].

Currently, industrial gas turbine designers are interested in dry low NOx emissions (DLE) combustion, with <25ppm NOx corrected to 15% oxygen required in all countries, but with <10ppm required in many areas of the World. Today low NOx has to be achieved in gas turbines with lower CO_2

emissions and higher thermal efficiency. A higher thermal efficiency is achieved by operating at higher turbine entry temperatures, which are associated with higher compressor outlet pressures. This makes the achievement of low NOx more difficult as NOx is a direct function of the combustion temperature and in diffusion type combustion increases with pressure (~$P^{0.5}$)[4]. The present work uses one of the most common types of low NOx combustors, radial swirlers[5] and aims to show that they can be adapted to operate with liquid biofuels so as to reduce the fossil fuel CO_2 emissions, whilst retaining their low NOx characteristics.

1.4 Gas Turbine Thermal Efficiency and Power

Nowadays, most electrical power plants use combined cycle gas turbines (CCGT) to achieve greater efficiency than what can be achieved with the simple cycle. A combined cycle generates steam from the waste heat in the exhaust of an industrial gas turbine, which in turn drives a steam turbine to generate additional electricity.

The Brayton cycle is characterized by two significant parameters: the pressure ratio and the combustion firing temperature (or turbine inlet/ entry temperature). The pressure ratio is defined as the compressor discharge pressure (P2) / compressor inlet pressure (P1).In an ideal cycle, turbine entry temperature (T3) is the highest temperature reached. The ideal thermal efficiency (ηt) is defined as the energy produced by the engine/energy contained in the fuel as shown in equation (1) [1].

ηt=(Turbine work done-Compressor work done)/Heat input from the fuel

$$\eta t = \frac{m_2 Cp(T_3 - T4) - m_1 Cp(T_2 - T_1)}{m_f C_P (T_3 - T_2)} \qquad (1)$$

Where m_1 is the air mass flow rate through the compressor (Kg/s)

m_2 is the exhaust mass flow rate through the turbine and equal to (m1+mf)

m_f is the fuel flow rate (Kg/s)

C_p is the specific heat of air at constant pressure (KJ/Kg.k).

In an ideal cycle, the working fluid is assumed to be air with a constant C_p that does not vary with temperature or with the composition changing after

combustion. This is an invalid assumption as C_p does vary by temperature and composition. It is assumed that the air is heated by a process that does not increase the mass, therefore, $m_1=m_2$, which yields the following equation:

$$\eta t=1-\frac{(T_4-T_1)}{(T_3-T_2)} \qquad (2)$$

In an ideal cycle $\boldsymbol{T_3/T_4=T_2/T_1}$, so the thermal efficiency of a simple gas turbine would be given by the equation below:

$$\boldsymbol{\eta t=}1-(T_1/T_2)=1-(T_4/T_3)=1-(P_1/P_2)^{\gamma-1/\gamma}=1-(P_4/P_3)^{\gamma-1/\gamma} \qquad (3)$$

$\gamma=C_p/C_v$, C_p and C_v are the specific heats at constant pressure and volume respectively. From the equation it can be deduced that an increase in P_2 and T_2 would increase the thermal efficiency. In addition, the thermal efficiency is maximized when T_3 (or combustion firing temperature) is at its highest value. As mentioned earlier, most of the power generations use gas turbines with a combined cycle to maximize the thermal efficiency of the cycle. The exhaust gas temperature in combined cycles are not required to be reduced which represent the critical point in terms of the efficiency. However, the thermal efficiency of an open cycle is low (30-35%) in comparison to a combined cycle (60%) [1-3].

1.5 Combustor design requirements

Gas turbine combustors vary in design depending on the specific application of the engine and all combustors have common functions that they must perform. A successful combustor design must satisfy a wide range of requirements where the relative importance of each requirement varies with the application of the gas turbine, and of course, some requirements are conflicting, requiring design compromises to be made [2, 6]. Thus, the strict regulation for pollutant emissions has recently led both designer and user of combustion devices to develop the technologies of gas turbine combustors to meet these regulations. Most design requirements reflect concerns over engine costs, efficiency, and the environment. The essential parameters for any gas turbine combustor are surmised as follows [2]:

1. High combustion efficiency (>99%) at all operating conditions (the fuel must be completely burned so that all energy is released from the fuel and no unburned fuel is emitted).
2. Outlet gas combustor temperature should be appropriate for the turbine blades (~1850K for aeronautical applications, 1750K for power applications).
3. Meet emissions legislation.
4. Low pressure loss (3-5% is common), as any pressure drop through the combustor leads to an increase in fuel consumption and reduces the power output.
5. Good flame stability, including both weak and rich extinction limits.
6. Consistently reliable ignition must be attained at very low temperatures, and at high altitudes (for aircraft).
7. Smooth combustion, with no pulsations or rough burning.
8. An adequate temperature outlet profile that is acceptable for the turbine inlet.
9. Useful life (thousands of hours), particularly for industrial use.
10. Multi-fuel use. Characteristically, natural gas and diesel fuel are used for industrial applications and kerosene for aircraft.
11. Length and diameter compatible with engine envelope (outside dimensions).
12. Designed for minimum cost, repair and maintenance.
13. Minimum weight (for aircraft applications).

1.6 Gas turbine alternative fuels

Fossil fuels dominate transportation, industrial energy, agricultural energy and electrical power generation sector since [7, 8]. Currently 25% of fossil fuel is consumed by the transportation sector and the aviation sector consumes about 13% of the transport fuel, which is the second biggest sector after road transportation. Furthermore, about 15,750 aircraft in commercial aviation operate on fuel derived from fossil fuels, contributing about 2-3% of global carbon emissions [9, 10].

Hydrocarbon fuels are organic compounds consisting entirely of carbon and hydrogen. Depending on the number of carbon atoms and their molecular structure, they can be classified as either gaseous, liquid, or solid

in standard conditions. Gaseous fuels have up to four carbon atoms present, whereas fuels with twenty or more are solid, and those in between are liquid [11]. Hydrocarbons in petroleum fuel are usually classified into three main groups: paraffinic, naphthenic and aromatic.

1) Paraffinic oils are straight chain with general formula (C_nH_{2n+2}) and it can be found mainly in the United States, North Africa, and Nigeria. The simplest hydrocarbons are methane and propane. However, depending on the source of the crude oil and the distillation process, aviation fuels contain about 60% paraffins. They have a higher hydrogen/carbon ratio, high gravimetric calorific value, lower density and freeze point compared to other types of hydrocarbon fuels.

2) Naphthenes are saturated hydrocarbons with general formula $(CH_2)_n$, the carbon atoms are linked to form rings instead of chains as in the case of paraffins. Their contributions to Jet fuel are about 25-35% and have high gravimetric heat of combustion and low soot formation. Cyclopropane, (C_3H_6) and Cyclopentane, (C_5H_{10}) are member of Naphthenes.

3) Aromatic hydrocarbons are unsaturated molecules, ring compounds containing one or more six-member rings with the equivalent of three double bonds. They contain less hydrogen and lower specific energy and have similar structure to naphthenes. The general formula of aromatics is (CnH2n-6) and benzene, toluene and napthalene are examples. The main advantage of aromatic compounds in the fuel is that they help to seal the high pressure aircraft fuel system. However, aromatic compounds have a higher tendency to form soot and a strong solvent action on rubber, which damages fuel systems. The aromatic content in aircraft fuels is limited to 20% [9].

The concentration of the three major types of compounds in a given base fuel is determined by chemical analysis. The conventional aviation jet fuel is a mixture of many different hydrocarbons and has an average composition of 60% paraffins, 20% naphthenes, 20% aromatics and contains about 500 ppm of sulphur. A key variation in the type of hydrocarbons in aviation kerosene is the hydrogen content or H/C ratio. Aromatics have a H/C close to 1 and aliphatic have a H/C close to 2. Thus, the H/C ratio or hydrogen content is a key parameter in aviation fuel specification and has been found to be a key correlator in aviation gas

turbine smoke emissions[12] and is part of the fuel specification. It will be shown in the present work that the H/C is a key correlator of the fuel effects that are investigated in the work on the aircraft APU fuel effects phase of this research.

There are many types of fuel used in industrial gas turbine combustors according to the application. These include natural gas, liquid distillate, diesel fuel, and residual fuel oil. Most industrial gas turbine combustors have dual NG/liquid fuel firing. This means you can switch between two kinds of fuel according the operational needs. However, in low NOx combustors it is only on NG that DLN can be achieved and most manufacturers still use a diffusion flame with liquid fuel and have water injector to control the NOx. The present work attempts to demonstrate low NOx performance using liquid fuels and comparison with NG is used to illustrate how close to this ideal has been achieved on liquid fuel.

The impact of pollutant emissions from combustion processes on the health and the environment have become great concern of the public and have led to extensive R&D in combustion technologies, fuels and other sectors to meet more and more stringent air quality and emissions regulations. Improved technology has the best prospect for reducing emissions as will shown in chapter 4&5 by using a low NOx combustor, while significant benefits will be demonstrated through the utilization of alternative fuels.

Biofuels including biogas, bioethanol and biodiesel have become more attractive recently as they are “carbon neutral”, as the plant absorb CO_2 emissions while they grow [7, 13, 14] and release it when the biofuel is burned. However, this process is not carbon neutral if carbon emissions are generated in the growing, harvesting and biomass to biofuel manufacturing process. This is known as the sustainability of biofuels i.e. what is the proportion of carbon reduction taking these upstream CO_2 generation issues into account. First generation liquid biofuels could have as much as 80% upstream CO_2 (Ethanol from corn in the USA for example), but 60% efficiency was typical for biodiesel. The production of biofuels should avoid competition with food production, as the availability of growing crops can be

affected by the limitation of the land for food. Biodiesel is one of the best available renewable liquid fuel sources [7, 8].

Biofuels offer reduced CO_2 emissions for both industrial and aero gas turbines. Industrial applications are more practical due to low temperature waxing problems at altitude. Any use of biofuels in industrial gas turbines must also achieve low NOx. Operation of gas turbines on biofuel alone is problematic due to the very high boiling point of vegetable oil methyl esters, typically around 325^{o}C. Operation with a second fuel that is easier to ignite is more common, such as the use of blends of liquid fuels with biofuel/diesel and biofuel/ kerosene. An alternative method of coping with the high boiling point of biodiesel is to co-fire with natural gas. The aim is for natural gas to provide the recirculating hot gases that will ignite the biodiesel. The comparison of co-firing with natural gas (NG) at different flow rate with the operation on liquid biofuel and blends with kerosene has been investigated.

There are greater restrictions on any candidate fuel in aviation sector as it must fulfill all the specification requirements for aviation fuel. More details about alternative fuels will be discussed later. There are significant interests in utilizing alternative fuels for aviation, due to supply security and increasing environmental concerns[15, 16]. These alternative fuels are not only required to reduce the carbon footprint of aviation but also not to cause adverse effects on NOx and particulate emissions[16, 17].

There are three reasons for using renewable fuels: fuel security, carbon reduction and NOx and soot reduction. There has been intensive research on feedstocks and process transformation of the biomass feedstock into aviation fuels. Aviation biofuels are more difficult to get approved than road transport biofuels as they require tighter fuel specification, flight testing and life cycle impact assessment of these fuels. They must also meet all the operational specification of current kerosene jet fuels [18]. Both synthetic and renewable jet fuels are the most common alternative fuels in aviation [19] and not the oxygenated methyl ester biofuels used in diesels. These Jet fuels such as Fisher-Tropsch fuels are aromatic and sulphur free which has good advantage of reducing particulate emissions[20]. However, oxygenated diesel biofuels have the additional benefit of soot reductions through the

incorporation of oxygenated components in the fuel which are known from diesel engine work to reduce soot emissions.

1.7 Gas Turbine Emissions and health impacts.

The impact of pollutant emissions from combustion processes on the health and the environment have become of great concern to the public[6]. Combustion processes in power generation and industrial heating plants, automobiles and aircraft engines and in domestic heating are the largest contributors to atmospheric pollution. Industrial gas turbine emissions are very low for CO and UHC but significant in NOx emissions at high powers. Industrial gas turbines do not operate at idle apart from at start up, but for aero-gas turbines CO and UHC emissions are high at idle conditions and hence are important for air quality at airports, together with NOx and soot which are high at the maximum power used at airports and hence contributes to airport air quality issues.

Gas turbine exhaust gas composition and their environmental impacts and sources are summarised in Table 1.There are two distinct categories of gas turbine emissions. The major exhaust gases are carbon dioxide (CO_2), water vapour (H_2O), Nitrogen (N_2) and Oxygen (O_2) and their concentration are present at percentage levels. Of these gases only CO_2 is a pollutant as a greenhouse gas[20]. The compositions of these major species can be calculated if the fuel composition and operating conditions are known. The second category are minor species that are environmentally harmful and harmful to human health: this includes carbon monoxide (CO), unburned hydrocarbons (UHC), particulate matter (PM), smoke (carbon), oxides of sulphur (SO_x) and oxides of nitrogen (NO_x) and are present in parts per million (ppm) concentrations. These cannot be calculated and require careful measurement.

The power generation sector contributes the largest share of CO_2 emissions at 40%. Thus, in gas turbines the dominant greenhouse gas is CO_2 which is a natural product of combustion and can only be reduced by using less fuel (less usage or better thermal efficiency) or alternative renewable fuels. Alternative fuels in gas turbines are the main theme of this research project. [2, 21].

Emissions of UHC and CO from gas turbines are very low at full power (base load) and increase at low power conditions such as in the vicinity of airports and for industrial gas turbines below 50% of peak power. A key issue with low NOx industrial gas turbines is achieving low NOx and low CO and UHC as the power is reduced to at least 50% power[4].

Aviation emissions are a relatively small compared to other sources and depend on fuel type, aircraft and engine type, engine load and flying altitude [22]. The need to find an alternative cost-effective environmentally friendly fuel [23] becomes essential when global warming and airport air quality issues are to be reduced. Also, the growing political and public pressures targeting air transportation to reduce its greenhouse gas emissions which are growing rapidly due to the rapid growth of the aviation sector.

Carbon monoxide (CO) is toxic and can cause asphyxiation, leading to death at high concentrations [2, 24]. Also, It is responsible on red action of the blood capacity to absorb oxygen[2]. At low concentrations, CO reduces the oxygen carrying capacity of the blood through the formation of carboxyhaemoglobins and this increases the heart's pumping rate to increase the supply of oxygen, which leads to heart related medical problems. CO also is taken part in the atmospheric reactions with sunlight and NOx that lead to the formation of ozone.

Some hydrocarbons are carcinogenic (benzene, toluene, aldehydes, polycyclic aromatic hydrocarbons [PAH]), however, the main concern for UHCs is the production of ozone when they react with NOx in the presence of sunlight [2, 24] . Ozone reduces lung functions and reduces the oxygen carrying capacity of the blood and hence influences the heart by affecting the flow of oxygen into the blood. This is why NOx is the primary pollutant of concern from gas turbines and is most significant at high power conditions [2, 21]. In industrial gas turbines, the formation of NOx is affected by the primary zone flame temperature, the residence time and any operation conditions which affect flame temperature [25], such as the compressor exit temperature, which is controlled by the engine pressure ratio.

NOx has in addition to the ozone formation problem, has an adverse effects on human health [24] through the NO_2 proportion of the NOx in the

gas turbine exhaust. NO_2 reduces the lung function in humans and increases the pumping rate of the heart due to the reduced oxygen flow. In addition NOx interacts with moisture and ammonia in the air to form small particles of nitric acid which cause certain respiratory diseases such as emphysema and bronchitis and can trigger heart disease. The formation of nitric acid also leads to acid rain which harms plant growth in sensitive soils, such as in Scandinavian forests.

NOx also interacts with common organic compounds including ozone to form toxic chemicals such as nitroarenes, nitrosamines and nitric radicals which can cause biological mutations. Many studies have shown that NOx can deplete the stratospheric ozone layer and increase the penetration of solar ultraviolet radiation which increases the risk of skin cancer [2, 21, 26].

An additional pollutant of concern is SO_2 which reacts with water in the atmosphere to form sulphuric acid, the second component of acid rain alongside nitric acid. The SO_2 is derived from the high sulphur content of aviation kerosene at around 400ppm [2]. SO_2 is also harmful to humans due to reaction with bodily fluids to form sulphuric acid, which irritates the lungs and reduces the oxygen flow to the blood. For industrial gas turbines operating on natural gas (NG) there is little sulphur content, but recent work[27] has shown that the sulphur compounds added to NG to make it smell give rise to sulphuric acid emissions which form a mist in the 10nm region. This will also be shown to be a factor in the present results. Biofuels contain no sulphur so that sulphuric acid aerosol emissions are eliminated if B100 is used. Roughly 98% of sulphur in the fuel is converted into SO_2 but about 2% is converted into SO_3 which leads to the formation of sulphuric acid aerosols and solid sulphate formation. Both of these give rise to ultra-fine particulate emissions from gas turbines. Sulphuric acid and sulphate emissions are ultra fine at around 10nm and these cause sunlight to scatter and this is a global cooling effect.

Particulate matter is of current concern in aero gas turbines due to two reasons: smoke visibility in military aircraft and during civil aircraft takes off; and due to the health hazards of ultra-fine particulates. The six cities study of air quality and health effect of particulate matter[28] showed that there was a correlation of PM10 mass in the air and hospital deaths. 1% extra people

died for every 10 μg/m^3 increase in PM in the atmosphere. This has also been found in many other studies in different countries around the world. The only medical explanation of this was first made by Seaton[29] and this was that the effect was caused by the passage of nano particles <50nm into the alveolar region of the lung and into the blood stream. This caused inflammation of the lung lining and a reduction in the oxygen carrying capacity of the blood. The nano particles in the blood caused the blood to thicken and both effects placed a strain on the heart. This has led to a major programme[29] on the measurement of particle size distributions in aircraft exhausts. This has shown that typically the particles have a peak number in the 10-30nm size range[30, 31]. The importance of the particle size distribution led to a significant part of the work being devoted to particle size distribution measurements in a practical diffusion combustion gas turbine APU and in a well-mixed low NOx industrial combustor.

Table 1: Gas turbine exhausts emissions burning conventional fuels[26].

Major species	**Typical concentration % volume**	**Source**
Nitrogen(N_2)	66-72	Inlet Air
Oxygen(O_2)	12-18	Inlet Air
Carbon Dioxide(CO_2)	1-5	Oxidation of fuel carbon
Water vapour(H_2O)	1-5	Oxidation of fuel hydrogen
Minor species pollutant	**Typical concentration (PPMV)**	**Source**
Nitric oxide(NO)	20-220	Oxidation of atmosphere nitrogen
Nitrogen dioxide(NO_2)	2-20	Oxidation of fuel-bound organic nitrogen
Carbon monoxide(CO)	5-330	Incomplete oxidation of fuel carbon
Sulphur dioxide(SO_2)	Trace-100	Oxidation of fuel-bound organic sulphur
Sulphur trioxide(SO_3)	Trace-4	Oxidation of fuel-bound organic sulphur
Unburned hydrocarbon (UHC)	5-300	Incomplete oxidation of fuel or intermediates
Particulate matter smoke	Trace-25	Incomplete oxidation of fuel or intermediates, fuel ash, inlet ingestion

1.8 Research Objectives and structure of the thesis

This thesis covers three main areas:

- Experimental studies of biodiesel as a fuel in a low NOx radial swirler gas turbine flame stabiliser. The work investigated the comparison of

the emissions between a waste cooking oil derived methyl ester (WME) and kerosene using a radial swirler industrial low NOx gas turbine combustor under atmospheric pressure and 600K preheated air. The pure WME (B100) and its blends with kerosene B20 (20% Biodiesel: 80% Kerosene), B50 (50% Biodiesel: 50% Kerosene) and pure kerosene were tested for and lean extinction limits and gaseous emissions as a function of equivalence ratio. Aldehydes emissions for B100, B20 and kerosene were measured and compared. The work also focused on comparison of co-firing with natural gas (NG) with the operation on the liquid biofuel and blends with kerosene at two combustor Mach numbers 0.017 and 0.023 respectively.

- The second part of the thesis, experimental studies of alternative aviation fuels using Auxiliary Power Unit (APU) to evaluate the gaseous and particulate matter emissions. The engine was fuelled with standard JetA1 fuel and was tested at two power settings. Up to eight different fuel blends, were tested for their gaseous emissions, volatile Organic Compounds (VOC) and particulate matter (PM) and compared to base fuel (JetA1). The work focused on the measurement of non volatile PM number and studied the efficiency of volatile particle removal (catalytic striper) using SAE ARP PM sampling line from APU.
- The third part of the thesis focused on hydrogen combustion using an Impinging Jet Flame Stabiliser with no Flashback and Low NOx. The objectives were to evaluate NOx emissions and combustion efficiency of direct hydrogen injection at constant pressure loss and compare it with premixed and direct propane injection. All test carried out at Mach number of 0.47, 4.3% pressure loss and 600k inlet air temperature.

Chapter 2 : Literature Review

2.1 Combustion fundamentals

There are three types of combustion in gas turbines: diffusion (non-premixed) flames; premixed flames and rapid mixing flames. In non-premixed combustion the fuel is injected into the combustion chamber in a different location to the air, where it burns upon mixing with the air. Most aero-engine combustors are of this type. In premixed systems, fuel and air are mixing before entering the combustion zone[2]. There are no practical combustors in production of this type. In rapid mixed combustion the fuels is injected with the air, but without premixing or with very short mixing passages and most ultra low NOx industrial gas turbines are of this type. The low NOx combustion system used in this work is of this type, with radial swirlers with fuel injection either at the exit throat or centrally, but the fuel is injected downstream of the combustor air inlet and not upstream as in a premixed system.

Conventional gas turbines Fig.2.1 have mainly used non-premixed combustion due to its wide flame stability and ease of ignition. Non-premixed flames have a much greater range of air-fuel ratio (AFR) over which stable combustion can occur, but NOx emissions tend to be higher due to diffusion combustion with local stoichiometric reaction zones. A conventional diffusion flame combustor design, as used in aero-engines consists of a primary zone, secondary zone and dilution zone. A constant airflow velocity is maintained and the fuel flow is then increased or decreased to control the overall air-fuel ratio (AFR) within the primary zone. The A/F is set to achieve the desired combustor exit temperature or turbine inlet temperature. Engine power is varied by decreasing this temperature from that for maximum power. The maximum power turbine entry temperature has increased since the gas turbine was developed as turbine blade cooling systems and materials have developed.

The H class industrial gas turbines have the highest turbine entry temperature of about 1750K, but the F class has about 1600K and this is currently the most common power generation gas turbine[32, 33]. The older E class has a turbine entry temperature of 1450K and this covers most

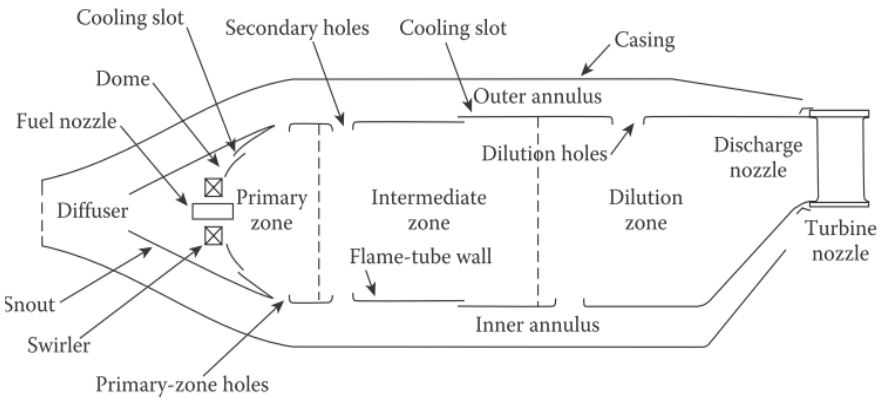

Figure 2.1: The components of a conventional combustor[2].

current power generation gas turbines. The thermal efficiency of the combined cycle gas turbines increases as the turbine entry temperature increases and is 60%-62% for the H Class and 58% for the F class[32].

For any given fuel and air mixture, there exists a precise AFR value in which combustion would leave both no unburnt fuel and no excess oxygen, called the Stoichiometric air-fuel ratio (AFR_{st}). Mixtures with higher AFR than AFR_{st} are termed lean as they have excess air, whereas mixtures with lower AFR values are termed rich as they have excess fuel. The AFR is normally given on a mass basis[2]. In diffusion burning there is a wide range of local A/F around the mean A/F and the primary zone is normally designed to be near stoichiometric overall at maximum power. Within this local zone will be rich and lean and the rich zone will give problems with CO and soot emissions and interface stoichiometric region will be where most NOx formation occurs. In well mixed or rapidly mixed combustion the aim is to mix the fuel and air before the primary combustion takes place[2, 24].

In practice lean combustion and hence low NOx is limited by the highest AFR (leanest) that stable combustion can occur. This is the weak extinction [2, 24] and Andrews et al. [21] have reviewed the published data on weak extinction for well mixed and premixed low NOx gas turbine flame stabiliser designs. This shows that the best weak extinction is co-incident with the lean flammability limit, which is Ø=0.5 at 300K and Ø=0.25 at 900K. For the 600K air inlet temperature used in the present work the lean flammability limit is Ø=0.4. The lean limit corresponds to the critical flame temperature at which a flame can propagate and this is 1400K for the lean limit determined by the European standard for lean flammability

measurement of gases. Table 2 shows the results of the review of published weak extinction critical flame temperatures[34]. This shows 16% of the 128 data points had a critical stability limit flame temperature in the 1400-1500K range. However, some of the flame stabilisers had such poor flame stability that they could not operate below 1800K and hence had no operational low NOx region. The present work used a radial swirler design with good weak extinction characteristics.

Table 2: Summary of the Weak Extinction Data in terms of critical weak extinction flame temperature and laminar burning velocity[34]

Flame Temp. K	Data Points	%	U_L m/s
1400 - 1500	21	16	0.05-0.075
1500 - 1600	68	53	0.075-0.13
1600 - 1700	20	16	0.13-0.16
1700 – 1800	10	8	0.16-0.18
1800 - 2000	9	7	0.18-0.26

2.2 Gas turbine Emissions regulations

The emissions legislation from stationary gas turbines varies from country and region depending on the individual governments and the current level of pollution in the area. The limits are usually for full power conditions, are expressed as part per million (ppm) on a dry gas basis, and corrected to 15% oxygen. In the USA, emissions are regulated by the Environmental Protection Agency (EPA) and 75 ppm of NOx emissions were the earlier limits for natural gas. At the present time, NOx limits are <25 ppm (governed by the federal government) and <10 ppm (in California). In Europe, emissions legislation is controlled by the European Pollution Prevention and Control Bureau (EIPPCB), with the NOx limit being <25 ppm for NG and <45ppm for liquid fuels. For stationary gas turbines working at full power the typical CO limit is from 10 to 40 ppm at 15% oxygen [1, 11, 24].

For aircraft engines the exhaust gas emissions must comply with applicable regulations governed by the International Civil Aviation Organization (ICAO). Emissions limits are more complicated due to the variation of power setting throughout a standard flight (much higher emissions during takeoff than when idle). Emissions are analysed using the

landing and takeoff (LTO) cycle at commercial airports, which consists of four power mode (thrust) settings: takeoff (100%), climb out (85%), approach (30%), and taxi/idle (7%), and does not include time spent in cruise. The LTO cycle emissions are calculated using equation (4), and cruise is not included because the current regulations do not stipulate the maximum NOx level for this mode. [11, 24].

Emissions (LTO) (g/KN) = Emission Index EI (g/kg fuel)*Engine SFC (kg fuel/hr KN)*Time (hr) (4)

2.3 Mechanisms of pollutant formation

2.3.1 Carbon monoxide (CO)

Carbon monoxide is a poisonous gas that forms carboxyhaemoglobin with blood, which reduces the oxygen carrying capacity of the blood and this puts a strain on the heart. For concentrations above 3000ppm death occurs after 30 minutes. However, in low concentrations it still acts on the oxygen carrying capacity of the blood. CO is also a reactive gas that takes part in ozone formation chemistry in the atmosphere. The emissions of carbon monoxide from conventional gas turbines are normally less than 10 ppm at maximum power, but often increase at low loads or part loads [2]. CO is formed through different routes[2, 26].

1) Equilibrium of CO, which is very high for rich mixtures and low for lean mixtures and can be calculated at the equilibrium adiabatic flame temperature.

2) Inadequate residence time to reach equilibrium CO (combustion chamber is too short)

3) Quenching of the oxidation of CO due to reduction of temperature too soon, such as dilution jets added too soon or film cooling air quenching primary zone rich combustion.

4) Poor fuel and air mixing, where local rich zones in an overall lean mixture create locally high zones of CO which do not mix sufficiently with the surrounding air to be oxidised. The net result is higher CO than equilibrium would predict for the overall mixed equivalence ratio.

5) The oxidation of CO increases strongly with pressure (~P^2) and thus experiments, as in this work, at atmospheric pressure can result in CO levels that are much lower at pressure.

All ways of forming CO occur at low-power conditions where the flame temperature and CO oxidation rates are lower than at full power. CO measured emissions can be much greater than the equilibrium CO [2, 26]. Thus, meeting the CO emissions standards requires complete oxidation to carbon dioxide with good mixing, high flame temperatures, high pressure, and long residence time to achieve the equilibrium of CO. For a combustor length of 330mm, Escott et al[35] showed that the critical flame temperature below which CO increased above equilibrium was 1700K and this has been supported by other researchers .

2.3.2 Unburned hydrocarbon (UHC)

Unburned hydrocarbons are the result of incomplete combustion of hydrocarbon fuel. As for CO this can be due to insufficient residence time[36], addition of quench air too soon and poor fuel and air mixing. For liquid fuels poor fuel atomisation can give another source of UHC[2, 26]. UHC like carbon monoxide, have unreleased chemical energy and thus give rise to the combustion efficiency. Escott et al. [35] showed that for a 330mm long combustor, the critical temperature for UHC to increase due to inadequate residence time was the same as that for CO at 1700K, above this temperature UHC emissions were very low at ~1ppm.

2.3.3 Particulate matter (PM)

Particulate matter (PM) is defined in diesel emissions legislation as any material collected on a specified filter paper when the exhaust is cooled by dilution to between 42 and 52^{o}C. In reality cooling of the exhaust sample by dilution only is impossible as this requires adiabatic dilution and real dilution systems have heat losses. Heat losses give rise to wall deposition of particles through a process of the rmophoresis, where fine particles in a gas that is hotter than the wall are transferred to the wall. Thus the design of the dilution system and the filter collection system all influence the particle mass. Particles mainly consist of a volatile fraction (from unburned liquid fuel and

lube oil) and from carbon emissions (which are subject to wall losses). The sample cooling process by dilution influences the volatile fraction and wall losses influence the carbon fraction. For gas turbine applications the aero sector has no agreed definition of what particle mass means and no agreed method of measurement. However, there are approximate methods of estimating particle mass (first order approximation methods) [37, 38] that estimate the volatile fraction form the total hydrocarbons, the sulphate fraction from fuel sulphur and the carbon fraction from the smoke number (filter reflectance or blackness). However, currently the water associated with the sulphates is not recognised as being part of the mass, even though there is 1.3g of water for every g of sulphates and the weight of the particle mass will always include water [22].

There are many sources that produce particulates, including industrial processes, power generation and transportation activities. Particulate matter emissions from combustion sources burning fossil fuels have raised particular interest in recent years from environmental regulatory agencies due to health effects [39]. The particulate matter is ranging from millimetre-sized residues and soot aggregates to ultrafine nuclei mode particles with only a few nanometres in diameter. Commonly, the large particles are removed or collected by cleaning devices. However, the smaller particles from combustion exhaust gases could be transported over hundreds of miles, whereby causing serious air pollution problems. Currently, PM10 and PM2.5 are regulated by various legislations for engine exhausts, air quality and industrial processes [22, 40] because sub-micrometre particles have a significant risk for human health and environmental quality.

It has been shown that the formation rate of soot is controlled by the physical processes of atomisation and air-fuel mixing. Thus, it is difficult to predict the rate of formation and final concentration from kinetic or thermodynamic data. Moreover, the smoke measuring unit is the SAE Smoke Number for aero engines [2], which is based on filter paper reflectance for a specified total volumetric flow through the filter. For industrial gas turbines the Von Brand Reflective Smoke Number (VBRSN) is sometimes used. If the number is greater than 93 to 95, the visible smoke is not present, e.g. natural gas has a smoke number of 99 to 100[2, 26].

2.3.4 Oxides of nitrogen (NOx)

The major pollutants from gas turbine engines are NOx emissions, with the term NOx expressing the combination of NO and NO_2. Nitric oxide (NO) is mostly formed in a combustion process, with factors favourable to NOx formation being those of high temperature, long residence time and high pressure. However, NO_2 is formed by oxidation of NO by HO_2 in the reaction zone in very fuel-lean conditions at low temperature, where a large amount of excess air is also present. The rate of the oxidation is too slow to give significant conversion in short residence time, and the concentration of nitrogen dioxide is generally lower than that of NO. Nitric oxide can be produced by four different mechanisms: thermal, nitrous oxide, prompt, and fuel nitrogen[2, 26].

2.3.4.1 Thermal NO

At elevated temperatures, thermal NO is produced by the reaction between nitrogen and oxygen in the air, and the significant rate can be produced at temperatures above approximately 1850 K [2, 26]. However, the reaction is slow below this temperature, hence the key of achieving ultra-low NOx. It is the most significant contributor to overall NOx formation in conventional combustion systems. Thus, thermal NO is mainly a function of the flame temperature which is heavily dependent on the overall combustor equivalence ratio. The combustor inlet temperature increases the flame temperature[26] an increase to the inlet temperature of 100 K can lead to increasing the flame temperature by about 50 K.

The three principle reactions controlling the production of thermal NOx were first recognised by Zeldovich [2]. The reaction rate is very slow at temperatures below 1850 K.

$$O_2 \rightarrow O_2$$
$$N_2 + O \rightarrow NO + N$$
$$N + O_2 \rightarrow NO + O$$
$$N + OH \rightarrow NO + H$$

The first two reactions were first determined by Zeldovich and the third reaction was added [41] to account for thermal NOx formation in rich

mixtures where atomic oxygen levels are low. Most modern gas turbines operate leaner with firing temperatures below 1800 K and so NOx should not be formed because NOx requires a higher temperature. It was found that the contribution of the total NOx emissions produced by a lean premixed combustor burning methane fuel is 60% thermal NO at around 1900 K and around a 0.8 equivalence ratio, whereas it was 5% at 1500 K and ϕ=0.6 using the same fuel [2, 41].

2.3.4.2 Prompt NO

The prompt NOx is termed by Fennimore[42] and is produced very early in the flame region by fast reactions in hydrocarbon flames, and increased markedly as the combustion chamber becomes richer [25]. It was found that prompt NO represents around 30% of the total NOx emitted from gas turbines under normal operation conditions [25]. It is not residence time-dependent (as in thermal NOx). Prompt NOx is more prevalent in rich flames, with its mechanism involving a complex series of reactions, and the most valid route accepted [36]. There are three routes of prompt NOx formation shown by different researchers. The first kinetic formation of prompt NOx is given by Fenimore [42] which involved reaction between hydrocarbon and N_2:

$$CH+N_2 \rightarrow HCN+N$$

(N) Formed NOx by thermal mechanism and HCN oxidises under lean condition to form NO as shown in the equations[43].

$$N+O_2 \rightarrow NO+O$$
$$HCN+OH \rightarrow CN \rightarrow CN+H_2O$$
$$CN+O_2 \rightarrow NO+CO$$

The reaction of N_2 and O is another route to form prompt NO as shown by Nicole et al [44], whereas Bozzelli et al [45]shown that the reaction of N_2 and H is also significant way to form Prompt NO. At 1500 K and ϕ=0.6 in lean premixed methane with air, 65% prompt NO of the total NOx has been found compared with 30% prompt NO at 1900 K and ϕ=0.8 using the same fuel [2, 41]. However, in industrial gas turbines, thermal and prompt sources dominate the NOx formation.

2.3.4.3 Fuel-Bound NOx

Fuel-bound NOx (FBN) can be produced by oxidation of nitrogen in the fuel and can represent a considerable proportion of the total fuel depending on the degree of nitrogen conversion. Most of the fuels used in gas turbine combustion contain no fuel-bound nitrogen and hence FBN can normally be ignored. Fuel oil or Diesel can contain up to 400ppm of FBN but is more typically 100ppm. Approximately 5ppm NOx at 15% Oxygen results from 100ppm FBN for lean well mixed combustion. In lean combustion all the FBN is converted to NOx. To reduce this conversion rich/lean combustion is required with the rich zone well mixed and at an equivalence ratio of ~1.6, where conversion of FBN into gaseous N_2 is the preferred reaction and NO production is low [2, 4].

2.3.4.4 Nitrogen Dioxide (NO_2)

Normally, NOx emissions are dominated by NO at base load, with a fractional contribution of NO_2 at part load. However, nitrogen dioxide is formed in the combustors by the oxidation of NO in low-temperature regions of the flame where a large amount of air is present as diluents [2, 41, 46]. NO_2 is a visible brown toxic gas with a level around 15 ppm. It is more stable than NO and is the essential intermediate for zone formation; this process will occur faster if NO_2 is emitted directly, rather than occur after NO. NO_2 is harmful to humans and causes reduced lung functions, asthma attacks and heart problems. Although nitrogen dioxide concentration is small compared to NO concentration, it is considered the major source of atmospheric pollutants. The mechanism of nitrogen dioxide begins with the reaction of NO with HO_2, OH, and O_2 [2, 41, 46].

$$HO_2 + NO \rightarrow NO_2 + OH$$
$$O_2 + NO \rightarrow NO_2 + ON$$
$$NO + OH \rightarrow NO_2 + H$$

However, it was proven that NO_2 converts back rapidly to NO at a high flame temperature. This is evidence that NO_2 is a transient intermediate species which exists at flame conditions. Hori reported that NO_2 is likely to

be formed in the mixing region between the hot combustion gas and the cool air stream near the combustor wall under very fuel-lean conditions. In aero gas turbines NO_2 decreases at low powers, especially at idle. In industrial gas turbines lean low NOx systems which have low primary zone temperatures can be >50% NO_2 in <10ppm NOx combustors[4].

2.4 NOx control methods

NOx emissions from industrial gas turbines are limited to less than 25 ppm in most countries. Thermal is the most important mechanisms of NOx formation in gas turbines and prompt NOx is only important for lean mixtures where thermal NOx has been eliminated . Thermal NOx can be reduced if the primary zone is lean and well mixed with temperatures below 1900 K. An effective way to achieve low NOx is by either decreasing the reaction temperature as the equivalence ratio decreases. Thus low NOx is achieved by combustor design (dry low NOx or DLN) and does not use water injection or exhaust gas recirculation (EGR) to reduce the flame temperature. DLN is the technique for low NOx that is investigated in part of this work.

However, for retrofit NOx reduction to a high NOx diffusion combustor water or steam injection used in the 1980s and is still used for liquid fuels by most manufacturers today. The introduction of a small amount of any diluents into the primary zone [2, 47] reduces the flame temperature, which reduces the NOx emissions. Reducing NOx emissions by an injection of water or steam (wet) into the gas turbine combustor has an impact on the cycle efficiency and may increases CO and UHC.

2.5 Dry low NOx gas turbine combustion

There are some requirements that should be met in the design of a dry low NOx combustor for stationary gas turbines. These requirements include meeting the emissions goals at base load for both liquid and gas fuels, stable combustion at all operating conditions, acceptable levels of combustion noise, and capability of switching from gas to liquid, and vice versa [2]. In this type of technique, the combustors are designed to be leaner to eliminate local regions of high temperature within the flame. However, the majority of stationary gas turbines operate with a large amount of access air,

with some being derived to the dilution zone to lower flame temperature beside combustion and cooling [26, 47]. In this approach, air injected as diluents, instead of water or steam, and low pollutant emissions are achieved, particularly NOx [47]. Moreover, a NOx level of 9 ppm at 15% oxygen has been achieved [47].

2.5.1 Low NOx gas turbine flame stabilizer

Flow recirculation plays a fundamental role in gas turbine combustion. In this regime the downstream flow becomes reversed before meeting the incoming fluid, where the two streams mix. Re-circulating flow is normally used to stabilise a flame that can otherwise be unreliable. The airflow pattern in the primary zone is essential for flame stability and there are many different types of airflow pattern being used in low NOx gas turbine combustors, including grid plates, jet mix, and axial and radial swirlers. Thus, there is one feature that is common to all their abilities to create a toroidal reversal flow which entrains and recirculates a portion of the hot combustion products to mix with incoming air and fuel to stabilise the flame, whereby resulting in better mixing and combustion [2, 21, 48].

Grid plate flame stabilisers were common in the earlier design of lean low NOx combustion. The fuel is injected directly into each air hole or slot in the grid plate to achieve rapid mixing and low NOx. Al-Dabbage and Andrews[49, 50] used a grid mix concept, with their results showing that low NOx was achieved with a much better flame stability compared to premixed combustion. Andrews and Ahmed [51] improved the concept by using slot-shaped air injection holes, with an improvement of the fuel and air mixing being achieved.

Swirl combustors are commonly used in the dry lean premixed mode to decrease NOx emissions in gas turbines. However, there are a few problems associated with this technique, including auto-ignition and acoustic resonance. Andrews et al. showed that fuel injection in the dump expansion (20 mm downstream the swirler exits) prevented problems associated with a long premix passage, such as flashback, auto-ignition and acoustic resonance [24, 50, 52].

A radial swirler and jet mix grid plate type flame stabilisers were used in this dry low NOx study with natural gas, biodiesel and hydrogen fuels respectively.

2.5.2Swirler aerodynamics

2.5.2.1 Characteristics of Swirl flow

Swirling flow as shown in Fig.2.2 is used for stabilisation, to improve the mixing pattern, and control the flame to achieve a minimum level of NOx emissions and a high intensity of combustion [2, 48, 53]. The swirling flow has a rotational velocity around a central axis in addition to an axial flow. It creates a toroidal reversal flow which entrains and recirculates a portion of the hot combustion products to mix with incoming air and fuel to stabilise the flame [2, 21, 48]. This type of recirculation zone (Fig. 2-2) provides better mixing and strong shear regions, high turbulence, and rapid mixing rates [2, 21]. The flow recirculation is generated by the low static pressure in the central core downstream of the swirler, which becomes low enough for creation of a reverse flow as the swirl number reaches a critical value of about 0.6 [2]. One of the main advantages of combustion swirling flow, is the importance of centrifugal forces which tend to accelerate the mixing of two flows having different densities [21].

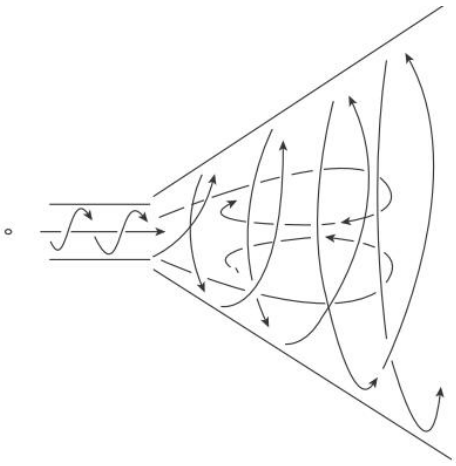

Figure 2.2: Recirculation flow [11].

2.5.2.2 Swirler type and configuration

Many low NOx gas turbines use swirling flows to the primary zone [2, 6]. However, the flow in this region has high shear stresses and strong turbulence intensity due to vortex breakdown, providing better mixing compared to bluff bodies [2, 6]. Axial and radial swirlers, as shown in Fig. 2-3, are used in both tubular and annular combustors depending on the application. The air is directed through angled passages which cause it to rotate about the combustor centreline. After entering the combustor, the swirling flow then expands, with a recirculation zone being formed. The size of the recirculation zone is increased as the vane angle and swirl number is increased and as the expansion ratio (D/d) increases [2, 21]. In the axial configuration the air enters the combustor directly from the compressor outlet in the axial direction, whereas in radial configuration the air passes across the combustor walls before making a 180° turn to enter the combustor. The radial swirler configuration is thus more suitable to reverse flow combustors.

Axial swirlers always have a large diameter compared to radial swirlers for the same flow capacity and pressure loss. The higher swirler airflow required for lean low NOx combustion requires larger flow capacity swirlers which require a larger axial swirler diameter. However, radial swirlers don't need a larger diameter and the flow can be increased by increasing the vane depth [36]. Radial swirl produces a stronger central recirculation zone and provides a widely dispersed, flat swirling mechanism attached to the swirl face, with their being more chance of fuel impingement on the wall compared with axial swirl [6]. A 45º eight flat bladed co-rotating radial double swirler was used in the present work.

Multiple or double swirlers can be arranged into either a counter-rotating or a co-rotating orientation. The effects of both configurations on the flow field have been investigated [6]. The major differences between co-rotating and counter-rotating are the distribution of turbulent kinetic energy and shear stress near the exit [6]. The performances of counter-rotating and co-rotating swirlers have been investigated, and found that the arrangement of counter-rotating is more desirable than its co-rotating counterpart [54]. This may be due to the strong shear layer and high intensity, which increase

the level of mixing in the downstream region of the fuel injector. However, low NOx emission levels were found with the co-swirl configuration compared to counter-swirling for both gaseous and liquid fuels [6]. Andrews et al [55-59] found that a counter-rotating radial swirler with vane passage injection has low NOx emissions compared to co-rotating which has better flame stability. Andrews et al [57, 58] reported that using a splitter plate between the two swirlers created a separation of the upstream airflow, which enhanced the flame stability with a central injector pilot. A 40mm splitter plate between the two 76mm outlet radial swirlers was used in the present work to enhance the flame stability and to improve the mixing.

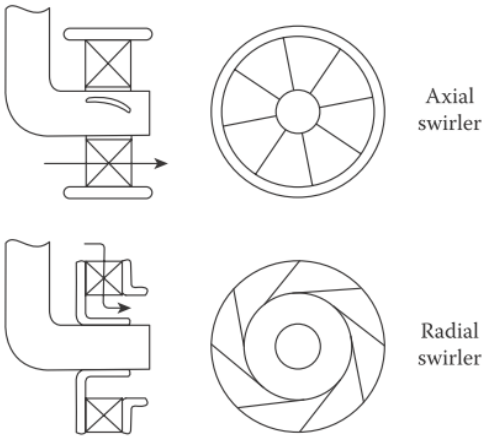

Figure 2.3: Axial and Radial Swirler[11].

2.5.2.3 Swirler number

The intensity of the swirling flow is denoted by the swirl number (S), which is defined as 'the ratio of the tangential and axial momentum' [2, 6, 21, 53]. The swirl number has a great influence on the shape and size of the recirculation zone. A swirl number around Sn>0.6 has been found to be required to produce a central recirculation zone and this is normally achieved with at least 30^{o} vane angle. Several investigations on the effect of Sn showed that the size of the central recirculation zone increased as the degree of swirl increased [2, 21]. The swirl number has a great influence on the swirler discharge coefficient (Cd), which is decreased with the increase in swirl number. This is due to flow separation on the swirl vane surfaces as the turning angle of flow is increased for high swirl [53].

Abdulsada et al. [60] investigated flashback and blow-off at three different swirl numbers using radial swirl at atmospheric pressure. Up to seven different fuels were tested, with their main conclusions being that flashback and blow-off limits are influenced by the swirl number, exhaust configuration and fuel type. High swirl numbers gave flashback limits with methane that were worse than the low swirl number.

However, this work on Swirl number is directly contradicted by the review of weak extinction by Andrews et al[34] for premixed and well mixed combustion. This shows that swirling and non-swirling flows can all achieve the fundamental flammability limits with critical temperatures in the 1400-1500K. There are some swirler and fuel injector designs that have poor flame stability, with critical temperatures >1800K, it is not true that this is a feature of swirling flow generally. One swirler that has particularly poor flame stability is the 'Low Swirl' axial swirler[61] that achieves flow swirler by putting an axial non-swirling flow on the centreline of an axial swirler with a large central hub. This has the effect of blowing out the central recirculation zone that gives swirlers their normally good flame stability. This has a critical flame temperature at weak extinction of 1760K.

Beer and Chigier [62] derived expressions for calculating the swirl number for various types of swirl.

$$\textbf{\textit{Sn}}= \frac{2}{3} * \frac{1-(D_h/d\ )^3}{1-(D_h/d)^2} \tan\theta \qquad \textbf{(5)}$$

However, this is for an axial swirler with a free discharge which is the situation in large furnace applications of swirlers. The swirl number is influenced by the combustor enclosure diameter D to swirler outlet diameter d and this is not taken into account by Eq. 5. Alkabie et al [63] have derived a geometrical equation for Sn for radial swirlers with no central hub, of the type used in the present work.

$$\textbf{Sn}= \frac{\sin\theta}{1+\tan^{-1}\theta} * \frac{A_3}{A_2 * C_C} \qquad \textbf{(6)}$$

Where Cc is the contraction coefficient of the radial vane passage jets.

2.5.2.4 Turbulence

A swirl stabiliser produces strong shear regions in the expanding shear layer between the inner and outer recirculation zones downstream of the swirler dump expansion. High turbulence is generation in these shear regions which is in free space well away from the walls or swirler. The turbulent kinetic energy comes from the energy loss in the swirler flow pressure loss. Reducing the swirler vane passage area for the same flow increases the passage velocity and the pressure, which generates more turbulence for flame stabilisation and fuel and air mixing[21, 53]. The distribution of turbulent kinetic energy downstream of a radial swirler with D/d of 1.8 is shown in Fig.2.4 using CFD by King et al. [64].

Andrews et al. [55] carried out CFD prediction for four different designs of radial swirlers with a 76mm diameter, with the outlet throat being 40 mm long and D/d=1.81, and they found that a strong shear layer was generated in sudden dump flow expiation at the swirler throat exit, as shown in the figure below [55]. In the present work, the swirler exit's diameter d was 76 mm, the combustor diameter D was 140 mm, and the ratio D/d was 1.84; this location was used for co-firing with natural gas.

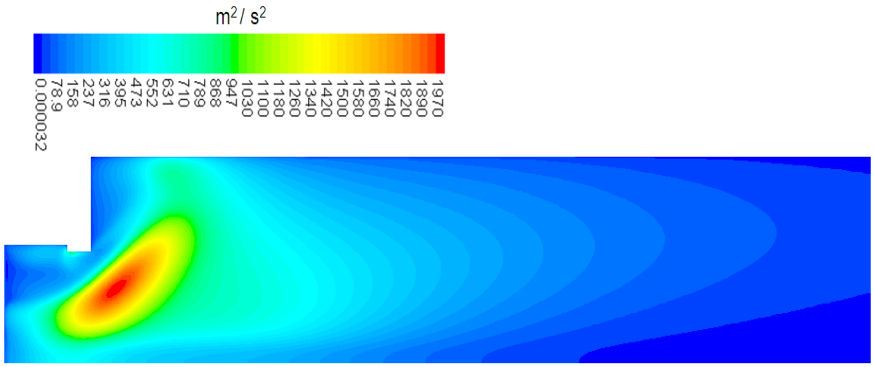

Figure 2.4: K-ε CFD predictions of kinetic energy of turbulence in the dump expansion[64].

2.5.2.5 Pressure loss

Generation of turbulence is accompanied by pressure loss in the combustor. Therefore, in combustor design an optimum compromise between the amounts of turbulence required for good mixing and minimum pressure loss should be taken into account. Both pressure loss and turbulence level depending on the minimum flow area of the system, and the amount of

turbulence level can be increased either by decreasing the depth/width of the swirler or by adding a restrictor in the flow. High turbulence energy can be created by increasing the aerodynamic blockage or by increasing the pressure drop across the swirler [21, 53]. In typical gas turbine combustors, the values of pressure loss is between 2 and 5% depend on the Mach number and can be calculated using equation 7 [21]. In the present work, the airflow was set to achieve reference Mach numbers of M=0.017 and 0.023 using the same stabiliser (co-rotating radial swirler). The higher Mach number increased the pressure loss from 1.5% at 0.017 to 2.7%.

$$\frac{\Delta P}{P} = \frac{\gamma}{2}\left(\frac{M}{C_D}\cdot\frac{A1}{A2}\right)^2 \qquad (7)$$

$$C_D = \frac{\dot{m}}{A_{th}\sqrt{2\rho\Delta P}}$$

2.5.2.6 Dump flow expansion

The D/d ratio is the dump flow expansion from the swirler outlet throat (d) to the combustor diameter (D) and it is an important parameter in low NOx combustor design. In this region a strong shear layer is generated, which stabilises the flame and mixes the fuel and air. Also, a peak turbulence level in a very small zone was found close to the dump expansion from the swirler as shown in Fig. 2.4. Two recirculation zones can be identified with a dump expansion swirler: central and outer recirculation zones. Thus, the size of the recirculation zone and the amount of air recirculated can be increased by increasing the hub size and diverging the swirl exit. Since larger recirculation zones increase residence time, which has an adverse effect on NOx formation, D/d should be limited. The typical values in gas turbine combustors for D/d are around 1.8–2, depending on the swirler discharge coefficient to pass at least 60% of the combustor airflow through the swirler [54, 65]. It has been showed that D/d ratios >2 are inappropriate for low NOx gas turbine combustors, as the swirlers are too small to pass the required amount of air at a typical 4% pressure loss[64].

It has been shown that rapid fuel and air mixing occur in the swirler dump expansion shear layer region. Kowkabi[21]found that higher combustion efficiencies and lower emissions of NOx were achieved with a lower expansion ratio combustor of 1 compared to a combustor with a high expansion ratio >1.5 and this agreed with other researchers[2, 65].

The injection of liquid and gaseous fuels into swirler outlet wall fuel has been shown by Alkabie and Andrews to have ultra-low NOx emissions. Andrews et al. [55] injected natural gas and propane 20 mm downstream of the swirler exit on the outer wall of the 76mm-in-diameter axial swirler at 600 & 740 K and atmospheric pressure. Their results showed that ultra-low NOx emissions were achieved. They used 20 mm to avoid problems associated with a long premix passage, such as flashback, auto-ignition and acoustic resonance.

2.5.2.7 Radial Swirl Design configuration

Fuels could be injected using radial swirler vane passage and this design has been put into production for gas and liquid fuels, in a modified format by Siemens small engines (Lincoln). Central 8 hole radially outward fuel injection also proved very effective for low NOx with liquid fuels. This is normally used as a pilot fuel location by many manufacturers[66, 67].

A potential problem with the use of radial vane passage fuel injection is that of flash back for natural gas and auto-ignition for liquid fuels. Alkabie and Andrews [68, 69] showed that low NOx emissions similar to those with vane passage fuel injection were generated with fuel injection at the swirler outlet throat wall, with the fuel injected radially inwards from the outlet throat wall at a 60^{o} angle from the wall to the upstream flow. The injection angle was intended to reduce deflection of the fuel in the downstream direction. At this location flashback and auto ignition is impossible as there is only 30mm from fuel injection location to the throat exit. However, to achieve this fuel injection location a 60mm long throat of 76mm diameter was added to the radial swirlers with 76mm outlet diameter. Fig.2.5&Fig.2.6 show radial swirl combustor and fuel injection configuration without and with throat respectively.

Previous work also investigated two pilot fuel locations: central and in the radial swirler dump expansion region. Both were effective in acting as a pilot region, but the central injection location had the best flame stability and the lowest NOx penalty and this was the pilot fuel location in all the present work

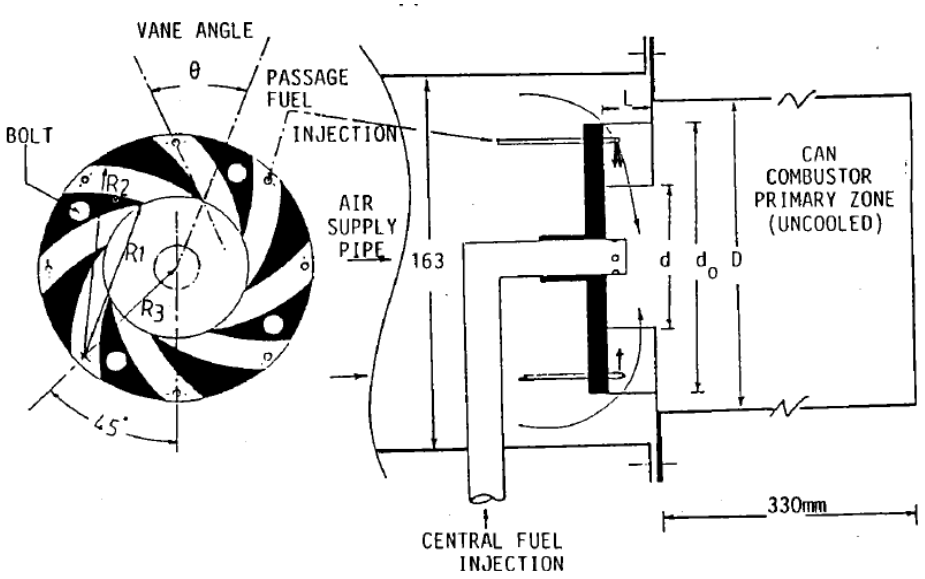

Figure 2.5:Radial swirl combustor and fuel injection configuration (without throat).

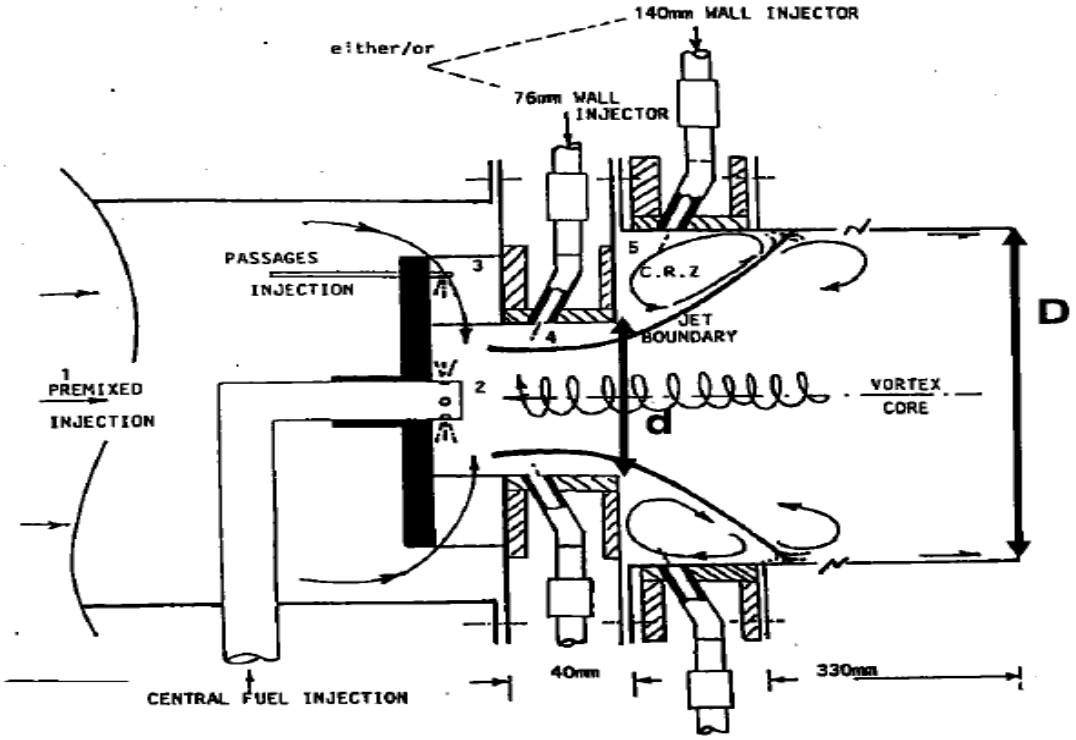

Figure 2.6:Radial swirl combustor and fuel injection configuration (with throat).

2.5.3 Effect of fuel injection location and mixing on NOx emissions using radial swirlers

Radial swirlers are widely used in dry low NOx combustors and typically pass about 60–80% of the total airflow at maximum power, depending on the turbine inlet temperature. However, the fuel injector's location and the design of radial swirlers are important and influence the NOx emissions and flame stability. There are several ways of fuelling radial swirlers: with a single fuel hole on the central vane passage [68, 70] or with three fuel holes per radial passage, as used by RR[71, 72].

The effective flow area of the swirler is important to determine the flow into the swirler. Equation 5 is used to calculate this area.

$$A_{sw}=n_v*s_v*w_v*C_d \qquad (8)$$

Where
n_v is the number of vanes
s_v is the vane gap
w_v is the vane width
C_d is the vane discharge coefficient=0.7

Andrews et al [54, 55, 73]investigated four different types of radial vane passage: curved passage, flat bladed passage, parallel rectangular passage, and circular passage. All swirlers had an outlet diameter of 76 mm and dump flow expansion from the swirler outlet throat (d=76 mm) to the combustor diameter (140 mm). The D/d ratio was 1.84, as in the present work. They injected natural gas into three different locations: vane passage injection with a radial fuel spoke with a single fuel injector hole for each vane passage, outlet throat wall fuel injection (as in the present work), and eight central radailly outward fuel holes.

The tests were carried out at a Mach number of 0.03 and inlet temperatures of 600 K and 740 K at atmospheric pressure. This Mach number represents around 60% of the combustor's total air flow in the primary zone. The results showed that the four different techniques used to manufacture the passages did not have a big influence on the results in terms of NOx emissions, with ultra-low NOx emissions being achieved. They produced similar NOx at both inlet temperatures with passage injection techniques at atmospheric pressure. However, it can be seen from Fig. 2.7 that RS1 and RS2 had lower NOx emissions with 76mm swirler outlet wall

injection, with RS5 and RS6 having lower NOx emissions with the swirler vane passage. Andrews also reported that [54] the best NOx emissions were for RS6 with circular vane holes which related to longer L/D of the circle vane. Thus, the stability margin of the flame was good and there was no acoustic pressure oscillation problem.

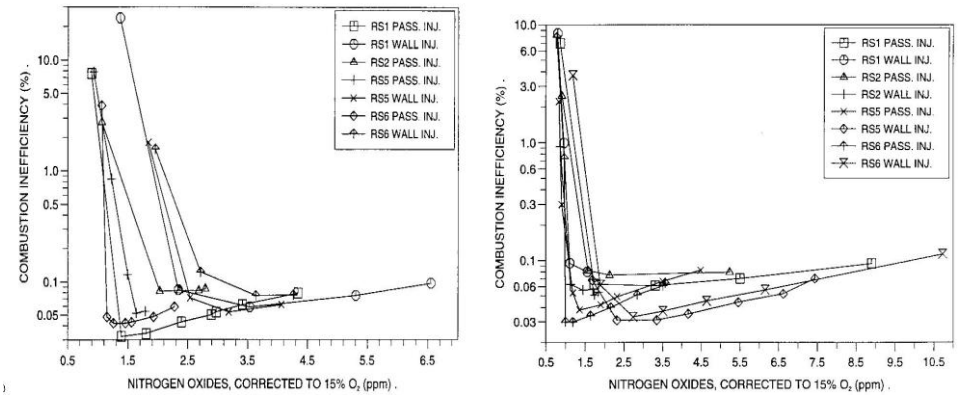

Figure 2.7: NOx at 15% oxygen as a function of the combustion inefficiency at 600K&740K for all four swirlers[54].

Flat vanes have been widely used in swirlers as they are cheap and easy to produce. However, curved blades are more aerodynamically efficient than flat vanes and have a higher flow capacity for the same pressure loss for the same swirler outer diameter. This is because curved vanes allow the incoming axial flow to turn gradually, which inhibits flow separation on the suction side of the vane[21, 53]

Radial swirlers have been used in the combustor primary zone, and have proven effective in achieving low NOx emissions using natural gas. The rapid mixing of injected fuel with the swirler airflow in the dump expansion shear layer, is required for a lean low NOx primary zone combustor. Vane passage fuel injection was shown by Alkabie and Andrews[68, 69] to have low NOx emissions (1 ppm was achieved). This design of radial swirlers has been used in some industrial gas turbines to achieve low NOx emissions with gas and liquid fuels [66, 67].

Andrews et al, have also shown that low NOx emissions could be achieved for gas and liquid fuel, which are similar to those with vane passage injection by injecting the fuel at the swirler outlet duct wall [54, 55]. They injected the fuel radially inwards from the outlet throat wall at a 60° angle from the wall upstream flow. In this region a strong shear layer is generated which stabilises the flame and mixes the fuel and air.

The maximum turbulence was found to be in the dump expansion shear layer, as predicted by King et al.[64, 74] using CFD. The results showed that the zone of peak turbulence was very close to the wall fuel injection location which gives good fuel and air mixing, as mentioned earlier.

King et al [64, 75] investigated three different designs of radial swirlers using CFD: dump expansion from the radial passage outlets, an outlet throat, and an outlet shroud. The purpose of the study was to improve the mixing to achieve low NOx. Their results showed that the addition of an outlet shroud to radial swirlers increased the pressure loss and produced higher turbulence. The predicted NOx emissions were reduced from 2.7 ppm in the radial swirler with a standard flange to 1.2 ppm with an outlet shroud. Moreover, the addition of a 60mm outlet throat to the radial swirler had a positive effect on performance by providing perfect fuel and air mixing by the end of the throat, and resulted in a 0.3ppm predicted NOx[64, 75]. For this reason an outlet throat to a large flow capacity radial swirler was used in the present work. The aim was to give more time for the slow evaporation of the biofuel.

Andrews et al[54, 65] carried out tests on the effect of wall fuel injection with an axial swirler at 600 and 740K inlet temperatures and atmospheric pressure combustion. They injected propane and natural gas from the outlet wall and compared the results with central fuel injection. Their results showed that rapid mixing occurred in the dump expansion shear layer by the outlet wall fuel injection, whereby resulting in ultra-low NOx emissions compared to central fuel injection. However, the central radial fuel injection had a wider combustion range (lower extinction limit), as shown earlier. Also, there was a good agreement between axial and radial swirlers in terms of NOx emissions with outlet wall fuel injection at similar test conditions[21, 54].

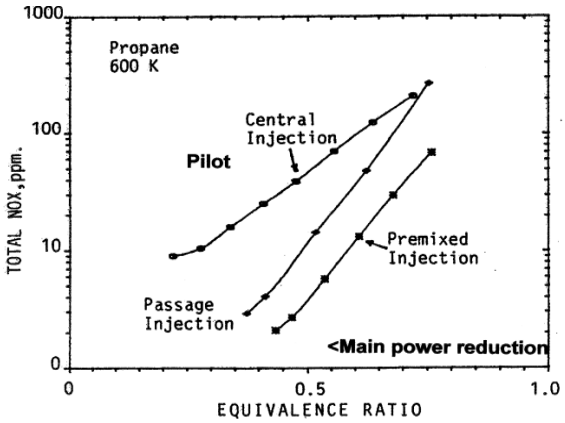

Figure 2.8: Comparison of central Radial Outward 8 Hole injection with passage and premixed injection[68, 69]

One of the main advantages of swirl flow designs is the centrifugal forces which tend to accelerate the mixing of two flows having different densities[76, 77]. This is beneficial to wall injecting, rather than central, by forcing lower-density hot gases to move inwards, whereas higher-density unburned gases were centrifugally forced towards the wall of the combustor. Andrews et al previously investigated the effect of doubling the vane swirler depth to achieve a higher flow and lower pressure drop by using a single swirler with central fuel injection and no downstream swirler exit throat; the results showed increases in the NOx emissions but improvement in the flame stability and power turndown[55] .

Central eight-hole radially outward fuel injection has a more stable flame for gaseous fuels, and also proved to be very effective for low NOx with liquid fuels[73]. This is normally used as a pilot fuel injection location by many manufacturers and will be used as a pilot fuel injection with liquid fuels in this work. This will be combined with the double radial co-flow swirlers that achieve a low pressure loss at the high flow rates of lean gas turbine primary zones. On gaseous fuels, this design had been shown to have very low NOx emissions, and the combination of the vane passage and central injection had shown very low NOx emissions over a wide range of equivalence ratios, indicating that a wide range of engine powers could be sustained [57, 58]. The present results show that the flame stabiliser configuration had good results for natural gas, but did not perform as well as on liquid fuels.

Alkabie and Andrews[68] were the first to demonstrate how dry low NOx could be achieved for gaseous and liquid fuels using the same fuel

injection location and flame stabiliser design. The tests were carried out at 600K inlet temperature and atmospheric pressure using a curved blade radial swirl with low fuel injection locations (passage and swirl outlet wall). Gaseous fuel (propane, natural gas) and liquid fuels (kerosene & gas oil) were used and injected into the vane passage with holes of 2.2 and 0.4 mm respectively[55], whereas the wall fuel injector holes were 3 mm and were inclined 30° upstream. The Mach numbers and pressure loss for the passage and wall were 0.02 and 0.014 & 5.1%, 4.2%, respectively. The results of NOx for four fuels in both cases were corrected to 15% oxygen and plotted as a function of the CO emissions, as shown in Figs.2.9&2.10 [68].

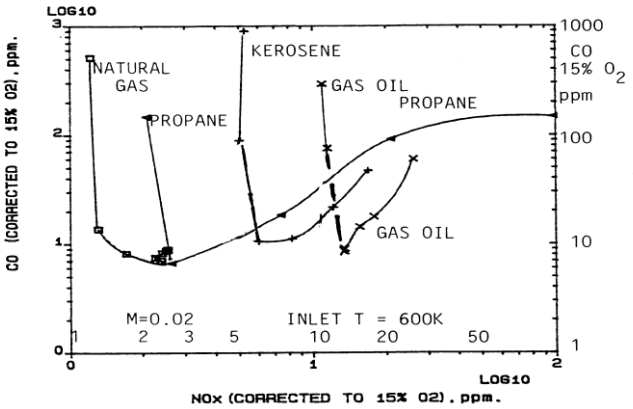

Figure 2.9: CO emissions as a function of NOx emissions with both corrected to 15% oxygen, radial swirler vane passage fuel injection at 600K and M=0.02[68].

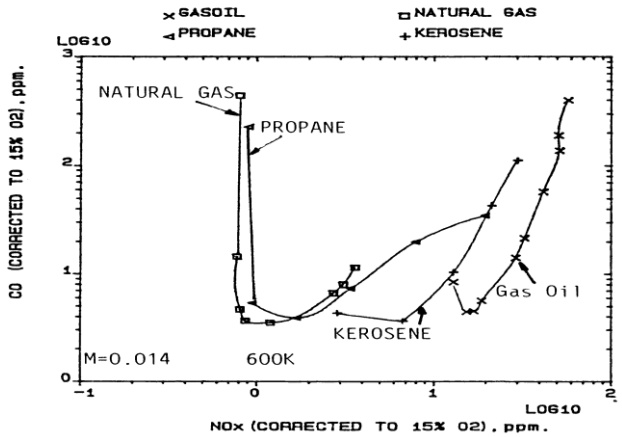

Figure 2.10: CO emissions as a function of NOx emissions with both corrected to 15% oxygen at 600K and M=0.014[78].

From the figures, it is shown that low ultra NOx was achieved for natural gas and similar to the original radial swirler results of Alkabie and Andrews[68, 69] as well as Burckner-Kalb et al[79]. They used wall injection

of premixed fuel and air using two tangential injectors[55]. For kerosene and gas oil, 25 ppm was demonstrated respectively. The higher NOx was from kerosene due to its flame having a richer central region with a peak temperature of 2050 K. In general, vane passage injection had better stability, whereas better mixing can be found in the outlet duct wall injection. The maximum turbulence was found to be in the dump expansion shear layer. Andrews et al [73] found that NOx emissions of liquid fuels were lower than for gaseous fuel, using central eight-hole radially outward fuel injection as shown in Fig.2.11.

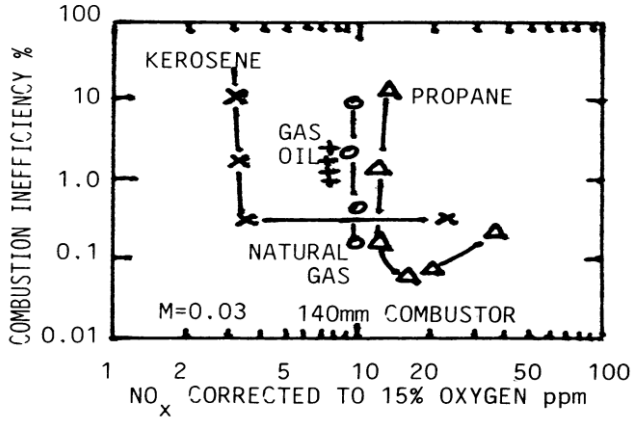

Figure 2.11: Combustion inefficiency as a function of NOx at 15% O_2 for a large airflow radial swirler (45° radial angle) with central radially outward 8 hole fuel injection[73].

Andrews et al [55] investigated radial swirlers using kerosene fuel with and without a central NG pilot. They compared two fuel injection locations at the inlet to the vane passages and 20 mm downstream of the 76mm diameter swirler exit through the wall. The test conditions were a 0.015 Mach number at 600 K and atmospheric pressure. 16 fuel injection holes and 8 injection holes were used for vane passage and 76mm wall fuel injection respectively. The results showed that 3 ppm of kerosene NOx emissions was achieved at Φ=0.6 and 600 K with the vane passage. These results are very similar to the performance with natural gas at the same conditions. Also, there was a large increase in NOx emissions with a central natural gas pilot compared to a vane passage without a pilot. The NOx increased from 3 to 15 ppm at Φ=0.5 and from 15 to 33 ppm at Φ=0.75 [55]. The NOx emissions were higher for 76mm liquid wall injection with a central pilot compared with passage injection. Their results showed that there was no acoustic

resonance at any test condition, as the addition of a pilot allowed richer Φ without acoustic resonance.

2.5.4 Applications of DLN in industrial sector

Early methods of NOx control were based on the use of water or steam injection. These methods successfully reduced NOx to levels of around 42 ppm using a variety of fuels. However, a high level of CO emissions and the cost of providing water and steam are the main drawbacks of these technologies. Legislators were also starting to seek lower NOx emissions, typically below 25 ppm, which could be achieved using DLN techniques. The majority of gas turbine manufacturers switched to Dry Low Emission (DLE) or Dry Low NOx (DLN) combustion systems to fulfil legislative demands. Dry low emission combustion technology in gas turbines is used in all industrial applications of gas turbines, but was led by the demand for DLN for electrical power generation. Alstom, Siemens Industrial Turbo-machinery, Siemens AG, General Electric (GE), Mitsubishi Heavy Industries (MHI) and Rolls-Royce (RR) are the major manufacturers of DLE engines to achieve low emissions. A large number of engine sizes are manufactured that range from 1 MW to 500 MW.

2.5.4.1 Siemens industrial Turbo-machinery

Siemens Industrial Turbo-machinery use a DLE combustor design as in Fig.2.12 which is based on the original work of Andrews et al[73] at Leeds University for a range of engines with power ratings from 4–13 MW. Current emissions levels are about 25 ppm for gaseous fuel and about 50 ppm for liquid fuel at 15% oxygen. This application uses a radial swirler with a reverse flow tubular combustor and impingement cooling. The main fuel is injected into the passages, with a pilot burner in the centre to improve flame stability. Examples of these engines include SGT400 Cyclone (13 MW), SGT300 Tempest (8 MW), SGT200 Tornado (7 MW), SGT100 Typhoon (5 MW), and TB5000 (3 MW). All these engines are designed and manufactured at Siemens Lincoln UK [2, 24, 36].

Figure 2.12: Siemens DLE combustor[6].

The G30 DLE combustor was adopted by the European Gas Turbine Company (EGT). The design of this system is to achieve good mixing at high flame temperatures to reduce NOx emissions as well as fairly poor mixing at lower firing temperatures to provide a good stability margin with low CO and UHC emissions. The G30 tubular combustor contains a radial swirler, swirler fuel injection system, mixing swirler exit passage, pilot burner, and dilution holes. Gaseous fuel is injected through the vane passage wall of each radial passage and mixed with the vane passage air in the downstream shear layer. The mixture is ignited and stabilised within the vortex core of the pre-chamber. [2, 36].

The central pilot is used to assist flame stability with the main vane passage fuel. This can be used as the only fuelling during start-up and up to a certain engine power level, which is often 40%. This design was developed for small engines with <10 MW (Typhoon/Tornado/Tempest). The Tornado single shift industrial engine achieves NOx, CO and UHC levels of 15, 10 and zero ppm, respectively, at base load [2, 6, 24].

2.5.4.2 Siemens AG

Siemens AG is another group of the global Siemens Corporation, manufacturing DLE gas turbine engines in the range of 68–253 MW. Most of the engines use an annular combustor with an axial swirler in their system, with the others using tubular designs. DLE combustion has been used since the 1980s, when vertical silo-type champers was used with low NOx burners at the top feeding downwards. In 1990, it was changed to a tubular design, and in 1994 the annular combustor was adopted which requires less cooling

air and provides shorter residence time and more homogenous temperature distribution[24].

Siemens use a large axial swirler with fuel injection through hollow swirl vanes with four fuel holes per axial vane passage. The design in shown in Fig.2.13 and has a central pilot with its own air flow. This was the first design to demonstrate <10ppm NOx for low turbine entry temperatures in 1990.

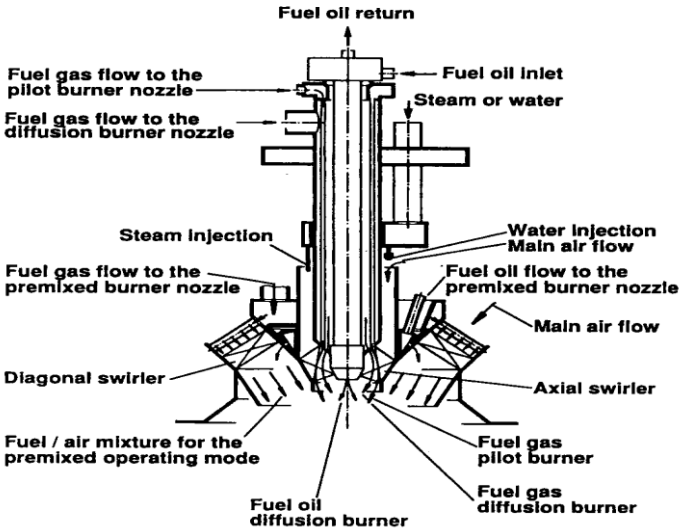

Figure 2.13: Siemens Axial Swirler[2]

2.5.4.3 General Electric (GE) DLN combustor

GE has been using DLN (Dry Low NOx) since the 1980s with the DLN1.0 combustor shown in Fig.2.14 [80, 81], which is still used for the E class gas turbines. This uses axial staging on pilot and main combustion, but uniquely switches the pilot flame off at high powers and used the pilot or primary combustor as a premixing zone for secondary main combustion with a central pilot. This is currently achieving <10ppm NOx in E Class engines [80, 81].

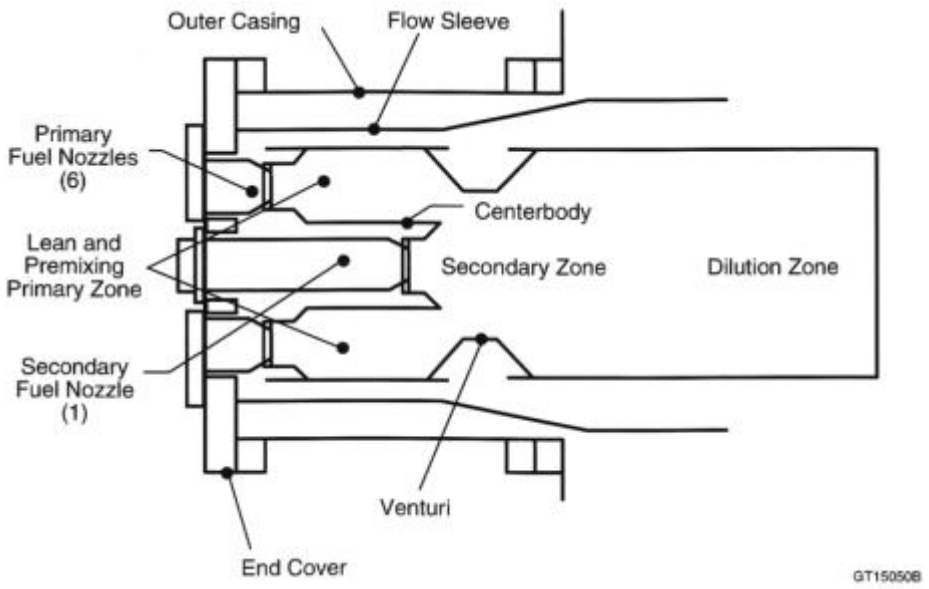

Figure 2.14: Dry Low Nox Combustor (DLN1.0)[81]

For the F, G and H Class higher firing temperature gas turbines and axial swirler was developed and the resulting combustor is DLN-2 as shown in Fig.2.15 and the latest version is the DLN2.6 axial swirler. This has five axial swirlers per can with each swirler with hollow blade fuel injection through holes in the blade surface[81]. They have separate fuel feeds to inner and outer holes and can fuel stage within each blade for enhanced power turndown in the low NOx mode. The NOx emissions for the H Class design are shown in Fig.2.16 [82]. This design has a weak extinction at the fundamental flammability limit[34] and hence has one of the highest power turndown capabilities in DLN technology.

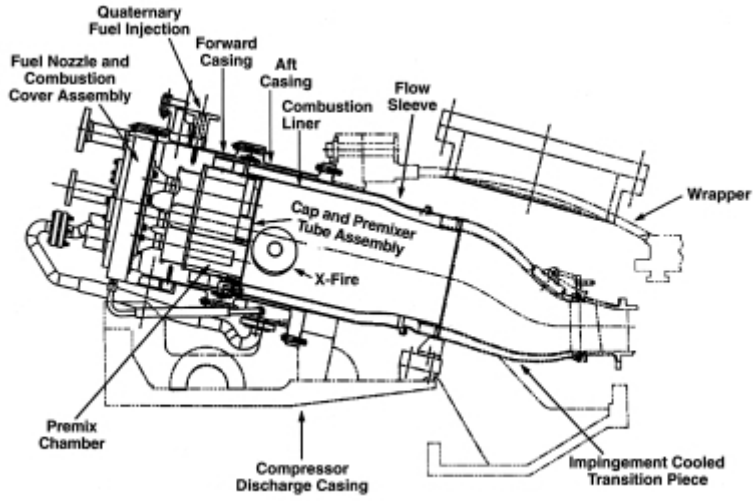

Figure 2.15: Dry Low Nox Combustor (DLN2)[81].

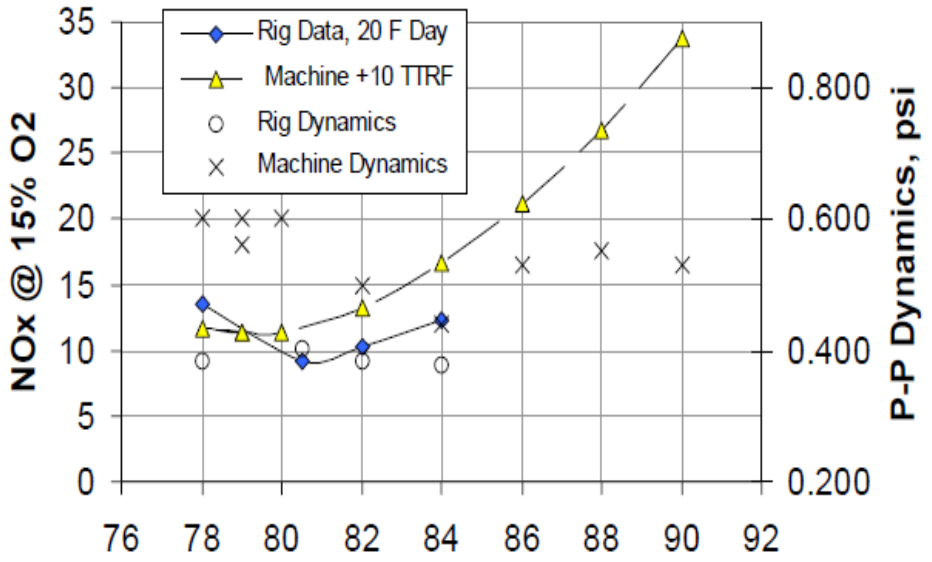

Figure 2.16: NOx emissions for H class design[82].

2.5.4.4 Alstom

In 1984, Alstom was the first company to manufacture the DLE gas turbine with GT13. GT13 used a silo combustor, with this approach using a large number of air fuel premixes to inject the mixture into the combustor. This approach was abandoned in 1990 and the EV burner was developed. The Environmental (EV) burner is used in their gas turbines with a power from 56 to 292 MW[83, 84].

The EV burner is a conical flame stabiliser cut in two and the two halves shifted to produce two slots along the cone wall, which act as tangential flow air inlets that are similar to radial swirler vane passages. A gas fuel injector is inserted along the slot with a number of fuel injection holes so that all the inlet air is fuelled[83, 84]. The design is shown in Fig. 2.17, and is effectively a form of swirler which is a hybrid between an axial and radial swirler, but with only two vane passages. The flame is stabilised in the free space near the burner outlet due to dump flow expansion and the generation of an expanding shear layer as for other swirlers.

One of the silo-type (one single large cylindrical combustor) combustors is the ABB GT11N gas turbine, which uses 37 EV burners all operating in the premixed mode. NOx emissions of 13 ppm were demonstrated at 643 K and

1.25 Mpa for base load [84, 85]. However, the annular-type combustor of this design can be seen in a single row of 18EV ABB GT10 (23 MW) and heavy-duty ABB GT13E2 (>150 MW), which has 72 EV burners with two stages. Moreover, the most recent development in EV burners is the GTX100 (43 MW) with thirty AEV burners and four air slots[86]. The emissions performances with gaseous fuels are 15ppm NOx and CO[85, 86].

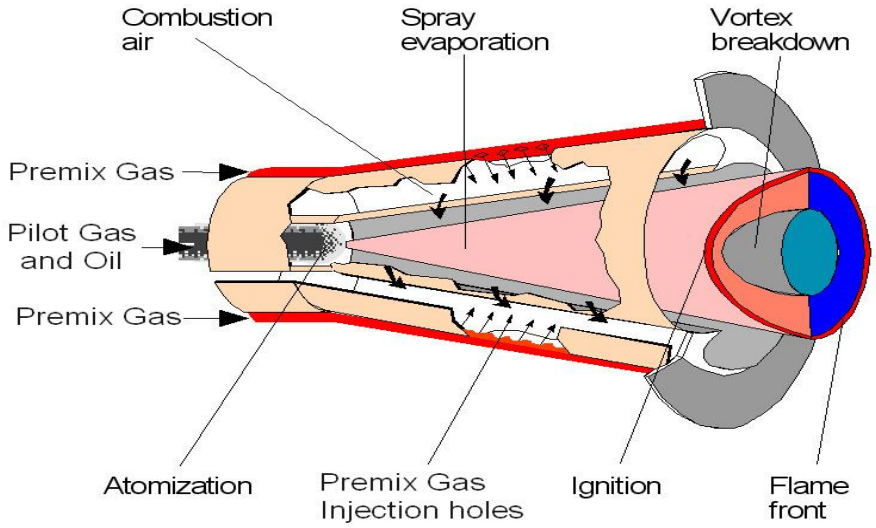

Figure 2.17: EV burner[86].

The main difference between the AEV and EV burner is the mixing section in the burner body downstream of the swirler. This is done by using four tangential slots along the cone with a simple cylindrical mixing length addition at the end of the EV burner as shown in Fig. 2.18 and termed the AEV [87-89]. The improvement in mixing in the AEV burner achieved low NOx emissions and NOx <10ppm for engine powers from 100% to 40%, as shown in Fig.2.19.

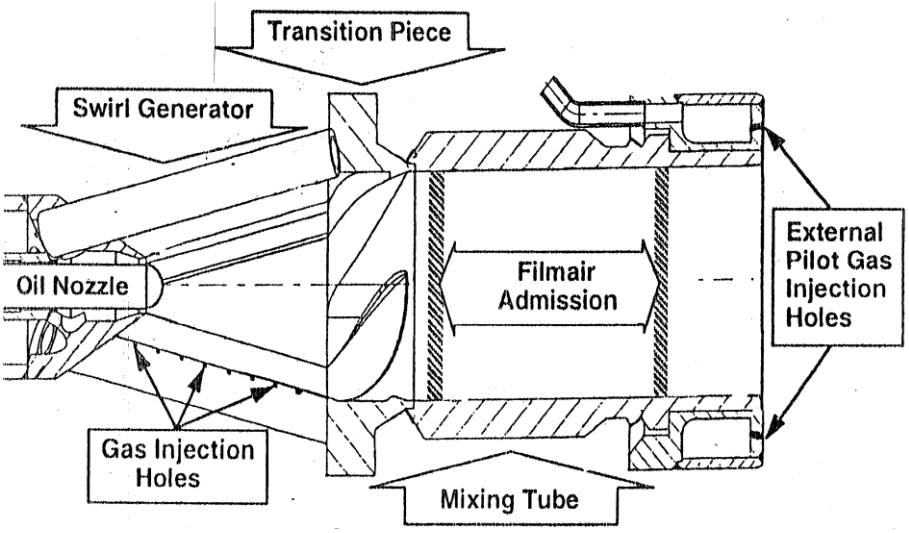

Figure 2.18: The advanced EV burner (AEV)[89].

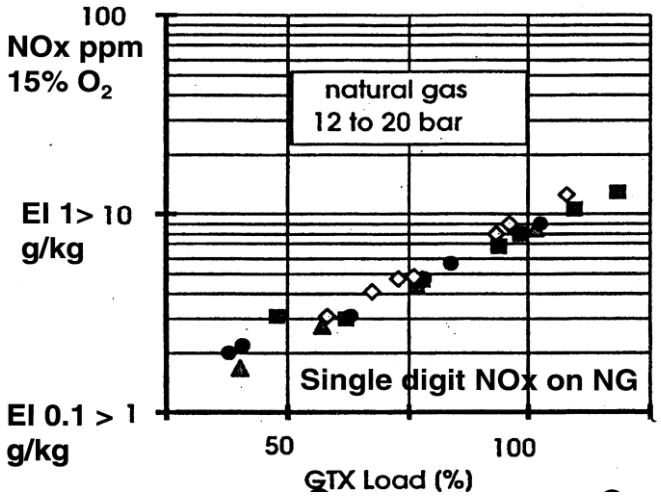

Figure 2.19: NOx emissions as a function of engine power for AEV burners[89].

2.5.4.5 Rolls Royce

This is an aero-derivative engine converted from annular combustor to can-annular for electrical power generation and pipe line pumping ranging from 25 to 70 MW, e.g. The RB211design is shown in Fig.2.20 and uses a two stage axially staged combustion to deal with the power turndown requirements The low NOx primary zone uses a counter-rotating radial swirler with vane passage fuel injection [90-92]. The original RR Trent (50-70MW) design initially used a three-stage combustion system, as shown in Fig.2.21, which achieved ~15 ppm of NOx. The latest version of the Trent uses a two stage combustion system and has replaced the counter-rotating radial swirler with a single vane passage swirler [90, 92, 93].

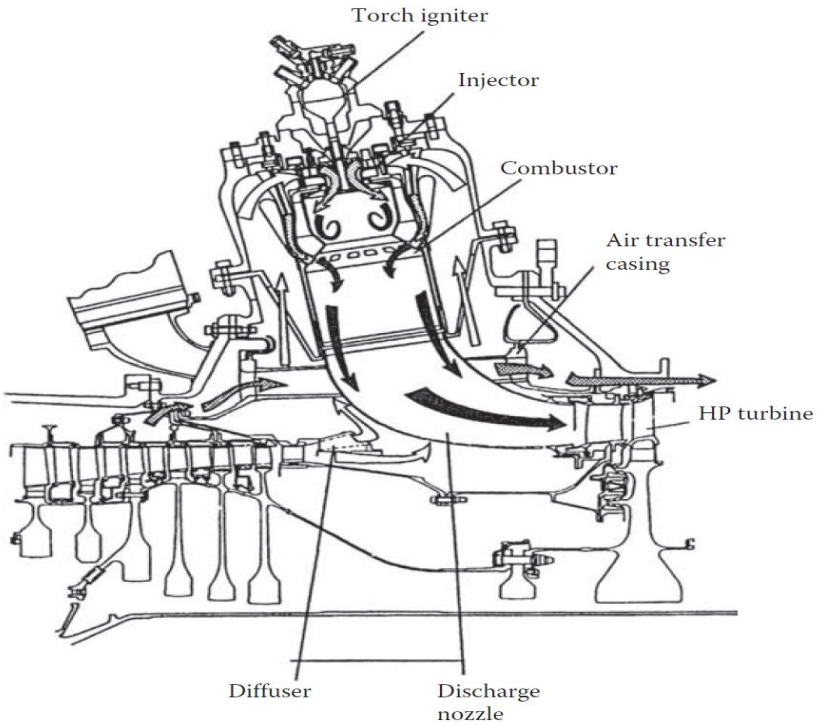

Figure 2.20: Rolls Royse Industrial RB211 DLE Combustor[90].

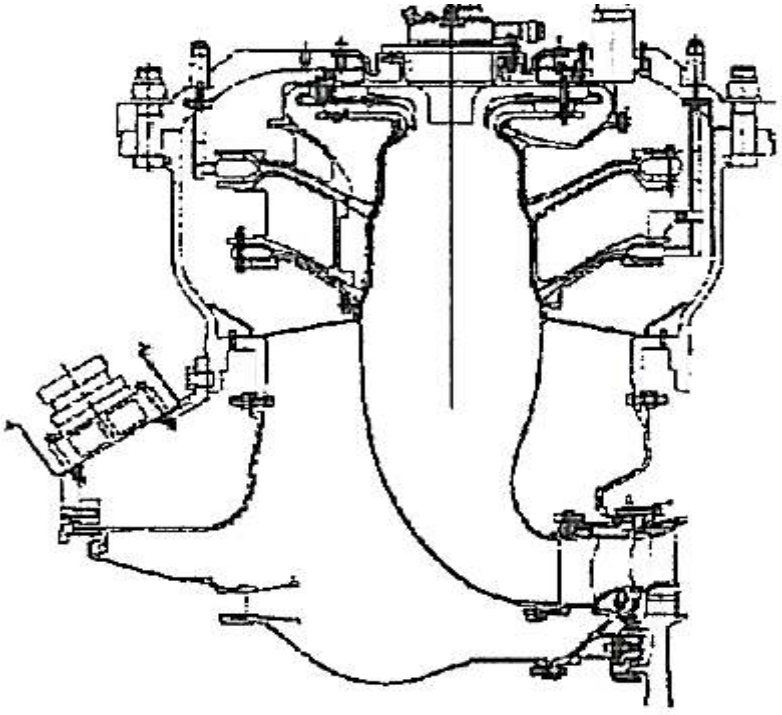

Figure 2.21: Rolls Royse Trent 50MW DLE Combustor[93].

2.5.4.6 Mitsubishi Heavy Industries (MHI) Can annular combustors

Can annular combustors are widely used in heavy duty gas turbines with large number and small size of axial swirler. Mitsubishi Heavy Industries (MHI) uses 8 swirlers per can as shown in Fig. 2.22, whereas GE uses five axial swirlers per can with the same design. MHI G series gas turbine is the largest steam cooled in the market and the first unit operated in 1997. The key issue of the G series design is to increase the turbine inlet temperature by taking advantage of the steam cooled combustor. NOx emissions has been reduced from 25ppm with MK7-4 to 15 ppm at 1500ºC in this design (M501 G)[32] as shown in Fig.2.23.

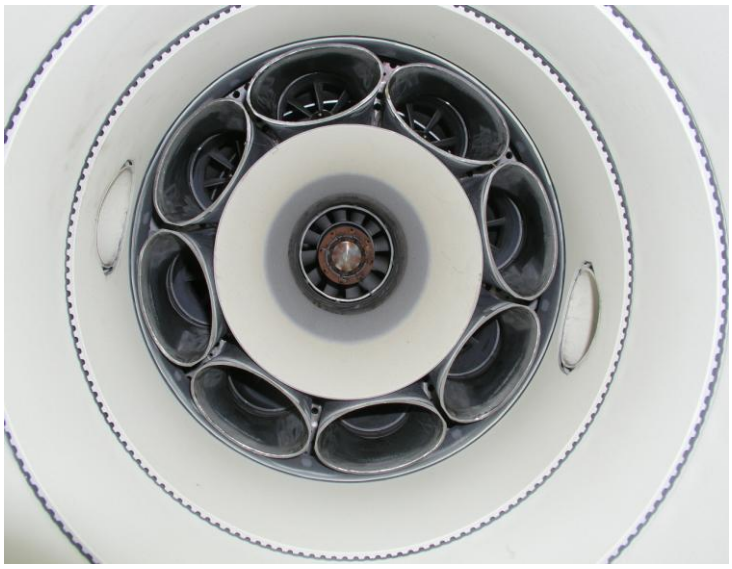

Figure 2.22: Eight axial swirlers with a short downstream mixing passage around a central baffle and central pilot axial swirler[94]

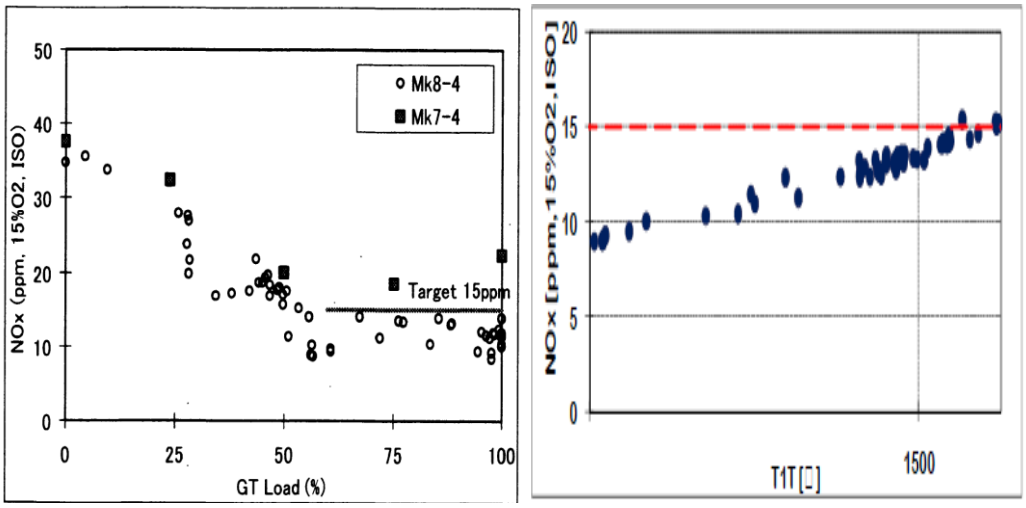

Figure 2.23: Nox Emissions MK7-4 and M501 G[32, 94].

2.5.4.7 Hitachi multi Cluster combustor

This is a rapid mixing flame stabilizer with no downstream premix passage and no swirling flow and round jet shear layers used for rapid air and fuel mixing with centreline axial fuel injection as shown in Fig. 2.24[95]. Hitachi H-25 gas turbines are used widely in power generation, general industrial use and in oil and gas field due to their high reliability and efficiency. It is equipped with 10 cannular combustors (cluster) connected by fire tubes and there are 36 fuel injectors in each cluster. Liquid and gaseous fuels can be used include NG, light distillate oil and kerosene. In the Hitachi H-25 dry method design, 25 ppm or less corrected to 15% oxygen was achieved at base load[95].

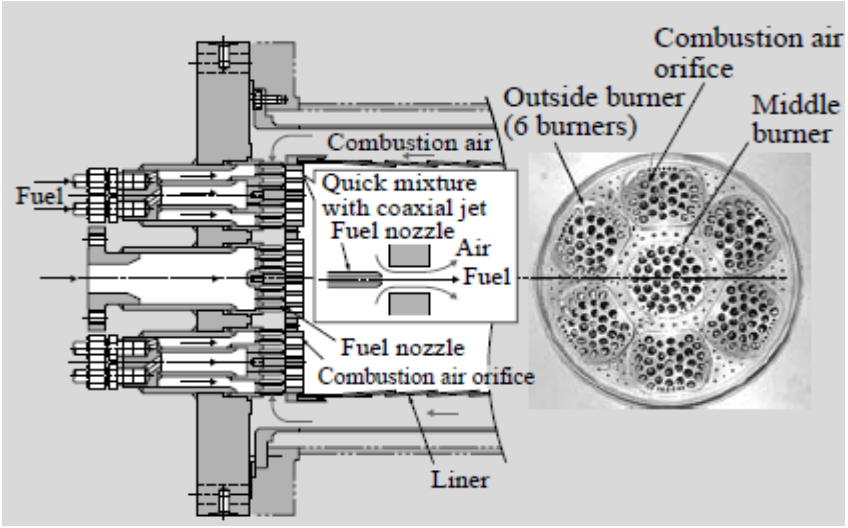

Figure 2.24: Structure of cluster burner.

2.6 Auxiliary power units (APU)

2.6.1Description and working principles

The substantial requirements of all aircraft for on-board electricity and hydraulic power compressed air have to be met. During the normal flight, these requirements can be obtained from the main engines using the gearbox; however, a mobile source of electric power or an auxiliary power unit (APU) can be used while the aircraft is on the ground. An APU is a small gas turbine mounted usually in the aft part of the aircraft, and is especially designed to meet on-board aircraft power demands. It can be used to provide electrical energy (115 V, 400 Hz) for aircraft systems during ground

time, air to the environmental control system (air conditioning) during ground time, and air (bleed air) for the main engine to start; it serves as an electric and hydraulic back-up system in flight. It is also used to start the main aircraft engines [96, 97]. Military aircraft use APUs to facilitate themselves in a wide range of operations, whereby making themselves self-sufficient and capable of rapid take-offs in a combat situation.

An APU is essentially a small gas turbine used for power generation in a similar way to an industrial gas turbine and not to produce thrust for propulsive power. There are various types of APU engines which are being used in different types of aircraft, depending on the aircraft engine size and type.

There are some important factors which should be taken into account when an APU is designed, including low volume, low noise, low weight, ease of maintenance, thermal efficiency, and overall cost. The earlier design of the APU was a single shaft with a large compressor providing about 30% of the inlet flow to be bled off. The power output is split into compressed air and electric power by the bleed valve. Due to the low thermal efficiency from old APUs, design modifications are being done to attain higher efficiency and lower emissions [96].

2.6.2 APU Emissions

Due to the significant amount of APU usage in an aircraft, especially during the aircrafts time at airports, it has contributed a significant amount in terms of emission pollution to the environment [96, 97]. The emissions from APUs are not a large source, but they are increasingly under scrutiny because these ground-level emissions can affect local air quality on and around the airport. The following pollutants are of interest for emission inventory and dispersion calculation purposes: Nitrogen Oxides (NOx), Hydrocarbons (HC), Carbon Monoxide (CO), Particulate Matter (PM), and Carbon Dioxide (CO_2). APU emissions from an aircraft has a great effect on the air quality of the airport and its vicinity due to the fact that the APU is the major source of power to the aircraft when it's at ground level; therefore, the measurement and determination of emissions from the APU of the aircraft can help the manufacturers and airport authorities to set policies and take steps to regulate its emission[96, 97]. Measurement of emissions from an

APU can be done by the use of probe sampling instrumentation consisting of measuring instruments, and can also be calculated if some operational conditions, like the aircraft type, fuel flow of APU, and the mode of operation, are known. Watterson et al[97] used equation (8) to calculate APU emissions from Heathrow and Gatwick airports, UK. The airports provided the standard averages of the APU running time prior to departure as well as one after arrival for all aircraft.

$$E_{LTO_{a,m,p,s}} = T_{a,m,s} \times F_{a,s} \times I_{a,p,s} \quad \textbf{(9)}$$

Where:

$E_{LTO_{a,m,p,s}}$ is the emissions in mode m of pollutant p for a specific aircraft type s at airport type a (kg)

a is the airport type

m is the mode (APU use prior to departure or APU use after arrival)

p is the pollutant

s is the specific aircraft type

$T_{a,m,s}$ is the time in mode m for a specific aircraft type s at airport type a (s)

$F_{a,s}$ is the fuel flow for an APU on aircraft type s at airport type a (kg s^{-1})

$I_{a,p,s}$ is the emission factor of pollutant p for an APU on aircraft type s at airport type a (kg / kg fuel).

2.7 Regulations for aviation and industrial gas turbine fuels

Some factors must be considered for alternative aviation fuels, including environmental effects, price, safety, and reliable operation. For civil aircraft, safety, reliability, low cost, and ease of handling are the main requirements, whereas for military aircraft, fuel cost is of secondary importance compared with availability, supply logistics, and the need for easy operation over a wide range of conditions. For industrial and marine gas turbines, very cheap fuels can be used, such as residual oil or surplus gas. Thus, any fuel proposed for aviation must have the following characteristics [9, 16, 98].

- High energy content to minimise fuel burn, operating cost and CO_2 emissions.
- Low freeze point, particularly for aviation fuels, to ensure fuel does not freeze at altitude.

- Good flow properties to ensure the fuel will flow as required through the aircraft fuel system.
- Suitable flash point to ensure the fuel can ignite in air as required.
- Good storage stability to ensure quality of the fuel is maintained with time.
- Compatibility with materials and components in the fuel system.

2.7.1 Aviation fuels

The fuel specifications for aircraft engines (e.g. the airframe, engine fuel system, and combustion chamber) are stricter than those of all other types of gas turbine. Aviation turbine fuels are used for powering jet and turbo-prop engine aircraft. Aviation kerosene fuels are composed of hundreds to thousands of different hydrocarbon components, with the differences between one batch and another being both molecular mass and abundance. There are two classifications of gas turbine fuels used in civil commercial aviation: Jet A-1 and Jet A — both are kerosene-type fuels, and Jet B — wide-cut kerosene (a blend of gasoline and kerosene), but are rarely used except in very cold climates [9, 16, 98].

Jet A-1: is a kerosene grade of fuel suitable for most turbine engine aircraft. It is produced to a stringent, internationally agreed standard, and globally utilised except in the USA. It has a flash point above 38°C and a freezing point maximum of -45°C. Jet A-1 meets the requirements of British specification DEF STAN 91-91 (Jet A-1), ASTM specification D1655 (Jet A-1), IATA Guidance Material (Kerosene Type), and NATO Code F-35.

Jet A: is a similar kerosene-type fuel that is produced to an ASTM specification and normally only available in the U.S.A. It has the same flash point as Jet A-1 but a higher freeze point maximum (-51°C). It is supplied against the ASTM D1655 (Jet A) specification.

Jet B: is a distillate covering the naphtha and kerosene fractions. It can be used as an alternative to Jet A-1, but because it is more difficult to handle

(higher flammability), there is only a significant demand in very cold climates, where its better cold weather performance is important. In Canada, it is supplied against the Canadian Specification CAN/CGSB3.23.

JP4: is the military equivalent of Jet B, with the addition of a corrosion inhibitor and anti-icing additives; it meets the requirements of the U.S. Military Specification MIL-DTL-5624U Grade JP-4. (As of Jan 5, 2004, JP-4 and 5 meet the same US Military Specification.) JP-4 also meets the requirements of the British Specification DEF STAN 91-88 AVTAG/FSII (formerly DERD 2454), where FSII stands for Fuel Systems Icing Inhibitor. NATO Code F-40.

JP5: is high flash point kerosene meeting the requirements of the U.S. It is widely used by the US Navy.

JP8: is the military equivalent of Jet A-1, with the addition of a corrosion inhibitor and anti-icing additives, and widely used by the Air Force. Comparisons of all fuels are presented in table 3.

Table 3: Aviation turbine fuels[11]

Property	Avgas	JP4	JP5	JP7	JP8/(Jet A/IetA1)
Formula	C_7H_{15}	$C_{8.5}H_{17}$	$C_{12}H_{22}$	$C_{12}H_{25}$	$C_{11}H_{21}$
H/C ratio	2.09	2	1.92	2.07	1.91
Boiling range (ºC)	46-145	60-240	180-260	190-250	165-265
Freeze point (ºC)		-62	-49	-44	-51, -45(JetA)
Heating value Kj/Kg		43.5	43	43.9	43.1
Specific gravity 16ºC	0.72	0.76	0.81	0.79	0.81
Aromatics (vol %)	25	10	19	3	18
Naphthenes		29	34	32	35
Paraffins		59	45	65	45
Sulphur (ppm)		370	470	60	490

2.7.2 Industrial Gas turbine fuels

Both gaseous and liquid fuels are used in industrial and marine gas turbine engines, with the choice of fuel being governed by economy and availability. Gaseous fuels have a wide energy-density range compared to liquid fuels, and most gaseous fuels can be accommodated in industrial

engines by suitable modifications to the turbine control system and fuel-handling equipment. Moreover, the most common gaseous fuel for industrial gas turbines is natural gas, which consists mainly of methane and a small amount of butane, ethane and propane. Also, some natural gas may contain about 15% carbon dioxide and nitrogen[11].

Examples of liquid fuels being used in gas turbines are No. 2-GT gas turbine fuel, No. 2 burner fuel, diesel oil, marine gas oil as well as heavy residual fuels. All these fuels required careful consideration in terms of pumping, atomisation and emissions.

2.8 Physical and combustion requirements of gas turbine fuels

The properties of the fuel are important, especially in aviation, to make sure that the fuel is injected, vaporised, and mixed with air in a combustion chamber before combustion can occur. The extent to which these processes are limiting combustion depends, to a very great extent, on the physical properties of the fuel. In the aviation systems, the fuel is required to operate over a wide range of conditions — high pressure and temperature at take-off, and low at cruise altitude.

2.8.1 Freezing point

Freezing point is an important property, especially in aviation fuel systems, and it is defined as the temperature at which solid particles or wax is present in the fuel. It measures the low temperature fluidity of fuel. It is a very important property because all aircraft operate at high altitude, where ambient temperature may be as low as (193ºK). However, aircraft fuel specifications require a maximum freezing point of 227ºK or 215ºK, depending on the type of service. As jet fuel is a mixture of different hydrocarbons, it means it does not freeze at one temperature. Thus, as the number of carbon atoms increased, the freezing point decreased and uses an iso-paraffin compound instead of a paraffin decrease freeze point [16, 99].

2.8.2 Flash Point

This is the lowest temperature at which a fuel can vaporise to cause an ignition in air. It measures flammability of the fuel to be used. It is used for classifying fuels from the viewpoint of fire risk. The minimum flash point of

Jet A fuel is 38°C, whereas the US Navy uses a higher flash point (around 60°C) with JP-5 fuel on an aircraft carrier due to safety reasons[16, 99].

2.8.3 Volatility Point

This measures the ability of the fuel to vaporise, which is controlled by the flash point and distillation in a kerosene-type fuel. High volatility provides easier light-up, improved stability, and higher combustion efficiency. However, the high volatility increases fire hazards due to excessive fuel evaporation losses at high altitude[11, 16].

2.8.4 Viscosity

Viscosity is a physical property that measures the chemical composition and temperature of the fuel. It is a measure of liquid resistance to flow. Viscosity is the most important fuel property as the higher viscosity delays the atomisation process. In practice, an increase in viscosity will lower the Reynolds numbers of the flow inside the atomiser, delay the atomisation, and produce a thickness sheet of the fuel at the exit end. The viscosity of gas turbine fuels depends significantly on its temperature; the higher viscosity of a fuel, the poorer the quality of atomisation and heavy oils is, and residual fuels must be heated before utilisation. The selections of proper atomisers in fuel-injection systems are important for providing satisfactory atomisation with fuel viscosities in the required range [11, 16, 100].

2.8.5 Sauter mean diameter (SMD)

SMD is defined as the diameter of the drop whose ratio of volume to surface area is equal to that of spray. Mean drop sizes for any given atomiser type are dependent on atomiser size, design features and operating conditions. Moreover, physical properties of the fuels and the properties of the surrounding medium are important in terms of atomisation quantity. Fuel density, temperature, viscosity, surface tension, and ambient air density are affecting the atomisation, whether with air-assist or air-blast atomisers. For pressure and air-blast atomisers, the SMD $\propto \sigma F0.6$[2, 101]

2.8.6 Surface Tension

Surface tension is a property of the surface of liquid which resists the formation of a new surface area, which is fundamental to the atomisation.

Thus, the higher surface tension resists formation of droplets from liquid fuel. Surface tension has a significant effect on fuel atomisation because of some typical values of surface tension and their variation with temperature[2].

2.8.7 Calorific value

Calorific value is a combustion property that represents the energy content per unit mass of fuel released during combustion under standard conditions. The calorific value is described as specific energy on a gravimetric basis which depends on the hydrogen-carbon ratio and its chemical composition, and is described as energy density on a volumetric basis. However, the heaviest fuels have the highest energy density, while the lightest fuels have the highest specific energy, and the choice of the aircraft fuel will depend on the type of aircraft and its application[2].

2.9 Alternative fuels

Due to the finite supply of petroleum fuels and increasing the demand for energy worldwide, development of alternative sources is becoming necessary. Renewable fuels are also in demand in order to reduce the carbon footprint of aviation. There are many alternative aviation fuels Fig.2.25 being considered by industry and research groups. The most viable alternatives are synthetic kerosene, Fatty Acid Methyl Ester (FAME), hydrogenated vegetable oils, liquid hydrogen, methane, and ethanol/methanol. For the short term, the synthetic liquid fuels of major interest will be largely derived from biomass, coal, oil shale/tar sands, and heavy oil. For the longer term, liquefied gaseous fuels (methane and hydrogen) are among the candidate fuels now being considered. All these fuels must be compatible with the engine and fuel-system requirements and with aircraft design features and operational procedures.

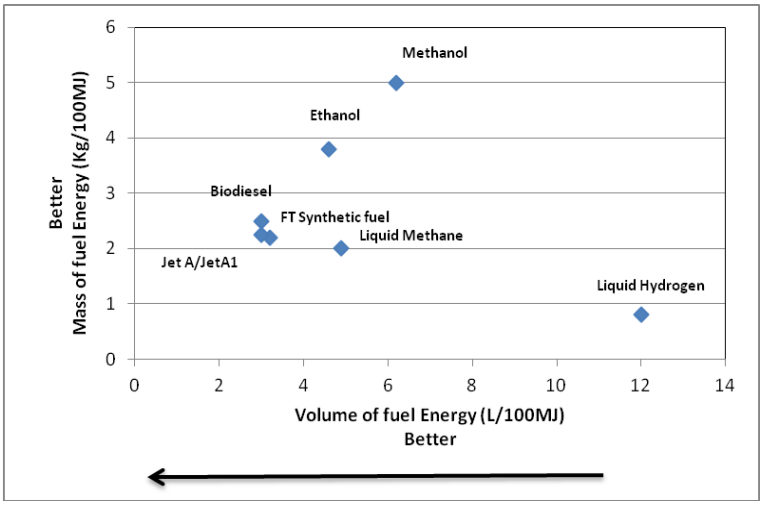

Figure 2.25: Alternative aviation fuels

2.9.1 Synthetic kerosene

Synthetic word is used to describe fuels derived from nonpetroleum feedstock, such as gas, coal and biomass [17, 102, 103]. Fischer-Tropsch (FT) is a process where the mixture of carbon monoxide and hydrogen (syngas) is converted into higher molecular weight of hydrocarbons Fig.2.26. The process begins with the gasification of the feedstock to produce a mix of carbon monoxide and hydrogen (syngas), which then goes through a catalysed chemical reaction to produce liquid hydrocarbons. The properties of synthetic kerosene are varying depending on the hydrogen to carbon ratio, catalyst, and process conditions. Since the FT synthesis starts with carbon monoxide, any source of carbon can potentially be used. If the synthetic kerosene is produced from coal, the conversion is called coal to liquid (CTL); natural gas (NG) can also be used as the starting material and is called gas to liquid (GTL), and most of the current plants use NG. Thus, biomass to liquid (BTL) is produced from biomass as a starting material by going through a gasification step to produce carbon monoxide. The main benefits of FT transportation fuels are that they are large, secure domestic supply, and clean burning fuel with very low nitrogen, aromatics and sulphur [17, 102, 103].

$$CO+H_2 \rightarrow (CH_2)_n+H_2O$$

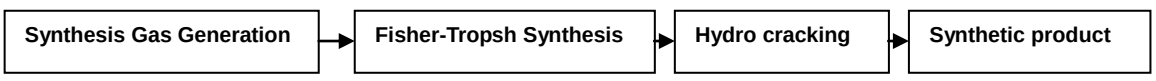

Figure 2.26: Production of synthesis product process

Synthetic kerosene has close to zero sulphur- and nitrogen-contained compounds compared to conventional jet fuel, with there being no SOx or sulphuric acid aerosol emissions. The fuel is also free of aromatic compounds, which will improve the thermal stability, lead to cleaner burning, and reduce fuel burn and CO_2 emissions. However, there are negative attributes of using synthetic kerosene with no aromatic compounds in aviation sectors, including poorer lubricating properties, lower volumetric heat content, a possible contributor to fuel system elastomer leakage, and increased CO_2 emissions during its manufacture. To increase the density of synthetic kerosene and avoid leaking, blending with conventional jet fuel is the solution, with many industries using 8% aromatic compounds as a guiding minimum[9, 104].

The process of Fischer-Tropsch (FT) was developed in Germany in 1956, and Sasol developed the technology further by operating a commercial plant in South Africa and using coal as the raw material. Thus, since 1999, the B50 (50% CTL and 50% normal kerosene) has been approved by regulatory bodies and used in aircraft fuelling in Johannesburg. B100 (100% CTL), produced by Sasol, was approved internationally in 2008 as fuel in commercial aviation [17, 98, 104].

The world's first commercial-scale BTL plant is underway in Germany with the Shell-Choren BTL plant being under construction. There are some challenges of producing BTL as alternative fuel in the aviation industry, including a large amount of feedstock to satisfy the fuel needed as well as the high capital cost of the plant that will increase the price of the fuel [98].
However, most of the current plants use NG as a source of synthetic kerosene, and Shell have operated 14,000 barrels per day in their commercial GTL plant in Malaysia for the last ten years. Also, 140,000 barrels per day are being constructed in the GTL plant of Shell in Qatar. Sasol Chevron also built a GTL plant in Nigeria, with an estimated 34,000 barrels a day since 2010. GTL in aviation will improve CO_2 emissions, air quality and fuel economy [11].

Several major companies are planning to build FT plants, with the yield of FT products expected to be one million barrels per day by 2020, some of

which could potentially be used as aviation fuel. Table 4 compares some properties of FT fuel with kerosene-based fuel[11].

Table 4: Specific energy, Density and Energy Density

Fuel	Specific energy (MJ/Kg)	Density @15˚c (g/cm^3)	Energy Density (MJ/L)
FT Synthetic fuel	**44.2**	**0.759**	**33.6**
Jet A/JetA1	**43.2**	**0.808**	**34.9**

2.9.2 Vegetable/plant oils, FAMEs and hydrogenated oils

2.9.2.1 Vegetable/plant oils

Many researchers have concluded that pure vegetable oils have a great potential to be alternative fuels for diesel engines [105]. However, they cannot be used directly in gas turbines because they can cause numerous engine problems. The higher viscosity and lower volatility of oils compared with diesel lead to engine cold-start problems, engine deposits, injector coking, piston ring sticking, and decreasing the combustion efficiency [106]. Therefore, these effects can be reduced or eliminated in different ways: the first way is by heating the vegetable oil to reduce the viscosity and lower the emissions or by dilution/blending with petroleum fuels. Another way is through the transesterification of vegetable oil to form an ester (biodiesel) to reduce the viscosity [105]. The main purpose of this process is to lower the viscosity of the fuel, which is the main drawback of the direct use of biodiesel that causes poor combustion [8, 107, 108].

2.9.2.2 Biofuels

Biofuels are produced from raw vegetable seed oils, palm oil, sugar beet, solid biomass, and other biomass-derived fuels. Ethanol, biogas and biodiesel are the main biofuels, and can be used in vehicles (cars, trucks), turbines, and boilers on the whole or blended with fossil fuels. Biofuels derived from agriculture products have renewable CO_2 emissions and are allowed to be discounted in carbon audits in most countries. There are also fiscal incentives to use biofuels in many countries that reduce the cost of electricity to the user [109].

There are many qualified biofuels in the European Union, including biodiesel (fatty acid methyl ester (FAME)). Its heating value is 30–50% lower

than typical coal. Liquid biodiesel is one of the most popular biofuels used in the transport sector. Several studies have shown that the characteristics of biodiesel are very close to diesel fuel and can be used in diesel engines with little or no modification [106, 110]. Although there are over 350 species of oil-producing plants, only a few can potentially be used for biodiesel production, e.g. rapeseed, sunflower, soybean, and oil palm.

FAMEs are produced through a transesterification process, as shown in Fig.2.27. It is defined as a chemical reaction of vegetable oils or animal fats with alcohol in the presence of a catalyst to form fatty acid methyl esters (FAMEs), and includes a glycerol by-product [107, 111, 112]. Methanol, ethanol, propanol, butanol, and amyl alcohol are alcohols used in the transesterification process. However, methanol is the commonly used alcohol in this process due, in part, to its cost and its physical and chemical advantages which allow it to quickly react with triglycerides [113].

The main advantages of biodiesel are high flash point, lower sulphur, and low hydrocarbon emissions and particulates. However, higher viscosity and lower heating value are the main drawbacks of biodiesel. The addition of biodiesel to Jet A fuel can reduce specific fuel consumption and increase thermal efficiency. Thus, the presence of oxygen in biodiesel (10–11%) by weight results in leaner combustion and more complete combustion. Table 5 compared some properties of biodiesel with conventional jet fuel.

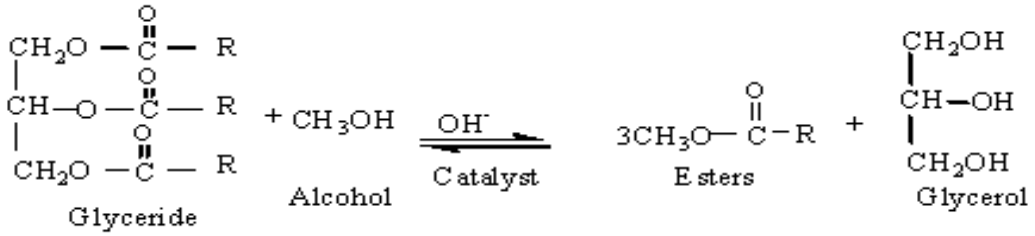

Figure 2.27: Transesterification process[109].

Table 5: Properties of biodiesel and conventional jet fuel[11]

Fuel properties	Biodiesel (typical)	Conventional Jet fuel
Flash point, °C	100	40-45
Viscosity at 40°C Cst	4.7	1.2
Sulfur, wt %	<0.05	0.05-0.15
Combustion heat, MJ/kg	36-39	43.2
Density at 15°C	0.87-0.89	0.80
Freezing point, °C	~0	<-40
Carbon number	C16-C22	C8-C16

2.9.2.3 Hydrogenated vegetable Oil (HVO)

HVO is obtained by converting unsaturated compounds into saturated compounds through the addition of hydrogen. It is more expensive than BTL production and less expensive than FAME production.

2.9.3 Orcryogenic fuels

Orcryogenic fuel refers to a condition where the material in gases faces normal, ambient conditions, has been cooled to its boiling point, and stored as liquid at low temperature, e.g. liquid hydrogen, liquid methane, liquid propane, and liquid ammonia.

2.9.3.1 Liquid hydrogen

Liquid hydrogen is the most environmentally friendly alternative fuel for both land and aviation, as there is no CO_2 emitted during the combustion; however, the CO_2 may be emitted during the production process of liquid hydrogen. There are many ways to produce liquid hydrogen, with the preferred methods being gasification of natural gas and biomass, as well as water electrolysis. It has high flame speeds, wide burning limits, easy ignition, and has a cooling capacity far superior to that of any other fuel.

Liquid hydrogen has very different properties to normal kerosene: it has very high gravimetric energy (120 MJ/kg versus 43.2 MJ/kg) and low volumetric energy content (8.4 MJ/l versus 34.9 MJ/l). The higher gravimetric energy will reduce the aircraft take-off weight, whereas lower volumetric energy requires a significant increase in fuel tank size. Also, liquid hydrogen has a boiling point about -252°C, which requires insulation and pressurisation of the fuel tank [9, 54].

There are numerous challenges associated with liquid fuel as an alternative fuel in the aviation industry, including supply, storage, handling, and distribution of pressurised liquefied liquid hydrogen. The tanks should be made from special materials (aluminium alloy, stainless steel), and modification to the combustor and fuel system components such as pumps, fuel pipes and valves is also required. All these challenges make it a long-term possibility as an alternative fuel in aviation. However, using hydrogen fuel cells to power aircraft in the near future may be a possibility.

2.9.3.2 Liquid Methane

Methane is also a cryogenically alternative fuel in a transition between normal kerosene and liquid hydrogen. It has good thermal stability and clean combustion. However, low density and low boiling point are the main drawbacks of the methane fuel. Methane, like liquid hydrogen, has a higher energy density by mass than kerosene (50 MJ/kg versus 43.2 MJ/kg) and a lower energy density by volume (21.2 MJ/l versus 34.9 MJ/l). Nevertheless, using methane as an alternative aviation fuel will require the same modification in the fuel system as described earlier for liquid hydrogen, but the reduction in takeoff weight and the increase in the fuel tank would not be as large as for liquid hydrogen; this is a result of energy density of liquid methane by mass and volume that is close to normal kerosene. There are many ways to extract methane, such as natural gas fields and methane hydrates, and it can also be produced from fermentation of organic matter under anaerobic conditions and from gasification of biomass. Liquid methane offers a 25% CO_2 reduction and a 60% increase in water vapour, but the negative attributes to methane production are that CO_2 may be emitting availability of sufficient and suitable biomass [11, 17, 114].

2.9.3.3 Liquid Propane and Ammonia

The properties of propane are very similar to liquid of methane in terms of lower specific energy and lower cooling capacity. It can be as a liquid at ambient temperatures by modest pressurisation of the fuel tank. The advantage of ammonia is its higher cooling capacity. However, it has a low heat of combustion, which is about 40% that of kerosene[11, 114]. Comparisons of all liquid alternative fuels with conventional kerosene are presented in Table 6.

Table 6: Properties of some alternative liquid fuels[11].

Property	Kerosene	Liquid Hydrogen	Liquid Methane	Liquid propane	Liquid Ammonia
Lower specific energy MJ/Kg	42.8	116	49	46	17.2
Boiling point (ºC)	150-300	-252	-162	-42	-33
Freeze point (ºC)	-50	-26	-182	-182	-78
Flame speed m/s	0.39	2.67	0.37	0.43	0.30

2.9.4 Alcohols

Alcohol fuels comprise hydrocarbons with one or more oxygen atom within the molecular structure, and have low calorific value.

4. Ethanol/ Methanol

Methanol is currently made from methane (direct oxidation), biomass (destructive distillation) or synthesis gas (coal gasification), depending on the production process. Methanol is poisonous, ash-free and has a minimal soot-forming tendency. It burns with a low-luminosity blue flame and a minimum of exhaust smoke, and has wide flammability limits. Moreover, the low flame temperature ensures relatively low emissions of nitric oxides.

Ethanol can be derived from petroleum or from biological feedstock; it is now being used as an automotive fuel in a 10% mixture with gasoline in Brazil and the USA. Ethanol and methanol have several properties that make them unsuitable to use as an aviation fuel. These include having low energy densities (27.2 MJ/kg and 19.9 MJ/kg respectively) and being of a hygroscopic nature (ability to attract water molecules); for these reasons, ethanol and methanol are only being considered for specific specialist applications [17, 108]. Table 7 present alcohol fuels properties compared to aviation kerosene.

The main advantages of oxygenate fuels are: lower carbon content and freeze point, higher flash point, lean mixture operation due to oxygen, and lower emissions. The drawbacks of alcohol fuels are toxicity of methanol, lower specific energy, being highly corrosive, and poor lubricity in pumps and injectors[17].

Table 7: Alcohol fuels properties[11]

Property	Kerosene	Methanol	Ethanol
Lower specific energy MJ/Kg	42.8	19.9	26.8
Relative density at 15.5ºC	0.8	0.797	0.794
Boiling point (ºC)	150-300	64.85	77.85
Freeze point (ºC)	-50	-95	-117
Viscosity at 293K (m^2/s)	1.65×10^{-06}	0.75×10^{-06}	1.51×10^{-06}
Surface tension (N/m)	0.02767	0.0226	0.0223

2.10 Fuel injection

Gaseous fuels (e.g. natural gas, syngas) will mix more rapidly with air than liquid fuels, which have to atomise and vaporise. However, mixing can occur after atomisation and does not require full vaporisation as this will be done by the flame front.. The optimum level of mixing is the major concern for gaseous fuels, especially those with low calorific values. Gaseous fuels are injected using plain orifices into the surrounding combustion air, which may be swirler. Liquid fuels for low NOx combustion are injected in the same way as gaseous fuels, but with a smaller fuel injection holes. A liquid jet injected into a crossflow of air gives good air blast atomisation, as well as good mixing. The evaporation rate of a liquid fuel droplet depends strongly on the droplet size: the smaller the size, the faster the rate of evaporation. In most low NOx gas turbine combustors, liquid fuel atomisation is achieved by air-blast atomisation. The fuel atomiser must produce a large number of droplets with a sufficiently large total surface area, and distribute the fuel droplets uniformly in the air stream to enhance the mixing process. Thus, complete evaporation of liquid fuel droplets and good mixing of fuel and air within a short distance are essential to achieve low emissions [1, 2, 100].

Fig. 2.26 shows the common method of achieving good atomisation. An air-blast atomiser was used in this work to inject biodiesel and its blends with kerosene; thus, the Sauter mean diameter was calculated for biodiesel and kerosene at both Mach numbers, with the results being discussed in chapter 4.

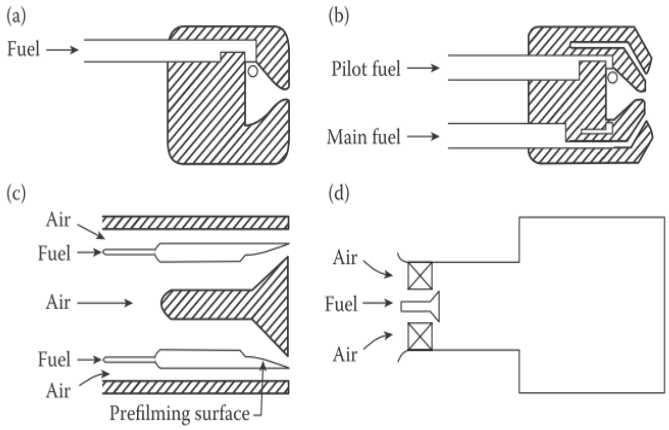

Figure 2.28: Common atomizer design: (a) simplex, (b) dual-orifice, (c) airblast, (d) premix-prevaporize[11]

Chapter 3 : Experimental Set Up and Instrumentations

3.1 Experimental Set Up

There are four different experimental set ups in the thesis, one for the combustion rig for biodiesel and hydrogen and two for APU.

3.1.1 Experimental Set Up for Low NOx burnber

Experimental set up for combustion and emissions of biodiesel and its blends with kerosene as well as NG co-firing will be described and the results will be discussed in chapter 4&5.

3.1.1.1 Combustion Rig

The apparatus used for the combustion experiments consisted of a combustion chamber, an air supply line, venture air flow meter, 250mm diameter air plenum chamber, a fuel supply line and an exhaust gas analyze system as shown in Fig.3.1. The combustion experiments were carried out at atmospheric pressure. The inlet air was heated to the required inlet temperature (600K) by 150KW electrical heaters prior to entering the combustion chamber. A 6.4mm wall thickness stainless steel uncooled combustor, cylindrical shape with an inner diameter of 140mm and length of 330mm was used in this study. The combustor length was a typical minimum size for aero gas turbines and was much shorter than most industrial gas turbines.

A 76mm outlet diameter radial double swirler was used to stabilize the flame and improve the mixing as shown in Fig.3.2. A 45º eight flat bladed co-rotating radial double swirler. The two swirlers were separated by a splitter plate with 40mm diameter outlet orifice Fig.3.3. The aim was to create a pilot region that used only 50% of the air flow from the upstream swirler, on gaseous fuels this had been very effective in achieving a weak extinction down to 0.1 equivalence ratio [57, 58]. All liquid fuels were injected through eight small holes (0.05mm) in the center Fig.3.4 of the rear wall of the radial swirler.

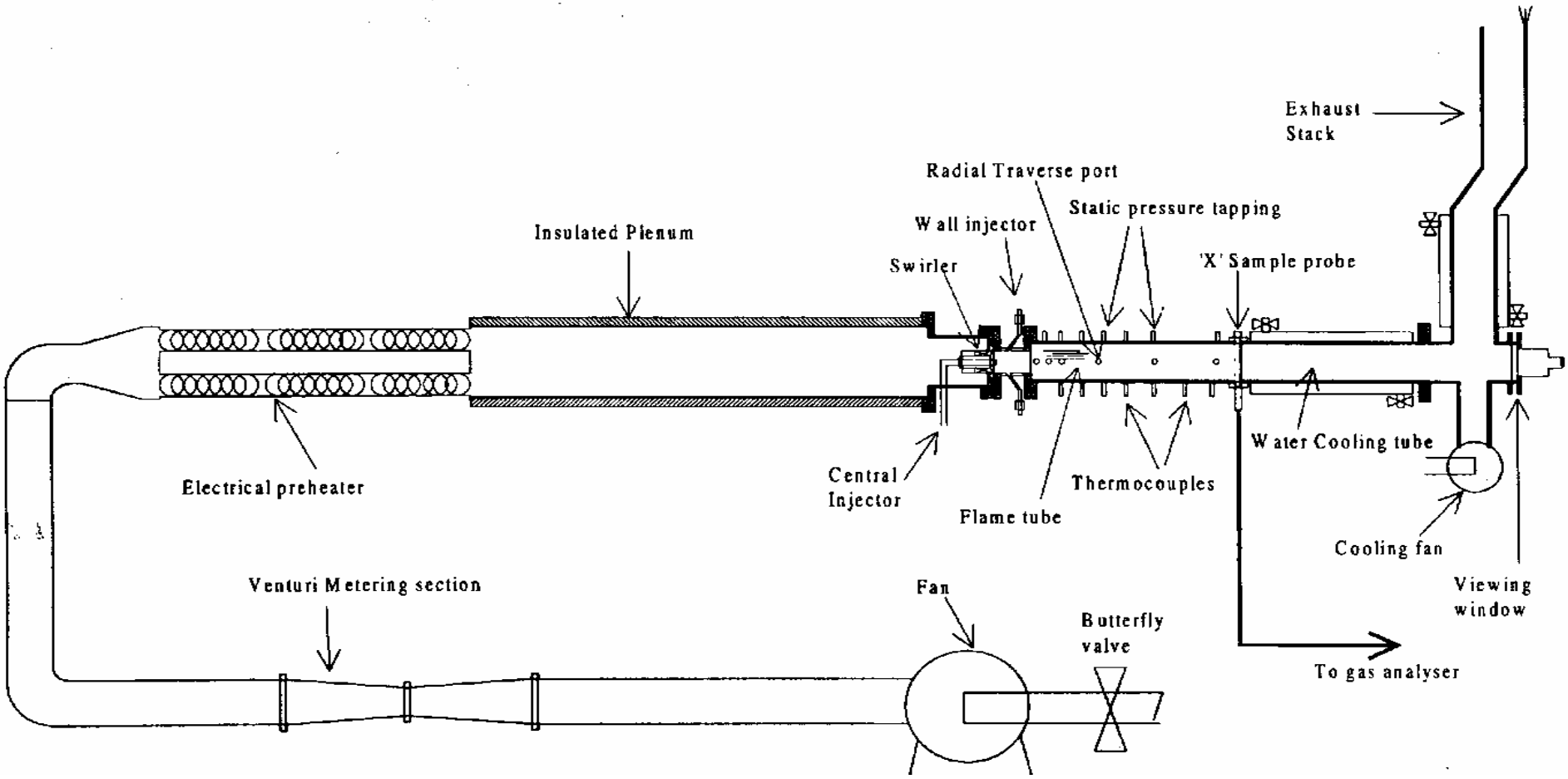

Figure: 3.1 Rig Test Facility[54].

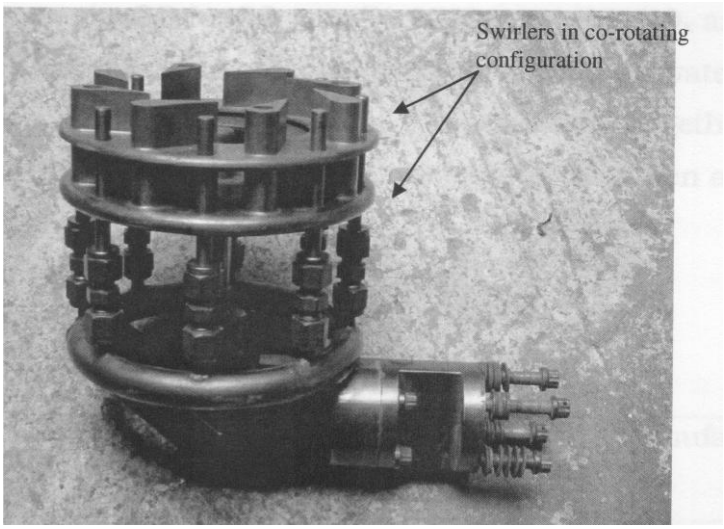

Figure 3.2: The co-rotating radial swirler assembly with radial passage fuel injection assembly

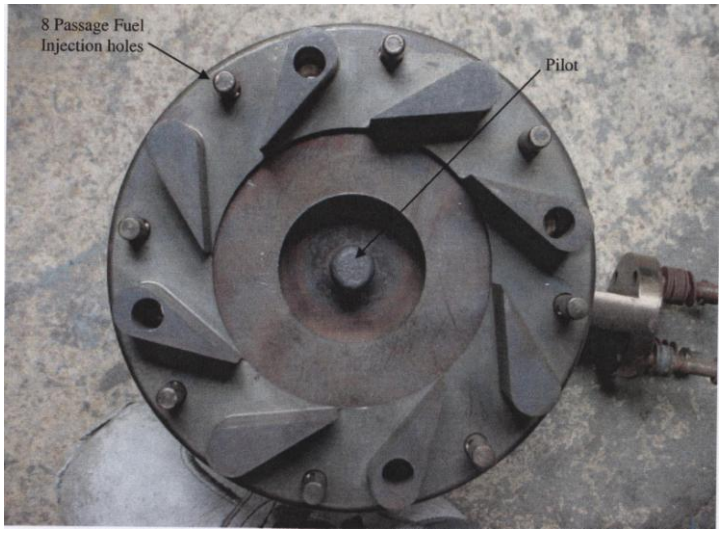

Figure 3.3: The 40mm diameter constrictor between the two radial swirlers and the central pilot fuel injector.

The swirler outlet throat was 76mm diameter and 40mm long and 8 equispaced fuel injection orifices were mounted in the wall of the swirler outlet throat. This was the fuel injection position for the natural gas used in this co-firing work. The wall injector for natural gas fuel had eight equispaced 3mm diameter holes, located 20mm from the throat inlet and inclined 30^{o} towards the upstream flow as shown in Fig. 3.5.

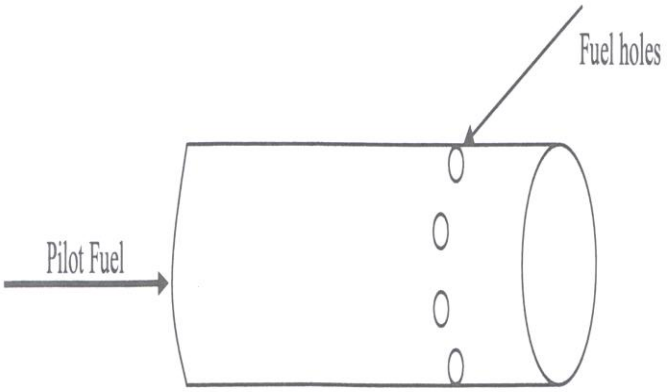

Figure 3.4: central fuel injection position

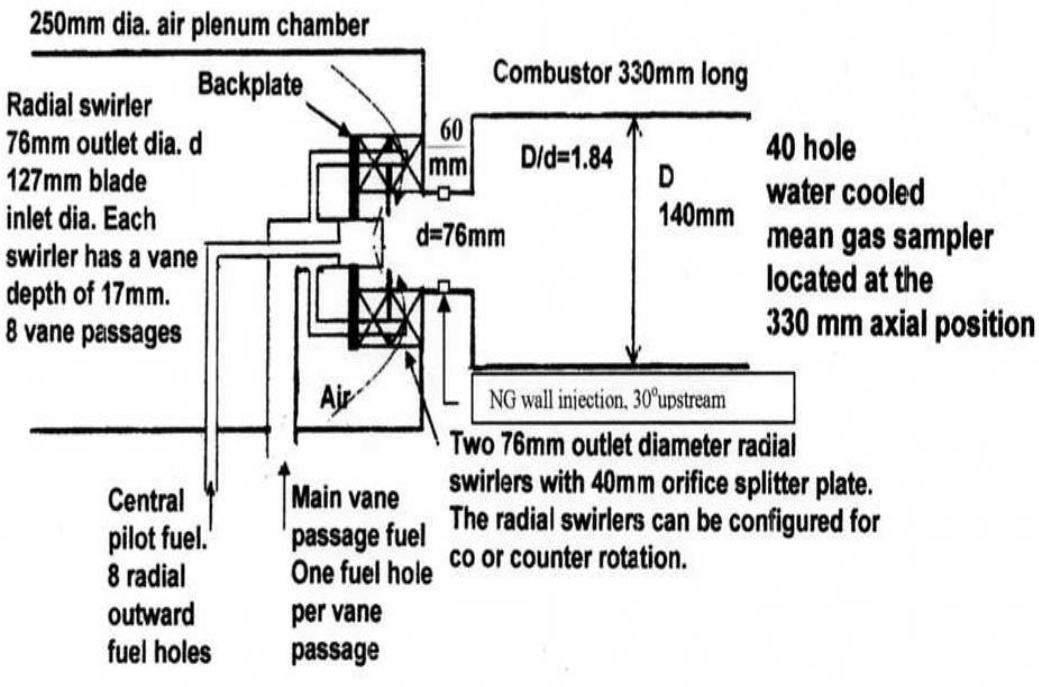

Figure 3.5: Schematic view of the geometry of the combustor [54].

3.1.1.2 Test Procedures

The test conditions were designed to achieve two references isothermal Mach numbers (0.017&0.023) at 600K in the 140mm diameter combustor at atmospheric pressure. The first Mach number typically represents ~40% of the total combustor airflow entering the lean primary zone through the radial swirler. Also, this Mach number represents a lower power simulation of an air staged combustor or combustor with air bleed or IGV air throttling. A lower Mach number gives an increased residence time and this will slightly

increase the NOx [59, 115, 116], so the present low NOx results are conservative. Whereas Mach number of 0.023 represents ~75% of the total combustor airflow entering the lean primary zone through the radial swirler. The inlet temperature was measured 100mm upstream of the swirler using chrome-alumel type K thermocouple. The ignition was carried out by electrical discharge from the spark igniters.

The experiment was started by setting the air flow necessary to achieve the desired reference Mach number of 0.017&0.023 and the electrical heater was switched on and left to achieve 600K. The higher Mach number (0.023) enabled the pressure loss to be increased from 1.5% at 0.017 to 2.7% in the present work. Natural gas was used as the starting fuel using wall fuel injection, which gave good fuel and air mixing with low NOx emissions.

Ignition of the methane-air used a high energy spark mounted at the shear layer impingement point 50mm downstream of the swirler throat exit. The liquid fuel flow rate was gradually increased to attain the desired equivalence ratio, while the methane flow rate was slowly decreased to zero. The change of equivalence ratio was achieved by adjusting fuel flows. As the different fuels have different stoichiometric air fuel ratio, the fuel flow rate was different for each fuel at a certain equivalence ratio.

The main equivalence ratio was leaner than 0.6 for the minimum NOx. Numerous investigators have shown that at this equivalence ratio or leaner well mixed combustion has minimal NOx dependence on pressure[68, 69].

3.1.1.3 Fuels and fuel delivery system

The biodiesel used in the test was WME (waste cooking oil Methyl Ester) made from a mixture of waste cooking oils such as rapeseed oil and sunflower oil. Its physical and chemical properties are presented in table1, along with kerosene. A commercial kerosene fuel produced in the UK was used for the pure kerosene test and blending stocks. This was not aviation kerosene and was very low in sulphur as it was manufactured alongside ultra-low sulphur diesel (typical S levels of 7ppm). Kerosene was stored in a 200 liters barrel whereas WME and blends were stored in a 40 liter tank. They were pumped from the barrel or tank and delivered to fuel injection points after passing through rotameters for measuring fuel flow. Two rotameters were used with different measurement ranges. These two

rotameters were calibrated for kerosene, WME and blends respectively as the density for these liquid fuels are different and thus the mass flow is different for the same indicated volumetric readings.

B100 (100%WME), (20% WME&80%K) B20, (50%WME&50%K) B50 and Kerosene (K) were injected and premixed with incoming air in a premixed fuel injector with holes on centers of equal area Fig.3.4. The fuel air ratio and equivalence ratio is increased in small steps by increasing fuel flow rate whereas keeping air flow rate constant. Table 8 presents physical and chemical properties of the fuels.

Natural gas was supplied from the mains via a boost pump at laboratory temperature (i.e. only the air was heated not the gas). For all the tests NG was supplied at a constant flow rate which achieved with the constant air flow a constant equivalence ratio, which is just inside the weak extinction limit. All the tests were conducted by establishing a stable NG flame at Φ=0.4 and then increasing the overall Φ by increasing the flow of liquid fuel at the central injector. Also the present work was carried out with NG flow rates that were not flammable and the overall combustion relied on heat release from both fuels. A range of NG equivalence ratios were investigated 0.18, 0.22 and 0.38 at Mach number 0.023.

Table 8: Physical and Chemical Properties of the Fuels

Property	Kerosene	B100	B50	B20	NG
Viscosity at 40ºC mm²/s	~ 2	5.10			
Density @15ºC kg/m³	800	884	842	816.8	0.717
Calorific Value MJ/Kg	46	39.8	42.9	44.76	55
Stoichiometric ratio	14.7	11.8	13.35	14.43	17.2
Carbon % mass	86	75	80.5	83.8	75*
Hydrogen % mass	15	11	13	14.2	25*
Oxygen% mass	~ 0	14	7	2.8	0

*NG is assumed all for methane

3.1.1.4 Emission measurement

3.1.1.4.1 Gaseous emissions

Mean exhaust plane gas samples were obtained using a 40 hole water cooled 'X' configuration gas sample probe Fig. 3.6, with sample holes on

centers of equal area. The sample gases were passed into a 190^{o}C heated sample line and on through a 190^{o}C heated filter and pump to a 190^{o}C heated gas analysis system. The gas analysis results were processed to provide a computed air to fuel ratio by carbon balance, combustion efficiency, mean adiabatic flame temperature and various pollution parameters. A chemiluminescence NOx analyzer (Signal Instruments, UK) was used with a vacuum ozone reaction chamber. It had a minimum scale of 1-4 ppm with a 0.05ppm resolution.

Natural gas was supplied from the mains via a boost pump at laboratory temperature and was analyzed for use in the gas analysis carbon balance. The NOx was measured hot on a wet gas basis, as were the unburnt hydrocarbons using a heated FID (Signal Instruments). The CO and CO_2 were measured on a dry gas basis using NDIR with Luft cell detectors (ADC). The gas analyses results were processed to provide air fuel ratio. Regulated emissions (NO, NO_2, NOx, UHC& CO) have been analyzed on dry basis and corrected to 15% O_2 over range of different fuel rate as recommended by the Environmental Protection Agency.

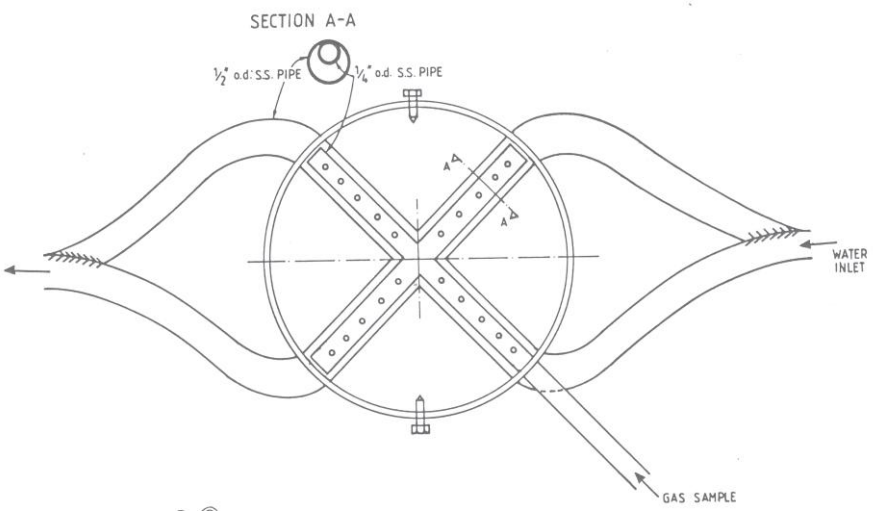

Figure 3.6: gas sample probe

A Gasmet CR-2000 Fourier Transform Infrared (FTIR) was used to detect and quantify three aldehydes: formaldehyde, acetaldehyde and acrolein. The exhaust sample was drawn at the same position as that for regulated emission analyzers by a heated sample line with its temperature

being controlled at 180ºC. One of the main objectives of using FTIR in this study is to get specified hydrocarbon information, including alkenes, aromatic hydrocarbon, and aldehydes[117]. FTIR will be discussing later in more details. The work in chapter 4 focused on aldehydes emissions due to their strong ozone formation potentials.

3.1.1.4.2 Particulate matter (PM)

It was anticipated that the particulate mass and number emissions would be extremely low for lean well mixed low NOx gas turbine combustion. Levels of particle number close to ambient air levels were anticipated. Consequently the same procedure was used as for ambient air sampling and no dilution of the sample gases was used. This was because the contamination introduced by filtered dilution air could be greater than the particles being measured.

Normally with diffusion type combustion in gas turbines and diesels the particle number is too high to directly enter a size analyzer and dilution of the sample to reduce the concentration is essential. Also the dilution is also done to cool the sample so as to condense volatile droplets and sulphuric acid droplets, which then give rise to nano-particles. However, in the present work there was no volatile HC with natural gas combustion and for the liquid fuels at the conditions used of stable operation well away from the weak extinction condition, the hydrocarbon emissions were very low at <20ppm and no significant volatile fraction was present. This is the situation in aero-engines at high powers with very low hydrocarbon emissions and hence very low volatile fraction. Thus, it was not anticipated that there would be a volatile component to condense in this work.

The raw hot gas sample from the multi-hole water cooled sample probe was above 200^{o}C and this was connected to the SMPS by a metal tube sufficiently long to cool the sample to a temperature low enough to enter the SMPS measurement system. The particle size equipment was located close to the combustion equipment so as to minimize transfer line lengths. The same system was used to measurement the particle number size distribution in the ambient air fed to the test rig prior to ignition. This was also measured with and without the electrical air heaters on. No filtration of this air was used

and the air was fed directly from outside the test room and this location was above an internal University road with very light traffic loading, but was 100m from a busy main road.

A Scanning Mobility Particle Size (SMPS) system with a Nano-Differential Mobility Analyzer (NDMA) and a Model 3025 Condensation Particle Counter (CPC) was used to determine the number concentration and size distribution of aerosols in the size range from 5 nm to 160 nm.

3.1.2 Experimental set up for APU

In this section, experimental set up for the measurements of combustion and emissions of alternative aviation fuels from APU will be described and the results will be discussed in chapter 6,7&8.

3.1.2.1 Description of APU Engine

An Artouste MK113 APU engine was used as a test bed for the emissions measurements as shown in Fig.3.7&3.8. It is located in Low Carbon Combustion Center at Sheffield University. It is a single spool gas turbine engine, in which a centrifugal compressor is driven by two stage turbine (Table 9) through a single rotating shaft [118]. All operating parameters of the engine such as fuel flow rate, RPM, exhaust temperatures, pressure and fuel consumption were monitored and recorded throughout the test. Table 10 present the nominal selected values for APU at idle and full power using JetA1 as fuel.

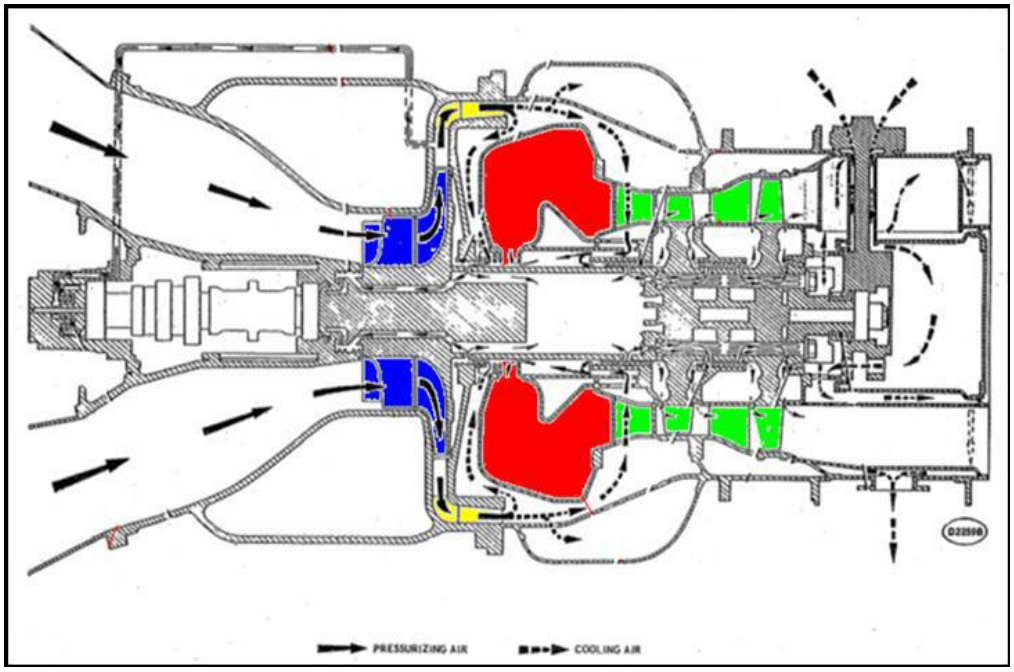

Figure 3.7: Schematic View of Artouste MK113 APU engine[119].

Table 9: APU Engine description

Component	Description
Type	Turbine engine driving generator and providing air bleed
Compressor	Single stage sided centrifugal
Combustion chamber	Annular
Turbine	Two stage axial flow
Overall dimensions	
Length	69.25 in
Width	22.4 in
Height	24 in

Table 10: measuring APU operating conditions

	RPM	Fuel flow rate (Kg h^{-1})	EGT ºC	Air fuel ratio
Idle	22540	51-53	500~506	61~67
Full power	34460	115-116	520~546	65~70

NB: 1. RPM-revolution per minute
2. EGT-exhaust gas temperature.

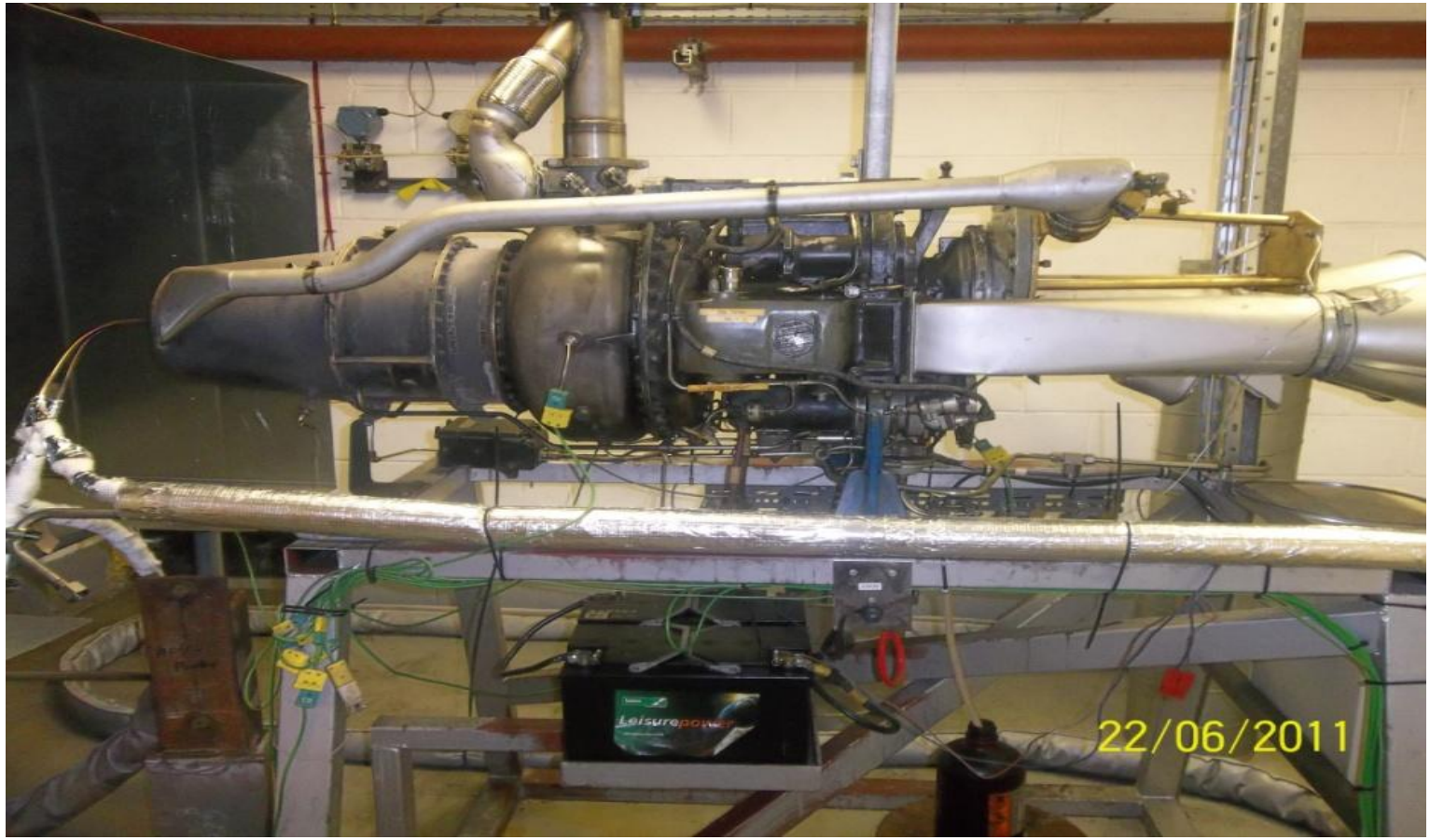

Figure 3.8: Auxiliary power unit

3.1.2.2 Fuel Composition

Conventional kerosene based JetA1 fuel was used a reference fuel. Five compositionally designed fuels were tested and supplied by Shell. Table 11 shows the composition, ratio of hydrogen to carbon, aromatics content, sulphur content and density of the testing fuels provided by Shell and no measurement were carried out in the lab due to confidentiality. Two separate fuel tanks were used for JetA1 and other testing fuels respectively. The second group of the fuel is provided by Sustainable Way for Alternative Fuel and Energy in Aviation (SWAFEA) include four candidate fuels and one baseline fuel JetA1. The compositions and properties of each fuel are presented in table 12. The neat conventional kerosene based JetA1 was used as the reference fuel. Three renewable fuel blends were tested. A neat GTL aviation fuel was also used as the second reference fuel without aromatics. All fuels were tested for engine exhaust particle number and mass size distributions. Again all measurement was carried by SWAFEA.

Table 11: Compositionally designed surrogate fuel properties

Fuel symbol	Fuel compositions	Sulphur ppm	H/C Ratio	Aromatics (%wt)	Cycloalkanes (%wt)	Density kg/m^3
JetA1	JetA1	400	1.89	20.5	13.5	801.9
A	70% Cycloalkane / 20% Aromatics / 10% GTL	<5	1.93	19.8	70	805.4
B	80% GTL / 20% Aromatics	<5	2.01	19.8	0	768.7
C	50% GTL / 40% JetA1 / 10% Other	42.2	2.02	11.58	5	777.3
D	95% Cycloalkanes / 5% GTL	<5	2.07	0	95	787.9
E	100% GTL	<5	2.19	0	0	737.6

Table 12: Alternative Aviation fuels properties

Fuel Symbol	Fuel compositions	Specific heat MJ/Kg	Sulphur ppm	H/C Ratio	Aromatics (%wt)	Density kg/m^3
JetA1	JetA1	43.2	669	1.89	16	803.5
E	100% GTL	44.4	<5	2.19	0	737.6
F	50% HEFA/ 50% JetA1	…….	…..	2.1	…….	…….
G	50%HVO/ 50%Naphthenic cut	43.5	10.8	2	35.33	806.8
H	10%FAE/ 90% JetA1	42.18	601	2	15.2	810
I	75% HEFA/ 25% JetA1	43.9	181	2.1	4.5	763.6

FAE: Fatty Acids Ethyl Ester
HEFA: Hydro- treated Ester and Fatty Acid

3.1.2.3 Emission measurement systems

3.1.2.3.1 Part I: Determination of particle line loss for gas turbine engine exhaust particle measurement

Overview

A direct probe sample extraction measurement method from the exhaust of an auxiliary power unit (APU) was used. Two stainless steel sampling probes were used at the exhaust outlet of the APU, with the aid of a stainless steel plate fixed behind the exhaust outlet to hold the sampling probe to sit just half way out of the exhaust diameter allowing for less than 7% space occupied at the exhaust as shown in Fig.3.8. One was used to check particulate signature during the test and the other one was used as a sampling system. The temperature of the exhaust was monitored using thermocouple to make sure it was above 160ºC before entering the heated line section. A 10-meter of heated line was connected to one of the probes and then followed a heated dilutor in which nitrogen gas was introduced with a temperature of 160 ºC and dilution ratio of 10:1 as shown in Fig.3.9.

The diluted exhaust gas sample was then connected to a 25 meters heated line. At the end of the 25 m heated line, a cyclone was set up to remove particles larger than 2.5 µm. A Vapour Particle Remover (VPR) was installed after the cyclone to remove volatile fractions of particles by heating and introducing the second dilution by nitrogen. The exhaust gas sample after the VPR was passed through several particle measurement instruments including two SMPS. A schematic view of the system set up is

shown in Fig.3.9. Several sampling points along the system were set up as noted in the Fig.3.9 and table 13. Two SMPS instruments were used to measure particle number concentrations and size distributions with one fitted with long Differential Mobility Analyzer(DMA) and the other one fitted with nano-DMA. These two instruments were connected to different sampling points in turn so the particle concentrations and size distributions at the different locations of the sampling line were determined. A DMS500 particle measurement instrument was employed at the fixed location (point 1) acting as a “policeman” to monitor the exhaust stability. All the measurements were undertaken when the engine was completely stabilized.

Nitrogen gas were used to set a zero calibration of the measurement instrument before the start of the testing thereby giving a much accurate reading when the sample is being passed through the line to the measuring instrument.

Dilution

Two stages of dilutions were applied. The first one (point 2) was the hot dilution (160ºC) with nitrogen with a dilution ratio of 10:1 to avoid coagulation of particle and condensation of water. The second dilution (point 4), also known as vapour particle removal (VPR) as shown in Fig.3.10, involved three sub-stage dilutions which are hot dilution sub-stage, evaporation sub-stage and cold dilution sub-stage with a total dilution ratio of 160:1. The condition of each stage is shown in table 13. Combining two stages of dilutions, an overall dilution factor of 1600 was being incorporated into the result. The use of the VPR was to determine the non-volatile PM present in the particle emitted and also reduce the particle sample temperature to ambient temperature. Correction factors (penetration factors) of 0.66, 0.75, 0.77 and 0.82 for particle diameter ranges 3.11nm – 15nm, 16nm-30nm, 31nm-50nm and 51nm-499nm respectively were incorporated into the results to take into consideration of the particle loss through the vapour particle remover (VPR). The actual dilution ratios were checked by the CO_2 concentrations measured at the point 2, 5 and at the engine out.

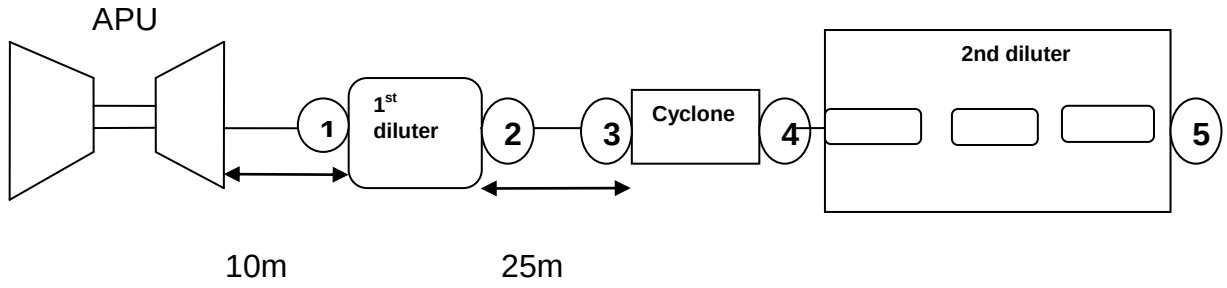

Figure 3.9: Schematic view of the sampling system set up

Table 13: First and second Dilution conditions

Conditions	Type of dilution	Dilutant	Dilutant temperature ºC	Dilution location from exhaust (meters)	Dilution ratio
First dilution	Hot dilution	Nitrogen gas	160	10	10
VPR Second and third dilutions	Hot and Cold dilution (2 stage dilutions)	Nitrogen gas	320 and 20	35	10x16

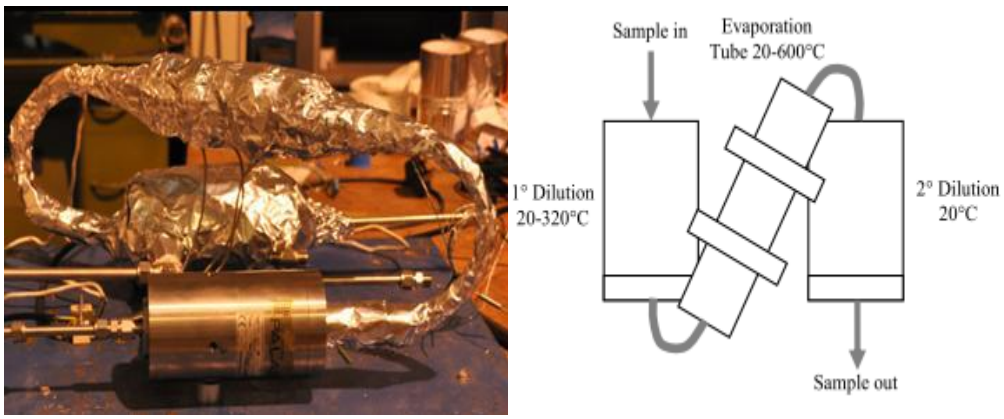

Figure 3.10: Vapor particle removal (VPR).

In the sampling system, the 25meters stainless steel line was used between first and second diluter to account line loss effect. Table 14 shows description of each point.

Table 14: Sampling test Points location.

Points Number	Location
Point 1	Upstream of the primary diluter (first dilution)
Point 2	downstream of the primary diluter(Dekati DI1000)
Point 3	After the 25m heated sample line
Point 4	After 1μm sharp cut point Cyclone
Point 5	After (VPR) – Second dilution

Catalytic stripper (CS)

A catalytic stripper (CS) was used to oxidize and remove volatile and semi-volatile particulate matter, typically organic carbon, which has been proved to have good removal efficiency[120]. Inorganic compounds such as sulphate are chemically absorbed the catalyst. This was done by passing the exhaust over the oxidation catalyst which was heated to 300°C. This method differs from other methods such as a thermal denuder that remove gas phase material via physical adsorption.

The catalytic stripper as shown in Fig.3.11 was connected to the sampling line at different sampling points (2, 3&5) and then connected to two SMPS instruments. So the non-volatile particles can be measured. The results were compared to the measurements without the CS fitted. The volatile particles can thus be determined. A line loss correction factor of 0.3 (30% loss cross the CS) were used and incorporated into the results. The CS flow rate was set to 1.5 L/min.

Figure 3.11: 1.5 L/min Catalytic Stripper (CS).

Particulate measurement instruments

Two scanning mobility particle sizers (SMPS) coupled with two CPCs (TSI Model 3025&3085) were employed to measure particle size distributions and mean particle diameter according to their mobility through an electric field. The first SMPS with nano-DMA for particle size range measurement of 3-51nm, while the second one with long-DMA was used for range 16-500nm. The sheath flow and sample flow are 15 L/m and 1.5 L/m respectively. The scan up time of 100 seconds and retrace time of 15 seconds were selected for SMPS. The high flow rate setting of the CPC at (1.5 L/m) was chosen.

3.1.2.3.2 Part II: Sampling System for Gaseous and PM emissions

Gaseous emission measurement

A stainless steel plate was fixed behind the APU exhaust so that the installed sampling probes would sit no further than half an exhaust diameter behind the engine exhaust plane as required per the Aerospace Recommended Practice. Three sample probes were mounted on the steel plate, two for PM measurement and the one for gaseous emission measurement. A schematic of the setup for the study is presented in Fig. 3.12.

The exhaust sample was extracted from the exit plane of the APU exhaust cone through a conditioned sampling probe, connected to a heated sample transfer line at 150ºC to avoid water vapour condensation and to minimize heavy hydrocarbon condensation when the samples reaches the analyzers. There was no dilution involved. This method eliminated the possible effect of plume age (dispersion) and dilution factors. The heated sample line spited between gaseous analysis suite and a smoke meter operated by Sheffield University. The gas analyses results were processed to provide air fuel ratio. The exhaust sample for FTIR was drawn at the same position as that for regulated gaseous emission analyzers by a heated sample line with its temperature being controlled at 180°C. The sample flow rate was 2-3 l/min. Major gaseous species (i.e., CO, CO_2, NOx) were quantified using a Gasmet CR-2000 Fourier Transform Infrared (FTIR)-based gas analyzer. The analyzer quantifies gas species concentrations by

measuring the absorption of an emitted infrared light source through the gas sample Standard gaseous were measured. However, UHC were measured using FID. FTIR was also used to measure volatile organic compounds (VOC) for each fuel at both conditions idle and full. Gaseous emissions and VOC results will be discussed later in chapter 7.

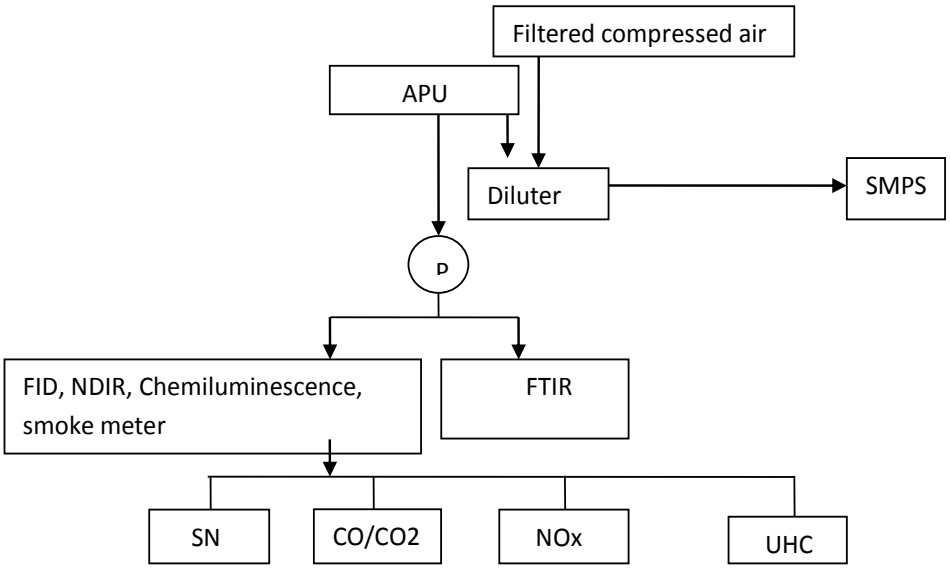

Figure 3.12: Schematic view of experimental set up.

Particulate sampling system

The exhaust sample was taken at the exit plane of the exhaust cone and immediately diluted by filtered dry compressed air using a fixed ratio (10:1) dilutor. The dilution at the probe tip prevented the condensation and agglomeration and gas to particle conversion in the sampling line as shown by some authors [121, 122]. Probe tip dilution is the most widely accepted dilution technique for sampling of turbine engine PM emissions. The particle inlet probe was designed to allow introduction of a concentric flow of dilution just downstream of the probe tip to eliminate the coagulation of particulates in the sample system. The filtered dry compressed was measured for particle concentration and size distribution as a background check. The particle concentrations in the filtered dry compressed air were found in a magnitude of hundred thousandth of exhaust gas particle concentrations. Therefore the compressed air had negligible interference to the exhaust particulate measurements. The exhaust samples for PM measurement were transported to a SMPS via 10 meter long, unheated, 5 mm diameter sample

line. Line losses were measured separately and applied for the results. More details about SMPS will be explained later. PM results will be discussed later in chapter 8.

During the test PM and gaseous emissions were sampled at an idle (no load) and full power (load). The APU was started with JetA1 and allowed to be stabilized for few minutes before it is switched to the testing fuels. The engine was set to run for approximately 6 minutes at idle (cold idle) then 6 minutes on full power before returning to idle again (hot idle). The cold idle condition were been considered to be the operational time of a the APU or the aircraft from the airport stand up until the aircraft reaches the runway for take-off, and the hot idle state were being considered to be the operational time at landing to taxi of the aircraft to the airport stand. This would help determine the effect and amount of particle emission at the various mode of operation.

3.1.3 Experimental set up impinging Jet Mix Flame Stabilizer

This is experimental set up for combustion and emissions of hydrogen fuel using impinging Jet mix flame stabilizer. The results will be discussed in chapter 9.

3.1.3.1 Jet Mix Flame Stabiliser

The Jet Mix flame stabiliser was developed by Andrews and co-workers [49, 50, 52, 123-133] as a means of stabilising premixed flames with the easy comparison with the same geometry with direct rapid fuel injection. It is shown in Fig.3.13 and consists of an air splitter that splits the combustion air into two jets, radial and axial and fuels the radial jet with a central fuel injector. Two radial flow proportions were investigated with 6% and 20% of the total air flow area in the radial jets. The 20% flow was achieved with 8 radial holes of 6.1 mm diameter and 8 axial holes of 12.4 mm diameter. For 6% radial flow, the radial jets were 3.2 mm diameter and the axial jets 12.3 mm diameter. The diameter of the radial hole outlet hub was 40mm and the axial holes were located midway between this hub and the combustor wall. The locally rich radial fuel jet can achieve mixing with the remaining air in two ways: direct impingement mixing with in-line jets and micro rich/lean mixing with offset jets [52]. Comparison with the original premixed results

[50] enabled the quality of the mixing in terms of NOx to be determined. The excellent fuel and air mixing qualities of two impinging jet with fuel in the radial jet was shown by Andrews and Abdul Hussain[50, 133] using a water flow visualisation test rig with the salt conductivity techniques as the fuel tracer. The Jet Mix system was developed to be capable of operating in a low NOx mode on liquid fuels using air assist atomisation in the jet impingement process and the excellent quality of the atomisation was demonstrated [125, 126, 128].

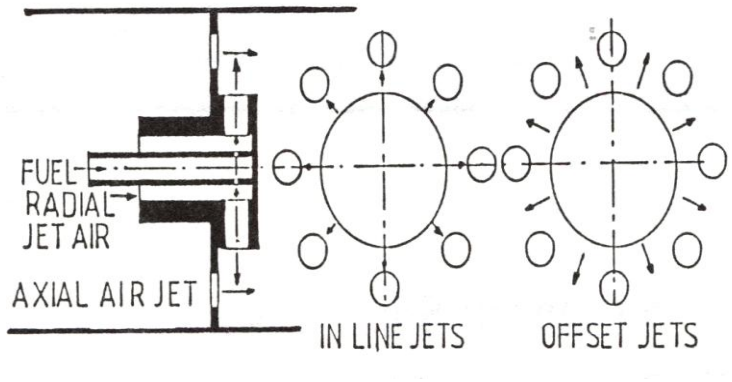

Figure 3.13: Jet mix Flame stabilizer [126]

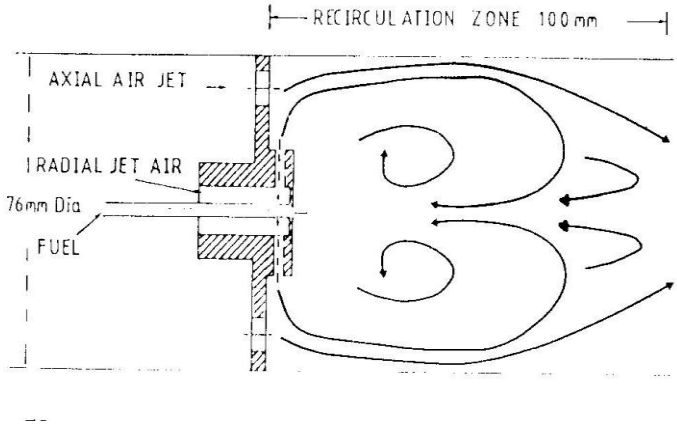

Figure 3.14 : Jet mix recirculation zone [125]

Water flow visualization was also used to determine the downstream aerodynamics, as shown in Fig.3.14 for in-line jets [125]. This shows a potential weakness of the design in that the mechanism used to form the two

air jets from one air supply involves a central 90° turn on for the radial air jets and this produces a central baffle or hub that is similar in effect to the central hubs used with axial and radial swirlers by some manufacturers. This recirculation zone aids flame stability in the same way as for swirl combustion, but it can also be a NOx limiter if the central zone burns hotter than the mean combustion due to mixing imperfections. Although the NOx emissions on propane and methane were very low with this Jet Mix design, as noted by Tacina[134], it was subsequently found to be not as low as could be achieved using radial and axial swirlers and the large central recirculation zone was a contributing factor to this as the radial rich jets did have a tendency to produce slightly rich regions here. This recirculation zone became larger if the Jet Mix flame stabiliser was simply scaled up for larger combustors and hence practical applications used many of these devices [135] which became a complex fuelling problem and also has some acoustic problems [135].

The radial air jet passage in Fig. 3.14 provides some preliminary fuel and air mixing as well as the initial atomisation air assistance for liquid fuels. The mixing rate between the fuel and air will depend on the pressure loss of the system as this governs the air jet velocities and the turbulent energy conveyed into the flow. The stability, combustion inefficiency and NOx emissions were affected by the proportion of primary zone air in the radial Jets, as shown in Fig.3.15. This shows that the inline Jets radial flows in the range 15-30% gave an extremely low NOx level of 10ppm at 15% oxygen with adequate combustion inefficiency [49].

In the present work the proportion of the radial jet air was of concern due to the ability of hydrogen to burn in the radial jet and possible stabilize inside the radial jet passages and burn out the flame stabilizer. This could not occur with hydrocarbon fuels as the air jet velocities were too high at 60 – 100m/s depending on the pressure loss. The radial jet flow is too high a velocity for hydrogen to flash back and the hydrogen and air are not mixed until turbulence is created in the downstream shear layer.

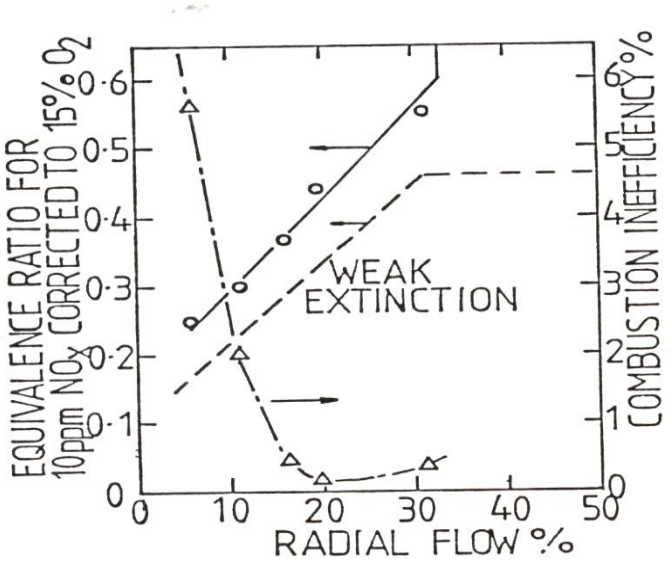

Figure 3.15: Equivalence ratio and combustion inefficiency at which 10ppm corrected NOx was achieved as a function of the % radial flow[123].

It was considered that the Jet Mix design could be safely operated on hydrogen without flash back into the radial jets. If the overall hydrogen equivalence ratio was 0.3 a 20% radial jet flow would produce locally Ø=1.5 in the radial jet and this is close to the maximum burning velocity of 3.5 m/s for hydrogen/air. However, acceleration by a factor of 20 by turbulence would be required for flash back into the radial jet.

However, the development of the flame downstream of the radial jet outlet in the axial jet shear layer would be rapid and faster for 20% radial jet air. This did prove to be a problem as the flame stabilizer operated hot on its front face with 20% radial air flow. The reduction of the radial air flow to 6% was investigated to reduce the temperature near the flame stabilizer. The radial jet at 0.3 overall equivalence ratio would have a very rich radial equivalence ratio of Ø= 5. Unfortunately, this is not the best configuration for low NOx emissions, as shown in Fig.3.15.

3.1.3.2 Rig Descriptions and Conditions

The atmospheric pressure test facility has been described previously [123-125, 136] and is shown in Fig.3.16. It consisted of a1.5m long 76mm diameter approach pipe, flame stabiliser, 330mm long 76mm diameter uncooled combustor, a 40 hole mean gas sampler which was water cooled, followed by entrainment of cooling air and then a bend in the exhaust pipe

with an observation window on the combustor centre line of a 90^0 bend. The air flow rate was measured by a Venturi then electrically heated to 600K. The 76mm combustor was a practical annular combustor depth and equivalent to a single burner test rig. The combustor was instrumented with wall static pressure tapping and thermocouples to measure the axial profiles of the temperature and static pressure which can be used to determine the recirculation zone size and heat release locations.

The Jet Mix combustor was operated at a very demanding condition equivalent to all the combustion air passing through the flame stabiliser and no air used for film cooling or dilution air. This is a reference Mach number of 0.05 for aero type gas turbines, on which many industrial gas turbine combustion systems are based. The actual Mach number was 0.047 in this work. The Jet Mix flame stabiliser was sized to have pressure loss at this high reference Mach number of 4.3%. This level of pressure loss is typical of practical industrial gas turbines. The main action of the flame stabiliser pressure loss is to produce turbulence for enhanced fuel and air mixing and for increasing the turbulent burning velocity to maintain a stable flame in the high velocity mainstream flow. However, turbulent enhancement of the burning velocity for hydrogen would not be as important as for propane. The main requirement of the pressure loss was to provide the turbulent energy to mix the radial hydrogen with the axial jet air. Providing turbulence to assist flame propagation was not a major priority for such a reactive mixture. For propane operation increasing the pressure loss has been shown to have benefits for NOx emissions[49, 123].

For the reasons given above M=0.05 is the flow condition that hydrogen gas turbine combustion should operate at as there is no need for dilution air for flame stability purposes and no film cooling air should be used as this makes the main combustion richer and hence increases the NOx [134]. For propane combustion this is a very demanding flow condition for complete combustion in the 330mm combustor length. For hydrogen with a much higher laminar burning velocity is should not be a significant problem.

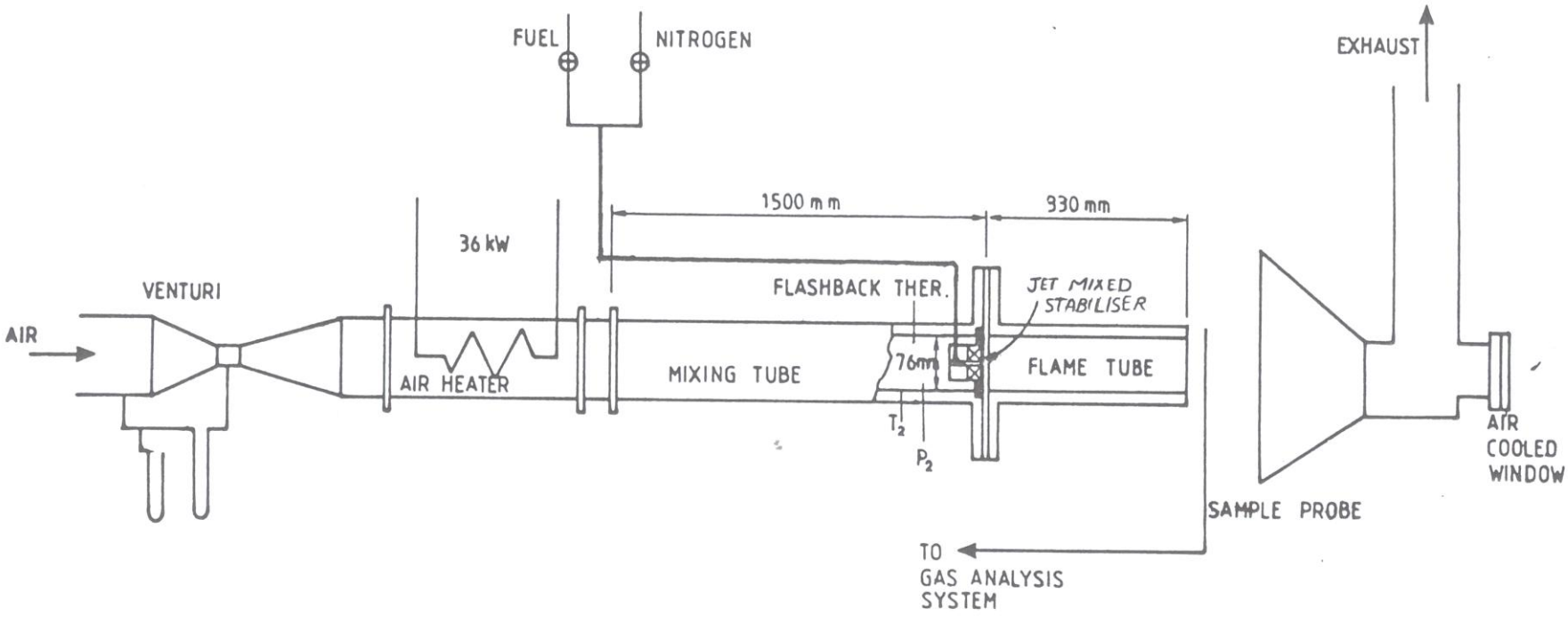

Figure 3.16: Schematic of the experimental rig[124].

3.1.3.3 Fuel supply and Injection

Two gaseous fuels were used in this work propane and hydrogen. The propane was injected directly and premixed mode, whereas, the hydrogen was not premixed due to the flashback risk and was directly injected at the flame stabiliser into the centreline of the radial jet and the NOx results have been compared at the same conditions. Propane was supplied from a bank of six liquefied propane cylinders. The hydrogen fuel was supplied from nine bottle interconnected array of high pressure hydrogen cylinders located outside the building.

3.1.3.4 Emissions Measurements

The mean gas sample was passed into a heated sample line and on through a heated filter and pump to a heated gas analysis system. NOx is reported on a wet gas basis. In addition to the usual analyser of Chemiluminescence for NOx a thermal conductivity hydrogen analyser was used. This had a 0-5% scale as was used to determine if any unburned hydrogen remained and hence was to determine if there was any combustion efficiency problem at the high combustor flow rate used and the short residence time. The results showed that the hydrogen was zero at nearly all test conditions and this shows that there was no hydrogen combustion efficiency problem. In contrast the comparator propane fuel had combustion efficiency problems as weak extinction was approached and this was determined through NDIR CO and FID UHC measurements.

The gas analysis results were processed to provide a computed air to fuel ratio, combustion efficiency, mean adiabatic flame temperature and corrected NOx emissions to 15%O_2, 600k inlet temperature was used to simulate high power industrial gas turbine operation.

3.2 Emissions Measurements Methodology

3.2.1 Aircrafts emissions Measurements Methodology

3.2.1.1 Gaseous emissions measurement

There are various methods being adapted to measure gaseous emissions includes: the International Civil Aviation Organization **(**ICAO)

methodology, the Environmental Protection Agency (EPA) methodology and probes sampling measurements. The ICAO and EPA based on some measured factors such as emission indices of each species, number of LTO cycle, emission factor, fuel flow and time in mode rate at every engine time of operation, number of engine used by aircraft type and type of the aircraft. Both methods can be used easily to measure CO, HC, SO_2, NOx and CO_2 species, however, high possibility of errors during the measurement can occur and provide not accurate results.

The use of probes is another method used in measuring of emission from the exhaust of an aircraft engine, the probe which is being fitted at the exhaust of the aircraft engine takes direct measurement of emission specie from the aircraft engine. The exhaust gas from the aircraft engine exit plane is cooled and connected to sample line for gas species measurements using gas analysis system or Fourier Transform Infrared (FTIR). In this study, gaseous emissions from APU burning alternative fuels were measured by FTIR.

3.2.1.2 Fourier Transform Infrared (FTIR)

The FTIR (Fourier Transform Infrared) spectrometer is a portable instrument that is capable of measuring 51 species including legislated CO, NOx, THC and CO_2 emissions as well as water, ammonia, N_2O, and many other hydrocarbon species.

A Gasmet CR-2000 Fourier Transform Infrared (FTIR) comprised an analyzer, heated sample lines, a portable sampling unit (filtering and controlling sample flow), and a laptop. it weighed approximately 30kg. The FTIR analyzer has a 2 meters sample cell with a sample flow rate of 2~3 l/min. It is capable of measuring concentration as low as 3~5ppm with 2% accuracy measurement range. The exhaust sample was drawn at the same position as that for regulated emission analyzers by a heated sample line with its temperature being controlled at 180°C to avoid condensation as the FTIR measurements are wet measurements. The FTIR is capable of measuring concentrations as low as 0.5~3 ppm, depending on the application. The FTIR measured both legislated emissions (CO, NOx, THC and CO_2) and selected non-legislated emissions (ammonia and speciated VOCs and nitrogen oxides) during the evaluation trials.

The Temet FTIR is an instrument uses Fourier Transform Infrared spectroscopy to measure gaseous emissions. Fourier Transform Infrared spectroscopy (FTIR) was development in early 1970s to provide a good way for monitoring trace pollutants in ambient air. This technique offered a number of advantages over conventional infrared systems, including sensitivity, speed and improved data processing. However, the main drawback of using the traditional infrared spectroscopy is the limitation of measurement of low concentration due to three reasons. First is the significant presence of water vapor, CO_2 and methane, which strongly absorb in many regions of the infrared (IR) spectrum. Consequently, the spectral regions that can easily be used to search for pollutants are limited to 760-1300cm -1, 2000-2230 cm -1, and 2390-3000 cm -1. Secondly, the sensitivity is not enough to detect very small concentrations in the sub-ppm level. Thirdly, spectral analysis was difficult since subtraction of background spectra had to be carried out manually[117].

The basic components of an FTIR are shown schematically in Fig.3.17. The infrared source emits a broad band of different wavelength of infrared radiation(IR). The IR source used in the Temet GASMET FTIR CR-series is a SiC ceramic at a temperature of 1550 K. The IR radiation goes through an interferometer that modulates the infrared radiation. The interferometer performs an optical inverse Fourier transform on the entering IR radiation. The modulated IR beam passes through the gas sample where it is absorbed to various extents at different wavelengths by the various molecules present. Finally the intensity of the IR beam is detected by a detector, which is a liquid-nitrogen cooled MCT (Mercury-Cadmium-Telluride) detector in the case of the Temet GASMET FTIR CR-series. The detected signal is digitized and Fourier transformed by the computer to get the IR spectrum of the sample gas.

Figure 3.17: Basic components of FTIR

However, regulated and unregulated emissions from Axially Power Unit (APU) are measured by FTIR, whereas, it was used to measure aldehydes

emissions from low NOx Burner using biodiesel and its blend with kerosene. Daham et al compared measured total hydrocarbon emissions using FID and FTIR and they concluded that the FTIR tended to underestimate THCs by compared to FID[137]. Therefore, the main objectives of using FTIR in this study is to get specified hydrocarbon information, including alkenes, aromatic hydrocarbon, and aldehydes.

3.2.1.3 Particulate matter (PM) Emissions Measurement

Particulate matter (PM) emissions from aircraft engines are of major environmental concern due their impact on global climate change, local air quality and human health. The PM generated from aircraft gas turbine engines can be classified into two major components; non-volatile (soot) and volatile PM. Non-volatile PM (or soot) is produced in the combustor and is present at engine exit temperature and pressure whereas volatile PM is formed in the near-field plume downstream of the engine through the gas-to-particle conversion of sulfur and organic gases [138-141]. The PM emissions generated by aircraft engines are nano-particles ranging in size from 5nm up to 100nm [37, 141, 142], contain a variety of toxic air pollutants, and are carbonaceous in nature.

Large number of very small particles generated from gas turbine engines has great impact on both human health and global climate. However, mass and number of PM should be considered when aviation PM emissions evaluated. Measurement methodology of particulate from aircrafts exhaust can be divided into two sections: sampling system and measurement instruments.

Sample probes and transport are the two critical aspects of the sampling system. Probes should be designed to minimize particle losses and agglomeration and suitable for all conditions. The selection of instruments is based on their availability, reliability, easy to use and the price.

Moreover, first Order Approximation (FOA) is being used to measure PM mass, it based on smoke number measurements.FOA is used to estimate particulate emission (PM); the volatile and non-volatile emission from certified commercial aircraft engines. The FOA v1.0 and FOA v2.0

method are estimate the total mass of the particulate based on aero engine smoke number (SN)[37, 38, 143, 144].

FOA v1.0 is used for measuring of non-volatile (black carbon or smoke) and the Smoke Number (SN) and fuel flow (FF) has to be determined for specific aircraft engine type at specific operation mode. Smoke number and fuel flow data can be obtain from ICAO 1992 databank to estimate the total mass of the particulate using Equation (10).

$$\mathbf{EI\ (mg/Kg) = 0.6(SN)^{1.8} * (FF)} \qquad \mathbf{(10)}$$

SN: the ICAO smoke number
FF: the ICAO fuel flow by mode in Kg/s

FOA v2.0 is a higher measurement version of FOA v1.0 which takes into account of volatile particulate emission and was developed in 2005. The measurement process also depends on the Smoke number and fuel flow of an aircraft engine type at specific operation mode (takeoff, climb, approach and taxi/idle), which can be obtained from the ICA0 emission databank.

$$\mathbf{EI\ (mg/Kg) = 2.4(SN)^{1.8} * (FF)} \qquad \mathbf{(11)}$$

SN: the ICAO smoke number
FF: the ICAO fuel flow by mode in Kg/s

The drawback of FOA v2.0 methodology does not express the major component of non-volatile and volatile of aircraft PM emissions. In 2007 it has been developed to include all components of PM to give accurate results and named as FOA v3.0. The components of volatile PM include fuel sulphur content; organics form unburned fuel and organics from lubrication oil[143, 144].

$$\mathbf{EI_{total} = EI_{vols} + EI_{nvols}} \qquad \mathbf{(12)}$$

EI_{vols}= sum of the components (Sulphates+ Fuel Organics + Lubrication oil Organics)

However, the FOA methodology based on smoke number measurements and do not provide the PM number and size of the PM which is required to assess the environmental effects of the PM emissions. There are several equipments of measuring particle numbers and their size distributions using

probe sampling technique include Scanning Mobility Particle Sizer (SMPS), Electrical Low Pressure Impactor (ELPI) and Differential Mobility Analyzer (DMS) etc. Each of these instruments has its features based on its measurements technique. It is believed that the time resolution; accuracy and size resolution are key parameters in the measurement of particle size distributions[141, 145]. SMPS as one of the commonly used methods [39], it was used to measure particulate number and mass and their distribution from both Low NOx gas turbine combustor and APU. Condensation Particle counter (CPC) is used for number count. Numerous studies from NASA, MS&T, and UTRC have shown that intra-instrument comparisons were in good agreements[142].

3.2.1.4 Scanning Mobility Particle Sizer (SMPS)

SMPS‘s are majorly been used in the measurement of aerosols size distribution over a range of sizes; 5nm to 1000nm, and are always been used together with condensation particle counter (CPC) which are both been connected individual to a computer to display the measured results using special software for easy interpretation. SMPS can be used in a wide range of application ranging from nano-particle measurement, atmospheric research, emission pollutant level research, condensation research, engine exhaust emissions, aerosol dynamic, to combustion research. A Electrostatic Classifier is also being used alongside the SMPS to classifier the particles into various sizes diameter of measurement before being scanned by the SMPS[146].

The selection of particle size measurement range in an electrostatic classifier is determined by the type of Differential Mobility Analyzer (DMA) been used; a TSI long-DMA and nano-DMA gives a particle size range of 10-1000nm and 4-160nm respectively as shown in Fig.3.19&3.20. the size selection mode of operation involves the electrical force balance in an electric field based on the particle net charge and drag force which is been experienced by the particle in the classifier.

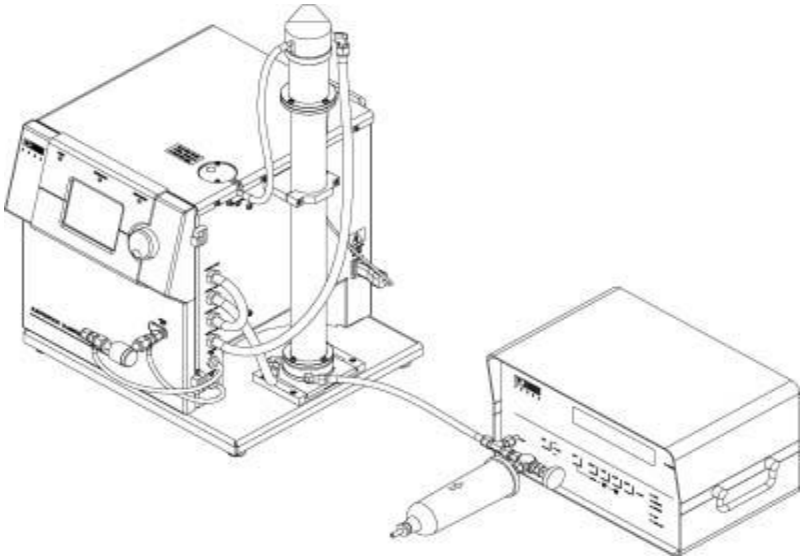

Figure 3.18: Model 3025 CPC with long-DMA[146]

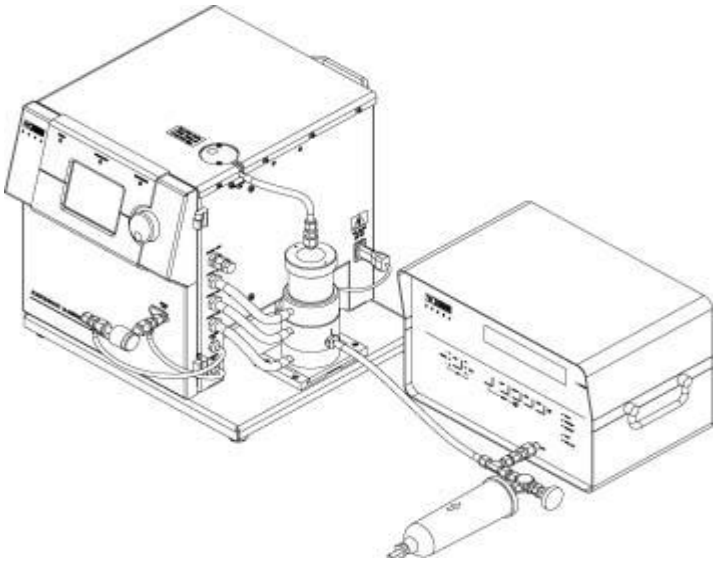

Figure 3.19: Model 3025 CPC with Nano-DMA[146]

The most important factor to be considered in the operation of the SMPS system in particle classification is the ratio of the sheath air flow rate and aerosol flow rate in the electrostatic classifier to be 10:1 which is mostly being achieved by ensuring that the excess flow rate, sheath flow rate, monodisperse and polydisperse flow rate are all equal. A bypass flow is been used in a nano-DMA to reduce the diffusion loss occurring in small particles through the DMA classifier. The bypass flow and sheath flow are been connected into one flow through the long-DMA or nano- DMA to increase the flow to attain a maximum flow of 15.1pm. The sheath flow rate

influences the particle size sample measurement, with low flow rate used for large particle size measurement and high flow rate for high sheath flow rate for small particle size measurement. The sample flow rate was set to be 0.41L/m.

A SMPS system with a Nano-Differential Mobility Analyzer (NDMA) was used to determine the number concentration and size distribution of aerosols in the size range from 5 nm to 160 nm. The SMPS is based on the principal of the mobility of a charged particle in an electric field (particle charger). The sample is sucked into the system and passed through an inertial impactor to remove the larger particles and then enter the NDMA to differentiate particles according to their electrical mobility, with only particles of a narrow range of mobility exiting through and counted with a Model 3025 Condensation Particle Counter (CPC). The entire system is automated. Data analysis is performed using a computer system with customized software[146].

3.2.1.5 Smoke Number Measurment (SN)

Smoke number was determined using a Richard Oliver smoke meter, Whatman (no. 4) filter paper and a reflecto-meter (BOSCH ETD 02050). The principle of the method is to measure the change in the absolute reflectance of the filter paper before and after the collection of PM on the filter paper by passing a set volume of sample (9.2cm^3 of exhaust) through the conditioned filter paper (Fig3.20). The smoke number measurement procedure involved inserting a piece of filter paper into the pre-conditioned sampling block of the Richard Oliver smoke meter. Once on condition, the user activated a solenoid which directed the exhaust sample through the conditioned sampling block. After sufficient volume had been sampled, the unit automatically returned to bypass mode and the filter was removed and its reflectance value measured. Three measurements were taken for each testing condition and average values were used.

Smoke numbers (SN) were measured for each engine setting for operation on JetA1 and the all alternative fuels and fuel blends. A minimum of three measurements were performed at each engine/fuel condition. For the measurement, raw exhaust samples (total of ~7.1 litres) were transferred via heated lines (150°C) to a smoke sampler where the smoke (carbon) sample was collected on a paper filter. Post-test analysis of each filter was

performed using a reflectometer to compare the opacity between a clean and stained filter. Excellent data reproducibility was observed for most multiple runs for each engine/fuel condition (<±5%).

Figure 3.20: Engine smoke measurement.

3.3 Emissions Calculation

3.3.1 Calculation of Air mass flow

Air mass flow was calculated using basic equation of the mass rate flow. From the Mach number definition

$$M=\frac{V}{a}=\frac{V}{\sqrt{\gamma RT}} \quad \text{..... (13)}$$

$$V=M*\sqrt{\gamma RT} \quad \text{(m/s)} \quad \text{..... (14)}$$

From continuity

$$\dot{m}=\rho*A*V \quad \text{(Kg/s)} \quad \text{..... (15)}$$

Where

M = Mach number, both Much number are used 0.017&0.023

γ = Ratio of specific heat, for air =1.4

$\dot{m}$ = Mass flow rate (Kg/sec)

A =Area (m^2).

V = Air velocity and sometimes referred as reference velocity (m/sec).

R = Gas constant, for air 287.04.

T =Inlet temperature (^oK).

a= speed of sound, a= $\sqrt{\gamma RT}$.

ρ = Density and for the air =1.29Kg/m^3

Equation (15) was used to calculate the air mass flow given the Mach number, air inlet temperature (K) and indicated flow rate in (Kg/sec).

3.3.2 Fuel flow calculation

Fuel flow calculations are performed for both gaseous (natural gas) and liquid fuel (kerosene and biodiesel).

For gaseous fuels all the rotameters were calibrated for natural gas by the manufacturer. Whereas, liquid fuel rotameters were calibrated for kerosene by the manufacturer. The rotameters had to be re-calibrated in order to get the actual fuel flow rate for biodiesel and biodiesel blend. This was done experimentally by allowing a quantity of B100, B50 and B20 to pass through the rotameters and measuring the indicated fuel flow rate, and also measuring the actual fuel flow rate at the fuel injection point. Every time the indicated flow rate given, the actual fuel flow rate was calculated using the equations. The following equations were used to correct the fuel flow rate for B100, B50 and B20 respectively.

Y= 0.5372X-0.0758 (16)

Y= 0.8117X-0.0596 (17)

Y=0.9564X-0.0455 (18)

All fuel flow rate measured in (L/min) and converted to m^3/sec. However, the mass flow rate for each fuel expressed as Kg/sec using the density of each fuel presented in table 8.

3.3.3 Equivalence ratio calculation

The actual air/ fuel ratio was obtained by two ways: actual measurements of air flow and fuel flow and calculated by carbon balance from the exhaust gas analysis. The Stoichiometric air/ fuel ratio for each fuel was calculated based on fuel compositions as shown in table 8.

The equivalence ratio (Φ) is defined as the stoichiomerttic air/ fuel ratio divided by the actual air/fuel ratio.

$$\textbf{Equivalence Ratio (}\Phi\textbf{)} = \frac{AFRS}{AFR} \qquad \textbf{(19)}$$

The air to fuel ratio can be calculated using the ratio of the measured air entrainment to the mass loss rate using the following equation:

$$\textit{Mass AFR} = \left(\frac{\text{Air entrained (kg/hr)} / 3.6}{\text{fuel mass loss rate (g/s)}} \right)$$

However, this method assumes that all the air entrained is used by the fire which gives misleading fire air to fuel ratio. As a result, Chan's AFR method, which is an advanced way of calculating a more accurate air to fuel ratio, was considered. Chan's AFR equation determines the air to fuel ratio based upon gas emission analysis as an alternative to the conventional direct air to fuel flow rate measurements. Carbon monoxide, carbon dioxide, oxygen and hydrocarbons are adequate for obtaining an accurate air to fuel ratio for the Chan's AFR equation.

A general formula for the composition of the fuel can be represented as $C_\alpha H_\beta O_\gamma N_\delta S_\varepsilon$

$$A/F_{Chan} = \frac{138}{12.011\alpha + 1.008\beta + 15.999\gamma + 14.007\delta} \times \frac{A_1\beta - A_2 + 2\alpha A_3 A_4 - 2\gamma(A_1 + A_5)}{2(A_1 + A_5)(2.0028) - 0.0014 \times 2A_3 A_4}$$

Where $$K = \exp\left[2.743 - \frac{1.761}{0.01T_{eq}} - \frac{1.611}{(0.01T_{eq})^2} + \frac{0.2083}{(0.01T_{eq})^3}\right]$$

T_{eq} = Equilibrium Temperature

K value of 3.5 was considered

$$A_1 = [CO] + [CO_2] + [HC]$$

$$A_2 = x[HC]$$

X = Ratio of Elemental Hydrogen to Elemental Carbon, an X value of 1 was considered

$$A_3 = [CO] + 2[CO_2] + 2[O_2] + [NO] + [NO_2]$$

$$A_4 = 1 + [CO]/([CO_2][K])$$

$$A_5 = [CO]/([CO_2][K])$$

The sotichiometric air to fuel ratio was calculated as in the following:

General formula for a CHO combustion = $C_\alpha H_\beta O_\gamma$

This would normally be expressed in terms of H/C and O/C ratios using y= H/C and z=O/C as CH_yO_z

$$CH_yO_z + a\ O_2 = b\ CO_2 + c\ H_2O$$

This is in volume units (molar balance)

Carbon balance gives 1 = b; Hydrogen balance gives y = 2c

Oxygen balance gives z + 2a = 2b + c = 2 +y/2

Thus a = [(2 + y/2) – z] / 2

The stoichiometric Air/Fuel= [(1 + y/4) – z/2] 137.94 / (12 + y + 16z).

Both methods were calculated and compared and the differences were about <18% as shown in table 15.

Table 15: comparisons of measured and calculated equivalence ratio.

Fuel	calculated	measured	diffrences
	Φ	Φ	%
	0.45	0.51	-14.61
K	0.49	0.55	-12.21
	0.62	0.71	-14.63
	0.67	0.77	-14.76
	0.40	0.47	-17.54
WME	0.42	0.45	-8.10
	0.48	0.49	-1.85
	0.49	0.57	-16.89
	0.44	0.49	-11.80
NG	0.49	0.53	-6.83
	0.55	0.59	-6.49
	0.60	0.68	-12.50

3.3.4 Emissions correction

All emissions were corrected to 15% oxygen using the formula recommended by the Environmental Protection Agency. The 15% oxygen in the exhaust represents typical conditions of full power stationary gas turbines of the 1970s era.

$$NOx_c = NOx_{obs} * \frac{5.9}{20.9 - O_2\%actual} \quad (20)$$

Where

NOx_c = corrected NOx to 15% (ppm)

NOx_{obs} = measured NOx (ppm)

O_2 = oxygen concentration in the exhaust gases %

This equation was used also for CO &UHC.

3.3.5 Mass Emission Calculation

The gaseous emissions measurements were on a volumetric basis. These were converted into a mass basis using the conventional method for the computation of emissions index (EI: g/Kg fuel).

$$EI=K*C*(1+A/F)*1000 \quad \text{(EI: g/Kg fuel)} \qquad (21)$$

Where

- K is conversion coefficient, which is the ratio of molecular weight of a certain emissions component to the molecular weight of the whole sample gas. The molecular weight of the exhaust sample gas is close to that of air and does not vary more than 1% for H/C ratios of about 2 irrespective to air/fuel ratio. For this reason, K is a constant per component.
- C is concentration of the monitored species, ppm or %. The equation has to be multiplied by10^{-6} (ppm) or 10^{-2} (%) respectively.
- A/F is the air/fuel ratio on a mass basis determined by wet based carbon balance or measured directly using lambda sensor.

For transient and total test cycle measurements, the EI was converted into emission units of g/sec using fuel consumptions. The fuel consumption could be measured directly using fuel consumption measurement system or by carbon balance method.

3.3.6 Combustion efficiency

Combustion inefficiency is calculated due to the inefficiency of unburned hydrocarbon and carbon monoxide measured at the combustor exit.

$$\eta = 1-\eta_{HC\ ineff} - \eta_{COineff} \qquad (22)$$

$$\eta = 1 - \frac{M_{HC} * MWT_{HC} * CV_{HC}}{CV_f}(1 + AFR) - \frac{M_{CO} * MWT_{CO} * CV_{CO}}{CV_f}(1 + AFR)$$

$CV_{CO=}$10.1 MJ/Kg

$CV_{CH4=}$ 50 MJ/Kg

$MW_{CO=}$28

MW_{HC}=16

3.3.7 Flame temperatures

The adiabatic flame temperatures for all fuels were calculated using the GASEQ developed by Morley[147] and the results will be discussed later. This method fixed a set of reaction products at a constant pressure to minimize the Gibbs free energy of the mixture. The software requires the information of reactants such as elemental mass composition and heating values of liquid fuels and the species of combustion products, which were N_2, H_2O, CO_2, CO, O_2, OH, H, O, H_2 and NO.

3.3.8 Estimation of OFP (Ozone Formation Potential)

The ozone control strategy requires some quantitative methods to determine the tendency of ozone formation for a particular substance. The use of incremental reactivity is an appropriate reactivity ranking scheme. The incremental reactivity (IR) of an organic compound is defined as the amount of ozone produced per unit mass of VOC added to an organic mixture, or:

IRi = ΔO3/ΔVOCi gO3/gVOCi

The maximum incremental reactivity (MIR) is the primary reactivity scale used in VOC control regulations for gasoline vehicles and aerosol coating in California [148, 149]and is developed using a box model. For the MIR box model calculation, NOx level is adjusted to result in the highest incremental reactivity. MIR conditions are likely to occur in VOC-limited urban air masses, where the mixture is most sensitive to organic compounds because of low VOC-to-NOx ratios. MIR represented the maximum possible ozone formation tendency under the optimum condition. The EI of OFP for a particular VOC is calculated by the following equation:

EI (OFPi) = MIRi*EI_{VOCi} gO_3/kgfuel (23)

Where EIVOCi is the EI of VOCi in g/kgfuel.

Reactivates by definition are the sensitivity of ozone concentrations to the mass of individual organic compounds added to the system, and therefore, different sensitivity analysis techniques can be applied for their assessment.

The EU environmental law requires 31 individual OFP precursor VOCs and NMHC (Non-Methane Hydrocarbon) to be measured[150]. Formaldehyde is listed as recognition of its significance in OFP, in which MIR of formaldehyde is 8.96gO_3/gVOC. The contribution of formaldehyde emissions to OFP will be discussed in chapter 4.

3.3.9 Emissions Index(EI)

Number based emissions index (EI n) is the number of particles per kilogram fuel burned and the following equation can be used to calculate it:

$$\mathbf{EI\ n = EI_{CO2} \times (N_0 / M\ (CO_2) \times 10^6} \qquad \mathbf{(24)}$$

EIn: The number of particles per kg fuel burned, P/kg-fuel

EI_{CO2}: mass emissions index of CO_2, 3160g/kg for JetA1.

$N_{0:}$ the number of the particles per unit of volume of exhaust sample, P/cm^3

M ($CO_{2)}$: mass of CO_2 per volume of exhaust samples, kg/m^3.

M (CO_2)=Cco_2 x (44/29)x ρ_{air},

$CO_{2:}$ is the CO_2 concentration, %.

$\rho_{air:}$ is the density of air, 1.2kg/m^3.

44 and 29 are the molar mass of CO_2 and air respectively.

Chapter 4 : Gaseous and Particulate Emissions of Biodiesel and its Blends with Kerosene in a Low NOx Gas Turbine Combustor

4.1 Introduction

Increasing oil prices, issues with security of supply, and concerns over climate change have accelerated the research and development of alternative energy sources such as biofuels, solar and wind energy [110, 151]. Biofuels derived from agriculture products have renewable CO_2 emissions and are allowed to be discounted in carbon audits in most countries. There are also fiscal incentives to use biofuels in many countries that reduce the cost of electricity to the user. One of the main drawbacks of biodiesel is the cost and sustainability. The use of waste cooking oils is one way to reduce the cost of biodiesel and utilize to waste cooking oil for better sustainability[152]. Blending of biofuels such as biodiesel and bioethanol with petroleum derived fuel has become more and more popular practice due to the need to reduce CO_2 emissions and concern over depleting oil reserves in road transport. EU directive 2003/30/EC launched a scheme to promote the use of biofuels in transport[153]. European fuel quality standards allow a B5 mix; i.e. 5% biodiesel, to be mixed with petroleum diesel without invalidating manufacturers warranties.

The application of biodiesel in gas turbine engines has been developing and yet still much less extensive as in the diesel engines. There has been some work reporting the biodiesel tests on the small and micro gas turbine engines[154-156] and heavy duty gas turbine engines[157, 158]. They found that the NOx emissions from biodiesel were in a comparable level and engine cold start could be an issue.

Liu et al[110] reported a biodiesel testing program on industrial gas turbines that the pure biodiesel (B100) derived from waste cooking oil was tested on the atmospheric and pressure testing rigs in the SGT-100 DLE combustion system to investigate ignition, emission and combustion dynamics using. They found that the biodiesel was easier to ignite at high air mass flow rates and harder at lower flow rates and the lean extinction limits had similar trend as well. The emissions results from pressure rig they

derived showed that biodiesel had lower NOx and CO emission than diesel and comparable UHC emissions with diesel.

The work in this chapter investigated the comparison of the emissions between a waste cooking oil derived methyl ester (WME) and kerosene using a radial swirler industrial low NOx gas turbine combustor under atmospheric pressure and 600K preheated air. More details about the rig, conditions and flame stabilizer are mentioned in 3.1.1 in chapter 3. The pure WME (B100) and its blends with kerosene B20 (20% Biodiesel: 80% Kerosene), B50 (50% Biodiesel: 50% Kerosene) and pure kerosene were tested for lean extinction limits, particulate matter and gaseous emissions as a function of equivalence ratio.

4.2 Results and Discussion

4.2.1 Influence of biofuels injection location

Initially it had been intended that WME would burn satisfactorily with vane passage fuel injection. This was attempted with central ignition of natural gas, but no cross light could be achieved and no flame could be stabilized on WME with this fuel injection location. The other fuel injection location that had demonstrated low NOx with natural gas was at the outlet throat wall. This was also investigated and again no cross light from a central natural gas flame could be achieved. Thus, the two positions for fuel injection that gave low NOx with gaseous fuels would not stabilize a flame with WME as shown in Fig.3.5 in chapter 3. Kerosene could be burned satisfactorily with low NOx when injected at these locations [55]. The reason for this was that the air inlet temperature of 600K was too low to vaporize the fuel, whereas with kerosene the much lower distillation range led to easy vaporization.

The only fuel injection location where WME flames could be stabilized was the central injector shown in Fig.3.5 in chapter 3. This had been shown in early work with radial swirlers, with no downstream outlet throat and a small depth radial swirler to have very low NOx characteristics on kerosene[55, 73]. However, the addition of the discharge throat in the present work did not perform as expected and the fuel and air mixing was not as good as without the throat and the NOx was higher for kerosene. The

reason is thought to be that the mixing occurs in the downstream shear zone in the expansion flow as shown earlier. The addition of the throat makes the central fuel injector remote from the shear layer mixing region. For WME negligible vaporization will occur in the exit throat at 600K. The main fuel vaporization route is through central recirculation of hot burned gases that recirculate back to the head of the radial swirler, where the liquid fuel is injected. This was why B100 WME could be burned without natural gas assistance, whereas for vane passage or outlet wall fuel injection no flame could stabilize, as there was no hot gas recirculation in these regions.

4.2.2 Weak Extinction

The weak extinction was determined at 600K and both Mach numbers 0.017&0.023 by igniting the flame with natural gas outlet throat wall injection and then turning off the natural gas once the combustor was hot. The fuel flow to the central injector was then gradually reduced at constant air flow until no flame was observed through the air cooled observation window mounted on the centre line of the combustor in a 90^{o} bend in the exhaust. The weak extinction was also accompanied by a sudden increase in hydrocarbon emissions. Table16 presents the weak extinction limits for all fuels that have been tested at M=0.017 and compared with the results of 0.023.

Biodiesel demonstrated lower lean extinction limit due to the oxygen content in the fuel. There was a considerable drop between B20 and B50, indicating that the mixing ratio of biodiesel to kerosene between 20 and 50 had a significant impact on lean extinction limit.

Each fuel was tested to the lowest equivalent ratio (leanest) that could maintain a stable flame and to the highest equivalent ratio (richest) that acoustic noise became unbearable. For B100 case, the upper end (richest mixture) was constrained by the appearing of a large amount of white smoke from around the flanges of the combustor due to the evaporation of unburnt biodiesel. This indicated that the low volatility of biodiesel, compared to kerosene, caused serious problems on fuel vaporisation and atomisation.

Table 16: Weak extinction limit for kerosene and WME and their blends at Mach numbers of 0.017& 0.023, inlet temperature 600K, 1 atm.

	Weak extinction (Ø)		Maximum phi at onset of acoustic resonance		Maximum Phi at white smoke	
Mach No.	0.017	0.023	0.017	0.023	0.017	0.023
Kerosene	0.46	0.62	0.66	0.93	….	…
B20	0.44	0.56	….	…	0.76	0.79
B50	0.36	0.47	….	….	0.5	0.66
B100	0.35	0.28	…	…	0.5	0.49

The weak extinction results in table 16 were unexpected, as WME B100 and its blends with kerosene were more stable than for kerosene alone at both Mach numbers. This could be due to worse mixing with WME, due to the longer vaporization period. This would aid flame stability, but at the expense of the increased NOx that is shown later. The influence of Mach number was also not expected, particularly the large reduction in the kerosene weak extinction at the higher Mach number and in contrast the significant improvement in B100 WME weak extinction. The B100 results indicate deterioration in mixing, in spite of the lower SMD at the higher Mach number. Improved atomization should result in better mixing but the B100 results do not behave as expected.

The deterioration in the weak extinction for kerosene at the higher Mach number is also difficult to explain as a weak extinction closer to the fundamental flammability limit is expected and this is Φ= 0.4, close to the weak extinction at the lower Mach number. It is considered that the central fuel injection with a large radial swirler vane passage depth, coupled with a relatively long exit throat, results in the fuel placement resulting in the shear layer high turbulence regions not being the main stabilization zone. The flame may stabilizer further upstream in the throat where velocities are higher and flame stability lower.

Also shown in table 16 is the practical phenomenon of white smoke. Although the combustion was enclosed, it was an atmospheric pressure test and at a particular equivalence ratio white smoke started to leak from the joints in the test rig and fills the room. Operating at richer mixtures was then

unsafe and the combustor had to be shut down. This is why there is only few data for B100 at very lean mixtures. A further feature of low NOx combustion is the onset of acoustic resonance. This can limit the Φ that can be operated as acoustic resonance cannot be tolerated in the test facility. There was no problem with acoustic resonance with WME blends but there was with kerosene. At the lower Mach number, the onset of acoustic resonance was at Φ=0.66, close to the desired operating range. However, at the higher Mach number acoustic resonance was not reached until Φ=0.93. Resonance is a coincidence of chemical and acoustic time constants in the combustor. Changing the Mach number increases the flow velocities and creates more turbulence and these changes the chemical time constant. This then enabled much richer mixtures to be operated without resonance.

4.2.3 Emissions from Liquid fuels at Mach number 0.017

Fig.4.1 to 4.6 show the emissions as a function of equivalence ratio for pure biodiesel (B100), kerosene and two blends (B20 and B50) at Mach number 0.017 with an air inlet temperature of 600K. The lower end of the curve represented the minimum equivalence ratio that the flame could be stabilized for each fuel. The high end of the curve represented a condition at which either the acoustic level or smoke or CO emissions were very high and considered intolerable beyond the point.

The upper limit for fuel/air richness in terms of equivalence ratio for B50 and B100 was at around 0.5. The richer fuel air mixture beyond this point caused heavy smoke around the combustor, indicating a fuel vaporization problem. The visual inspection of the combustor after disassembling had proved the existence of a considerable amount of unburned fuel. The kerosene and B20 had been tested with wider ranges of equivalence ratio than B50 and B100 because there were no such smoke problems and the tests had been carried out until the acoustic level and CO emissions were very high, where the equivalence ratio reached 0.65 for kerosene and 0.75 for B20.

4.2.3.1 CO emissions and UHC emissions

The CO emissions as function of equivalence ratio for biodiesel, kerosene and blends at Mach number 0.017 and air inlet temperature 600 K

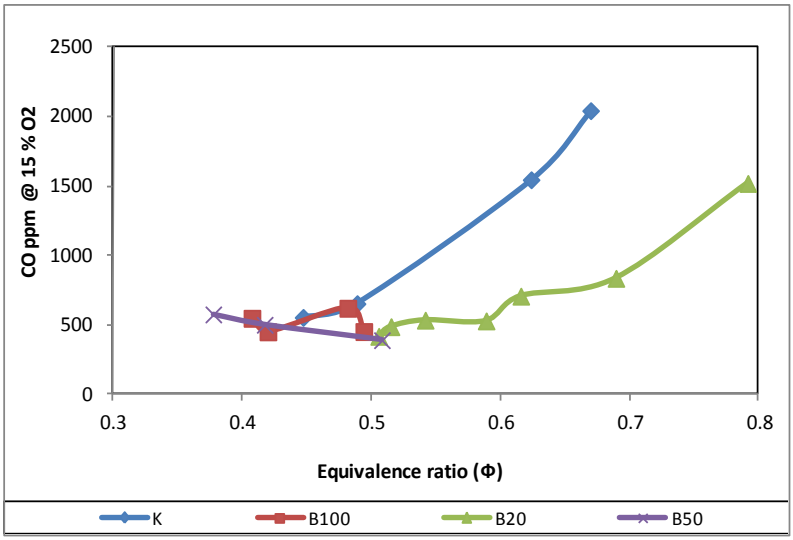

Figure 4.1: CO emissions as a function of equivalence ratio for pure biodiesel, its blends and kerosene.

were presented in Fig.4.1. The tendency of CO formation is due to incomplete combustion which may correspond to low flame temperature and insufficient time. The results showed that as the percentage of biodiesel increased, CO emissions decreased. The B100, B50 and kerosene had the same level of CO emissions at the equivalence ratio of ~0.4. However, the B50 had the lowest CO emissions overall. By the comparison of B20 with kerosene, it can be seen that the CO emissions were at the same level at Ø=0.4 for both fuels and started to increase at different gradients as the equivalence ratio increases. The ratio of increase in CO for kerosene was approximately twice as much as that for B20, indicating the effect of oxygen in biodiesel on CO emissions reductions.

Fig.4.2 shows the UHC emissions as a function of equivalence ratio for pure biodiesel, kerosene and blends at Mach number 0.017 and air inlet temperature 600K. The UHC emissions were reduced as the fuel air mixture became richer. This is due to that the flame temperatures were increased as the equivalence ratio increased. For kerosene the equivalence ratio had to be in the range of large than 0.6 to get a large fall in UHC emissions, which were comparable to biodiesel and blends and this was corresponding to that the flame temperature reached 1600K or above. B20, B50 and B100 much lower maximum UHC emissions at lower equivalence ratio ranges (lean) even the flame temperatures were lower than kerosene. Almost no UHC emissions were observed if the fuel air mixture was richer enough.

This indicated that oxygen in the biodiesel helped the oxidation of hydrocarbons and made the equivalence ratio range for low UHC became wider. B100 has higher UHC emissions than B50, which could be attributed to the discrepancy in vaporization ability as the B100 had lower volatility and higher viscosity than B50. The results demonstrated that the introduction of 20% of biodiesel in kerosene would be able to make a big impact on UHC emissions, due to that the fuel born oxygen in the biodiesel can increase the efficiency of the conversion of hydrocarbons.

Fig.4.3 presents the combustion inefficiency as a function of equivalence ratio for all fuels. The graph show that the combustion inefficiency for all fuels <1.2%. However, biodiesel and its blends (B20&B50) had lower combustion (<0.8%) inefficiency compared to kerosene fuel overall operating conditions. The main reason is due to higher CO emissions of kerosene especially at richer conditions.

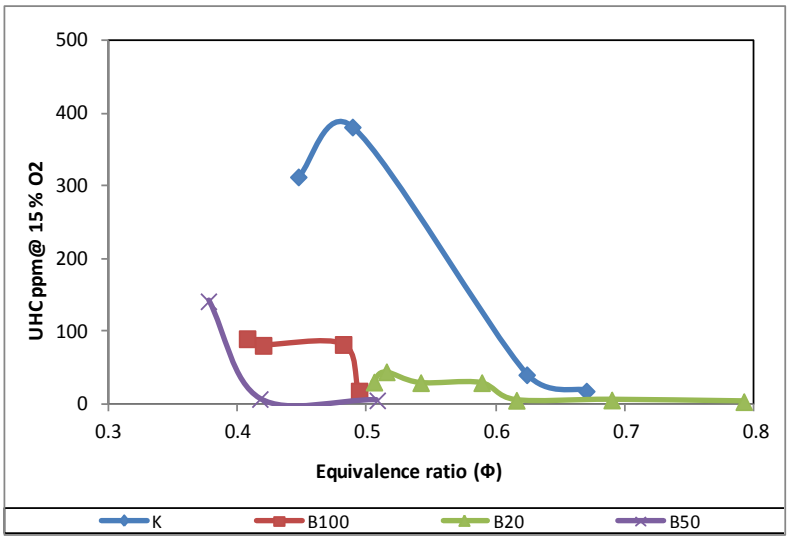

Figure 4.2: UHC emissions as a function of equivalence ratio for pure biodiesel, its blends and kerosene.

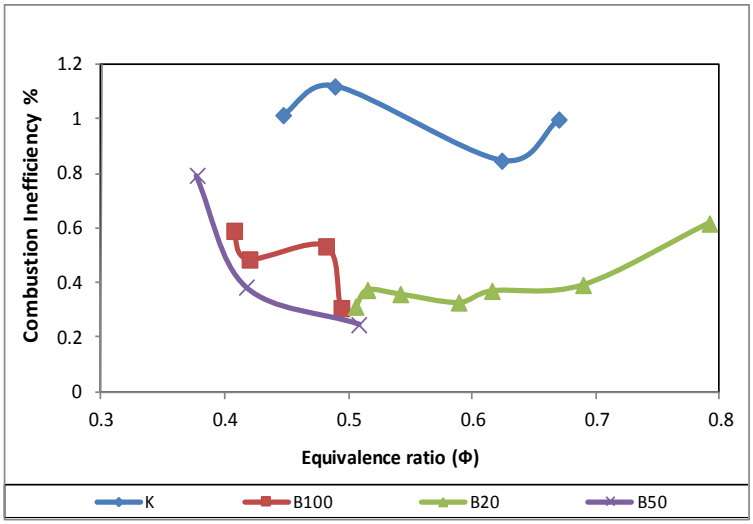

Figure 4.3: combustion inefficiency as a function of equivalence ratio for pure biodiesel, its blends and kerosene.

4.2.3.2 NOx emissions

Fig.4.4& 4.5 present the NOx emissions as a function of equivalence ratio and flame temperature for pure biodiesel (B100), kerosene and two blends (B20 and B50) at Mach number 0.017 with an air inlet temperature of 600K respectively.

The B50 and B100 produced significantly higher NOx emissions than kerosene and B20 when the equivalence ratio was 0.45 to 5, which was the range that all four fuels were able to be tested. The NOx emissions from B50 and B100 were very close and about 27% higher than B20 and kerosene. The higher NOx emissions from biodiesel were considered to be related to the oxygen content in the biodiesel. The NOx emissions from B20 were notably lower than that from kerosene when the equivalence ratio was 0.65 and this gap between kerosene and B20 was getting smaller when the fuel air mixture was richer and finally diminished at the equivalence ratio of 0.5.

The lower NOx from biodiesel in the relatively rich zone was considered that the oxygen in the biodiesel assisted combustion whereas in the relatively lean zone, the oxygen in the biodiesel started to cause adverse effect on NOx. This is supported by the decreasing gap in NOx emissions between kerosene and B20 with reducing equivalence ratio. The results also show that the flame temperatures had a positive linear correlation with equivalence ratio for all the fuels. The flame temperatures for all fuels were

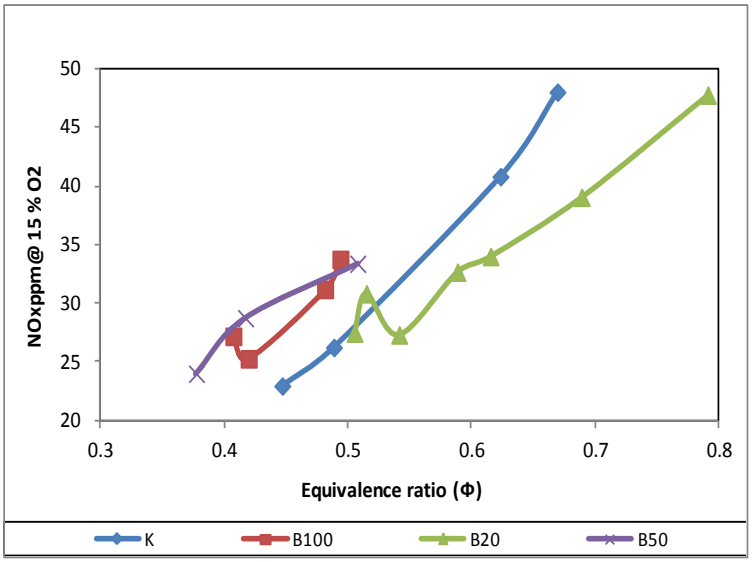

Figure 4.4: NOx emissions as a function of equivalence ratio for pure biodiesel its blends and kerosene.

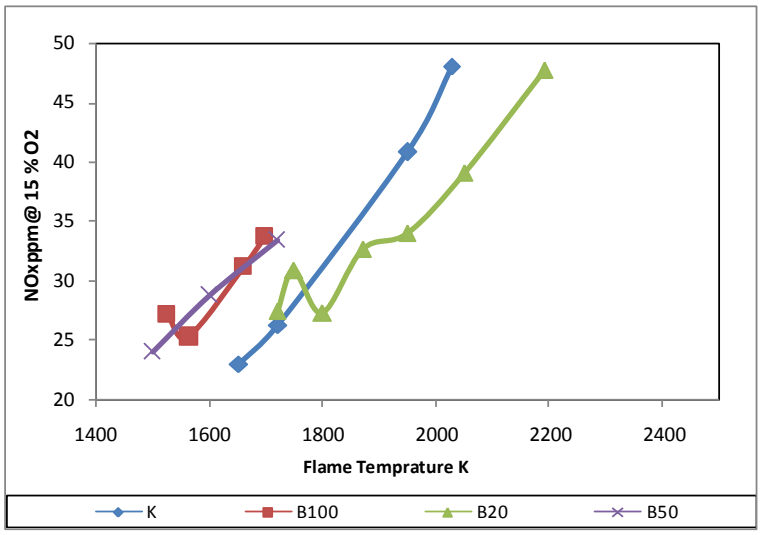

Figure 4.5: NOx emissions as a function flame temperature for pure biodiesel its blends and kerosene.

very close. The NO emissions were measured, along with NOx measurements and the same trend as that for NOx emissions was observed.

From NOx and NO measurements, the NO_2 emissions were obtained. The ratio of NO_2/NOx in percentage was calculated and presented in Fig.4.6. The NO_2 fraction was inversely correlated to the equivalence ratio. i.e. the lean mixtures favor more NO_2 emissions. The NO_2 fractions were in the range of about 40~70% overall for all fuels and various equivalence ratios. There is a trend indicating that the NO_2 fractions were decreasing as the share of biodiesel increasing. i.e. the NO_2 fractions were in the order of:

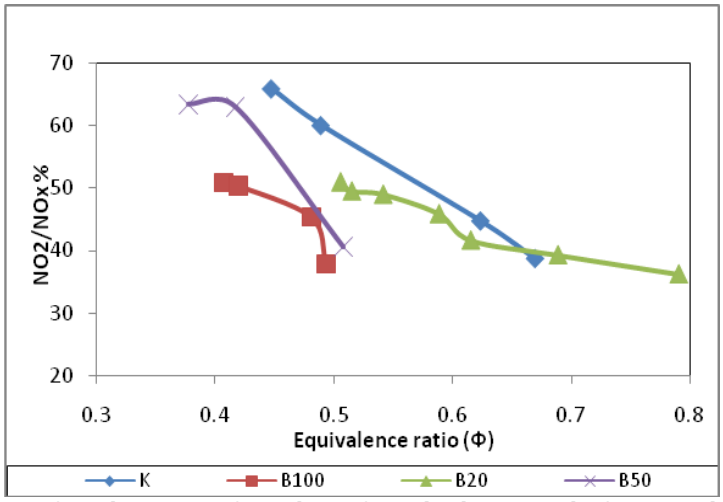

Figure 4.6: NO_2 fractions as a function of equivalence ratio for pure biodiesel, its blends and kerosene.

kerosene>B20>B50>B100. The B100 and B50 showed lower lean extinction limits than kerosene due to the oxygen content in the biodiesel.

4.2.4 Emissions from Liquid fuels at Mach number 0.023

The previous section investigated the same flame stabiliser as in this section with kerosene and WME blends at a relatively low primary zone operating Mach number of 0.017 and pressure loss of 1.5%, which is equivalent to a heat release loading of about 5 MW/m^2bar. This is a condition beneficial to fuel oxidation due to high residence times. The results showed NOx increased for B100 and B50 but with B20 the same NOx as for kerosene was found. However, the inlet temperature was set to achieve a reference Mach number of M=0.023. This was higher than in the previous section using this flame stabilizer. The higher Mach number enabled the pressure loss to be increased from 1.5% in the previous work to 2.7% in the present work.

Figs.4.7 to 4.12 present the emissions as a function of equivalence ratio for pure biodiesel (B100), kerosene and two blends (B20 and B50) at Mach number 0.023 with an air inlet temperature of 600K. All emissions results are corrected to 15% oxygen for 600K inlet air temperature and Mach number of 0.023. Again, the lower end of the curve represented the minimum equivalence ratio that the flame could be stabilized for each fuel. The high end of the curve represented a condition at which either the acoustic level or smoke or CO emissions were very high and considered intolerable beyond the point. Unfortunately, these limiting conditions were

different for the four liquid fuels, as shown in table 16. This resulted in no equivalence ratio at which results for all four fuels were obtained. The main problem was B100 where the white smoke problem prevented operation at any Φ that the other fuels were tested at.

4.2.4.1 CO and UHC Emissions

The CO, hydrocarbon and combustion inefficiency results are shown in Figs.4.7 to 4.9. The CO emissions of B100 were decreased as the equivalence ratio increased, which is the expected trend for equilibrium CO. B20 increased the CO relative to kerosene but B50 reduced the CO for the same equivalence ratio. All the CO emissions were very high due to the rich mixtures used and the high equilibrium CO at these Φ. At Φ=0.5, the B100 CO emissions are low as are the B50 results and these are lower than for kerosene. This is the well known effect of oxygenated biofuels in reducing CO emissions.

Fig.4.8 shows the UHC emissions as a function of equivalence ratio for pure biodiesel, kerosene and blends at Mach number 0.023 and air let temperature 600K. The UHC emissions were very low for all fuels for Φ>0.5 and this is the high flame temperature region. B100 was operated leaner than this with lower flame temperatures and slower HC oxidation. At Φ=0.7 the HC were significantly lower for B20 and B50 compared with kerosene. Again, as for CO, this is due to better oxidation with fuels that contain oxygenates.

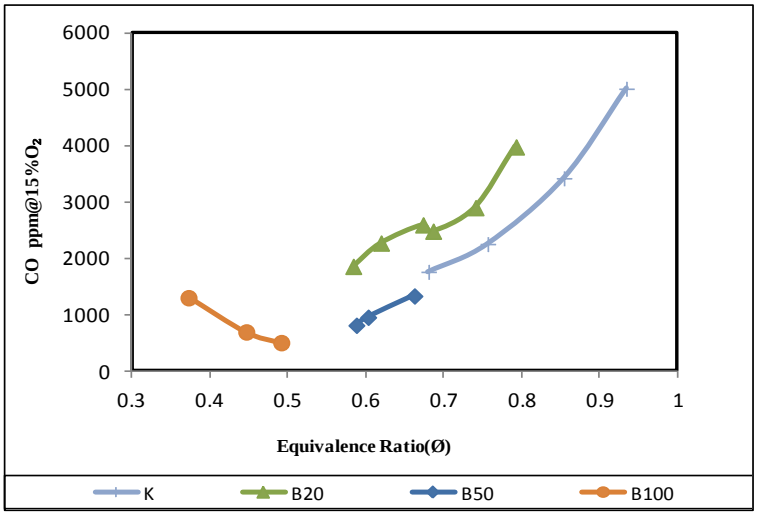

Figure 4.7: CO emissions as a function of equivalence ratio for pure biodiesel, kerosene and blends.

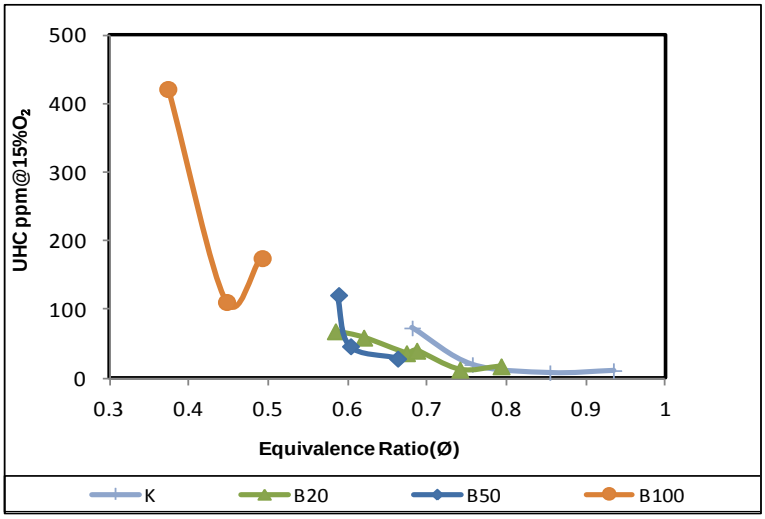

Figure 4.8: UHC emissions as a function of equivalence ratio for pure biodiesel, kerosene and blends.

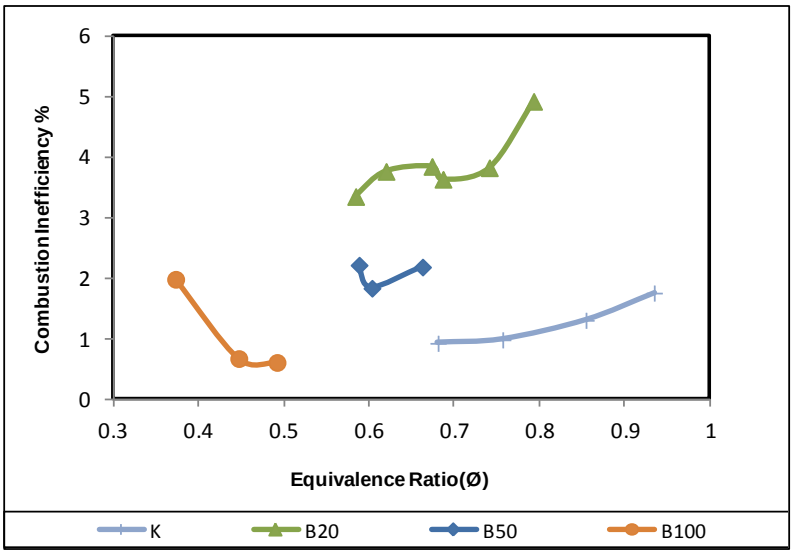

Figure 4.9: Combustion Inefficiency as function of equivalence ratio for pure biodiesel, kerosene and blends.

The energy content of the CO and UHC mass emissions give the combustion inefficiency as shown in Fig.4.9 as function of equivalence ratio for all fuels. The results in the graph show very low combustion inefficiency <3% for all fuels except B20. However, B20 has poor combustion inefficiency overall operating conditions due to higher CO emissions.

4.2.4.2 NOx emissions

NOx emissions corrected to 15% oxygen are shown as a function of both the equivalence ratio in Fig.4.10 and flame temperature in Fig.4.11. The NOx results show that B20 and B50 have higher NOx than for kerosene and B100 has higher NOx than B50 at the Φ where both had results. Although

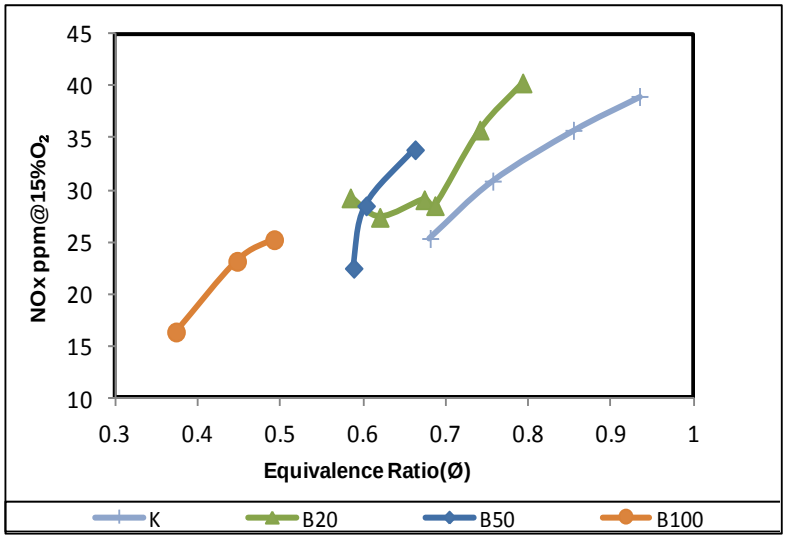

Figure 4.10: NOx emissions as a function of equivalence ratio for pure biodiesel, kerosene and blends.

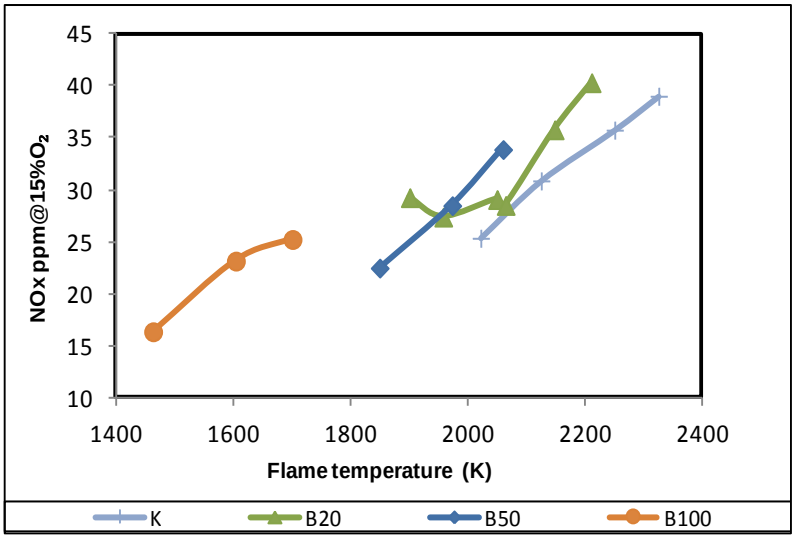

Figure 4.11: NOx emissions as a function of flame temperature for pure biodiesel, kerosene and blends at M= 0.023.

the trends are similar for the four fuels, the increased NOx for the biofuel blends and B100 can be seen for the same flame temperature.

NO was measured for all fuels among NOx and the results showed that all the influence of biofuels on NOx is entirely through the influence on NO. This indicates a direct increase in thermal NO with biofuels and this is likely to be due to deteriorated mixing relative to kerosene, due to the slower evaporation of WME. The NO_2/NOx ratios as a function of Φ for all fuels are shown in Fig.4.12. The results showed that there is little significant influence of biofuels on the NO_2 emissions. The oxygen content in biofuels may have given an additional NO oxidation route in the flame, but there is no evidence

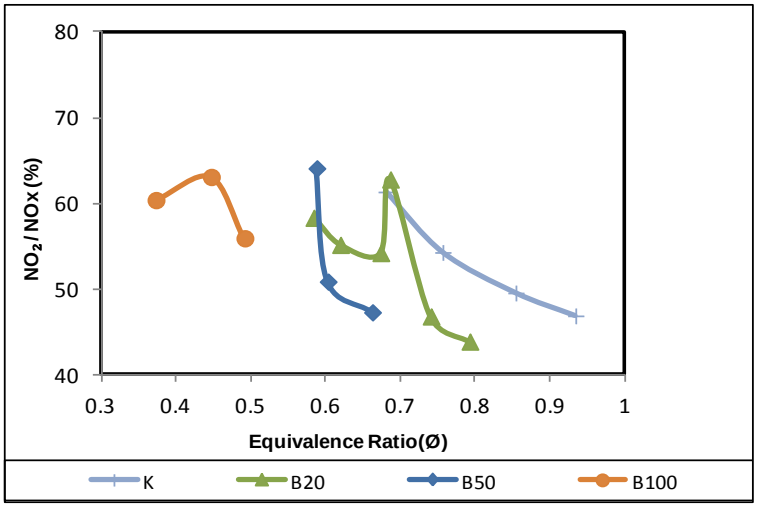

Figure 4.12 NO_2/ NOx as a function of equivalence ratio for pure biodiesel, kerosene and blends.

for this. As the NO_2 is not increased with WME but the NOx is, the result is a decrease in NO_2/NO ratios with WME blends for the same equivalence ratio, as shown.

4.2.5 Sauter mean diameter SMD Calculation

Sauter mean diameter (SMD) of the droplet size is defined as the ratio of the volume to surface area and usually used to characterize the drop penetration and heat and mass transfer. The SMD in the present work is calculated and compared for all fuels according to the Lefebvre equation [2, 21, 101, 159] for air blast atomization.

$$SMD = 1\times10E-3*\left[\frac{\sqrt{\sigma\rho L}}{\rho AVA}\right]^{0.5}*\left(1+\frac{1}{AFR}\right)^{0.5}+6\times10E-5\left[\frac{\mu L^2}{\sigma\rho A}\right]^{0.425}*\left(1+\frac{1}{AFR}\right)^{0.5} \quad \textbf{(25)}$$

Where:

SMD: Sauter mean diameter	(µm)
AFR: air fuel ratio	
VA: air velocity	(m/s)
µL: fuel viscosity	(m^2/s)
ρA: air density	(kg/m^3)
ρL: fuel density	(kg/m^3)
σ: surface tension	(kg/s^2)

Liu and el al [110] measured and compared the droplet size of biodiesel and diesel fuels. They concluded that biodiesel has larger droplet size than diesel fuel at the same conditions. Also their results showed that besides fuel

properties, atomization and fuel-air mixing process have big impact on emissions especially NOx. Their results were in a good agreement with this work as the inlet air velocity increased, the mixing and atomizing of fuels is improved and thus the NOx emissions decreased at higher Mach number.

The SMD for kerosene and pure biodiesel were calculated and compared at Mach numbers 0.017 and 0.023 as shown in Fig.4.13. This shows that for M=0.017 biodiesel had a larger (x 1.27) droplet size than kerosene at the same conditions. Biodiesel has a higher viscosity compared to kerosene fuels and this increases the drop size. The graph also shows that at the higher Mach number of 0.023 used in the present work, the higher air velocities reduced the SMD. At the higher Mach number WME had an SMD that was a little lower than for kerosene at M=0.017. Kerosene SMD decreased from 44 to 36 μm compared with a decrease of 57 to 46 for WME. However, all the drop sizes were in the range below 70μm where kerosene sprays burn like gaseous fuels. The higher Mach number enabled the pressure loss to be increased from 1.5% at M=0.017 to 2.7% at 0.023 using this flame stabilizer. The associated higher velocities in the radial swirler vane passage increased and this reduced the spray drop size.

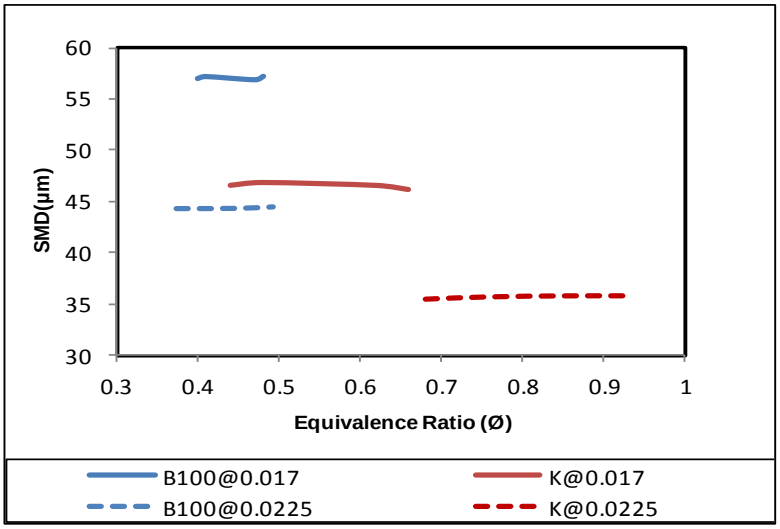

Figure 4.13: SMD comparison for both fuels at reference Mach numbers of 0.017 and 0.023.

4.2.6 Effect of Mach number on emissions

The emissions results for kerosene, B20, B50 and WME (B100) measured in this study are compared at both Mach number 0.017 and 0.023

with the same flame stabilizer and 600K air inlet temperatures. The results are plotted in Figs.4.14 to 4.19 as a function of the equivalence ratio for 600K inlet temperature and both Mach numbers 0.017 and 0.023.

4.2.6.1 NOx emissions

The influence of Mach number (M) on NOx emissions is shown in Figs. 4.14&4.15. At Φ=0.7 the kerosene results show a large reduction in NOx at the higher M with reduced residence time and higher pressure loss. This indicates the influence of improved mixing at the higher pressure loss. At this equivalence ratio thermal NOx is important and this reduces when mixing is improved. For B100 the only common equivalence ratio is for Φ=0.5 (~1750K) and this also shows lower NOx at the higher (M), but the change is much smaller than for kerosene at Φ=0.7. At the lower Φ flame temperatures are outside the thermal NOx range which is why the influence of M on NOx is smaller. Fig. 4.15 shows the influence of (M) on NOx for B20 and B50. In both cases at the same Φ the higher (M) reduces the NOx, indicating a reduction in thermal NOx due to the shorter residence time and better mixing at the higher pressure loss of the higher(M) operation.

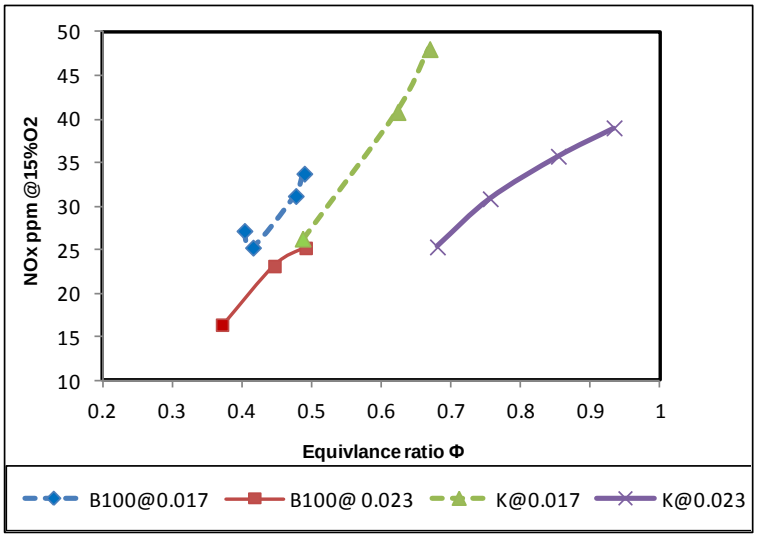

Figure 4.14: comparison of NOx emissions for B100&K at different Mach number.

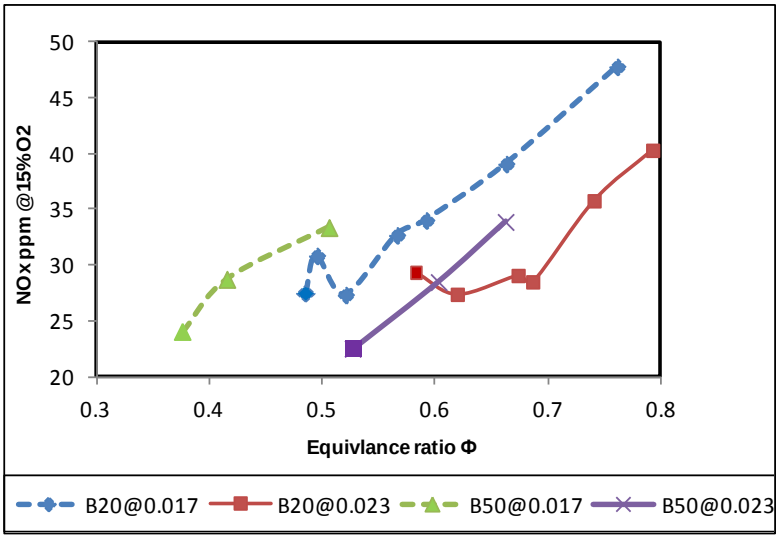

Figure 4.15: comparison of NOx emissions for B20&B50 at different Mach number

4.2.6.2 CO Emissions

The CO emissions as function of equivalence ratio are shown in Figs.4.16 &4.17. Comparison of kerosene with B100 in Fig.4.16 shows little influence of M for the same Φ. There is some evidence at Φ=0.4 of higher CO with B100 at the higher M and this would be due to the reduced residence time for CO oxidation. The B20 and B50 blends had a greater influence of M as shown in Fig.4.17. The B50 results are in agreement with Fig.4.17 with a small increase in CO at the higher M. The very large increase in CO at the higher M for B20 was unexpected.

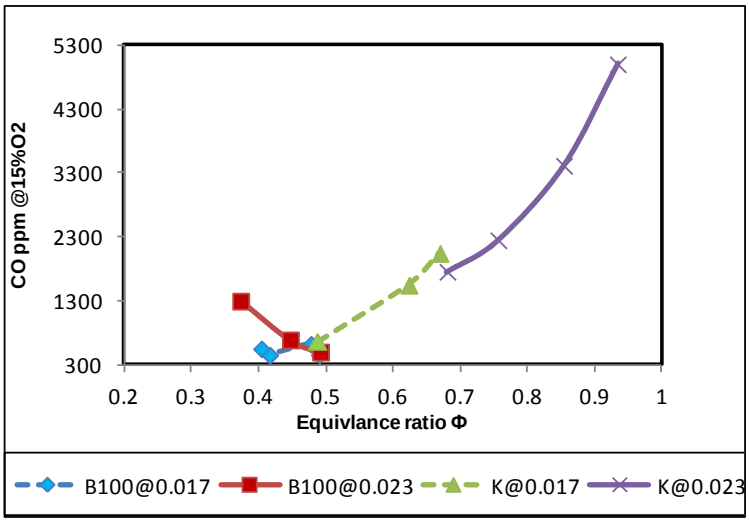

Figure 4.16: comparison of CO emissions for B100&K at different Mach number.

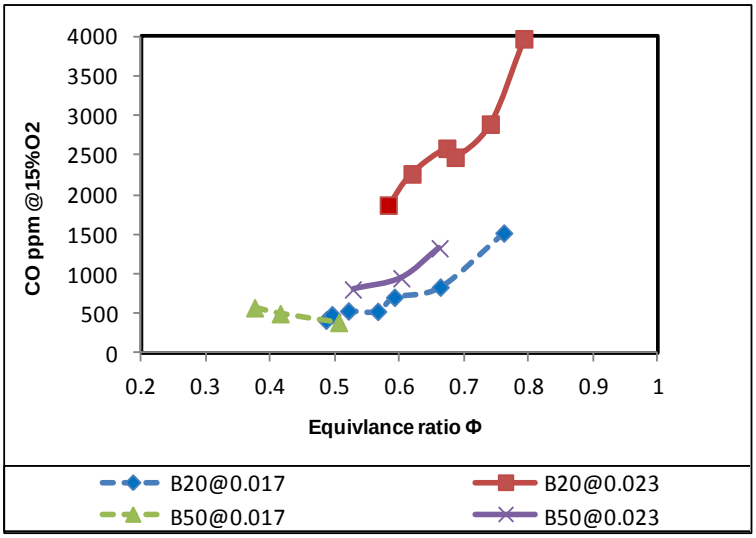

Figure 4.17: comparison of CO emissions for B20&B50 at different Mach number.

4.2.6.3 UHC Emissions

Comparison between two Mach numbers for kerosene, pure biodiesel (B100) and blends (B20, B50) fuels regarding UHC emissions are shown in Figs.4.18&4.19. The results show that the emissions of HC increased at higher Mach number due to the reduced residence time. The results also show there was no significant increase in HC with WME, in spite of the very high boiling point. The equivalence ratio trends are strongly influenced by the difference in weak extinction discussed above.

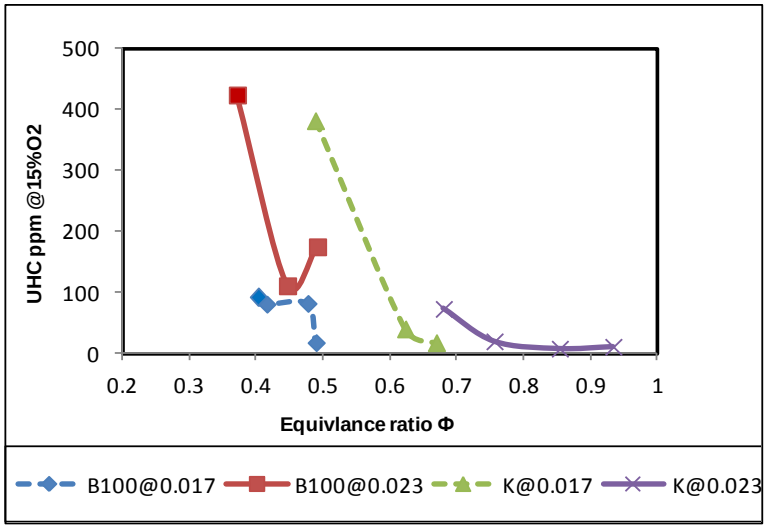

Figure 4.18: comparison of UHC emissions for B100&K at different Mach number.

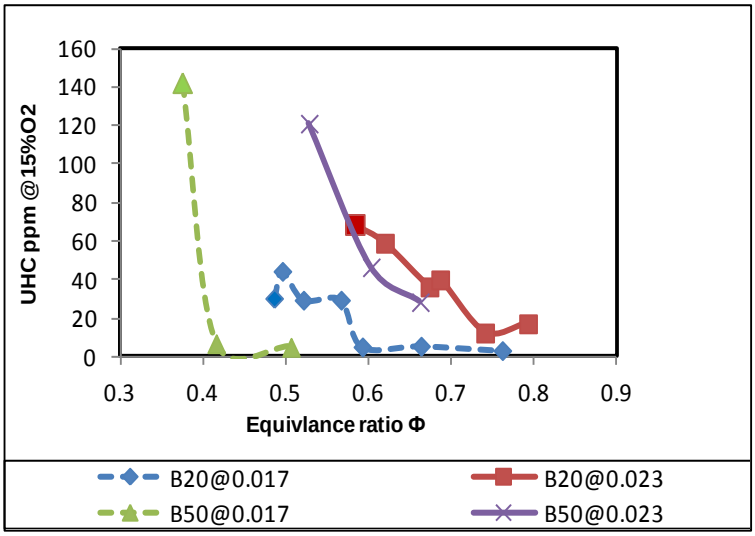

Figure 4.19: comparison of UHC emissions for B20&B50 at different Mach number

4.2.7 Aldehydes emissions of biodiesel and its blends

4.2.7.1 Introduction

There are much limed studies investigated the unregulated emissions from biodiesel such as carbonyl compounds (CBCs) especially aldehydes. These compounds are playing an important role in atmospheric chemistry and urban air. Also, they are a source of major health concern and important precursors to free radical ozone[160]. It is reported that formaldehyde, acetaldehyde acrolein and methyl ethyl ketone are the main species of carbonyl emissions from the exhaust and are toxic, mutagenic and even carcinogenic to human body [161, 162].

Traffic emissions are one of the most important sources of formaldehyde and acetaldehyde pollutions in urban air. The formation of them is a result of incomplete combustion of fuel. There are two pathways of formation of formaldehyde and acetaldehyde in urban air: primary and secondary. The primary source is emitted directly from the vehicles through exhaust gases. The secondary sources are formed from photo oxidation of other volatile organic compounds (VOCs) emitted from exhaust. Formaldehyde is the most dominant aldehyde in vehicle exhaust emissions. Both formaldehyde and acetaldehyde are classified as a probable human carcinogen by EPA in 1987 and exposure to them can cause irritation of the eyes, nose and respiratory tract.

The relationship between engine conditions and formaldehyde emissions has been studied in a diesel engine and the results showed that

at lowest load condition formaldehyde emissions was more than twice as high as that at the higher load conditions[163]. Lin et al investigated the emissions of carbonyl compounds from a heavy duty diesel engine using five different biodiesel. The study summarised that formaldehyde was the major carbonyl in the exhaust accounting for 70.3 ~75% of the total CBC concentration for all fuels. The effect of aldehydes emissions with equivalence ratio in light duty diesel engine was studied by Zervas et al [163]. They concluded that aldehydes decrease as the equivalence ratio increase and they represent from 8 to 16% of the pollutants detected[163].

There is a knowledge gap in aldehydes emissions from gas turbines, especially formaldehyde. Li et al [160] investigated unregulated emissions from micro gas turbine engine using FTIR. They found that the major detected aldehydes (formaldehyde, acetaldehyde and acrolein) had similar level of emissions at low power (<20% of maximum thrust) and at maximum power (>60% of the thrust), formaldehyde emissions increased rapidly. Formaldehyde has a strong potential to form ozone and is classified as an active ozone formation precursor. Ozone is irritant gas that can pose hazards to mucous membranes of eyes and respiratory tract,

The work in this chapter compared the emissions between a waste cooking oil derived methyl ester (WME) and kerosene using a radial swirler industrial low NOx gas turbine combustor under atmospheric pressure and 600K preheated air. The pure WME (B100) and its blends with kerosene (B20) and pure kerosene were tested for formaldehyde, acetaldehyde and acrolein emissions. The OFP was assessed for ozone formation potentials.

4.2.7.2 Combustion characteristics of aldehydes

Salooja studied the role of aldehydes in combustion inside a furnace. He studied the pre-flame and ignition behaviors of a number of statured and unsaturated aldehydes[164]. The main conclusions can be drawn:

- Aldehydes vary in their influence on the oxidation reactions at different pre-flame stages and on ignition.
- The aldehydes reactivity does not increase with molecular weight.
- Acetaldehyde is the most effective promoter.

Wei el at[165] also studied the aldehydes emissions mechanisms from blend fuel using spark engine. They concluded that the emissions of formaldehyde and acetaldehyde are controlled by two factors: initial temperature and gas flow velocity (i.e. residence time). Also, no HCHO and CH3CHO will emitted when the temperature too high or too low due to rapid consumption and the frozen generation respectively. In this study, the air flow rate was fixed and thus the residence time was constant. Therefore the aldehydes emissions were dependent on the consumption that would be accelerated at higher temperatures.

4.2.7.3 Aldehydes emissions as a function of equivalence ratio

Figs.4.20 to 4.22 represent aldehydes emissions measured by the FTIR in ppm as a function of equivalence ratio (Ø) for all three fuels under atmospheric pressure and 600K inlet temperature with Mach number 0.023. The three aldehyde species are formaldehyde (HCHO), acetaldehyde (CH_3CHO) and acrolein (C_2H_3CHO).

Only two FTIR measurements were taken for B100 at the equivalence ratio of 0.37 and 0.45. The effort for a FTIR measurement at the equivalence ratio of 0.49 was failed due to the heavy white smoke and consequently terminated the test.

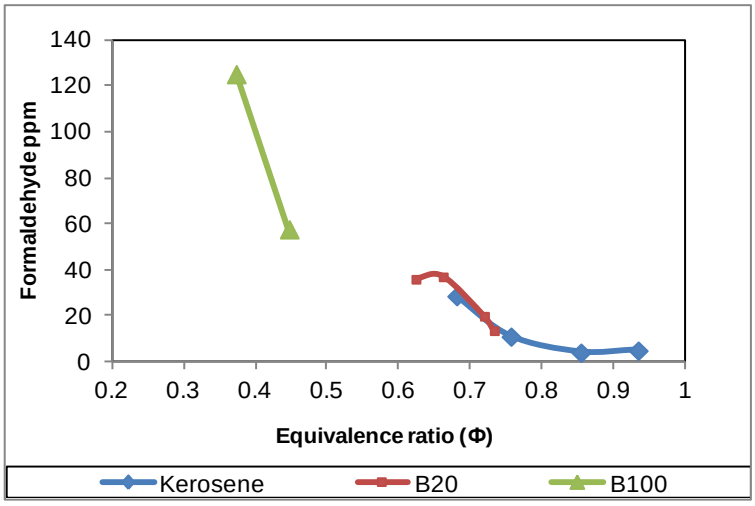

Figure 4.20: Formaldehyde as a function of equivalence ratio

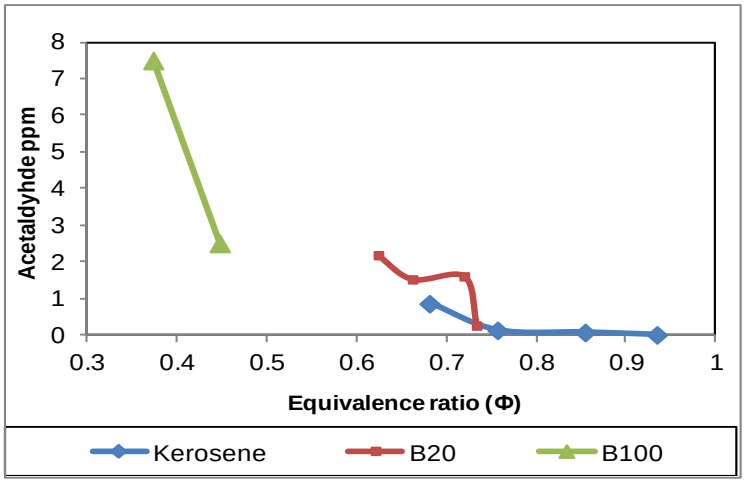

Figure 4.21: Acetaldehyde as a function of equivalence ratio.

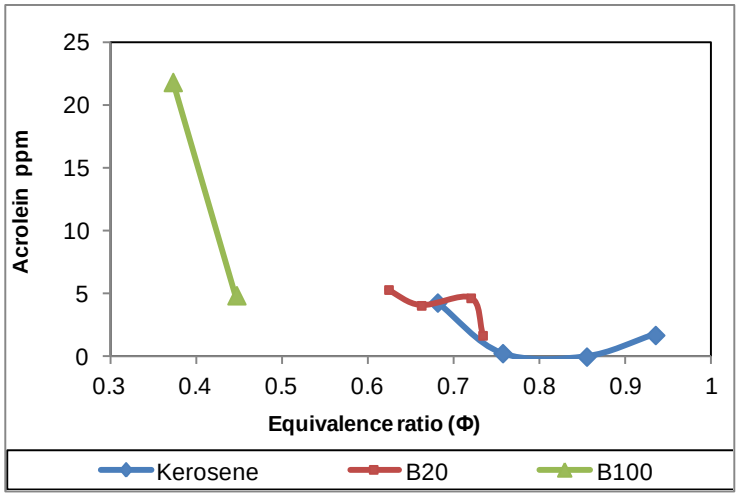

Figure 4.22: Acrolein as a function of equivalence ratio.

The results showed that formaldehyde is the dominant aldehyde species for all three fuels. B100 had significantly higher formaldehyde emissions than B20 and kerosene. It is notably that the equivalence ratio for B100 was remarkably lower, which resulted in lower flame temperatures compared to B20 and kerosene (Fig.4.26). This suggested that the flame temperature is a major factor that affects the formation of formaldehyde. The oxygen content in the fuel seems to have little impacts on formaldehyde formation by comparison of B20 with pure kerosene results where there was overlapped range of equivalence ratio. The same trends were found for acetaldehyde and acrolein. The concentrations of acetaldehyde were close to the detection limit of the instrument for B100 and lower than the detection limit for B20 and pure kerosene. There were notable acrolein emissions for B100 and very low levels for B20 and pure kerosene.

The aldehydes are intermediate combustion products. Their formation is mainly due to incomplete combustion which is directly linked to combustion temperatures. The strong correlation between aldehydes and flame temperatures suggested that the formation of aldehydes were greatly decreased when flame temperatures increased to above 1600K. The concentrations of aldehydes were converted into EI as a function of equivalence ratio for all three fuels as shown in Figs.4.23 to 4.25. This will enable the estimation of mass emissions from fuel consumption.

The EI of formaldehyde for B100 from Ø=0.44 to Ø=0.37 is increased by a factor of 2.75 (1.6 g/kg fuel to 4.2g/kg fuel, larger than that of by concentration ppm (factor of 2.15, 58 ppm to 125ppm) as shown in Fig.4.23. This is due to a larger exhaust flow rate at lower equivalence ratio than that at higher equivalence ratio. The similar differences appeared to acetaldehyde and acrolein. This emphasizes the importance of EI as a measure of emissions, especially at low equivalence ratio or high air fuel ratio.

The EI values of aldehydes for B20 and kerosene were much lower than that of B100. The peak value of formaldehyde emissions for B20 was (0.89g/kg fuel) at Ø=0.62 and decreases (0.3g/kg fuel) as the fuel air mixture getting richer to reach Ø=0.73. The direct comparisons between different fuels were difficult due to different ranges of equivalence ratios. However, there was a small overlap range in equivalence ratio for B20 and kerosene at around Ø=0.7, where the B20 did not seem to have higher formaldehyde emissions.

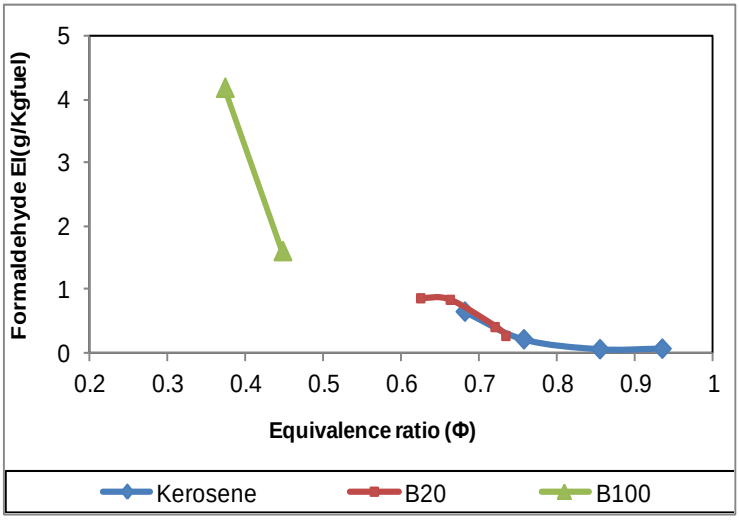

Figure 4.23: Formaldehyde as a function of equivalence ratio.

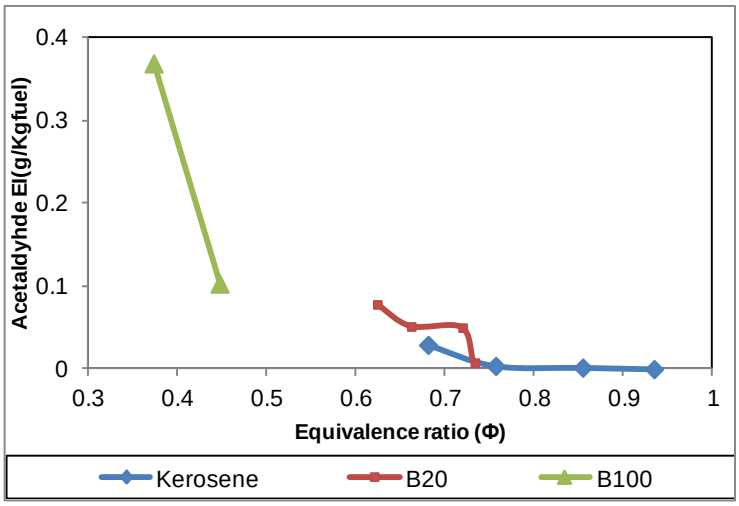

Figure 4.24: Acetaldehyde as a function of equivalence ratio.

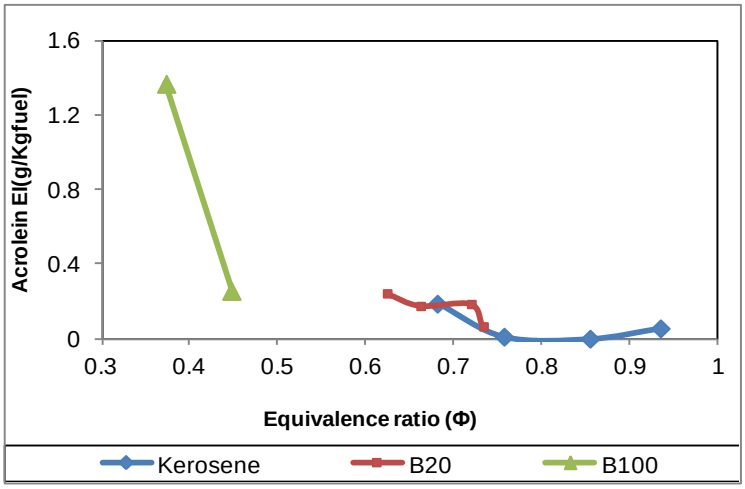

Figure 4.25: Acrolein as a function of equivalence ratio.

4.2.7.4 Formaldehyde emissions as a function of flame temperature

Combining the resuts in Figs.4.23 to 4.25, it is clearly shown that aldehydes emissions are a function of flame temperatures regardless of fuel types. It is therefore worth further investgating the relationship between the aldehydes concentrations aginst flame temperatures. As acetaldehyde and acrolein concentrations were very low at higher equivalence ratios, which contrained the accuracy of the measurement, only formaldehyde concentations were further invesigated. All formadehyde concentrations in ppm from three different fuels were plotted against flame temperatures as shown in Fig.4.26. A good polynominal fit between formaldehyde concentration and flame temperature was shown. In fact, a good linear fit existed between 1600 and 2200 K. The same trend is shown in Fig.4.27 for formaldehyde EI.

The formaldehyde emissions in ppm and EI were normalised to the maximum values as shown in Figs.4.28& 4.29. As the results represented a relative change from a particular equivalance ratio for all three fuels it could be used to predict other fuels such as B50 foramdehyde emissions trend based on limited measurements.

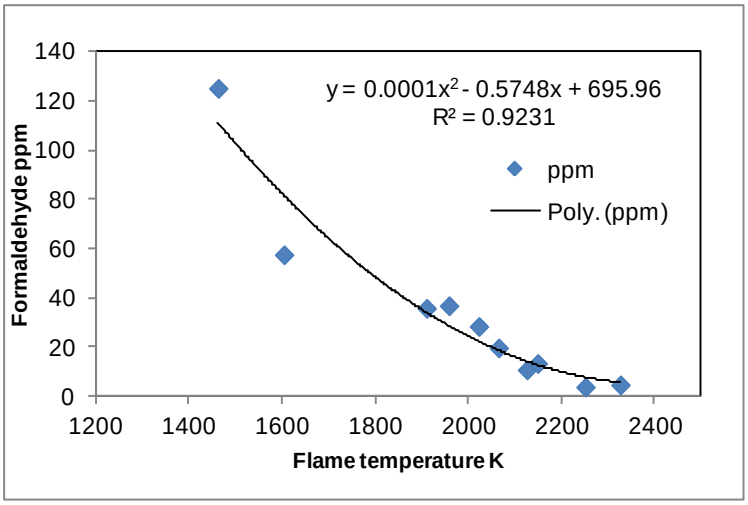

Figure 4.26: Formaldehyde concentrations as a function of flame temperature

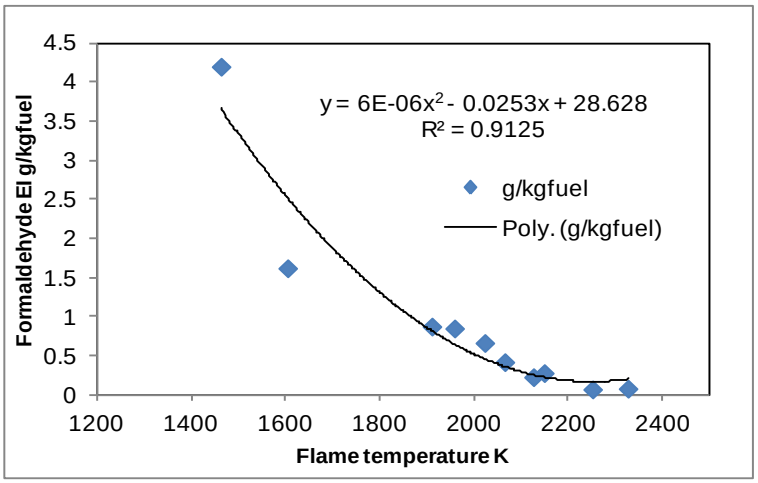

Figure 4.27: Formaldehyde EI as a function of flame temperature.

It is worth noting that industrial gas turbines for electrical power operate at high pressure around 20bar and aero gas turbines at take-off could reach up to 60bar. The influence of pressure on emissions should be considered. The relation between the thermal NOx and pressure was reviewed by Andrews[24] and showed that the thermal NOx increased as the pressure rose. The strong influence of the pressure on NOx emissions occurred near Stoichiometric region.

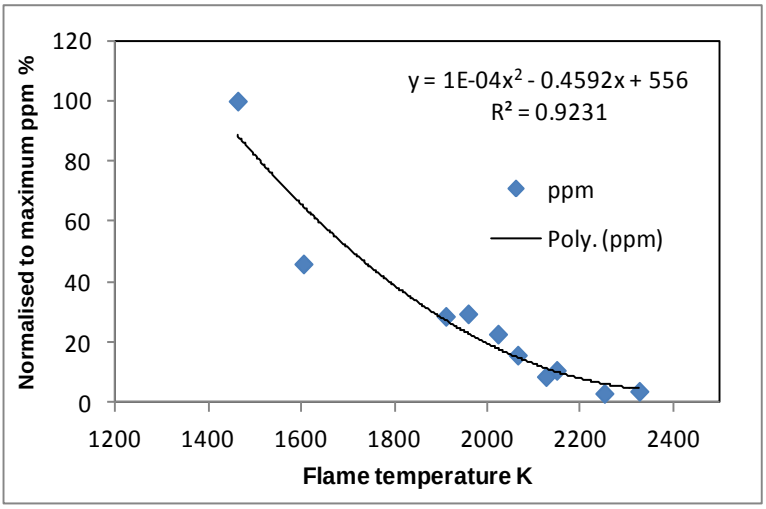

Figure 4.28: Normalized formaldehyde concentration as a function of flame temperature.

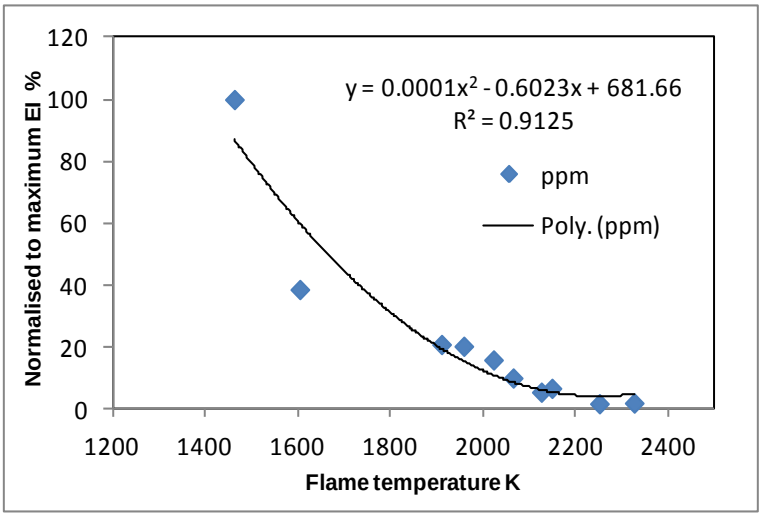

Figure 4.29: Normalized formaldehyde EI as a function of flame temperature.

The evidence for a ~0.5 pressure exponent for thermal NOx in lean burn combustion was observed. Liu etc investigated the biodiesel emissions on an industrial gas turbine and found that the CO and hydrocarbon emissions decreased as the inlet pressure increased[110], this may suggest that the increase of pressure leads to a reduction in aldehydes emissions. However, no literature or report on the influence of pressure on aldehydes emissions has been found.

4.2.7.5 Total hydrocarbon emissions and aldehydes fractions

The total hydrocarbons (THC) for three fuels at different equivalence ratios were measured by a FID as presented in table 17, along with total aldehydes concentrations (converted to methane equivalent) and their

fractions of total hydrocarbons. The THC emissions were similar for kerosene and B20 at all tested equivalence ratio ranges. The B100 had significantly higher THC emissions because of lower equivalence ratio and flame temperatures. Further increase of equivalence ratio would raise the flame temperature and then reduce hydrocarbon emissions for B100.

However, the further increase of fuel flow for B100 was constrained by a large amount of white smoke due to inefficient fuel evaporation. This is very different from diesel engines where a much high fuel injection pressure is usually used and thus fuel spray and atomisation for B100 in diesel engines are in a much better situation. By comparison with B20 and kerosene, the results in table 17 shows that B20 produced more overall aldehydes emissions in terms of concentration and percentage of the THC at the similar equivalence ratio ranges, although the THC emission levels were similar for B20 and kerosene. The total aldehydes emissions were considerably high for B100 and yet their percentages were not higher than other two fuels. For B20 and kerosene, the THC concentrations were at similar levels over the testing ranges of equivalence ratios, the concentrations and fractions of aldehydes were reduced significantly as the equivalence ratio increased. This indicated that as the fuel air mixture was getting richer, the flame temperature increased and aldehydes emissions were reduced while the THC remained. So the composition of the THC emissions changed.

Table 17: The percentage of Aldehydes to THC

	Ø	THC ppmC1	Aldehydes ppmC1	Aldehydes %
kerosene	0.68	100	43	43.2
	0.75	104	12	11.5
	0.85	109	4	3.7
	0.93	114	10	8.8
	0.62	104	56	54.1

B20	0.66	104	52	50.2
	0.72	104	37	35.7
	0.73	105	19	18.2
	0.37	680	206	30.3
B100	0.45	717	77	10.8

4.2.7.6 Assessment of OFP

The OFP of formaldehyde emissions at different equivalence ratios were determined using equation 23 and results in Fig.4.23 for three fuels and presented in Fig.4.30. The results show the maximum possibility of ozone formation by formaldehyde emitted. The results in terms of gO_3/kgfuel enable the estimation of OFP as a function of fuel mass flow and thus total mass of OFP for a given fuel mass. The OFP of formaldehyde was also plotted as a function of flame temperature as shown in Fig.4.31.

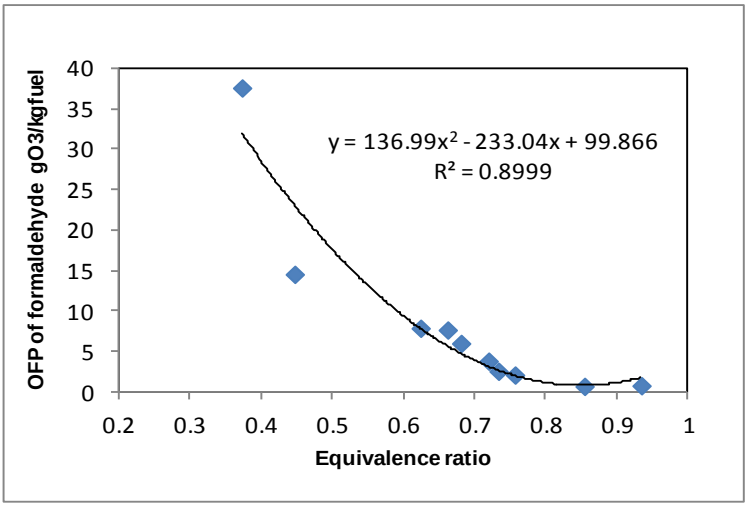

Figure 4.30: OFP of formaldehyde as a function of equivalence ratio for three fuels.

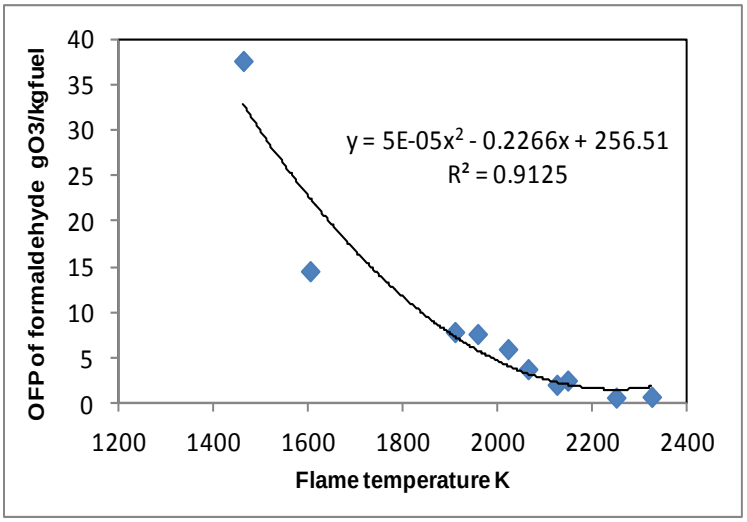

Figure 4.31: OFP of formaldehyde as a function of flame temperatures.

4.2.8 Particulate emissions

The PM emissions results for NG, kerosene and B20, B50, B100 measured in this study by SMPS were compared for 600K inlet temperature and two Mach numbers, 0.017 and 0.023. All the results at the lower Mach number were compared at ~0.5 equivalence ratio, whereas the higher Mach number the equivalence ratio was at ~ 0.55 – 0.58. The higher Mach number had a lower residence time but higher turbulence levels due to the higher flame stabilizer pressure loss. These Mach numbers are representative of aero combustors with about 50% of the combustor airflow through the primary zone. At the 0.023 Mach number the combustion intensity was 9 MW/m^2bar.

4.2.8.1 PM from cold and Hot Air

The ambient air fed to the combustor would have particulates in it from the local air supply. These were measured on the test rig using the same gas sampling system as for the combustion particle size emissions. The results are shown in Fig. 4.32 and the action of the electrical air heater was to increase the particulate emissions. This was probably due to metal dust particle release from the heating elements as well as from the connecting pipe work walls. Comparison with measurements made using the same SMPS instrument under ambient air roadside sampling is shown in Fig. 4.33

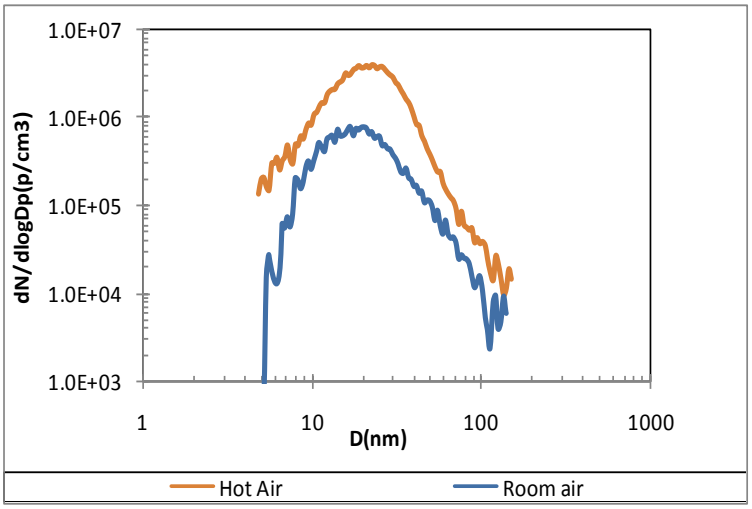

Figure 4.32: Particle size distribution in the cold and hot air feed to the combustor.

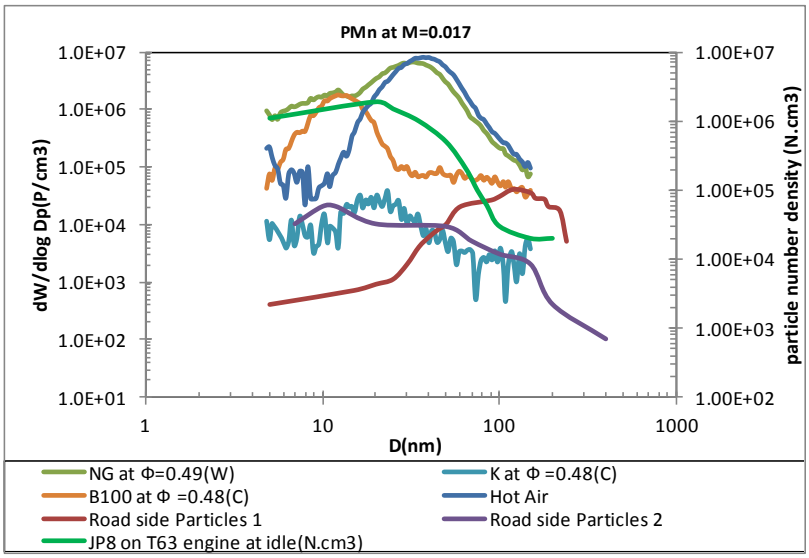

Figure 4.33: Particle size distribution for cold air compared with a congested traffic roadside air sample 1[166] and open country no other traffic air sample 2 [167] and two of the present combustion size distributions in number/m^3 units.

Fig.4.33 shows that the unfiltered ambient air used in this work had significant particle number with a size distribution that peaked at 20nm for cold air and 30nm for hot air. Comparison of this with a typical roadside ambient air measurement from the work of Lingard et al. [166] shows a very different ambient size distribution. At the roadside agglomerated and ultrafine particles had time to coagulated and increase in size and reduce in peak number. This is helped at the roadside by the presence of other particles from vehicle exhausts and roadside dusts. In contrast the results of Kittleson[167], shown in Fig. 4.33 for clean country air with no other particulate source, showed a peak number at 20nm but significantly lower

number than in the present work. These results were close to the present kerosene results as shown above.

Ambient urban air has a significant hydrocarbon contribution of an aerosol at 20nm. In the present work it would be expected that all components of ambient air apart from inert solid particles would be destroyed in the flame zone. Thus apart from ash particles the present measured particles are considered to be formed in the lean flames. For the kerosene results the contaminants in the air supply to the burner were mainly destroyed in the flame and few new particles were formed.

The measured particles were essentially the ash particles from the inlet air as carbon and hydrocarbon aerosols in the air would be destroyed in the flame. The higher particle numbers with the biofuel blends and B100 were due to the inferior mixing that occurs with the less volatile fuels and their larger drop size due to their higher viscosity. The present results compare well with the solid particle results of Han et al. [31] for an aircraft exhaust plume at the engine out plane. This had a peak number at 6 x 10^6/cm^3 at 30 nm, which are very similar to the present results as showen in Fig.4.33 for NG and B100. The much higher results than the present ones for kerosene is likely to be due to the sulphuric acid aerosol from the aviation fuel used in the work of Han et al.[31].

The cold air particle emissions were lower than those measured for natural gas combustion, but higher than the measurements for kerosene as shown in Fig. 4.33. The combustion levels with natural gas were only slightly higher than those of ambient air. However, as legislators are reluctant to allow the deduction of particles from ambient air from the combustor emissions, no attempt has been made to correct the results for the contribution from ambient air. Any hydrocarbons and carbon in the air would be oxidised in the flames at the 1700K flame temperature at which most of the results were obtained. With the direct undiluted exhaust gas sample particulate measurements used in the present work, the problem of the particles from dilution air directly affecting the measurements have been avoided. The particle concentrations are sufficiently low in the raw samples for particle losses in the hot pipe transfer to the SMPS particulate measurement system to be negligible.

4.2.8.2 Particle Size Distribution for Natural Gas

The natural gas particulate results were taken with the natural gas injected through the wall of the radial swirler outlet throat, as shown in Fig. 4.33 in number per kg of fuel and mass emission index units. The configuration tested was a well-mixed low NOx fuel injection location [54] and low particulate emissions were expected. Fig. 4.34 compared particle number and mass size distributions for all fuels at the same equivalence ratio.

The results show that natural gas had higher particulate emissions than for the liquid fuels, apart from B20 which was higher at M=0.017 and B100 which had higher particle number at M = 0.023. The peak number occurred at 10nm at M = 0.023 and 30nm at M = 0.017. The lower turbulent mixing at the lower Mach number may have contributed to the higher number and larger size of the particulates. The cumulative mass emissions calculated from the particle number were computed from the mass size distribution in Fig.4.34. The cumulative mass of particulates was 3.3 mg/kg_{fuel} at M = 0.017.

The gaseous emissions results for these tests at M=0.017 are shown in Fig. 4.35. These show that the CO and UHC emissions at the condition the particle size were taken, Ø = 0.49, were close to zero and this indicates that mixing was good.

The NOx emissions were 10 ppm, which is not ultra-low NOx and this indicates that the wall fuel injection location was not producing perfect mixing, where 1-2 ppm can be achieved in the best low NOx systems. However, this unmixedness is unlikely to be so bad that local rich zones occur that would generate soot. Hence there is no combustion reason for the particle number to be so high with NG.

Spang et al.[27] have shown that the sulphur compounds added to natural gas, to give it a smell, can be a source of sulphuric acid aerosol emissions. They measured particulate emissions from a small natural gas fired gas turbine. They measured a peak particle number at 10nm, similar to the present work. They showed that the particle mass emissions increased from 20 to 60 $\mu g/m^3$ for fuel sulphur levels from 0 to 15ppm.

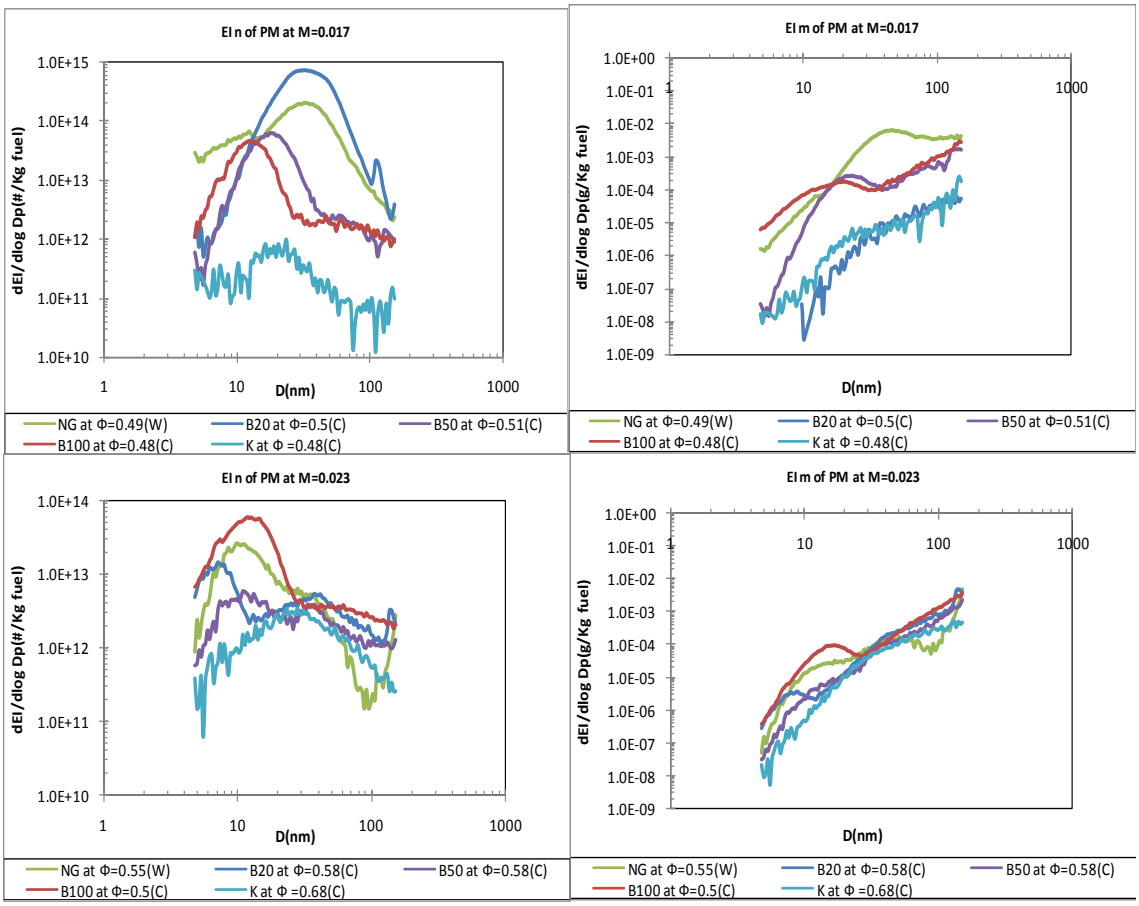

Figure 4.34: Comparison of particulate number and mass size distributions of all fuels at the same equivalence ratio

For a typical NG S level of 4ppm the measured particulate emissions was 30 μg/m^3 and assuming an operating A/F at 60/1 for the Capstone gas turbine this converts to about 1.6 mg/kg$_{fuel}$. This is a little below the present results for NG and indicates that NG sulphur levels was a likely cause of at least half of the measured PM emissions on natural gas.

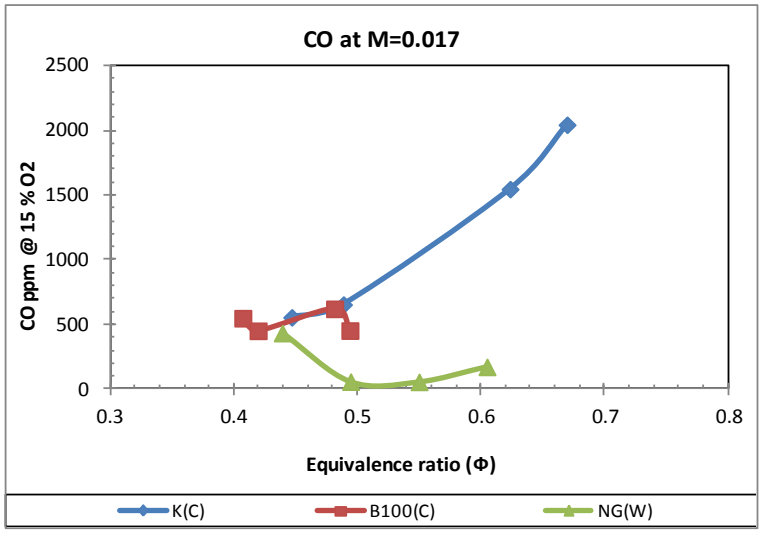

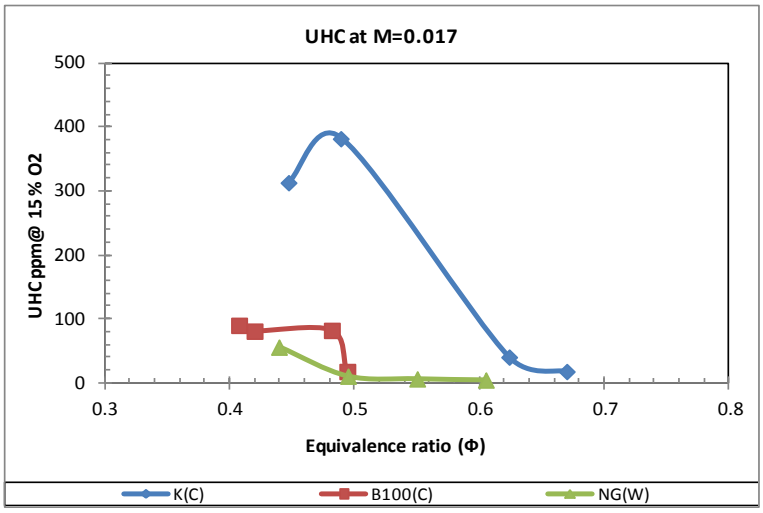

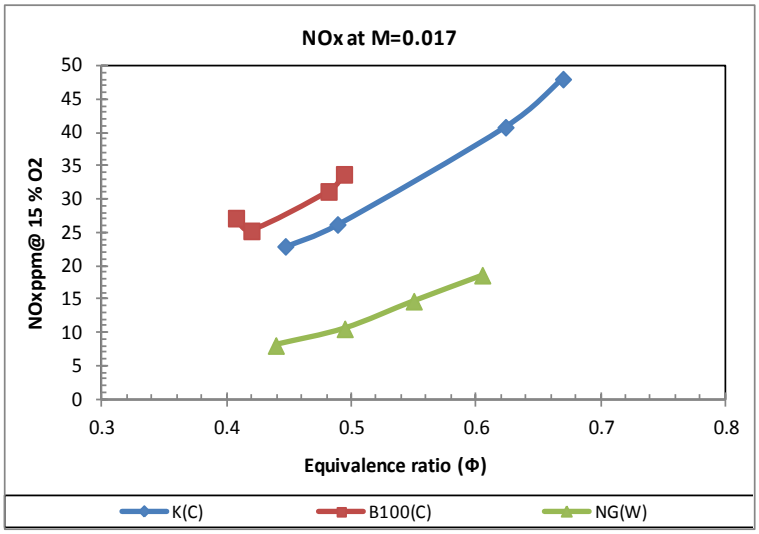

Figure 4.35: CO, UHC and NOx emissions corrected to 15% oxygen as a function of equivalence ratio.

4.2.8.3 Particulate matter of biodiesel and its blend with kerosene.

The number and mass size distributions recorded for all fuels are shown in Fig. 4.34. The number of particles was converted into mass using

the usual spherical particle with density 1000 kg/m^3 assumption. The figure also shows EI_n (number/Kg-fuel) and EI_m(g/Kg-fuel) for all fuels. In general, the higher Mach number reduced the PM emissions for both number and mass due to the better mixing at the higher pressure loss for the higher Mach number (1.83 times the pressure loss of the lower Mach number at the higher Mach number). The shorter residence time would give a lower particle coagulation time and hence a smaller particle size for the peak number. This was only found for B50 and the other liquid fuels had the reverse influence with larger particle size for the peak number at the lower Mach number, although much of this increase was due to the use of richer mixtures, especially for kerosene. The kerosene particle number results in Fig. 4.33 and 4.36 were extremely low, relative to the other fuels tested and were similar to clean ambient air.

The emissions results also showed that kerosene was different to NG and B100 as it had much higher CO and UHC, at 600 and 400ppm respectively at the test condition the particle size were taken. This could indicate the presence of an unburnt fuel aerosol in the particles measured, but one was not detected in the 10nm area where such particles would occur. These high emissions indicate that the flame had not burned to completion in the 330mm length downstream of the swirler outlet plane. Kerosene is more volatile than B100 or blends B20 and B50 and in the swirler throat is more likely to have evaporated and hence be better mixed that for B100. This flame would then be closer to its weak extinction and the flame would take longer to develop. This increases the NOx emissions through the prompt mechanism, as shown in Fig. 4.35. The better mixed flame with little time at high temperature then produces very few new particulates.

In contrast B100 does not evaporate at the 600K air inlet temperature and relies on the hot central recirculation for evaporation. This results in lower mixing and high NOx, through the thermal mechanism. This produces a hotter flame near the swirler exit in the central region, which has the low UHC shown. This unmixedness then produces some particulates in the flame, although at a low level due to the pyrolysis resisting oxygenated fuel, with its lower soot formation tendency. B100 particle number was lower than

NG due to the sulphur compounds added to NG. B20 at M=0.023 was the only result with a nuclei and agglomeration mode with peaks at 8nm and 40nm. The 8nm peak is likely to be a UHC aerosol effect.

The peak size (mode size) based on the particle number distribution are summarised in table 18. This shows that for all the fuels the peak number of particles occurred in the 15 – 30 nm range, apart from B20 at M=0.023. The particle total number and total mass, derived from the particle number, are summarised in table 19 and compared with some other aero gas turbine measurements in table 20 and with some industrial gas turbine measurements in table 21. The NG gas mass results in table 19 are similar to those measured on a filter paper in an industrial low NOx gas turbine[168] as shown in table 21.

Table 18: Particle size for peak number

Fuel	M=0.017	M=0.023
NG	30nm	15nm
Kerosene	20nm	30nm
B100	10nm	15nm
B50	20nm	15nm
B20	30nm	8nm

Table 19: Total particle mass and number

	Leeds low NOx burner at M=0.017		Leeds low NOx burner at M=0.023	
	Total PM mass mg/Kg	Total PM number P/Kg	Total PM mass mg/Kg	Total PM number P/Kg
NG	3.41	1×10^{14}	0.28	1.14×10^{13}
K	0.023	3.9×10^{11}	0.15	2.14×10^{12}
B20	0.91	3×10^{14}	0.59	7×10^{12}
B50	0.4	2.1×10^{13}	0.33	3.8×10^{12}
B100	0.34	1.5×10^{13}	0.68	2.5×10^{13}

Table 20: Comparison with JetA1 and Biodiesel PM from APU

NASA's DC-8 aircraft APU using JP-8 as Fuel [5]		
EGT ºC	Number concentration (p/cm^3)	Mass concentration mg/Kg
330	7.76×10^{07}	480
475	6.65×10^{07}	380
550	4.75×10^{07}	250
620	3.96×10^{07}	220
Sheffield University APU at full power EGT 460ºC		
Fuel	Number concentration (p/cm^3)	Mass concentration mg/Kg
Biodiesel	1.46×10^{09}	514
JetA1	3×10^{08}	175
GTL	8×0^{07}	14.6
Low NOx Combustor this work		
Ø=0.5	Number concentration (p/cm^3)	Mass concentration mg/Kg

M=0.017		
B100	6.26×10^{05}	0.539
B50	9.2×10^{05}	0.607
Kerosene	1.49×10^{04}	0.224

Table 21: Comparison with Other Low NOx Combustors[27].

Low NOx Industrial gas turbine (filter paper measurement)					
	Engine	Type	MW	Mass concentration mg/Kg	
				NG	Fuel oil
	Tempest	DRW01 RW047	7.9	12 8	73 138
	Cyclone	MW037 MW012	13.4	4 N/A	52 100
	Trent 970-84	aero engines	300ppm fuel S	N/A	32

Leeds Low NOx Combustor Ø=0.5, M=0.017 using SMPS		
Fuel	Number concentration (p/cm^3)	Mass concentration mg/Kg
NG	3.45×10^{06}	3.34
B100	6.26×10^{05}	0.539
B50	9.2×10^{05}	0.607
Kerosene	1.49×10^{04}	0.224

The present kerosene results in table 20 were much lower than any reported from diffusion flame aero or industrial combustors in tables 20 and 21. This is also shown in Fig. 4.36 for the particle size distributions. The present results may be representative of future lean burning low NOx aero gas turbines and indicate that there will be drastically reduced aero nano-particle emissions. A key difference between the present atmospheric pressure tests and engine tests is the impact of higher pressures on particulate emissions. Some indication that this is not a large effect for premixed flames can be obtained from particle size measurement in SI engines with premixed port fuel injection.

The combustion process occurs at peak pressures in the 50-100bar range, depending on the engine power and compression ratio, with similar air compression temperatures as in a gas turbine. Some published measurements for SI engine particle number size distribution are compared with the present results in Fig. 4.37. This shows that the two gasoline measurements span all of the present results, indicating that for lean premixed combustion pressure has no major impact on particle number.

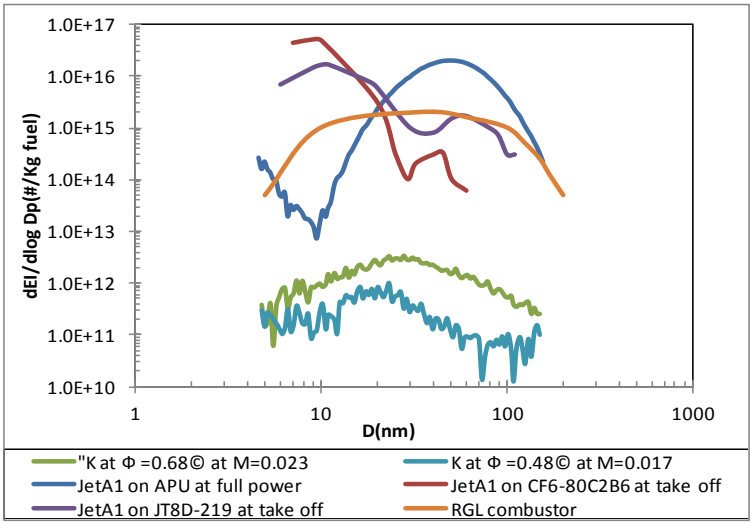

Figure 4.36: Comparison of the present results with literature measurements of particle size in number/kg$_{fuel}$ units. The Jet A1 APU results are from Li et al. [43]; the JT8D-219 and CF6-80C2B6 results were from Herndon et al. [169] and the RQL combustor results were from Bhargava et al.[142].

The premixed SI engine results also show that the present well mixed lean gas turbine combustor results are representative of the particulate levels in future lean burning aero engines and indicate that extremely low particle number and mass will be achieved. This indicates that any environmental problems from particulate emissions from current diffusion combustion aero-engines will dissappear as future lean burning low NOx aero combustors are put into service.

The present results showed that B100 produced a lower number of particles with small size compared to B20 which had the highest number and larger size. The higher the fraction of biodiesel, the lower the particle number and the smaller the size. This was expected as biofuels, which are oxygenated, have lower soot emissions when used in diesel engines and should give lower soot in gas turbine applications.

This would then give lower particle number. Similar behaviour was observed for the higher Mach number with lower number of particles and smaller size (nucleation mode). The PM mass distributions for all fuels are presented in Fig 4.34 as g/kg. B100 and B50 had close mass distributions at lower Mach number; while Kerosene showed lower mass at lower Mach number. A similar mass distribution for all fuels at higher Mach number was found.

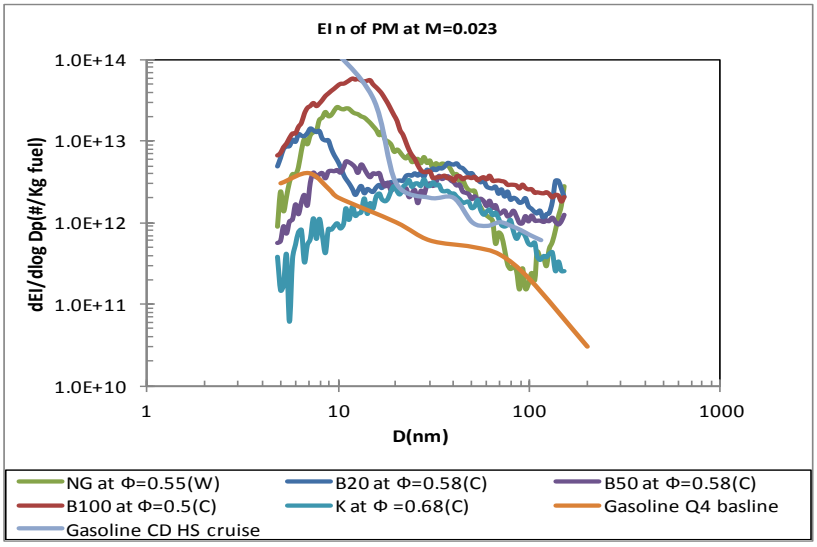

Figure 4.37: Comparison of particulate number emissions per kg of fuel for the present work with measurements in the exhaust of premixed combustion SI engines. Gasoline Q4 baseline [170], Gasoline CD HS cruise[171].

In general the EI_n and EI_m size distributions have similar relative characteristics to those reported by other authors [30, 142, 169]. Table 22 shows comparison of the total EIm, EIm, GMD and GSD for all fuels.

Table 22: Total EIn, EIm, GMD and GSD for all fuels.

M= 0.017	Number				Mass			
Ø=0.5	PN(p/cm^3)	EIn (p/Kg)	GMD	GSD	PM(g/m^3)	EIm (g/Kg)	GMD	GSD
NG	3.45 x10^6	1.04 x10^{14}	20.8	1.96	8.87 x10^{-7}	2.32 x10^{-5}	100	1.67
B100	6.26 x10^5	1.56 x10^{13}	13.9	1.69	1.37 x10^{-5}	0.00033	92	1.75
B50	9.21 x10^5	2.1 x10^{13}	18.4	1.53	1.78 x10^{-5}	0.00040	74	2
B20	1.26 x10^7	3.1 x10^{14}	32.2	1.47	7.11 x10^{-7}	1.7x10^{-5}	90	2
K	1.49 x10^4	3.92 x10^{11}	20.8	1.96	8.87 x10^{-7}	2.32 x10^{-5}	100	1.67

4.3 Conclusions

A waste cooking oil derived methyl ester biodiesel (WME) has been tested on a radial swirler industrial low NOx gas turbine combustor under atmospheric pressure and 600K. The pure WME and its blends with kerosene (B20 and B50) and pure kerosene were tested for lean extinction, gaseous emissions and particulate matter (PM) as a function of equivalence ratio. The experiments were carried out at a reference Mach number of 0.017& 0.023. The inlet air to the combustor was heated to 600K. The following conclusions have been drawn:

1) The lean extinction limit has been tested and is related to the fraction of biodiesel. The more the fraction of biodiesel, the lower the lean extinction limits.
2) The reduced emissions and lower extinction limit with biodiesel is considered due to the oxygen content in the fuel, which assisted the combustion process.
3) At lower Mach number, B50 and B100 produced significantly higher NO_X and NO emission and lower NO_2 emissions than B20 and kerosene. The increases in NOx by B50 and B100 were approximately 27% compared to B20 and kerosene. B20 produced lower NOx and NO emissions when the equivalence ratio was richer than 0.55 and 0.6 respectively compared to kerosene, and a similar level of NOx with kerosene when the equivalence ratio was smaller than 0.55. The NO_2 fractions in NOx were in the range of 40~70% for all fuels and conditions and inversely proportional to biodiesel shares in fuels.
4) Pure biodiesel and its blends showed lower CO emissions than kerosene. The difference was getting greater when the fuel air mixture was richer.
5) Blends and pure biodiesel had much lower UHC emissions than kerosene until the equivalence ratio reaching 0.65 where all fuels produced a similar level of UHC emissions.
6) At higher Mach number WME and its blends (B50, B20) had lower CO, UHC emissions and higher NOx emissions than the kerosene.
7) As the Mach number or residence time increased, the NOx emissions decreased for all fuels.
8) CO and UHC emissions decreased as the Mach number increased due to the shorter residence time.
9) Biodiesel has larger droplet sizes than kerosene at the same conditions. The big difference in the droplet size of both fuels is due to dynamic viscosity. The effect of Mach number was to significantly reduce the SMD at the higher M and this was responsible for the improved mixing at the higher M.

10) PM mass emissions of about 1mg/kg for gas and liquid fuel and B100 could be burnt without any major increase in particle number emissions.
11) The measured size at which the peak particle number occurred was similar to that for aero engine, but the number level was much lower.

The effects of pure WME (B100) and blend (B20) fuels on aldehydes emissions and OFP were investigated and compared with pure kerosene on a low NOx radial swirler combustor and the main findings are:

1) The experiment results showed that the dominant aldehyde in the exhaust is formaldehyde, which could be accounted for up to 50% of the total hydrocarbon emissions for B20 at low equivalence ratios
2) Aldehydes emissions were reduced as equivalence ratio increased. This is attributed to increases in flame temperatures, which were found to have a significant influence on aldehydes emissions.
3) There is a good correlation between aldehydes emissions and flame temperatures regardless fuel types, which could be potentially, used for predicting aldehydes emissions for other fuel types based on equivalence ratios.
4) The comparison between B20 and kerosene showed slightly higher aldehydes emissions in terms of concentrations for B20 than pure kerosene but with similar fractions of the total hydrocarbons. B100 produced much higher aldehydes, especially formaldehyde emissions at low equivalence ratio, along with high total hydrocarbon emissions. The low volatility of B100 induced the fuel evaporation problem and confined the fuel air mixture within a very narrow equivalence window and restrained the test towards higher equivalence ratios.
5) The OFP of formaldehyde emissions was assessed and showed a strong correlation with equivalence ratio and flame temperature regardless of fuel types.

Chapter 5 : Biodiesel co-firing with NG in a low NOx gas turbine combustor

5.1 Introduction

Interest in the use of liquid biofuels as renewable fuels has increased rapidly in recent years as they offer a retrofit means of reducing CO_2 emissions from transport and energy generation engines. Biodiesels obtained from methyl/ethyl esterification of fatty acids from vegetable oils, animal fats or used frying oils has been the focus of most studies and was used in the present work[162]. This work is concerned with the application of biodiesels in low NOx gas turbines for industrial power generation, where there are fiscal incentives to generate green electricity. Also existing low NOx gas turbines have dual liquid fuel capability and hence can easily be operated on biofuels.

Operation of gas turbines on biofuel alone is problematic due to the very high boiling point of vegetable oil methyl esters, typically around 300^{o}C. Operation with a second fuel that is easier to ignite is more common, such as the use of blends of liquid fuels with biofuel/diesel and biofuel/ kerosene, which has been investigated in the previous chapter. The work in the previous chapter showed that biodiesel had difficulties in fuel vaporization and had higher NOx emissions and lower CO& UHC compared to kerosene fuel.

One of the main drawbacks of biodiesel is the cost and sustainability. The use of waste cooking oils is one way to reduce the cost of biodiesel and utilize the waste. There are substantial researches on the applications of biodiesel in diesel engines, either pure biodiesel B100[152, 172, 173] or blended with diesel such as B5 (biodiesel 5%, diesel 95%), B10 (biodiesel 10%, diesel 90%) [109]. The success of biodiesel in diesel engines has trigged on increasing interests in using biodiesel as an alternative fuel for gas turbine engines [155-157] In comparison with diesel applications work on the use of biofuels in industrial gas turbines for power generation is relatively scarce.

Biodiesel has a very narrow distillation range around 300^{o}C and is therefore a difficult gas turbine fuel to burn as B100, especially in small industrial gas turbines where the compressor exit temperature is only just

above the boiling point of the fuel. The difficulty in vaporisation of the fuel makes conventional well mixed low NOx gas turbines on biodiesel a severe design challenge. Co-firing with natural gas offers a solution to these combustion problems

The work in this chapter is continuous of the pervious chapter, it is investigated the comparison of co-firing with natural gas (NG) with the operation on the liquid biofuel and blends with kerosene at two combustor Mach numbers 0.017 and 0.023 respectively. Waste cooking oil derived methyl ester (WME) was used as the biofuel and this was used alone (B100) with co-fired with NG and B20, B50 blends with kerosene co-fired with natural gas. The test conditions were atmospheric pressure and 600K preheated air as shown in Fig.3.1. Also, in the present work operation with a minimum proportion of natural gas was investigated so that the maximum biodiesel proportion and the maximum CO_2 benefit could be achieved. The problem of burning biofuel in low NOx combustors was illustrated by attempts to inject the natural gas in the well mixed combustion locations of vane passage and the present outlet throat wall injection as shown in Fig.3.5. Both of these locations worked fine with kerosene[68, 69] but did not ignite with biofuels as discussed in previous chapter. Hence, co-firing with central injection of biofuel was the only option for the swirler configuration that was used in this work.

The original work of Alkabie and Andrews[68, 69] that demonstrated the low NOx capability of radial swirlers with outlet throat wall fuel injection was carried out at 0.014 reference Mach number. The main difference with the previous work was that for the higher air flow capacity (higher radial swirler vane passage flow area) and the swirler pressure loss was much lower at 1.2% compared with the 5% of the previous work with smaller swirlers. This would normally make the turbulence levels lower and hence the mixing would be reduced. Also the air atomization of the fuel would not be as good, as the smaller vane passage area gives higher velocities and hence better atomization.

This was the fuel injection position for the natural gas used in this co-firing work. This swirler outlet throat wall injection has been shown previously to give very good mixing with natural gas and kerosene fuels [55,

68, 69]. Near premixed performance has been demonstrated in terms of low NOx and weak extinction [16, 17, 19]. An alternative natural gas location could have been in the vane passages, but this was not investigated here although it has been shown to have ultra-low NOx characteristics with natural gas [54].

5.2 Results and Discussion

5.2.1 Weak extinction limit

The weak extinction limits have been tested for all fuels at higher and lower Mach number as shown in Fig.5.1&5.2 respectively. For co-firing, the flow rate of natural gas (NG) was fixed at 145l/min (Ø= 0.4) at both conditions. In general, for liquid fuels only combustion, biodiesel demonstrated lower lean extinction limit due to the oxygen content in the fuel. There was a considerable drop between B20 and B50, indicating that the mixing ratio of biodiesel to kerosene between B20 and B50 had a significant impact on lean extinction limit. For co-firing tests, the overall equivalence ratio of both fuels was the summary of the NG equivalence ratio plus biodiesel equivalence ratio. So the data was higher than liquid fuels. Nevertheless, it showed that the B50 co-firing with NG had lower lean extinction limits.

Fig.5.1 shows the comparison of the weak extinction limits with and without co-firing with NG for all fuels at higher Mach number (0.023). The weak extinction results are rather unexpected as B100 has the best weak extinction and in all cases the addition of NG swirler outlet throat wall injection deteriorates the weak extinction. B100 is the most difficult fuel to burn on its own and with central fuel injection (which was the only fuel injection position that a stable flame could be achieved) the B100 fuel is vaporized by the central reverse flow of burned gases, which extend to the back face of the swirler where the central fuel injector is located. However, mixing of the B100 with the air will be poor and this gives the extended flame stability. In contrast the natural gas that is injected through the throat wall is very well mixed by the turbulent shear layer close to the throat outlet and this leads to a flame stability of Φ =0.37 close to the fundamental flammability limit for premixed gas and air at 600K.

With the constant NG flow set to achieve an overall Φ of 0.4 the flame is just inside the weak extinction. When liquid fuels are added through the central injector the effect is to deteriorate the weak extinction of the NG flame and produce a combined fuel stability that in every case is worse that for the liquid fuel alone, especially for B50 and B100. It should be appreciated that with the NG flame at Φ=0.4, the equivalence ratio of the added liquid fuel is very low and so the liquid fuel flame will not stabilize on the central injector. For example with kerosene, the weak extinction was 0.71 and with NG at 0.4 the effective local kerosene Φ was 0.31, outside the weak extinction of kerosene alone. With B100 the weak extinction of the two fuels together was nearly the same as NG alone. With B20 and B50 the weak extinction was considerable worse than NG alone. It is clear that the combined fuels do not produce a flame that behaves at the mean equivalence ratio as it would if only the liquid or NG fuels were used alone. The behaviors of weak extinction at lower Mach number (0.017) for all fuels are similar to that at 0.023 as shown in Fig.5.2.

One explanation of the results is that the near limit NG flame recirculates hot burned gases to the back plate of the swirler and the liquid fuel cools the gases as heat is absorbed to vaporize the liquid. However, the liquid fuel concentration is too low to establish a pilot flame and the net result is a cooling of the main NG flame and deterioration in the flame stability.

However, the delayed burning of the liquid fuel results in improved mixing when it does co-burn with NG and these results in the reduced NOx emissions that were found. In future work the NG fuel will be used as a central pilot fuel where it can be operated much leaner than in the present main NG fuel premixed mode. In this case the liquid fuel will be injected either through the throat wall or in the vane passage, then more of the heat release will come from the liquid fuel, but the overall flame stability will be controlled by the central NG pilot. This was not attempted in this work as liquid biofuels were found not to burn at all if they were injected into the vane passage or outlet throat wall without co-firing NG fuel. The biofuels would

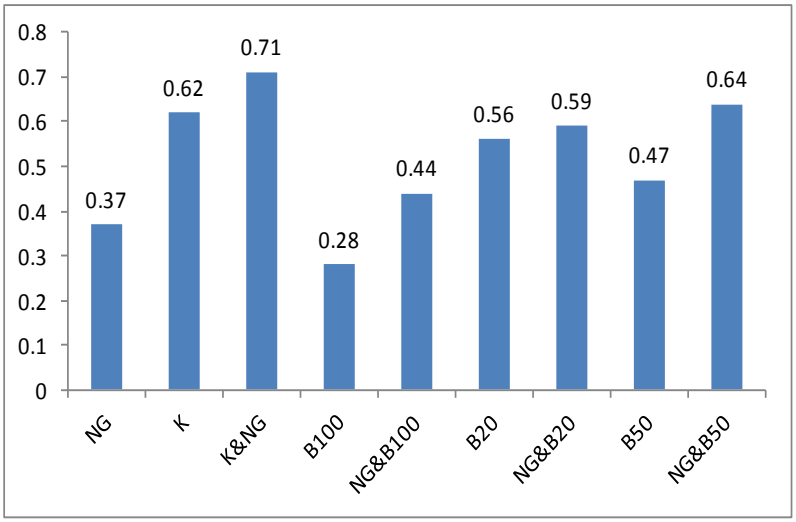

Figure 5.1: Comparison of weak extinction limit (Ø) with and without co-firing for all fuels at 0.023.

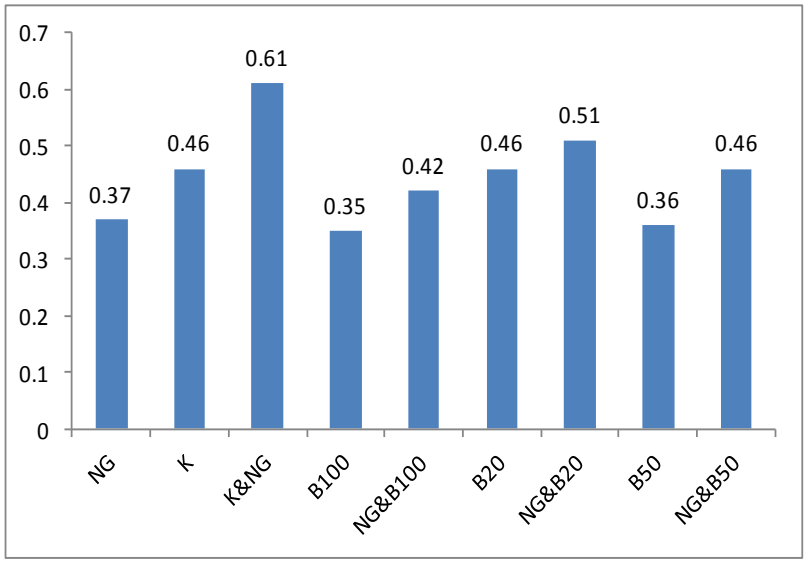

Figure 5.2: Comparison of weak extinction limit (Ø) with and without co-firing for all fuels at 0.017.

only stabilize a flame in the central injection location and this was why adding premixed NG was investigated in the present work.

5.2.2 Emissions from Liquid fuels Co-firing with NG at Mach number of 0.017

The co-firing tests were carried out using liquid fuels (K, B100, B20&B50) with natural gas. The flow rate of NG was fixed at 145 l/min (Φ =0.4), which was the lowest NG flow rate that the flame could be stabilized and indicated the lean extinction limit of NG for this configuration. The tests were started with NG only without blends at 145 l/min and then gradually introduced the liquid fuels. All emissions results have been plotted as a

function of equivalence ratio and compared with results in the previous chapter (without NG co-firing).

Figs.5.3&5.4 show the CO emissions as a function of equivalence ratio for all fuels with and without NG co-firing at Mach number 0.017 and inlet temperature 600K. Both graphs show that there an increase in CO with equivalence ratio which is due to the equilibrium CO trends. Fig.5.3 show that NG co-firing with extended the combustible range of B100 and reduce CO emissions for both K and B100. At Ø ~0.68, K with NG co-firing, CO emissions were reduced up to 75%. Thus, with the introduction of blends(B20&B50), the equivalence ratio increased and CO emissions decreased as shown in the Fig.5.4. The CO emissions reached a very low level at around 0.5 of equivalence ratio and then were gradually increasing after Ø >0.55. For both B20 and B50, it has been found that the CO emissions were reduced dramatically by NG co-firing from 400-500 ppm to around 100 ppm, a factor of 4~5. The lean combustion, good fuel air mixing and higher flame temperatures will favour the reduction of CO emissions. However, too lean mixtures would result in a reduced flame temperature that would increase CO emissions. Therefore, the lowest CO emissions at ~0.5-0.55 of equivalence ratio indicated the optimum to compromise between air fuel ratio and flame temperature.

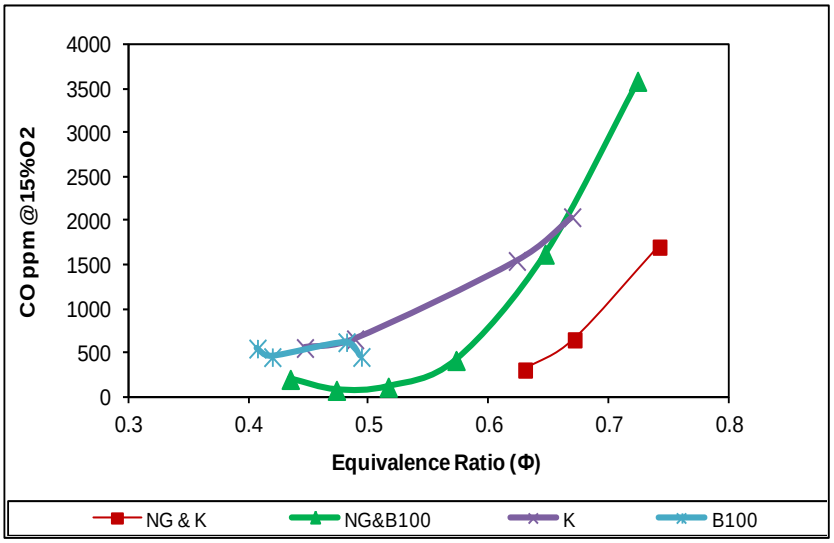

Figure 5.3: CO emissions as a function of equivalence ratio for K&B100 with and without NG co-firing.

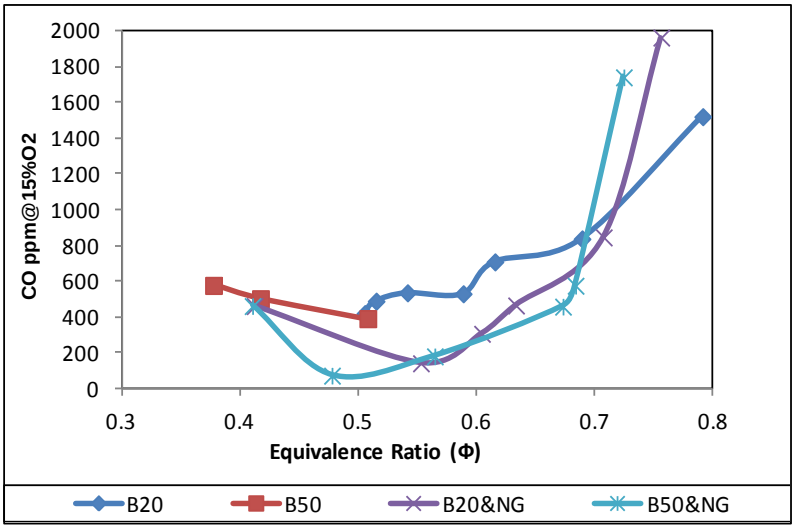

Figure 5.4: CO emissions as a function of equivalence ratio for B20&B50 with and without NG co-firing.

The UHC emissions as a function of equivalence ratio for all fuels with and without NG co-firing were shown in Fig.5.5&5.6. There is a significant reduction in UHC emissions for B100 and K when co-firing with NG as shown in Fig.5.5 and less than 30ppm has been achieved among all combustible operating range. Fig.5.6 also shows that, there were massive reductions in UHC emissions after B20 and B50 were added, which were from 430 ppm down to ~5 ppm. The UHC emissions were kept at a constant level regardless the change of the equivalence ratio from 0.45 to 0.73. It has been found that for B20 without NG co-firing, the UHC emissions decreased to ~5 ppm when the equivalence ratio was increased to 0.6 and over, whereas with NG co-firing, the UHC emissions were at ~5 ppm throughout the range of equivalence ratio being tested (0.45 to 0.73). B50 co-firing with NG also showed a low level of UHC emissions for all conditions. This suggested that NG co-firing is particular benefit to the relatively lean combustions.

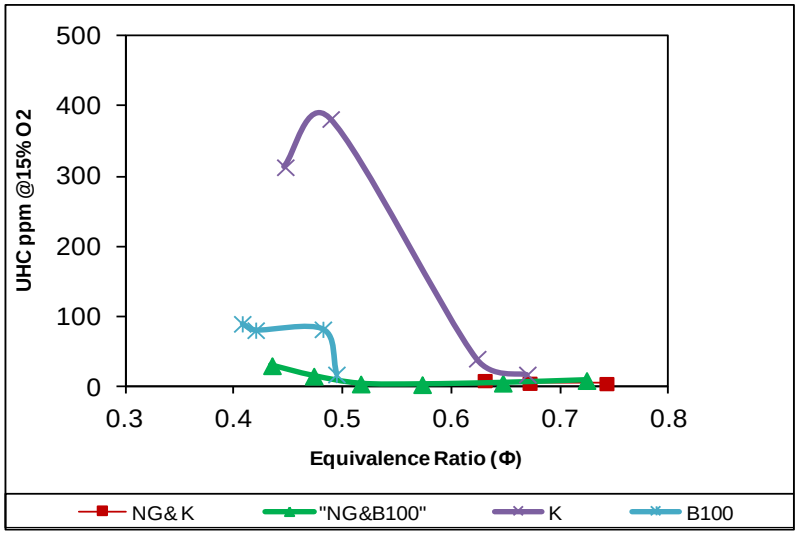

Figure 5.5: UHC emissions as a function of equivalence ratio for K&B100 with and without NG co-firing.

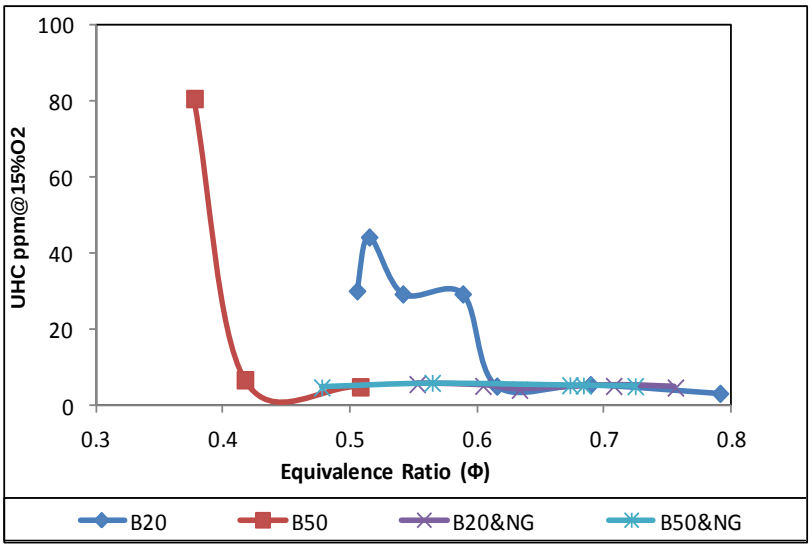

Figure 5.6: UHC emissions as a function of equivalence ratio for B20&B50 with and without NG co-firing.

The energy content of the CO and UHC mass emissions give the combustion inefficiency and this is shown in Figs.5.7&5.8 as a function of the overall equivalence ratio for all fuels. In these plots the equilibrium CO has been treated as combustion inefficiency. Figs.5.7&5.8 show very low combustion inefficiencies in the region that low NOx occurs. However, the operational range of equivalence ratios is severely limited by the poor weak extinction characteristics of the different fuelling combinations.

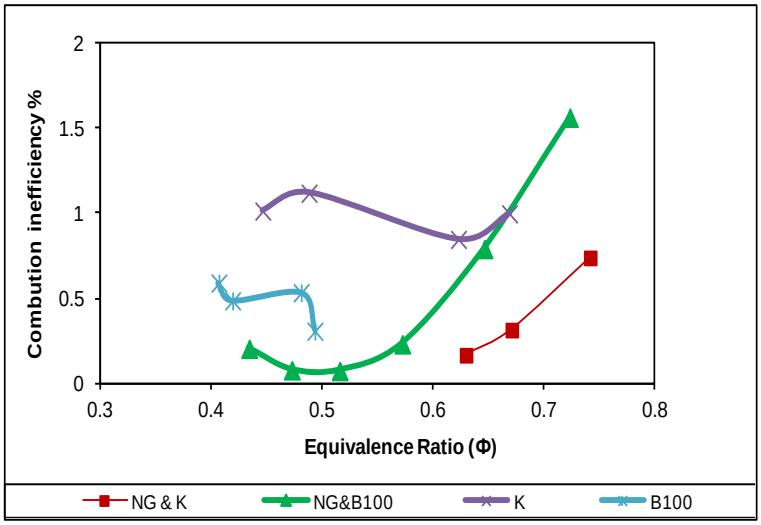

Figure 5.7: Combustion inefficiency emissions as a function of equivalence ratio for K&B100 with and without NG co-firing.

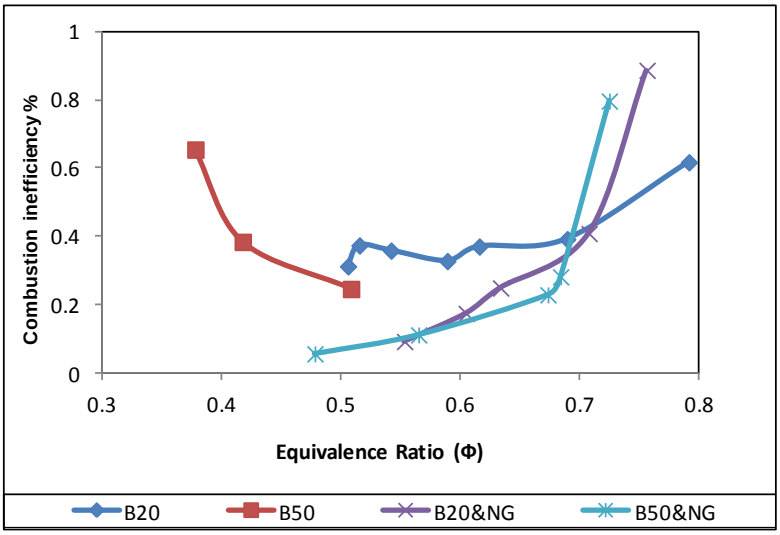

Figure 5.8: Combustion inefficiency emissions as a function of equivalence ratio for B20&B50 with and without NG co-firing

Figs.5.9&5.11 shows the NOx emissions corrected to 15% oxygen as a function of equivalence ratio for all fuels with and without NG co-firing and as a function of flame temperature in Figs.5.10 &5.12. The results of B100 and K in Figs.5.9&5.10 show the expected increase in NOx emissions with increasing equivalence ratio and flame temperature. The results also show that at Φ =0.5 the B100 NOx results are reduced from 35 ppm to 15ppm when co-fired with NG. Φ =0.5. For Ø=0.65, the NOx for kerosene is reduced from 55 ppm to 35ppm when co-fired with NG. B100 and NG flame had NOx ~ 10ppm, which is a flame temperature of 1300K, whereas <25ppm for kerosene and NG flame at 1650K. The co-firing with NG extended the combustible range of B50 from 0.5 to 0.7. Without NG co-firing, a large

amount of smoke was observed for B50 at Ø =0.5 around the flanges of the combustor and consequently the test could not be continued for richer mixtures. With NG co-firing, only a small amount of smoke was observed for B50 at Φ=0.5. The graphs also show that there are some moderate reductions in NOx by co-firing for B20 and significant reductions for B50. The reductions of NOx by co-firing for B20 were mainly in the relatively lean end by approximately 30%. The reductions of NOx by co-firing for B50 were approximately 50~70%.

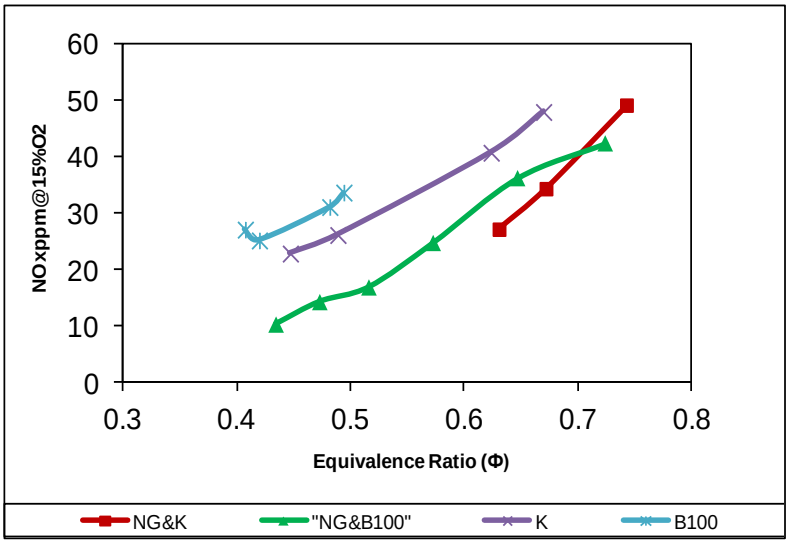

Figure 5.9: NOx emissions as a function of equivalence ratio for K&B100 with and without NG co-firing.

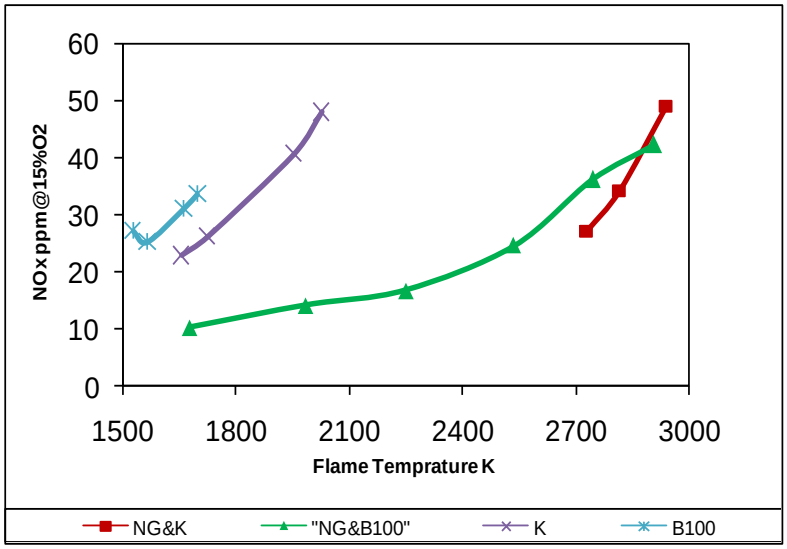

Figure 5.10: NOx emissions as a function of flame temperature for K&B100 with and without NG co-firing.

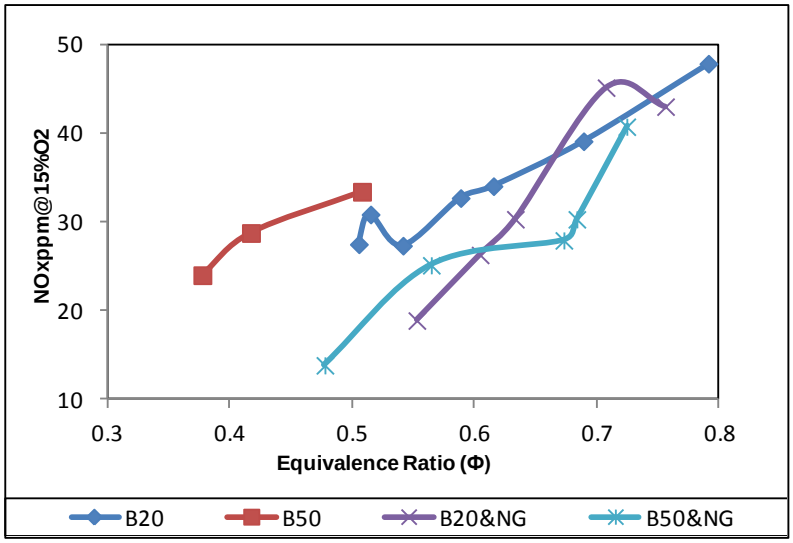

Figure 5.11: NOx emissions as a function of equivalence ratio for B20&B50 with and without NG co-firing

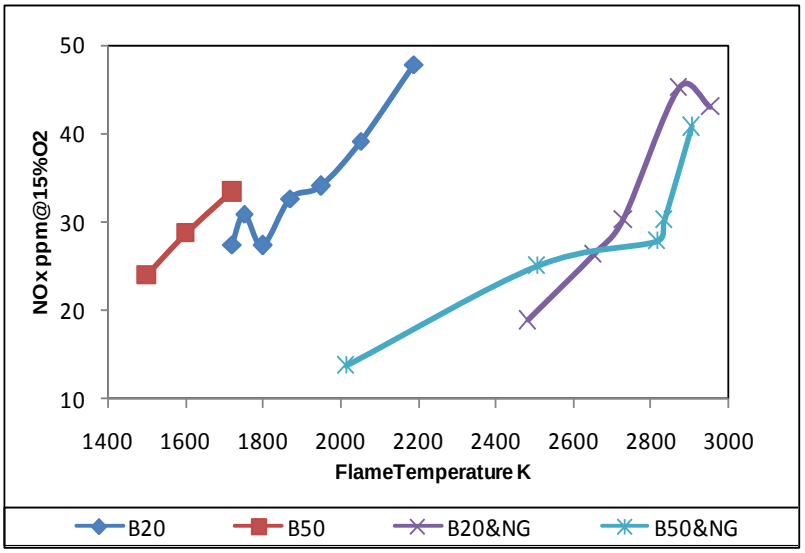

Figure 5.12: NOx emissions as a function of flame temperature for B20&B50 with and without NG co-firing.

Figs.5.13&5.14 presents the NO_2 fraction against NOx ratio for all fuels with and without NG co-firing. Fig.5.13 shows that B100 had more NO_2 with NG but kerosene had less NO_2 with NG. The graph also shows that NG co-firing reduce NO_2 fraction especially with kerosene fuel. The results in Fig.5.14 show that NO_2 fractions for co-firing of blends with NG were not sensitive to the changes of equivalence ratio and kept at a relatively constant level of approximately 30%, much lower than the NO_2 fraction of NG only, which was 75%.

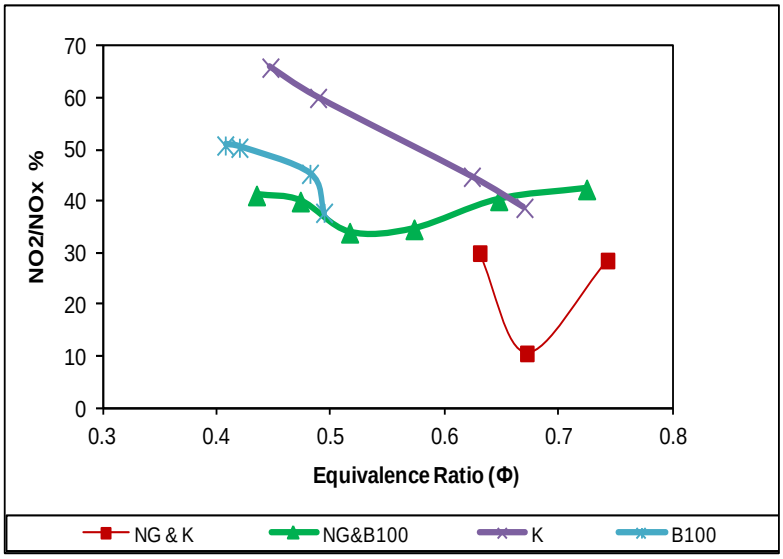

Figure 5.13: NO2/NOx emissions as a function of equivalence ratio for K&B100 with and without NG co-firing.

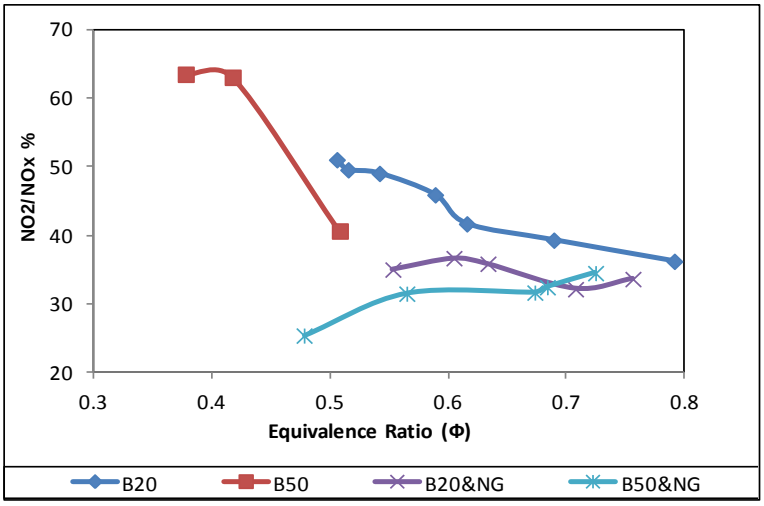

Figure 5.14: NO2/NOx emissions as a function of equivalence ratio for B20&B50 with and without NG co-firing.

5.2.3 Emissions from Liquid fuels Co-firing with NG at Mach number 0.023

Figs.5.15&5.16 show the CO emissions as a function of equivalence ratio for all fuels with and without NG co-firing. As mentioned earlier the increase in CO with equivalence ratio is due to the equilibrium CO trends. Fig.5.15 shows little influence of NG co-firing on the CO emissions for the liquid fuels alone. The increase in CO for very lean mixtures is due to the approach of weak extinction. For B100 where poor fuel atomization is expected and hence potentially poor fuel vaporization, higher CO than for kerosene was anticipated, but the figure shows that this was not the case.

This indicates that vaporization is controlled by the high temperature recirculated gases on the radial swirler centerline where the liquid fuel injector is located. For B20 and B50 blends as presented in Fig.5.16 shows that the effect of NG addition on CO emissions is more complex. For B50 and B20 fuels the addition of NG reduces CO for the same Ø. For B50 Fig.5.16 shows that for Ø =0.65, CO was reduced from 1200 for B50 alone to 400ppm with NG. For B20 at Ø =0.6 the CO was reduced from 2200ppm for B20 alone to 1000ppm with NG. This was due to the improvement in overall fuel and air mixing when premixed NG was used in conjunction with central injection of liquid fuels.

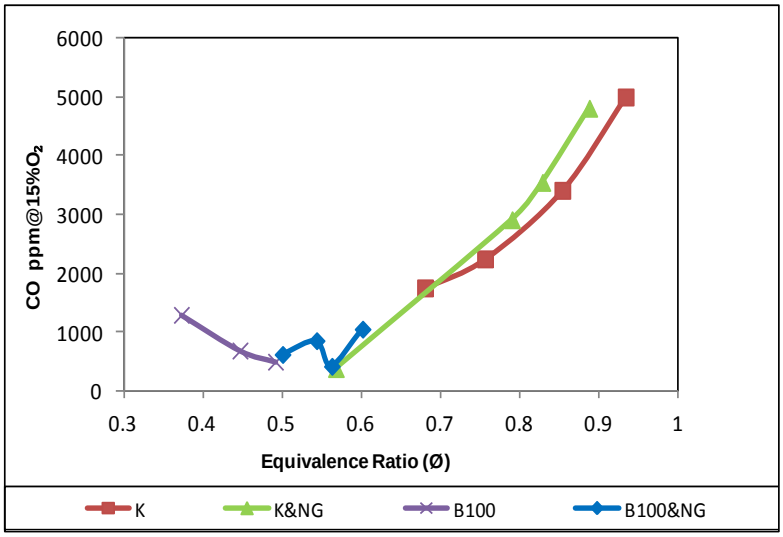

Figure 5.15: CO emissions as a function of equivalence ratio for K&B100 with and without NG co-firing.

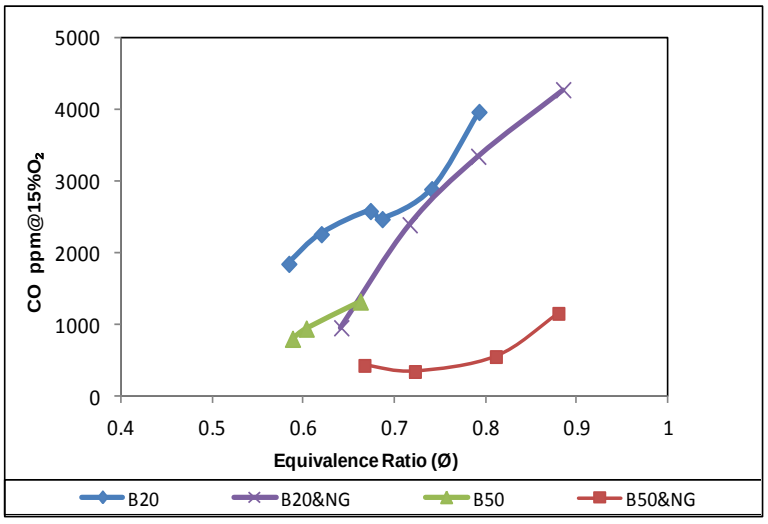

Figure 5.16: CO emissions as a function of equivalence ratio for B20&B50 with and without NG co-firing.

The comparisons of UHC emissions for all fuels with and without NG co-firing are presented in Figs.5.17&5-18. Fig.5.17 shows that for kerosene and B100 there was little change in UHC when co-firing with NG was used, for the same Φ. The figure also shows that UHC increase as the lean stability is approached, but for richer mixtures there were very low UHC emissions. Fig.5-18 shows a more significant influence of NG premixing on UHC emissions. For B20, the UHC was reduced when co-fired with NG and for B50 the UHC were strongly increased. The reasons for these opposite trends is difficult to explain, but are considered to be linked to the changes in fuel and air mixing when premixed NG flames are present.

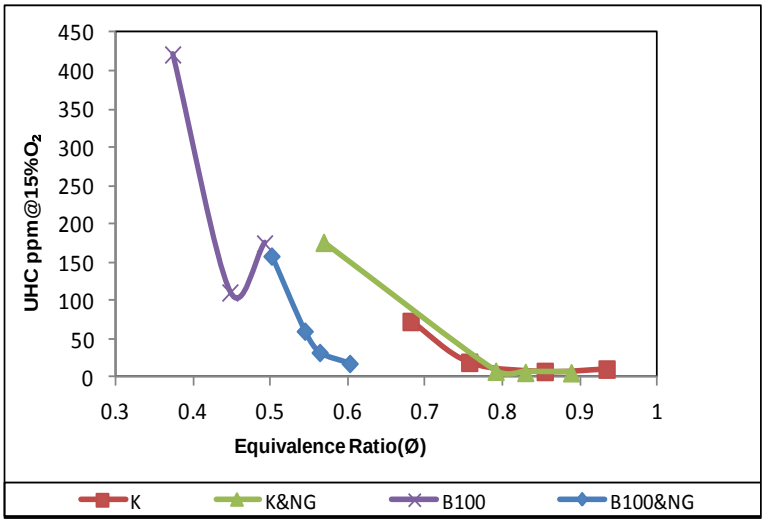

Figure 5.17: UHC emissions as a function of equivalence ratio for K&B100 with and without NG co-firing.

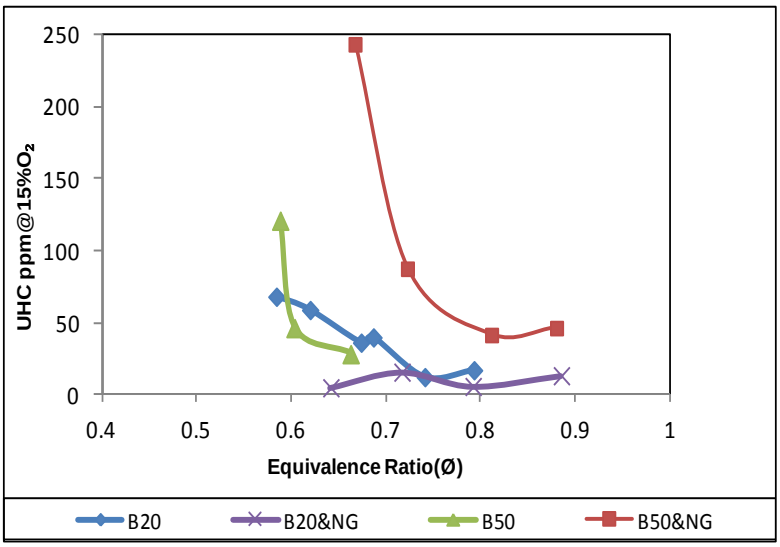

Figure 5.18: UHC emissions as a function of equivalence ratio for B20&B50 with and without NG co-firing.

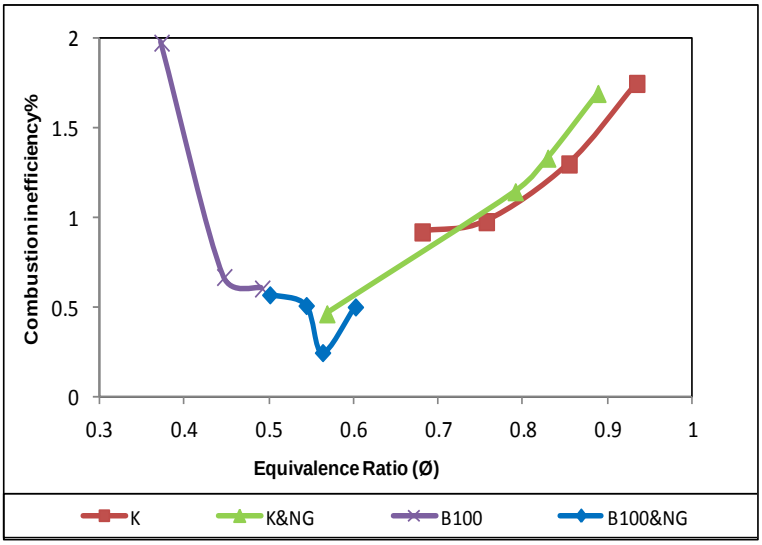

Figure 5.19: Combustion inefficiency as a function of equivalence ratio for K&B100 with and without NG co-firing.

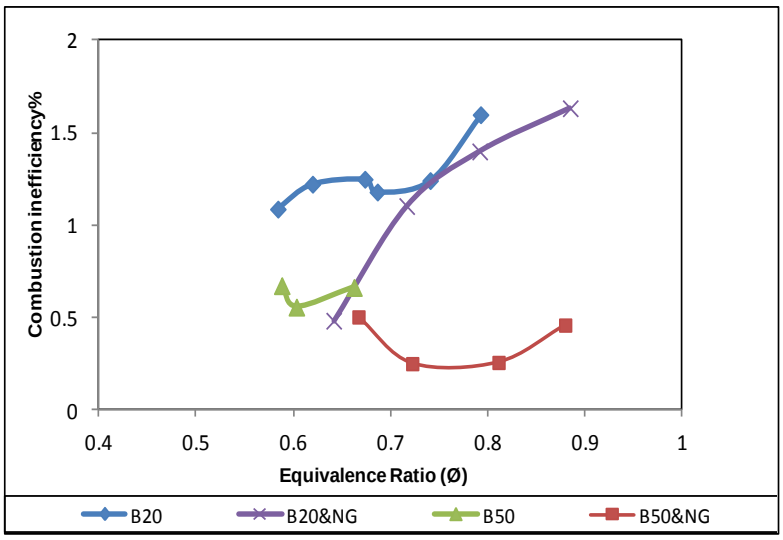

Figure 5.20: Combustion inefficiency as a function of equivalence ratio for B20&B50 with and without NG co-firing.

Combustion inefficiency results are shown in Figs.5.19&5.20 for all fuels with and without NG co-firing. Both graphs show that low combustion inefficiency for all fuel when co-fired with NG, especially B20 and B50 where less than 0.6% was achieved. At Ø =0.55, lowest combustion inefficiency (<0.3%) for B100. At this equivalence ratio, the lowest CO and UHC were generated for B100 when co-fired with NG.

Figs.5.21&5.23 show the comparison of NOx emissions as a function of equivalence ratio for all fuels with and without NG co-firing and Figs.5.22&5.24 as a function of flame temperature. Figs.5.21&5.22 show that the kerosene and NG flames had NOx <10ppm at Ø =0.6, which is a flame temperature of 1900K at the 600K inlet temperature. For the lowest

NOx measured at 7 ppm the flame temperature was 1800K. This is the region where thermal NOx has been eliminated if the fuel and air are well mixed. The radial swirler exit throat wall fuel injection gives good mixing and the NG combustion is effectively premixed. With liquid fuels injected at the central injector the mixing with air is not well mixed and locally rich zones are created which results in relatively high NOx emissions for the liquid fuels alone. The poor mixing helps the flames to have good flame stability. When liquid fuels are added to the NG flame the effect is to decrease the NOx emissions compared with only liquid fuels. Fig.5.21 shows that for Ø =0.7 the kerosene NOx results are reduced from 25ppm to 17ppm when co-fired with NG. For Ø =0.5 the NOx for B100 is reduced from 25 to 17 ppm when co-fired with NG.

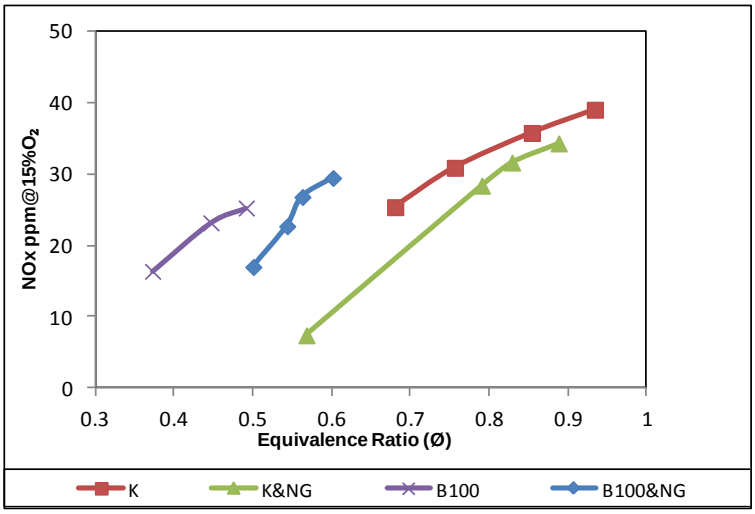

Figure 5.21: NOx emissions as a function of equivalence ratio for K&B100 with and without NG co-firing.

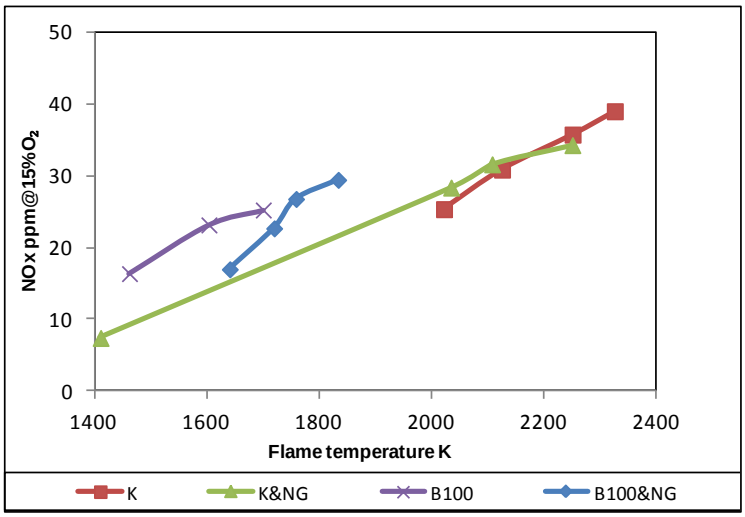

Figure 5.22: NOx emissions as a function of flame temperature for K&B100with and without NG co-firing.

For the blended fuels in Figs.5.23&5.24, at Ø =0.65, NOx is reduced from 34 to 9 ppm when B50 is co-fired with NG. There is a lower benefit for B20 as at Ø =0.65 the NOx was only reduced from 28 to 25 ppm. The reduction in NOx in all cases is due to the overall improvement in the total fuel and air mixing when a premixed NG/air flames at Φ=0.4 is present. For B50 and B100 with co-firing there were no smoke problems. Also there were no acoustic problems until the overall Ø was close to 0.9. This could not be achieved with only NG fuel and this is a further indication that the addition of the centrally injected liquid fuel to the near premixed near limit NG flame deteriorates the fuel and air mixing of the NG flame and this is beneficial in terms of control of acoustic resonance but is not beneficial for NOx.

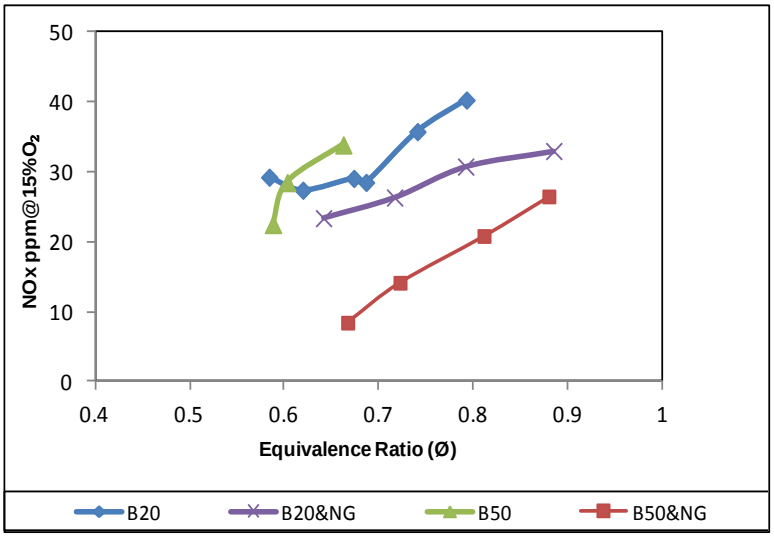

Figure 5.23: NOx emissions as a function of equivalence ratio for B20&B50 with and without NG co-firing.

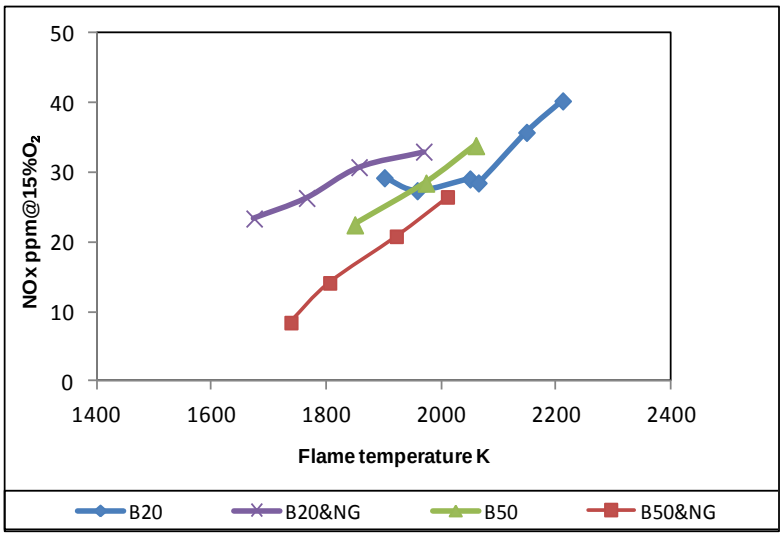

Figure 5.24: NOx emissions as a function of flame temperature for B20&B50 with and without NG co-firing.

Figs.5.25&5.26 present the NO_2/NOx ratios for all fuels with and without NG co-firing. Fig.5.25 shows that kerosene had more NO_2 with NG, but B100 had less NO_2 with NG. Fig.5.26 shows that at Ø =0.65 B20 had less NO_2 with NG and B50 had more NO_2 with NG then with the blended liquid fuels alone. There is clearly a complex influence on the flame conversion of NO into NO_2 that is influenced by the presence of premixed NG.

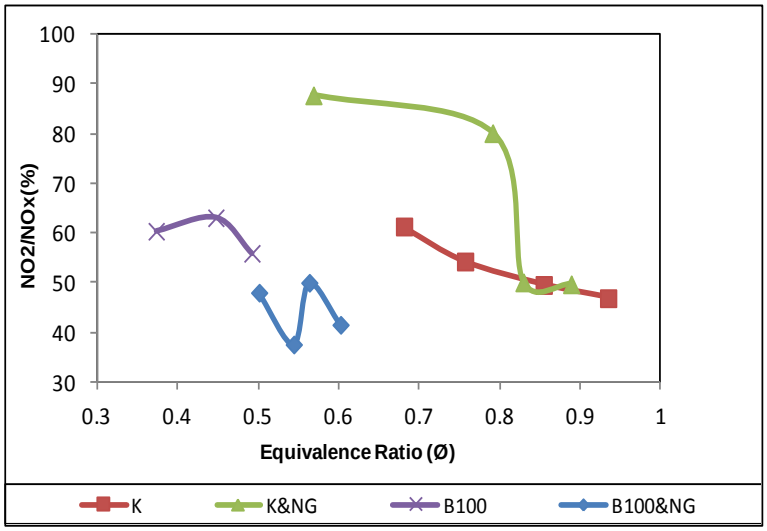

Figure 5.25: NO_2/NOx emissions as a function of equivalence ratio for K&B100 with and without NG co-firing.

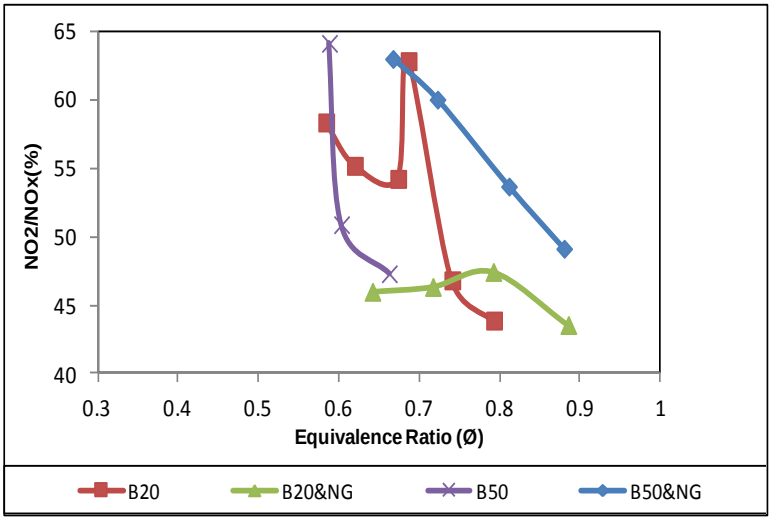

Figure 5.26: NO_2/NOx emissions as a function of equivalence ratio for B20&B50 with and without NG co-firing.

5.2.4 Effect of natural gas proportion when co-fired with biodiesel and kerosene at M=0.023

5.2.4.1 Weak extinction limit

Each fuel was tested to the leanest equivalent ratio that could maintain a stable flame and to the highest equivalent ratio (richest) that acoustic noise became unbearable. For BD (B100) and NG co-firing with BD case, the upper end of the curve (richest mixture) was constrained by the appearing of a large amount of white smoke from around the flanges of the combustor due to the evaporation of unburned biodiesel. This indicated that the lower volatility of biodiesel, compared to kerosene, caused serious problems on fuel vaporisation and atomisation. Only three equivalent ratios were tested for BD due to heavy white smoke.

These limiting equivalence ratios, Ø, are given in table 23, which also summarises all the fuelling configurations that were investigated. NG wall injection had a very good weak extinction close to that expected from fundamental flammability considerations[174]. However, the rapid mixing in this design led to the onset of acoustic resonance at Ø=0.55, which was leaner than has been found for single radial swirlers [54]. NG at the weak extinction, which is not normally a stable flame condition was operated with no problems when co-fired with BD central fuel injection, but there was no overall gain in the weak extinction or major change in the Ø for the onset of acoustic resonance (Ø=0.58 overall).

Table 23: Weak extinction Ø and the Ø limits constrained by white smoke or acoustic resonance.

Fuel	Weak extinction Ø	Maximum Ø at onset of acoustic resonance	Maximum Ø for white smoke
NG(W)	0.37	0.55	……..
NG(C)	0.25	0.63	
K(C)	0.62	0.93	……...
K (W)	0.39	0.75	-
BD(C)	0.28	……	0.49
K(C)&NG(W) at $Ø_{NG}$=0.18	0.71	0.88	……

K(C)&NG(W) at $Ø_{NG}$=0.22	0.64	0.86	…….
BD(C)&NG(W) at $Ø_{NG}$=0.18	0.46	……	0.6
BD(C)&NG(W) at $Ø_{NG}$=0.38	0.41	…….	0.58

(W) = Wall fuel injection; (C) = Central fuel injection

Central injection of kerosene is shown in table 23 to have a very poor weak extinction, which was worse than a premixed system would have. This was surprising as previous work with central injection with kerosene, but in simpler swirler configurations with a single radial swirler and no downstream throat [55, 68, 69] there was a very good weak extinction. It is likely that in the present work the depth of the double swirler and the length of the outlet duct that acts as a mixing passage, results in kerosene being better mixed by the time it reach the dump expansion swirling shear layer. However, this still does not explain why its stability was worse than for a premixed system. The poor kerosene central injection flame stability makes the NG co-firing tests not very good in terms of flame stability as there is no improvement on the poor stability of the kerosene central injection results.

A further issue with the central injection kerosene results was that it was very resistant to acoustic resonance up to Ø=0.93. If the weak extinction results indicate near premixed performance then this is normally accompanied by poor acoustic resonance resistance. This has not occurred in this case and the two unusual effects are probably linked. These results indicate that there is a controlling flame stability zone that is locally premixed but through which all the fuel does not flow. The fuel that does not pass through the premixed zone does not find a location in the flow to burn efficiently and this leads to the poor flame stability and high hydrocarbon emissions as will be shown later. With the premixed flame stabilising zone being isolated and not filling the combustion area, the conditions for acoustic resonance are not met. Internal flame compositional traverses and CFD investigations are required to validate this hypothesis. This indicates that the

flame stabiliser geometry investigated is not ideal to use with liquid fuel as a central ‘pilot’.

Kerosene works fine in this geometry when used as a main fuel using wall fuel injection and the excellent combustion efficiency and NOx results for this are shown later. The table also shows a weak extinction for kerosene injected in the wall location (using smaller fuel holes than for NG) has a premixed weak extinction performance and a wide operational range before acoustic resonance occurs. However, BD would not ignite when injected at this location and so it is not an option for co-firing with BD.

BD with central injection has completely different flame stability to that of kerosene and table23 shows that it is stable down to Ø=0.28, a conventional central injection pilot fuel performance. However, it is shown below that the CO and HC emissions were very high at Ø=0.36 and hence it can be assumed that as weak extinction was approached there was a continuing deterioration in the combustion efficiency. The fuel vaporisation relies on the central recirculation of heat from the main combustion zone. It is possible that this fuel is mainly contained upstream of the splitter orifice between the two radial swirlers, as shown earlier.

With co-firing with NG the stability deteriorates considerably and appears to have a near premixed flame stability, in spite of the poor atomisation expected with BD. This is unexpected as with NG pilot and NG main the flame stability is controlled by the pilot and the overall flame can burn leaner than the premixed limit[58]. When the NG main Ø was only 0.18 (which is well outside the flammable range) the overall weak extinction with co-firing was changed from 0.28 for BD to 0.46 with co-firing. It is significant that the sum of the BD Ø and the NG Ø exactly equals the weak extinction with co-firing. Also it is significant that when the NG Ø with B100 central injection is increased to 0.38 the overall weak extinction is 0.41.

This indicates that B100 does not have the conventional action of a pilot fuel when combined with premixed main fuelling. A possible explanation of the results, which is essentially the opposite hypothesis for kerosene discussed above, is that with B100 pilot there is a local zone which is not fully premixed but where all the fuel vapour accumulates and only part of the air. As the B100 fuel flow is decreased this zone approaches the premixed

weak extinction. When premixed NG is added to the air only part of this fuel enters the flame stability zone and the flow of BD has to be increased to maintain the temperature of this zone. Hence, the weak extinction deteriorates. This hypothesis needs internal flame traverses and CFD modelling to confirm its validity.

The unusual weak extinction results and the above interpretations are central to understanding the equally unusual emissions results. However, the emissions results do generally support the above hypothesis.

5.2.4.2 Kerosene Emissions Results

The carbon monoxide and unburned hydrocarbon emissions as a function of equivalence ratio are shown in Figs.5.27&5.28. CO emissions vary with equivalence ratio with higher levels as mixture get richer due to equilibrium CO increasing. There is also a combustion inefficiency contribution to CO emissions and this is due to inadequate residence time and poor fuel and air mixing. The present results show that the CO emission increase as the weak extinction is approached and the Ø that this occurs over is related to the weak extinction, but occurs considerably before the weak extinction in most cases with co-fuelling. The CO trends for most of the fuelling situations are similar but limited by the weak extinction. Only methane central injection has a weak extinction leaner than that for premixed combustion and this is the only fuelling that shows an increase in CO in the near region due to lack of residence time at the lower temperatures of lean combustion.

The UHC emissions were controlled by the weak extinction. They were low for high Ø but increased as weak extinction was approached. The energy content of the CO and UHC mass emissions give the combustion inefficiency and this is shown in Fig.5.29 as a function of the overall equivalence ratio for all fuels. In these plots the equilibrium CO has been treated as combustion inefficiency. The figure shows very low combustion inefficiencies in the region that low NOx occurs. However, the operational range of equivalence ratios is severely limited by the poor weak extinction characteristics of the different fuelling combinations.

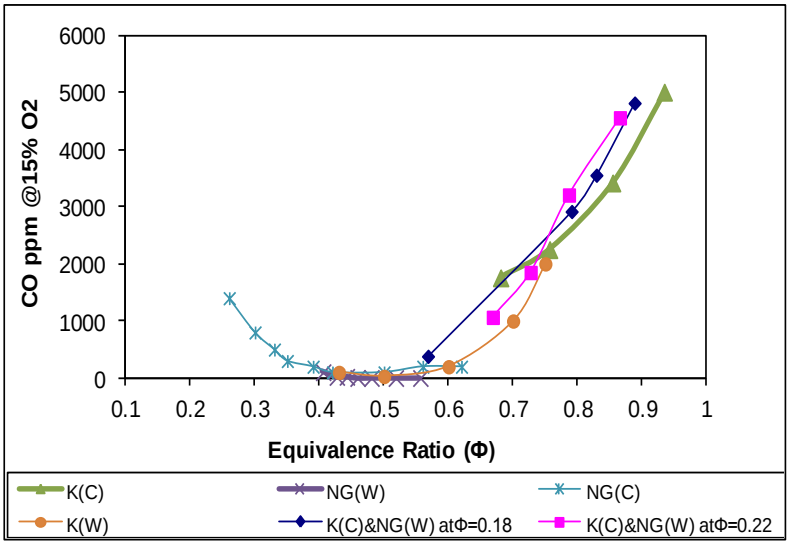

Figure 5.27: CO as a function of equivalence ratio for kerosene (central& wall), Natural Gas (central& wall) and NG co-firing with K at Ø=0.18& Ø=0.22.

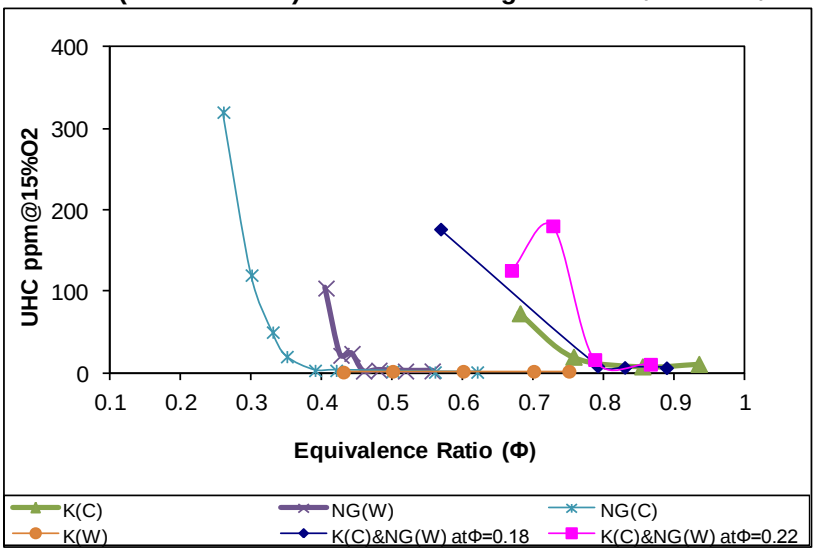

Figure 5.28: UHC as a function of equivalence ratio for kerosene (central& wall), Natural Gas (central& wall) and NG co-firing with K at Ø=0.18& Ø=0.22.

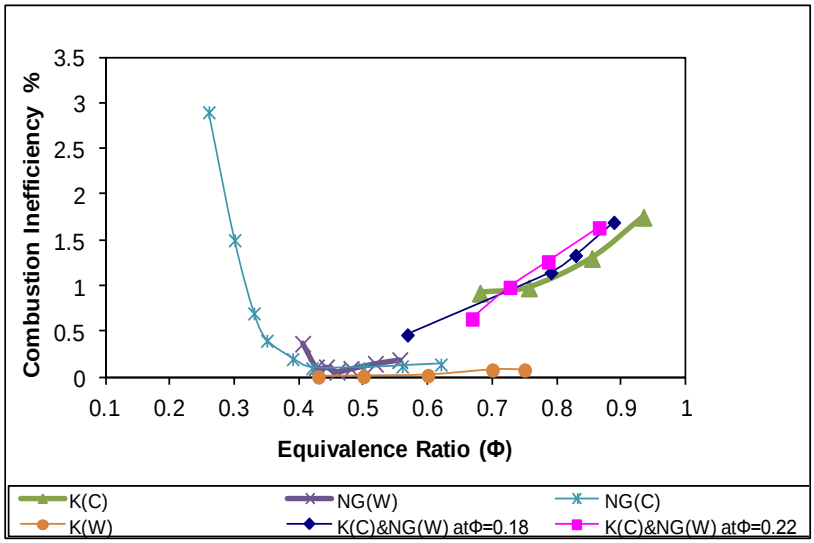

Figure 5.29: Combustion inefficiency as a function of equivalence ratio for kerosene (central& wall), Natural Gas (central& wall) and NG co-firing with K at Ø=0.18& Ø=0.22.

NOx emissions corrected to 15% oxygen are shown as a function of both the equivalence ratio in Fig.5.30 and flame temperature in Fig.5.31. The flame temperature plots are the most significant as they take into account the differences in calorific value of the fuels and the discussion will be mainly in relation to the temperature plots. For each fuelling configuration the results show the expected increase in NOx with increasing equivalence ratio and increasing flame temperature. However, there were some unexpected relative effects. Central injection NG has higher NOx than outlet throat wall fuel injection as has been shown previously [54, 55, 58, 68, 69].

However, the kerosene wall fuel injection NOx results were lower than those for NG, especially at higher temperatures. These are the lowest NOx of all the configurations tested, but this was not a fuel injection location that could be made to work with BD. Central injection kerosene was unstable at the equivalence ratios that the wall fuel injection with kerosene could operate. However, there was an overall equivalence ratio region around Ø=0.7 and the central injection NOx was much higher. However, when central injection of kerosene was combined with wall injection of NG at a NG Ø =0.18 the NOx was the same for the same flame temperature. It also had lower NOx than for central NG but higher than for wall NG. These results show that there is no practical advantage of co-firing with kerosene and show that kerosene is a much better fuel for wall fuel injection with perhaps central NG fuelling to act as a pilot for leaner operation.

Fig.5.32 shows the NOx corrected to 15% oxygen as a function of combustion inefficiency. This shows that only kerosene and NG wall injection had ultra-low NOx characteristics and the best results in terms of NOx and combustion inefficiency were for kerosene. All attempts to achieve good NOx results with co-firing with NG failed due to the flame stability problems discussed above. The kerosene results for co-firing would not lead to a decision to use this mode for BD/NG co-firing.

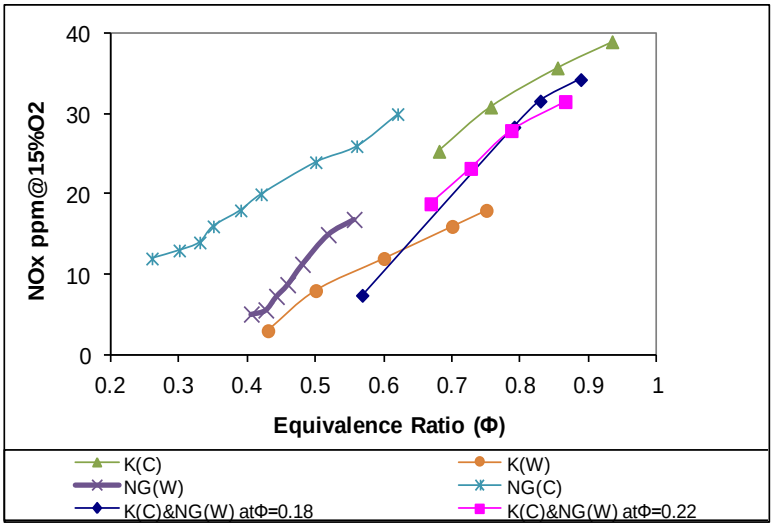

Figure 5.30: NOx as a function of equivalence ratio for kerosene (central& wall), Natural Gas (central& wall) and NG co-firing with K at Ø=0.18& Ø=0.22.

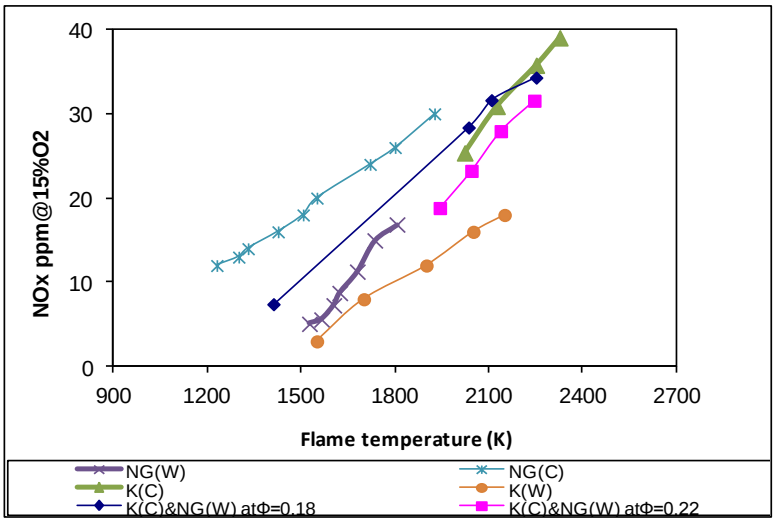

Figure 5.31: NOx as a function of flame temperature for kerosene (central& wall), Natural Gas (central& wall) and NG co-firing with K at Ø=0.18& Ø=0.22.

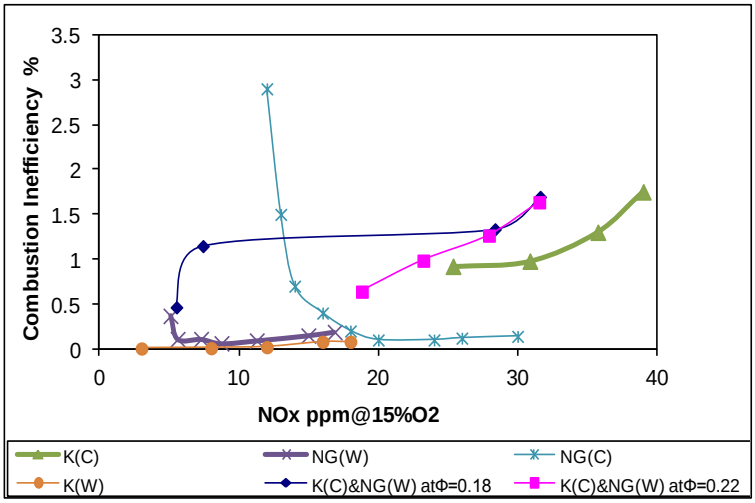

Figure 5.32: Combustion inefficiency as a function of NOx for kerosene (central& wall), Natural Gas (central& wall) and NG co-firing with K at Ø=0.18& Ø=0.22.

Fig.5.33 presents the NO_2/NOx ratios and shows that all co-firing modes had a greater proportion of NO_2. Kerosene co-firing with NG at the low NG flow rate Ø=018 had more NO_2 compared to the higher flow rate co-firing (Ø=0.22). NO_2 is formed in flame reactions zones by the conversion of NO to NO_2 by reaction with HO_2 in the flame reaction zone. To have a large NO to NO_2 conversion, as in the present work, the flame reaction zone has to be extended so as to have HO_2 radicals over a large distance in the flame and to have low flame temperatures, which is a requirement for low NOx, Co-firing essentially lengthens the flame zone starting near the central injector with one flame and the second main fuel flame burning in the products of combustion of the upstream flame.

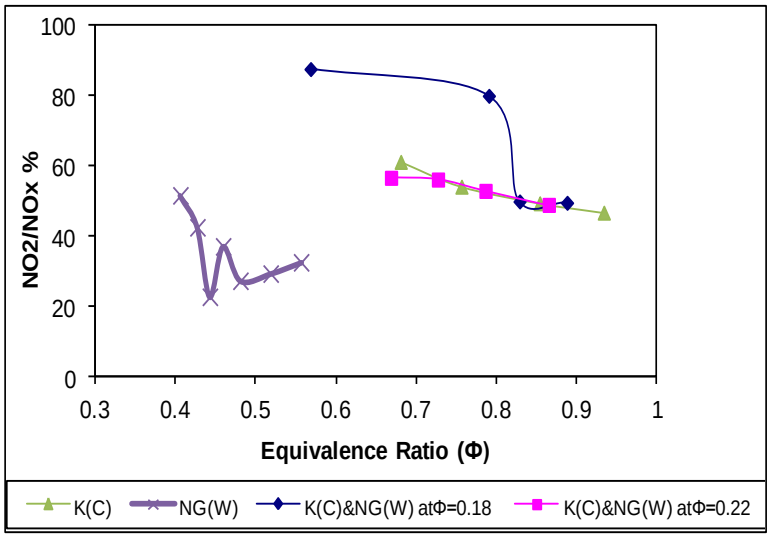

Figure 5.33: NO2/NOx as a function of flame temperature for kerosene (central), Natural Gas (wall) and NG co-firing with K at Ø=0.18& Ø=0.22.

5.2.4.3 Biodiesel Emissions Results

The CO, hydrocarbon and combustion inefficiency results are shown in Figs. 5.34 to 5.36.There was no biodiesel wall injection data available as it was unable to establish a stable flame. The increase in CO with equivalence ratio is due to the equilibrium CO trends. The increase in CO and UHC for very lean mixtures is due to the approach of weak extinction. The BD results for central injection were not very good with high CO and UHC due combustion inefficiency and not to equilibrium CO effects. For BD poor fuel

atomization and poor fuel vaporization is expected and the CO and UHC were higher than all the other fuelling configurations tested.

The NG central and wall results showed very good combustion inefficiency and the central injection results had efficient combustion in the lean region. Work is required to optimise the proportion of BD fuel used so that the maximum NG consumption can be reduced with the greatest CO_2 savings. This central fuel injector location forms a good pilot flame for natural gas low NOx combustion and was the only fuel injection location that biodiesel combustion could be stabilised as the region injected the fuel into the hot recirculating gases on the centreline that is a feature of radial swirl lean low NO_X combustion. The biodiesel results were compared with equivalent tests for kerosene as the central injection fuel.

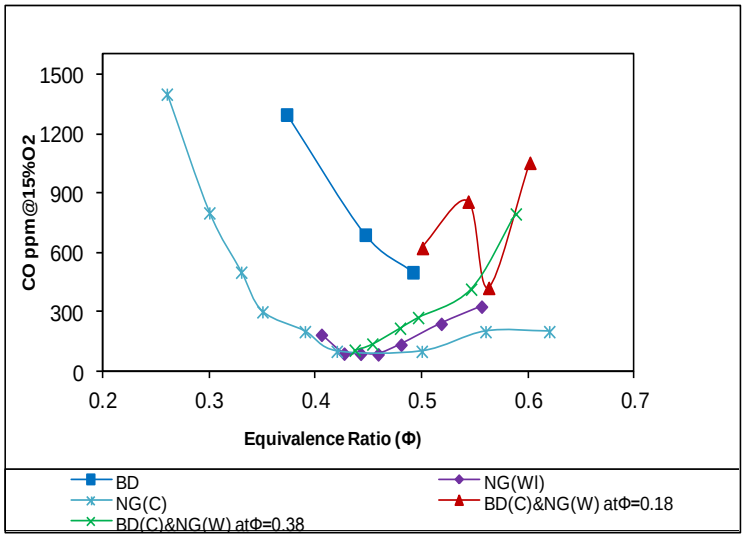

Figure 5.34: CO as a function of equivalence ratio for Biodiesel (central) and Natural Gas (central& wall) co-firing at Ø=0.18& Ø=0.38.

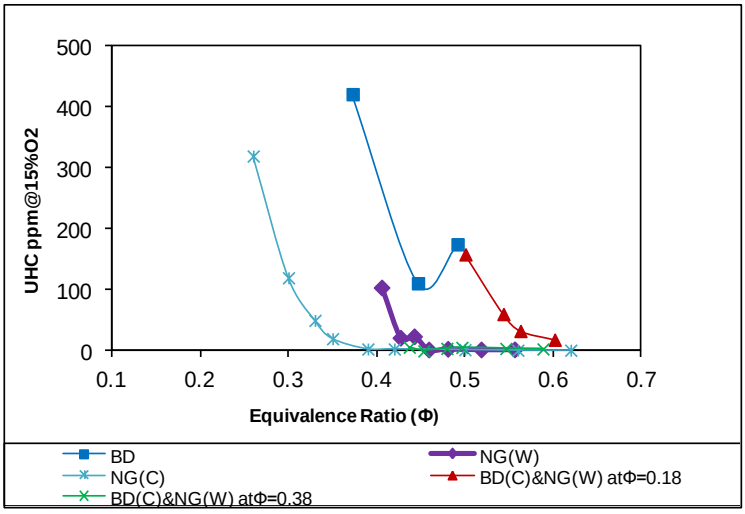

Figure 5.35: UHC as a function of equivalence ratio for Biodiesel (central), Natural Gas (central& wall) and NG co-firing with K atØ=0.18&Ø=0.38.

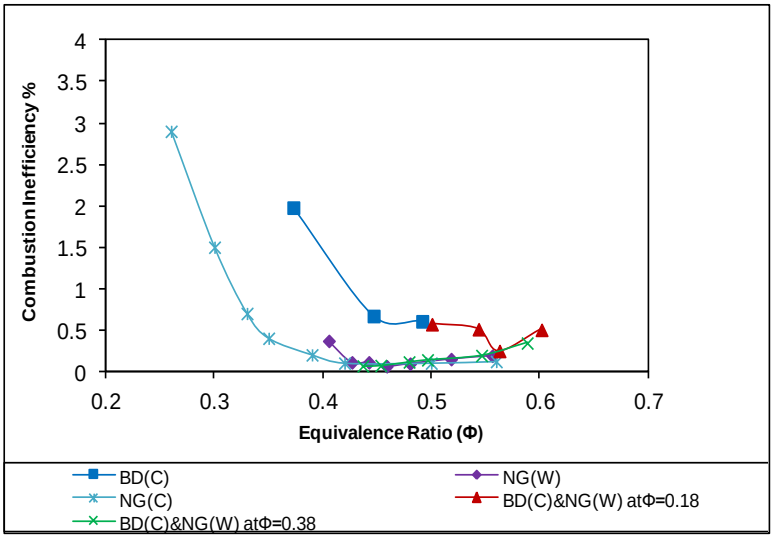

Figure 5.36: Combustion inefficiency as a function of equivalence ratio for Biodiesel (central), Natural Gas (central& wall) and NG co-firing with K at Ø=0.18& Ø=0.38.

The NOx emissions are shown as a function of the equivalence ratio in Fig. 5.37 and flame temperature in Fig.5.38. The NG central injection results had much higher NOx than the near premixed wall injection. BD had the same NOx for central injection as for NG for the same flame temperature as shown in the figure. When BD was the central injection fuel and NG the same wall injection the resultant NOx was significantly reduced from that of BD central injection. The NOx was higher than for NG alone for the same flame temperature but was relatively low and could be design to meet NOx emissions regulations below 25ppm.

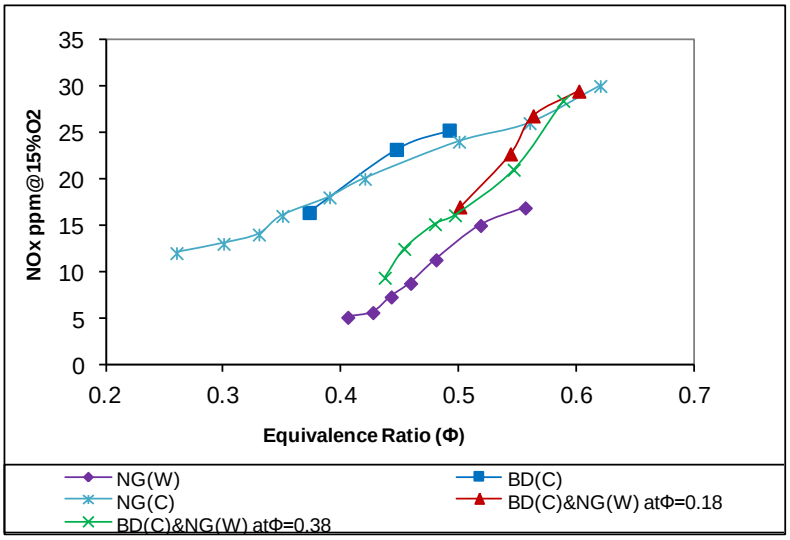

Figure 5.37: NOx as a function of equivalence ratio for Biodiesel (central), Natural Gas (central& wall) and NG co-firing with K at Ø=0.18& Ø=0.38.

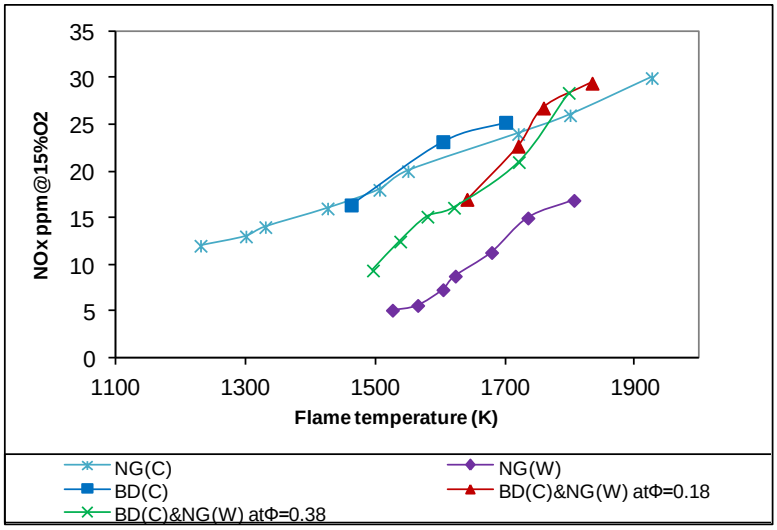

Figure 5.38: NOx as a function of flame temperature for Biodiesel (central), Natural Gas (central& wall) and NG co-firing with K at Ø=0.18& Ø=0.38.

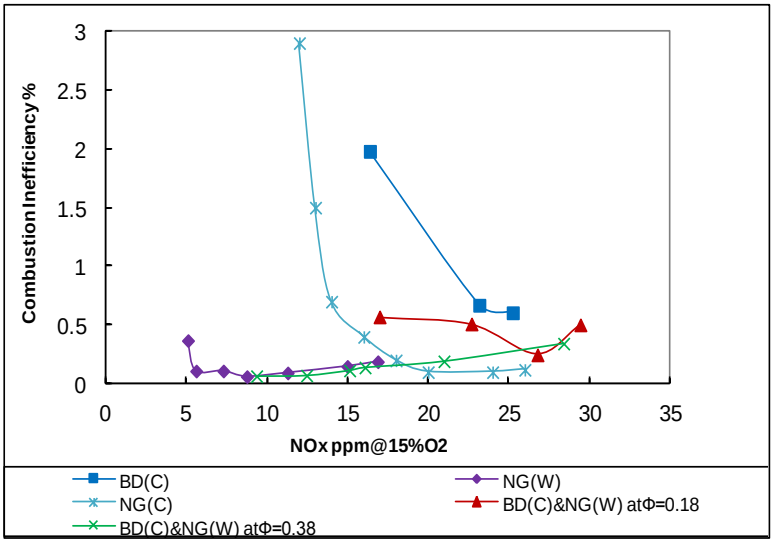

Figure 5.39: Combustion inefficiency as a function of NOx for Biodiesel (central), Natural Gas (central& wall) and NG co-firing with K at Ø=0.18& Ø=0.38.

The NOx emissions corrected to 15% oxygen in Fig.5.39 show very good NOx emissions for co-firing with 10ppm NOx corrected to 15% oxygen starting at 8ppm with mainly gas fuelling but as BD is added increases to 25ppm as B100 is increased. This is effectively increasing power on BD with no change in NG. This could translate to engine operation from 50 to 100% power on BD with power to 50% from NG. This would present a significant CO_2 saving and a major cost saving if there was a fiscal incentive attached to the CO_2 saved, as there is in many countries.

The NO_2/NOx ratios are shown as a function of Ø in Fig.5.40. This shows lower ratios than in Fig.5.33 for kerosene co-firing. The BD central injection results had the highest NO_2/NOx ratio and this indicates a slowly

developing low temperature flame which promotes the NO and HO_2 radical reaction to form NO_2. The lowest NO_2 was for NG wall injection at around 30%, but the addition of BD in co-firing only increased this to around 40%. In most circumstance these levels will be sufficiently low for the NO_2 emitted not to be visible (about 15ppm is visible in a stack).

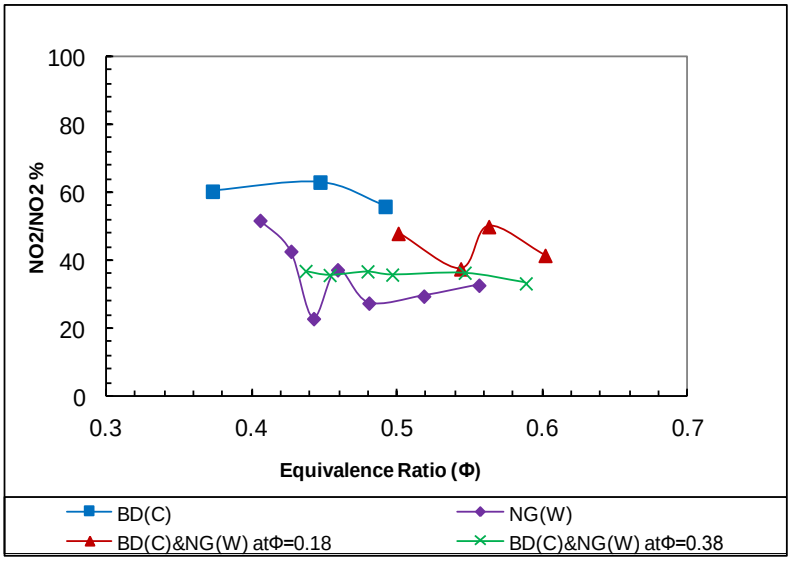

Figure 5.40: NO_2/NOx as a function of equivalence ratio for Biodiesel (central), Natural Gas (wall) and NG co-firing with BD at Ø=0.18& Ø=0.38.

5.3 Conclusions

A waste cooking oil derived methyl ester biodiesel (WME) has been tested on a radial swirler industrial low NOx gas turbine combustor under atmospheric pressure and 600K. The pure WME and its blends with kerosene (B20 and B50) and pure kerosene were tested for lean extinction and gaseous emissions as a function of equivalence ratio with and without co-firing with natural gas (NG). The central fuel injection was used for liquid fuels and radial swirler outlet throat wall injection was used for NG. The experiments were carried out at reference Mach number of 0.017 and 0.023. Also natural gas proportion on emissions at higher Mach number was investigated. The following conclusions have been drawn:

1) The lean extinction limit has been tested and is related to the fraction of biodiesel. The more the fraction of biodiesel, the lower the lean extinction limits. The reduced emissions and lower extinction limit with biodiesel is considered due to the oxygen content in the fuel, which assisted the combustion process.

2) The weak extinction results showed that for all the liquid fuels studies the addition of premixed NG deteriorated the flame stability of the liquid fuel flames. Alternatively the results show that the addition of liquid fuels to premixed NG flames deteriorates the weak extinction of the flame. The liquid fuel flames, especially those with the high boiling point WME, do not burn in the central zone and are vaporized in the premixed NG flame. This acts to cool the flame and this deteriorates the flame stability.
3) At M=0.017, by co-firing with NG, the NOx emissions were reduced up to 30% for B20 and 50~70% for B50. The level of NOx emissions using co-firing was lower than any liquid fuel without co-firing. The NO_2 fractions were reduced by co-firing and maintained a constant level of 30~40% regardless the change of the equivalence ratio.
4) The CO emissions for B20 and B50 were reduced by a factor of 4~5 by NG co-firing. The NG co-firing also reduced UHC emissions when the equivalence ratio was leaner than borderline conditions, which was φ=0.4 for B100 and φ=0.6 for B20, where the UHC emissions would increase significantly without NG co-firing at lower Mach number.
5) The NG co-firing enabled the B50 to be tested using richer mixtures without causing smoking problems around the combustor. This indicated that the NG co-firing helped the vaporization of the fuel and thus be useful for more viscous fuels such as biofuel and blends at M=0.017.
6) At higher Mach number, the NOx emissions were below 10ppm with kerosene co-fired with NG for Φ<0.6. With the addition of NG for the same Φ there was a reduction in NOx compared with the liquid fuel alone, for the same Φ. This was greatest for B50 with NG when NOx was reduced from 34ppm to 9 ppm when premixed NG was present. This reduction in NOx was due to the improvement in overall mixing of fuel and air by injecting liquid fuel into a near premixed main flame.
7) The presence of premixed NG flames strongly reduced the CO emissions at the same Φ, particularly for B50 and B20/NG flames.

8) UHC emissions were relatively low for B100 indicating that fuel vaporization was not a major problem. This indicates that the central fuel injection of liquid fuels is vaporized by the recirculation of burnt gases on the centerline of the radial swirler. This process is not strongly dependent on the atomization of the fuel at M=0.023.

The Effect of natural gas proportion co-fired with biodiesel and kerosene at M=0.023 has been investigated and main conclusions surmised as a following:

1) Co-firing of B100 was practically feasible with no major problems. The central fuel injector location forms a good pilot flame for natural gas low NOx combustion and was the only fuel injection location that biodiesel combustion could be stabilised, as the region injected the fuel into the hot recirculating gases on the centreline that is a feature of radial swirl lean low NOx combustion When B100 was the central injection fuel and NG the same wall injection the resultant NOx was significantly reduced from that of B100 central injection.
2) The NOx was higher than for NG alone for the same flame temperature but was relatively low and could be design to meet NOx emissions regulations below 25ppm. This is effectively increasing power on B100 with no change in NG. This could translate to engine operation from 50 to 100% power on B100 with power to 50% from NG. This would present a significant CO_2 saving and a major cost saving if there was a fiscal incentive attached to the CO_2 saved, as there is in many countries.
3) The key problem was very poor flame stability for kerosene with central injection. In contrast the B100 as a pilot fuel had an excellent performance in a co-firing mode, but not well on its own.

Chapter 6 : Determination of particle line loss for gas turbine engine exhaust particle measurement

6.1 Introduction

Aircraft and other airport activities in the airport have great effects on the air quality of both the airports and the neighboring regions. Emissions from aircraft are not only injected into planetary boundary layer, but also, into the upper troposphere and lower stratosphere [9, 15, 139]. Particulate matter (PM) affects the air quality and has been classified as a potential health hazard according to Environmental Protection Agency (EPA) of the USA [175].

The national Ambient Air Quality Standards set limits for PM2.5 on a 24hr and annual basis. The measurement of the aircraft engine PM emission provides knowledge on the magnitude of effect this emissions contribute to the environment and would help both the aircraft manufactures and airport authorities to take actions to reduce emission levels by adopting various methods from manufacturing of low emission aircraft engines, effective use of aircraft route of operation to the use of low emission technology infrastructure in the airport. [141, 176].

There are no regulatory and certified methods for direct sampling and measurement of PM emitted from aircraft engines. As the emission regulation is getting stringent, there is a need to develop a concept sampling system in terms of components, manufacturer and operability to standardize PM measurement. ICAO has planned to introduce particle number regulation for aircraft engines in 2016 for non-volatile particles[177]. Thus, there is a need to quantify the fractions of volatile particles and determine the line losses for non-volatile particles. A VPR and CS were used to remove volatile particles in this chapter to provide a non-volatile exhaust sample to the number counting instruments.

Due to safety rules and standards from the aircraft engine exhaust testing, a certain distance from the engine exhaust is required before the extraction of test sample can be taken. In reality there would have been a significant of chemistry and diffusion occurred before the exhaust sample can be extracted for measurement. So it is crucial to determine the particle loss during transportation in the sample line. The major factors affecting the

particle loss in the sampling line include the residence time, coagulation of particles and wall losses due to collisions etc [178]. Particle losses varied depending on particle compositions and sampling system configuration such as dilution method and sample flow rate etc. Timko et al[179] estimated particle losses of aircraft engine exhaust and found it was about 30% for particles ranging from 30nm to 300nm and 80% for particles range 10nm or less.

The work in this chapter investigates the particle line losses for total and non-volatile PM using SAE ARP PM sampling line from the APU engine. The details of the engine has been described in section 3.1.2. Jet A1 was used as fuel.

6.2 Results and Discussion

In order to obtain the complete exhaust size distribution from 5-400nm, both results of nano and long SMPS data were used to analyse particle size distributions. At each sampling point both SMPS were used to measure the number and size distribution with and without CS. Particles at point (1) could not be measured as there is no dilution available. Table 14 shows description of each point.

6.2.1 Determination of total particle losses through sampling lines.

Figs.6.1&6.2 present particle size distributions for point 2&3 at idle and full power respectively using JetA1 fuel. All results show mono modal distributions and there are noticeable losses along the 25 meters sampling line for PM across the entire size distribution with higher losses for the smaller sized PM. As seen in Fig.6.1, the peak particle concentration at particle size (~ 25 nm) at idle power is 40% higher than that of the same particle concentration after 25meter sample line. This shows that a significant amount of particle loss over the 25meter sampling line, this is as a result of increase in the rate of coagulation and particle wall line loss taking place over the 25meter line thereby resulting in the overall decrease in the

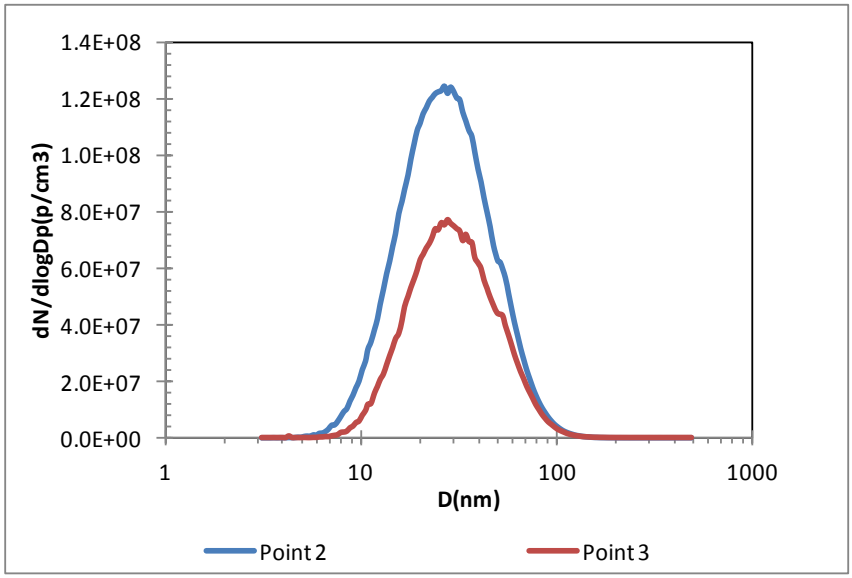

Figure 6.1: Particle size distributions measured at different sampling points at idle.

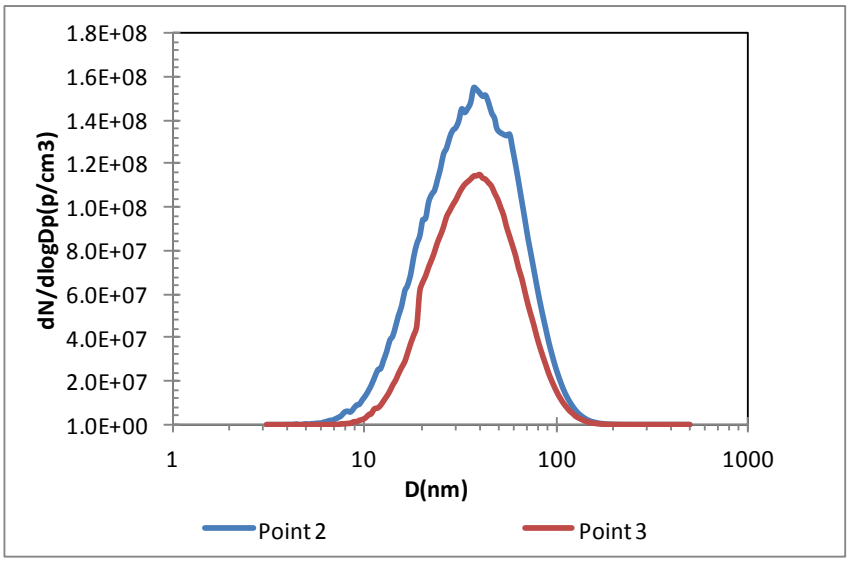

Figure 6.2: Particle size distributions measured at different sampling points at full power.

particle concentration after the 25 meter sampling line. Whereas at full power ~35% of the particles were lost in the sample line as shown in Fig.6.2.

Fig.6.3 shows the measured particle penetration factor generated for idle and full power conditions. For the particle size less than 10nm, about 70-100% of the total particles were lost in the sample line at both power conditions (idle and full power) as shown in Fig.6.3.The loss was 25-50% for particulate in the size range of10-100nm. The figure also shows that as the particle size increases, the loss in the sample line decreased to reach 0% loss for particles larger than 100nm at full power. The penetration factors for all particle sizes in this study are slightly higher than that found by Lobo et al

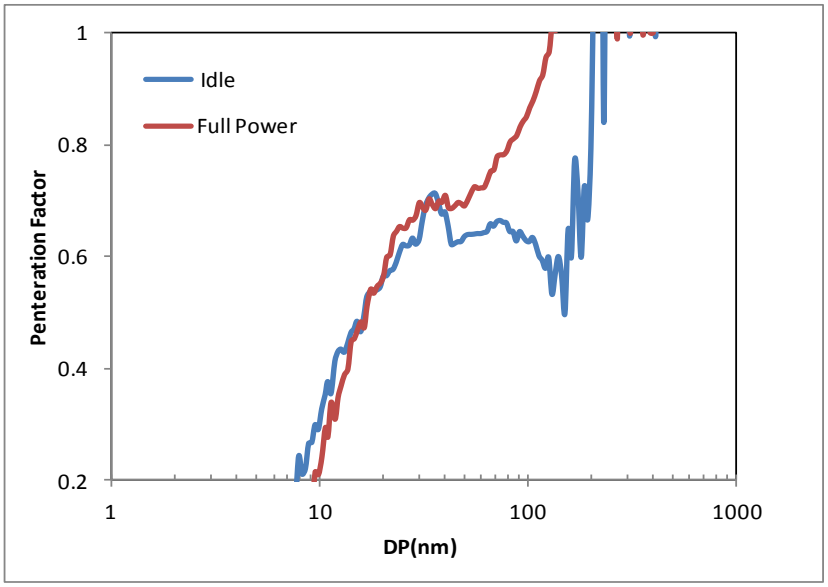

Figure 6.3: Penetration factor at idle and full power mode.

using a truck diesel engine at the same conditions. In this research the dilution was added at 10m downstream of sampling probe which could significantly have enhanced particle formation. Wong et al suggested that the dilution must be introduced upstream of a critical location which corresponds to the onset of particle formation microphysics about 1m downstream of the probe tip. This also fit with the conclusions stated in SAMPLE II that the higher losses occurred with increased residence time and line length [119, 180].

6.2.2 Determination of the non-volatile PM through sampling line

Figs.6.4&6.5 represent the results of particle size distribution for each point at Idle and full power with and without catalytic stripper (CS). The total and non-volatile particle concentration have been measured and compared. The function of the CS was to remove the volatile particles present in the exhaust sample by oxidation.

Fig.6.4 represents the total and non-volatile PM at point 2, 3 and 5 during idle power respectively. The result in the figure shows that at each point there is lower number concentration after CS compared to total PM and the reduction was across the entire size distribution as the volatile particles have been removed. Fig.6.4 showed that the difference between total particles to non-volatile is about 25%, 30% and 12% for point 2,3 and 5 respectively. These percentages represent the amount of volatile particles

being detected and removed by CS at each point. The particles at size 26 nm (±2) have the highest amount of total and non-volatile particle concentration at point 2&3.

At full power there is a higher combustion temperature in the combustion chamber than at idle power operating condition, resulting in lower amount of VOC gas emitted which resulted in lower amount of volatile particles produced as shown in Fig.6.5. For point 2 at idle and full power, the non-volatile PM represents about 75% of the total particles, whereas P3 non-volatile particles at full power higher than at idle. Fig.6.5 also showed non-volatile PM has been reduced from 88% at idle to 78% at full power resulting in higher number of volatile particles emitted.

.

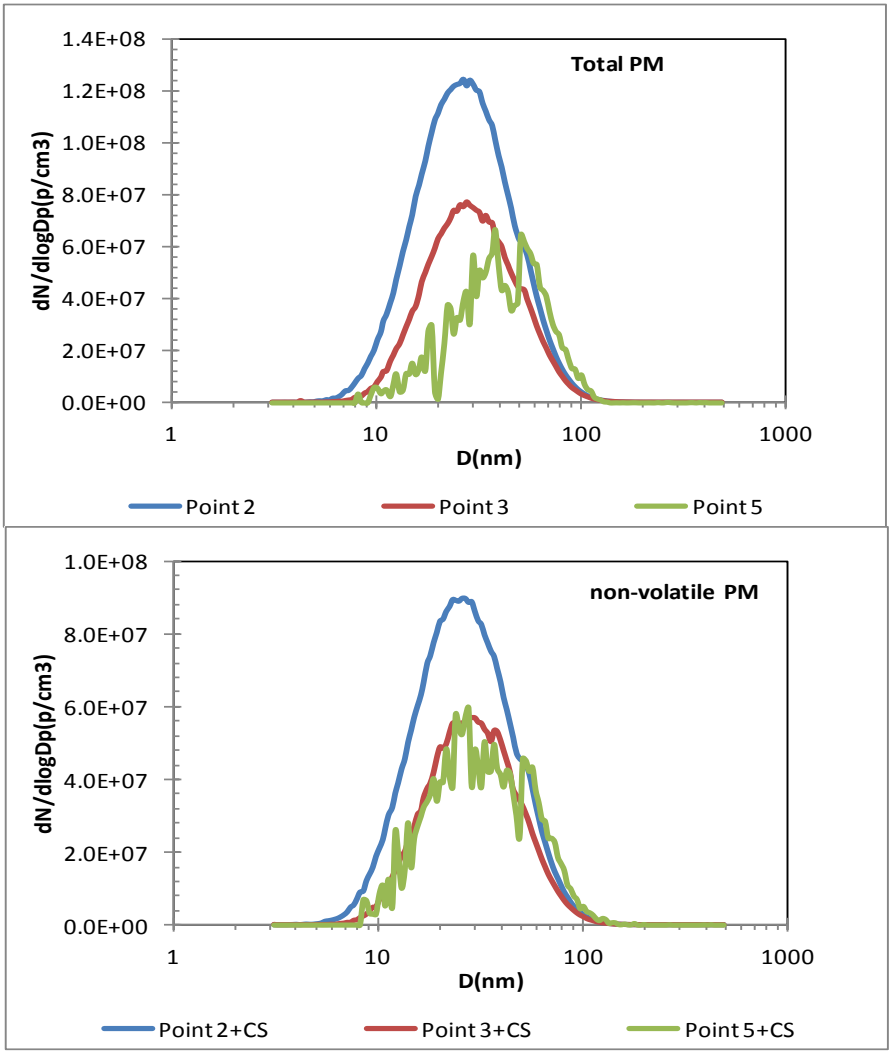

Figure 6.4: Total and non-volatile particles for different sampling positions at different sampling positions at idle.

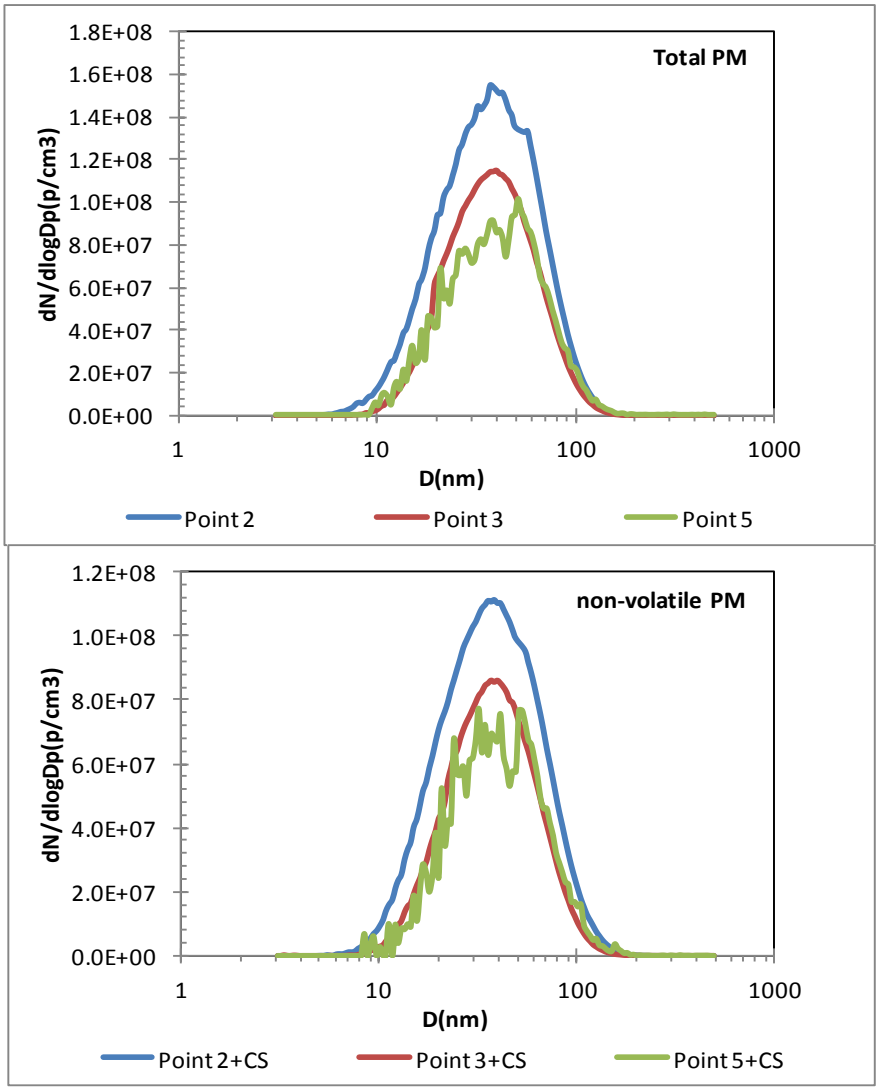

Figure 6.5: Total and non-volatile particles for different sampling positions at full power.

Fig.6.6 presented penetration factor for non-volatile particles at idle and full power conditions. Similar observation has been seen as in Fig.6.3, for the particle size less than 10nm, about 70-100% of the total particles were lost in the sample line at both power conditions. However, for particles between 10nm and 100nm the loss was 25-50% and there was no loss for particles larger than 100nm especially at full power mode

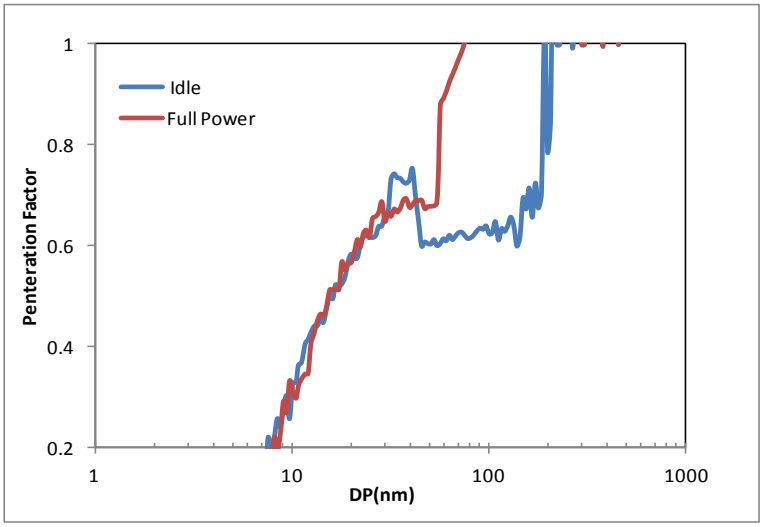

Figure 6.6: Penetration factor at idle and full power for non-volatile PM.

6.2.3 Comparison of total number, Geo mean diameter and Standard deviation at different points

Figs.6.7 to 6.9 represent Geometric mean diameter, standrad diviation and total particle concentrations for each point at idle and full power using JetA1 as a fuel. Geometric mean diameter increases with increasing fuel flow rate for all points and the average mean diametr is 26nm and 30nm at idle and full power respectivly. The results of geometric standrad diviation is presented in Fig.6.7 and is independet of fuel flow rate with averge value of (1.45-1.5). it is related to the width of the size distrbution. Total particle concentration generally increases with increasing fuel flow rate as shown in Fig.6.8. Point (2) has got the highest number of the total for both conditions, whereas the total concentarion for point (3) and 5 at full power is similar.

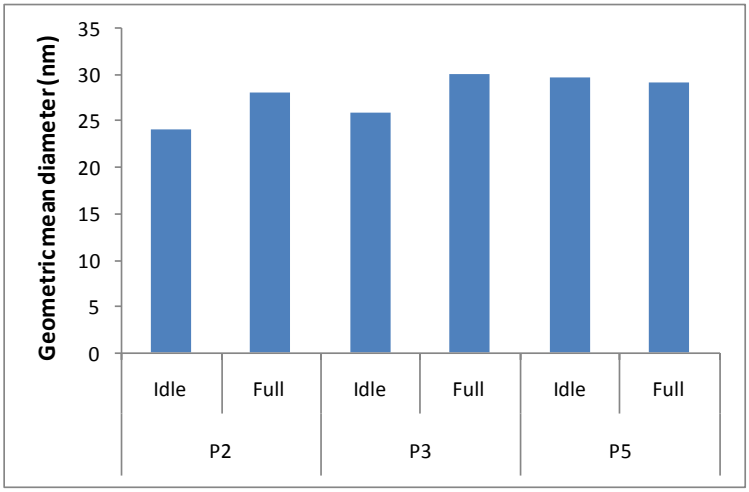

Figure 6.7: comparison of Geometric means Diameter of point 2, 3 and 5 at idle and full power.

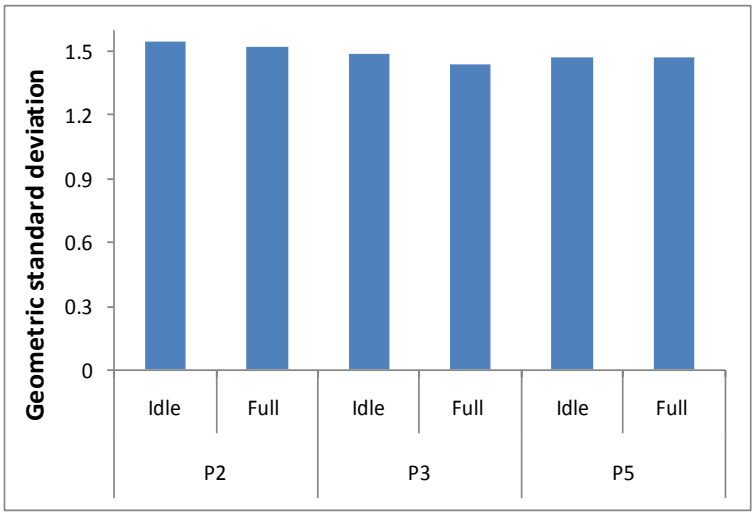

Figure 6.8: comparison of Geometric standard Deviation of point 2, 3 and 5 at idle and full power.

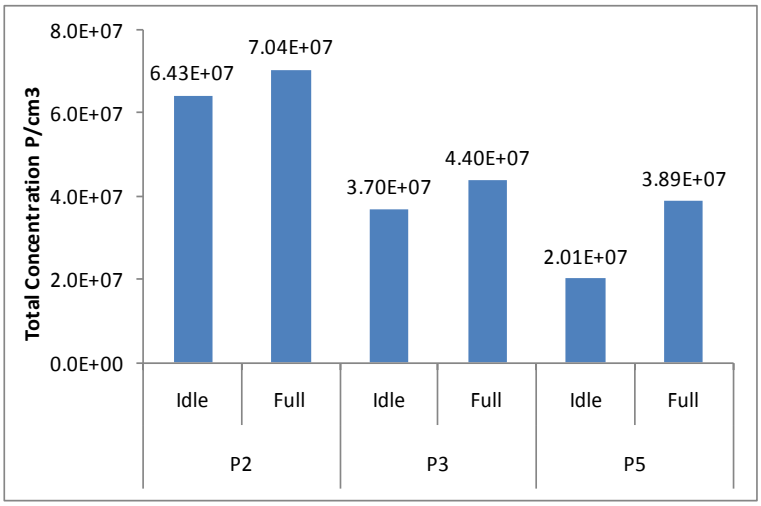

Figure 6.9: comparison of total concentration of point 2, 3 and 5 at idle and full power.

Fig.6.10 presented Particle loss for total particle concentrations. The total particle number concentration for point 3 is about 40% and 35% lower than that for point 2 at idle and full power respectively. Whereas at point 5 about 70% and 50% of the particles lost and removed by VPR at idle and full power compared to point 2.

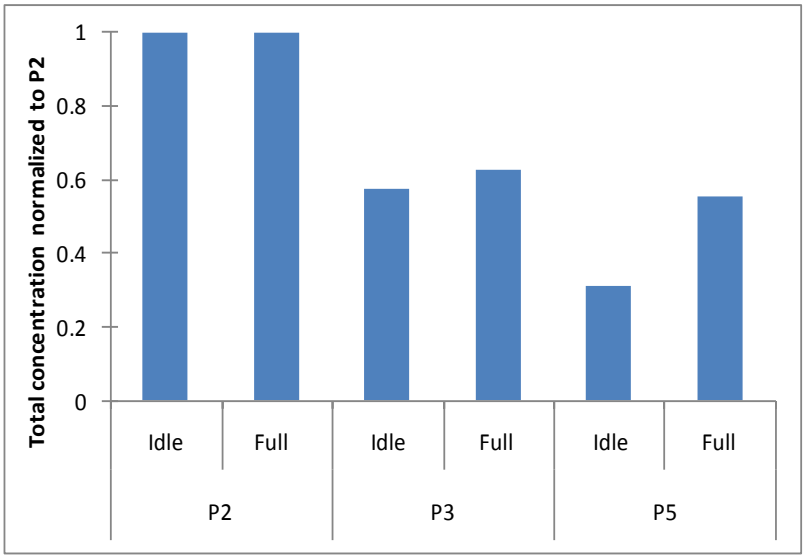

Figure 6.10: Total particle concentrations normalized to P2.

6.3 Conclusions

Results of measurement of particle number size distribution from an auxiliary power unit (APU) of an aircraft at idle and full power are presented to investigate the particle line loss of the sampling system. The following findings can be drawn from the results:

1) All results show mono modal distributions and there are noticeable losses along the sampling system for PM across the entire size distribution with higher losses for the smaller sized PM and the majority of PM losses in the sampling line occur between sampling point 2 &3.
2) At idle and full power a significant amount of 40% (±5) PM concentration was lost over the 25m sampling line. This was due to the coagulation and wall losses over the 25m sampling line. A correction factor can be implemented on further test using a 40% PM line loss over a 25m sampling line to determine the precise emission at the exhaust tip of the APU.
3) The volatile PM concentration emitted at full power was very low and almost lost totally over a 25m sampling line due to coagulation and wall line loss.
4) There is a higher amount of volatile PM emitted at idle power compared to that emitted at full power. This shows that the amount of hydrocarbons emitted at idle power is higher than that emitted at full power.

5) The results of the particle concentrations show a range of 10^{05} particle/cm^3 to 10^{08} particle/cm^3. At idle power peak PM size concentration is recorded at 26nm (±2) particle size having concentration of 1.27×10^{08} particle/cm^3 and at full power 49.6nm (±2) particle size with concentration of 1.69×10^{08} particle/cm^3.
6) Geometric mean diameter increases with increasing fuel flow rate for all points and the average mean diametr is 26 &30 nm at idle and full power respectivly. Geometric Standrad diviation is independet of fuel flow rate with averge value of (1.45-1.5). Total particle concentration generally increases with increasing fuel flow and point 2 has got the highest number of the total at idle and full power, where as the total concentarion for point 3 and 5 at full power is similar.

Chapter 7 : Comparison of Alternative Fuels Emissions from an Auxiliary Power Unit (APU) Engine.

7.1 Introduction

There is presently a strong interest in utilizing alternative fuels for aviation due to negative environmental consequences of conventional petroleum fuels. There are many types of petroleum alternatives are being considered include synthetic fuels derived from the Fisher-Tropsch process and biomass derived fuels[103, 181]. Synthetic fuel is a liquid fuel derived from various sources such as coal, natural gas (NG) and biomass in which carbon monoxide and hydrogen are converted to liquid hydrocarbons in the presence of metal catalyst such as iron, cobalt or nickel [182, 183]. The absence of aromatic content and purities of synthetic fuels are the main advantages compared to conventional fuels[183]. Hydro-processed vegetable oils (HVO) or Hydro-processed renewable jet fuels are the renewable aviation fuels that are derived from vegetable/plant oils and animal fat. As the feedstock's of vegetable oils and animal fat are limited, there is a competition between road transport and aviation for the demand of these feedstock's[19] [20].

The transesterification process of vegetable oils and animal fat to make biodiesel is easy and cheaper and has been widely used. This puts an extra pressure on the renewable aviation fuels, which must demonstrate a clear advantage in environment to compete with road transport regardless other obstacles such as cost. So there is a need to fully understand the environmental impact of alternative aviation fuels before they can be deployed in mass. However, there is a challenge for the utilization of alternative fuels that need a full understanding of the environmental impact of alternative fuels. The speciation of hydrocarbon pollutants will contribute to the understanding of the impact of air transport on global (cruise mode) and local air quality (airport) issues.

Edwin et al [8] carried out a comprehensive test using seven alternative fuels in six gas turbine engines for gaseous and particulate emissions. They found that all alternative fuels reduced particulate emissions significantly but the reductions on gaseous emissions were limited. The relative reductions

were higher at lower engine power than that at higher engine power. The reductions were greater for older engines than newer engines.

Timko et al[103] tested four alternative and blend fuels using CFM56-7 as a test engine for regulated emissions, volatile organic compound (VOC) and particulate emissions. They concluded that NOx emissions were reduced by 10%, 5%, 29% and 23% for 100% FT, 50% FT, 40% FAME blend and 20% FAME blend compared to JetA1 respectively. There were 31% and 25% reduction in CO for 100% FT and 40% FAME compared to JetA1 at idle (7%) respectively.

In this study, the gaseous and particulate matter emissions of APU were evaluated. Details about the engine, fuel properties and experimental set up were described in section 3.1.2. The engine was fuelled with standard JetA1 fuel and was tested at two power settings. In addition, two set of fuels (Compositionally designed surrogate fuel and alternative aviation fuels) were tested and compared to base fuel. Gaseous and volatile organic compounds will discussed in this chapter, whereas, Particulate matter will be discussed in chapter 8.

7.2 Experimental Results and Discussion

7.2.1 Gaseous Emissions

7.2.1.1 Compositionally designed surrogate fuels

Gaseous emissions were measured using a FTIR Gasmet CR-2000 analyzer and the undiluted sample was drawn through a gas probe and transferred to the instrument via a heated sample line (150°C) as recommended by the SAE.

APU gaseous emissions including carbon monoxide (CO_2), carbon monoxide (CO), total hydrocarbon (UHC), and nitrogen oxides (NOx) were measured at idle and full power and converted to their perspective emissions indices using the conventional method for the computation of emissions index (EI_m) using equation (24) and presented in Figs.7.1 to7.5 respectively.

The measured CO_2 emission index is presented in Fig. 7.1, Fuels A, B, and D had very close hydrogen/ Carbon ratios (~2), the amounts of CO_2 emissions are similar. Despite fuel C has similar H/C ratio to fuels A, B, the amount of CO_2 is higher. However, CO_2 decreased as hydrogen to carbon

ratio increased and GTL had the lowest CO_2 about 2940 g/kg with H/C ratio about 2.2 compared all fuels. As mentioned earlier, the high H/C ratio in fuel E resulted in higher water vapour, which is shown in Fig.7.2. It is also shown in Fig.7.2 that JetA1 produced the lowest amount of water vapour due to its lowest H/C ratio. The higher water vapour emissions have no air quality concerns but in the context of aviation, this may have impact on the formation of contrails.

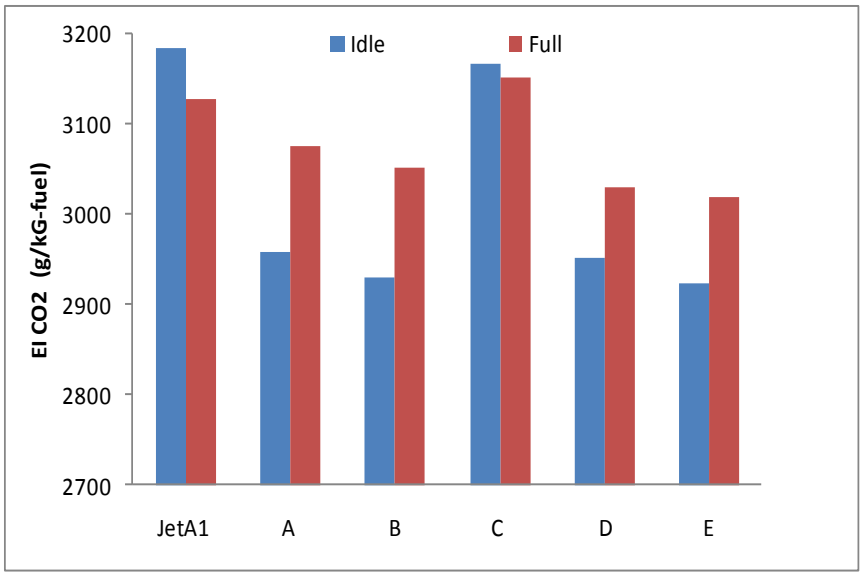

Figure 7.1: EI (CO_2) emissions (g/kg-fuel) for all fuels at idle and full power.

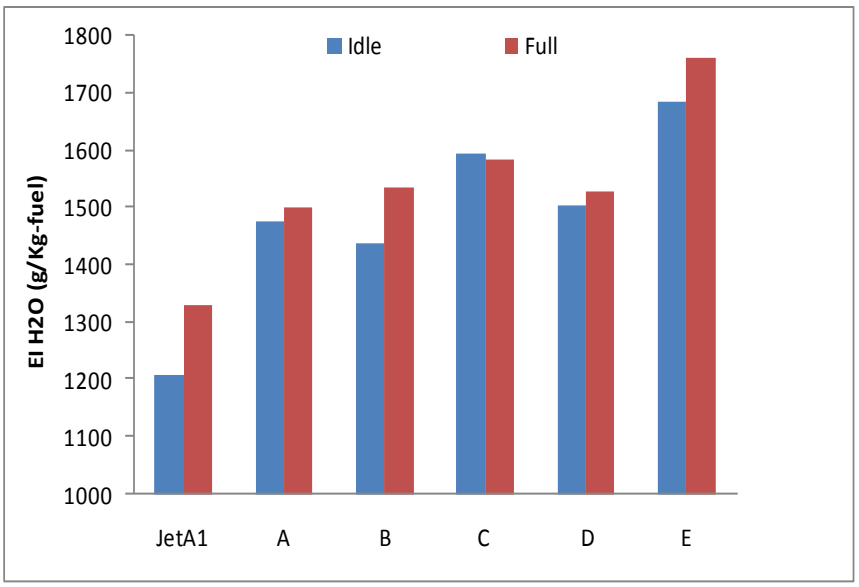

Figure 7.2: Comparison of Water Vapor (EI m) for all fuels at idle and full power.

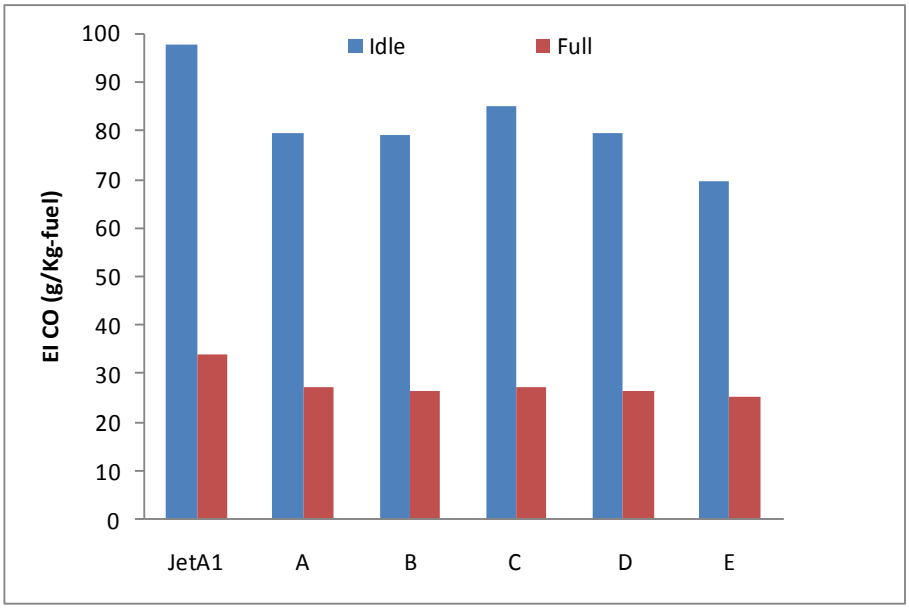

Figure 7.3: EICO emissions (g/Kg-fuel) for different fuels at idle and full power.

In general, the trend of the graphs show that CO and UHC decrease with increasing of the engine power whereas, NOx increases with the power as reported. The higher CO and UHC are due to incomplete combustion at lower combustor temperature. The CO emissions index ranges from 69-97g/Kg depending on fuel type and the higher fuel energy content, the lower CO emissions and this is in good agreements with published work[122]. Fig.7.3 showed that at idle reductions of 18% of CO emissions were observed for fuel A, B and D and 12% for fuel C relative to JetA1, whereas 28% reduction for the GTL fuel (E). Thus, at full power EI-CO emissions were reduced by 20% for all fuels compared to base fuel as illustrated in Fig.7.3.However, Cycloalkane and aromatics have no impact on CO emissions and fuel energy content was the dominant of CO emissions reduction.

Fig.7.4 showed EI m-UHC for all fuels and the behaviour of UHC is similar to CO as the UHC decreased rapidly with increasing the power for all fuels and EI m-UHC value ranging from 14-26g/Kg fuel at idle and 2.8-4 at full power. At idle; the (A-D) fuels registered a 17% reduction of UHC relative to JetA1, whereas a 44% reduction for the GTL (E) fuel was reported in this particular APU. At full power, UHC emissions for all fuels are similar relative to JetA1 except GTL where a 20% lower than the value of JetA1.

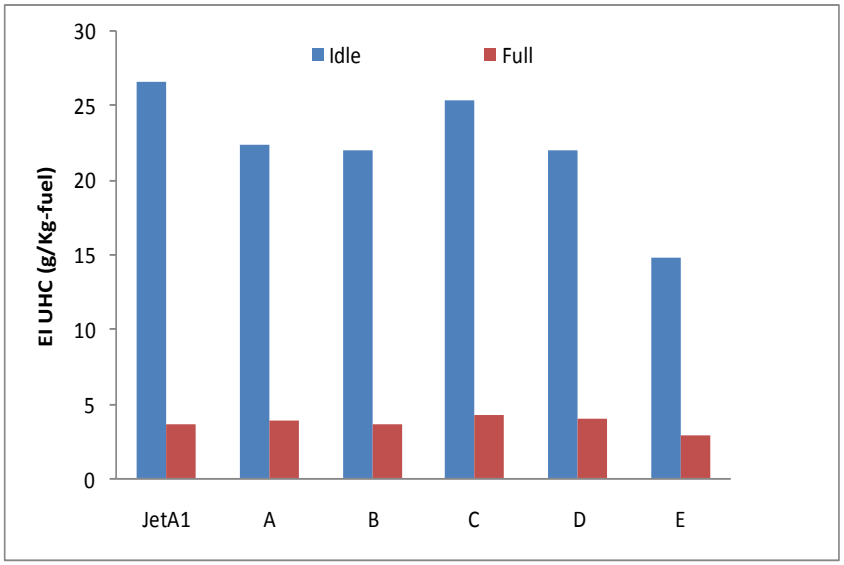

Figure 7.4: EI-UHC emissions (g/kg-fuel) for different fuels at idle and full power.

Fuel E (no aromatics) demonstrated lower CO and UHC emissions especially at idle. These observations are in good agreement with other studies in literature[19, 118]. Thus, the improved efficiency resulted in an increased combustion temperature and hence slightly elevated NOx level.

NOx emissions (g/Kg-fuel) and NO_2 fraction (%) are presented in Figs.7.5&7.6 respectively. In general, combustion of all fuels resulted in lower NOx emissions at idle mode compared to full power due to lower flame temperature. The flame temperatures for all fuels were very close. The result showed that there are no significant differences in NOx emissions for all fuels at both conditions. NOx EI is ranging from 2.17-2.2 g/Kg fuel at idle and 3.2-3.84 g/Kg fuel at full power and reductions in NOx emissions from 6-16 % depending on the chemical combustion of the fuels compared to JetA1 fuel. These findings are in good agreements with other studies [122, 184, 185]. The results also concluded that fuel properties have little impact on NOx emissions compared to primary zone flame temperature and combustor residence time which are low in this study.

NO_2 as an important urban air pollutant is required to monitor as part of air quality control in Europe. The fraction of NO_2 in NOx emissions is increasingly an important factor that could affect local air quality in airports and its vicinities. NO_2/NO_x ratio for all fuels at idle and full power was determined and presented in Fig.7.6. The APU NO_2/NO_x ratio is high at idle and low at full power for all fuels and various from 51-57% at idle and 32-

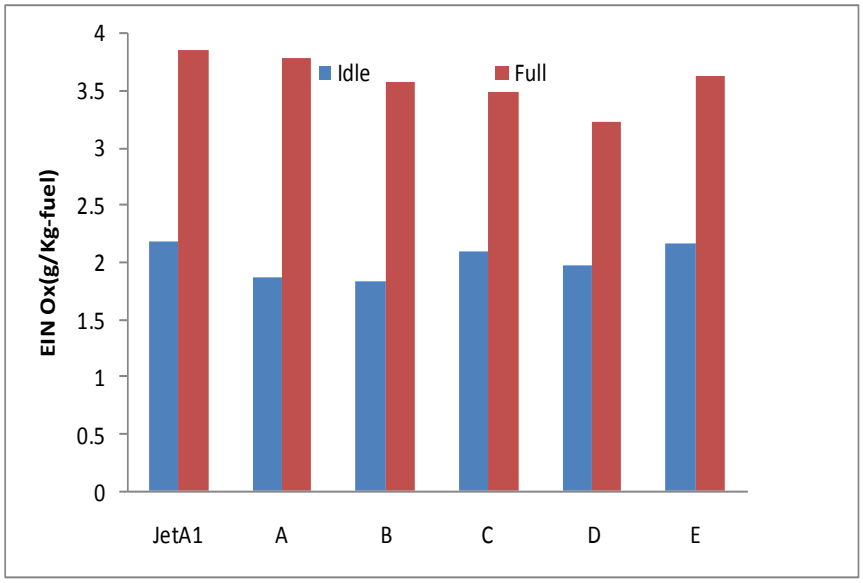

Figure 7.5: NOx emissions (ppm) for different fuels at idle and full power.

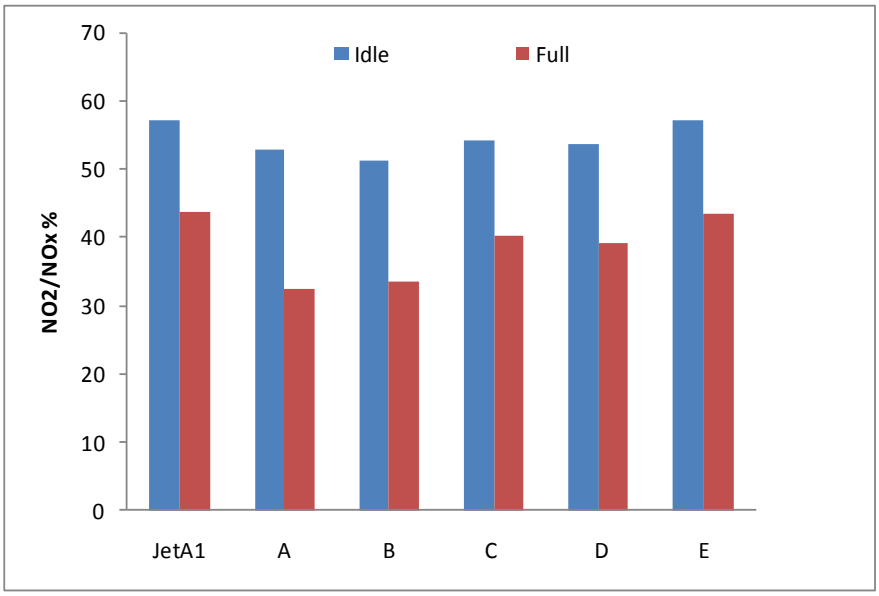

Figure 7.6: NO2/NOx (%) for different fuels at idle and full power.

43% at full power. This ratio is significantly lower than that reported by Wood et al at idle using CFM56 engine[186]. However the results showed that fuel composition has no effect on NO_2/NOx ratio and rapid conversion of NO to NO_2 at low thrust resulting in high NO_2 fraction were observed[185, 186].

The EI*m* results of all five fuels were normalized to JetA1 for idle and full power conditions and are shown in Figs.7.7&7.8. It is clearly shown that at idle the most notable changes were UHC and CO emissions. Figs.7.7&7.8 show a significantly lower CO and UHC emissions (5-25%) and (5-45%) were observed with the fuel blends respectively at idle. This could be

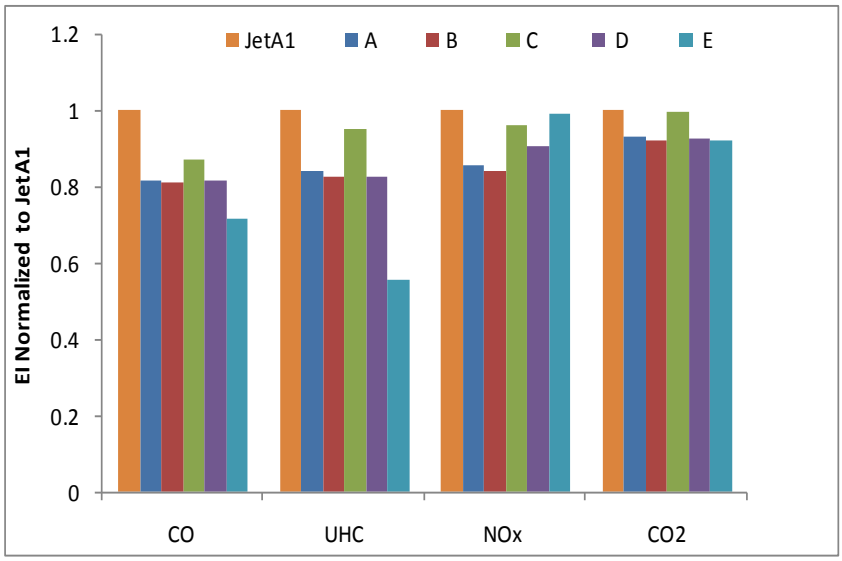

Figure 7.7: EI normalized to JetA1 at Idle condition.

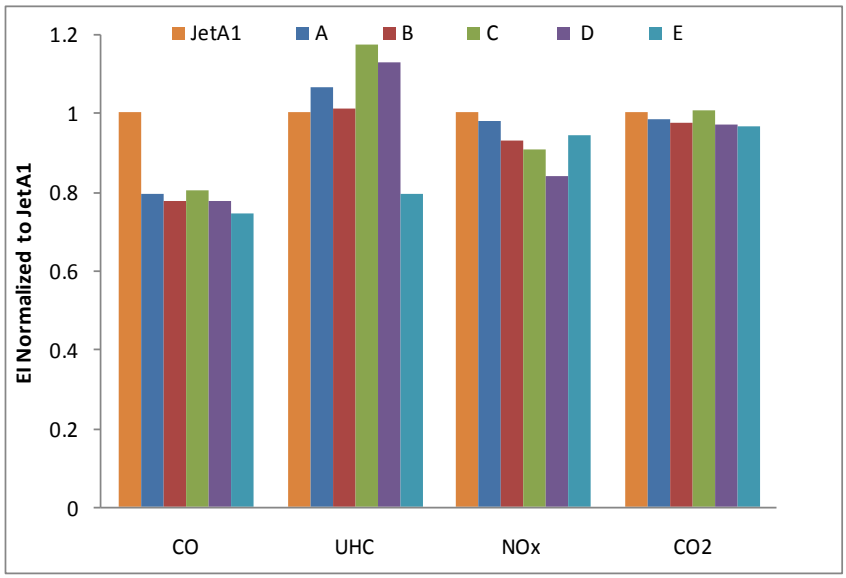

Figure 7.8: EI normalized to JetA1 at full condition.

attributed to the environmentally favourable chemical composition (lower carbon-to-hydrogen ratio, i.e., lower carbon number) which contributes to improved combustion characteristics particularly at lower combustion temperatures (idle). Test data also show negligible differences in nitrogen oxide emissions between the fuels at both conditions.

7.2.1.2 Aviation Alternative fuels

Gaseous emissions from both synthetic and renewable jet fuels measured from APU engine are illustrated in Figs.7.9 to 7.14 for all fuels tested. The results showed emissions index (EI $_m$ g/kg-fuel) for CO_2, CO, UHC, NOx and NO_2 fraction respectively. Also EIs for all fuels normalized to

JetA1 at idle and full power are shown in Figs.7.15&7.16. As anticipated, CO decreased and NOx increased as the engine power increased.

The measured CO_2 emission index is presented in Fig.7.9, Fuels F, G, H and I had similar hydrogen/ Carbon ratios (~2), the amounts of CO_2 emissions are similar. However, CO_2 decreased as hydrogen to carbon ratio increased and GTL had the lowest CO_2 about 3000 g/Kg with H/C ratio about 2.2 compared all fuels. As mentioned earlier, the high H/C ratio in fuel E resulted in higher water vapour emissions, which is shown in Fig.7.10. It is also shown in Fig.7.10 that JetA1 produced the lowest amount of water vapour due to its lowest H/C ratio. The higher water vapour emissions have no air quality concerns but in the context of aviation, this may have impact on the formation of contrails.

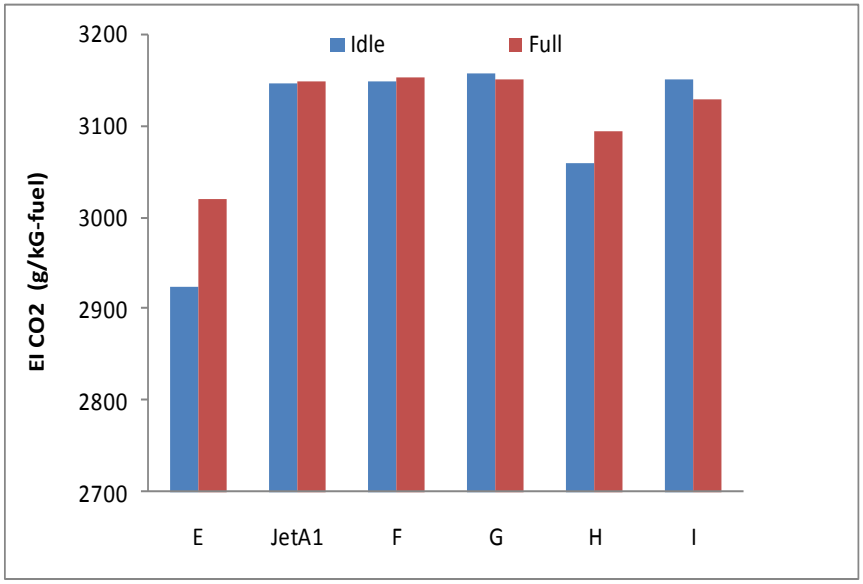

Figure 7.9: EICO_2 emissions (g/Kg-fuel) for different fuels at idle and full power.

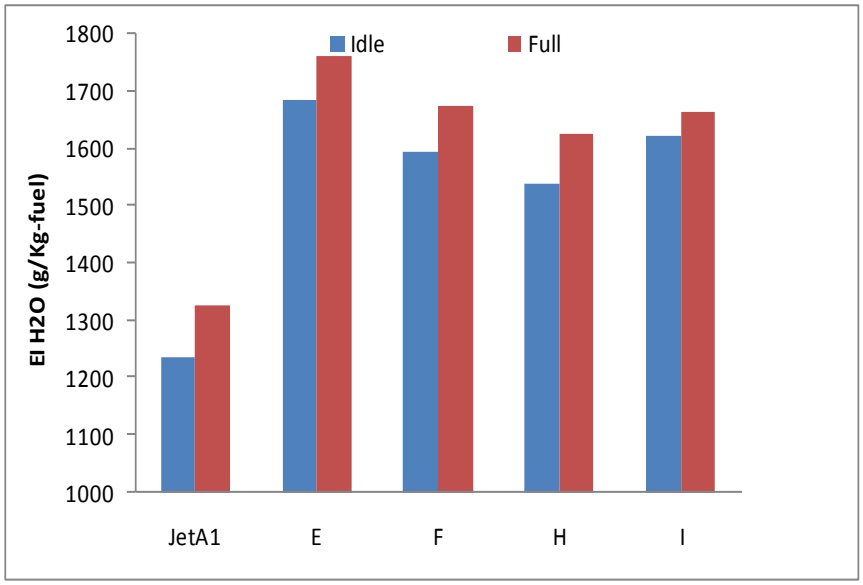

Figure 7.10: Comparison of Water Vapor (EI m) for all fuels at idle and full power.

The EI of CO and UHC emissions for all fuels are presented in Figs.7.11&7.12. The results for all fuels are similar and at full power. The CO average values were 75-90 g/kg at idle and ~25 g/kg-fuel at full power. The UHC average emissions were 15-25g/kg at idle and ~4g/kg at full power respectively. Significant reductions in CO and UHC emissions were observed for fuel E (GTL). At idle condition, fuel E reduced CO and UHC EI by 29% and 44% respectively relative to JetA1. At full power, fuel E reduced UHC emissions by approximately 44% compared to JetA1 but there was almost no CO reduction. Besides fuel E, other fuels also showed the reduction of CO such as fuel F, G, H and I with a figure of 14%, 12%, 22% and 14% respectively compared to JetA1 at idle. However, a reduction of 8% was observed for fuel F and I, whereas, fuel G and H were reduced by 3% and 16% respectively at idle power as shown in Fig.7.11.

The reductions of UHC emissions by other fuels were moderate, 18% reduction with fuel H, 11% reduction for fuel G and I relative to JetA1. The remarkable reductions in CO and hydrocarbon by fuel E were due to its higher H/C ratio (2.19). These observations are in good agreement with other studies in literature [187, 188].

The reductions in UHC by alternative fuels are reflected in particle emissions as will be shown later. JetA1 had the highest UHC and thus the highest particle numbers and mass. The fuel E had the lowest UHC and therefore the lowest particle number and mass emissions. The correlation

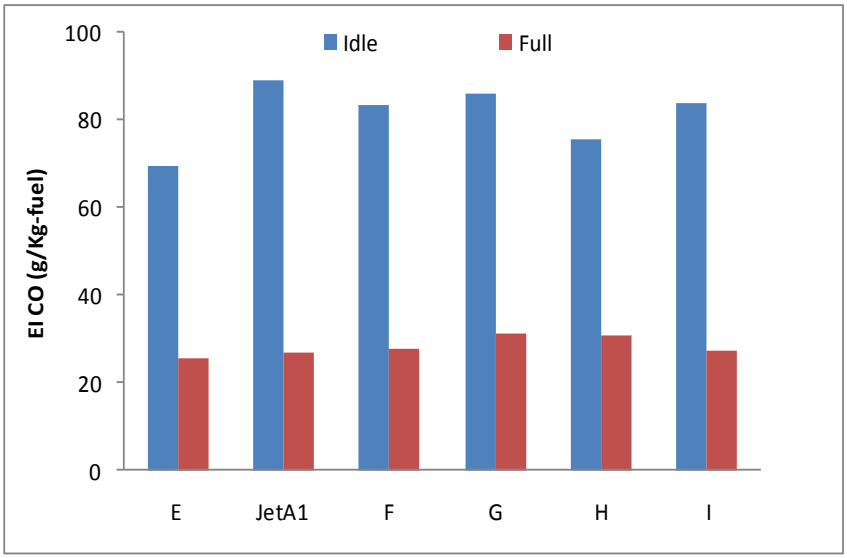

Figure 7.11: EICO emissions (g/Kg-fuel) for different fuels at idle and full power.

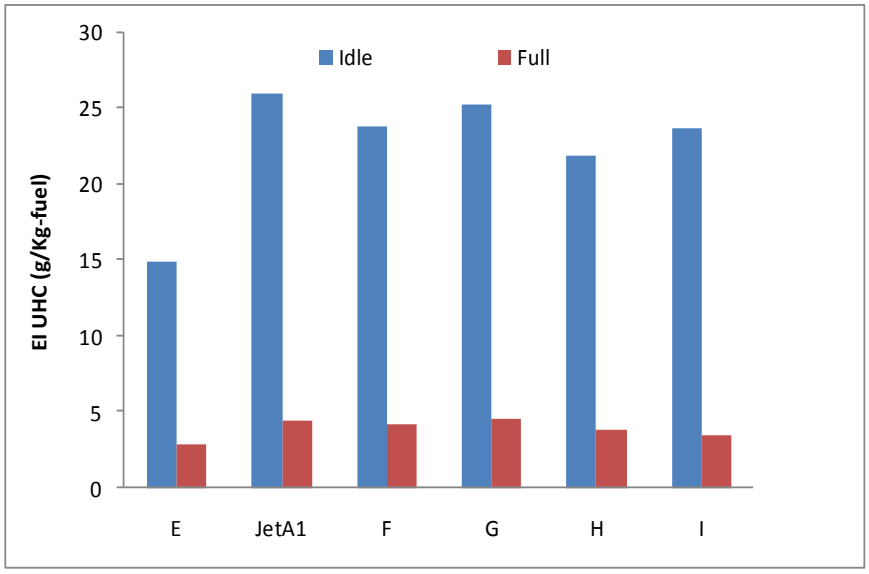

Figure 7.12: EIUHC emissions (g/Kg-fuel) for different fuels at idle and full power.

was thought to be related gas-to-particle conversion and condensation effect.

EI $_m$- NOx (g/kg-fuel) for all fuels are presented in Fig.7.13. NOx emissions for all fuels had a value of ~3.5 g/kg-fuel at full power and ~2.1 g/kg-fuel at idle. HEFA blend fuel (F) had slightly lower NOx emissions at full power compared to other fuels. At the idle condition, NOx emissions were slightly greater for fuel (G) ~2.3g/Kg than JetA1 (2.2g/Kg), whereas the GTL fuel (E) and HEFA blend fuel (I) had lower NOx emissions (~2g/Kg) relative to JetA1. Overall, all fuels showed similar NOx emissions. This conclusion is in good agreements with other people's research [187-189], that alternative

fuels produced the similar or slightly lower NOx emissions compared to JetA1.

NO_2/NOx fractions for all fuels are presented in Fig.7.14 for idle and full power conditions respectively. The results showed that NO_2 made a major contribution to the total NOx at idle (53-57%), whereas at full power NO_2 contributed 34-40% of total NOx. These findings are very close to Timko et al using PW308 engine and Wood et al using APU of CFM56 [184, 186]. These results showed that NO_2 has an opposite trend compared to NO and NOx, higher at idle and lower at full power and it is not flame temperature dependent. It is considered that the higher NO_2 fractions at idle were due to more oxygen available at idle to oxidise NO into NO_2.

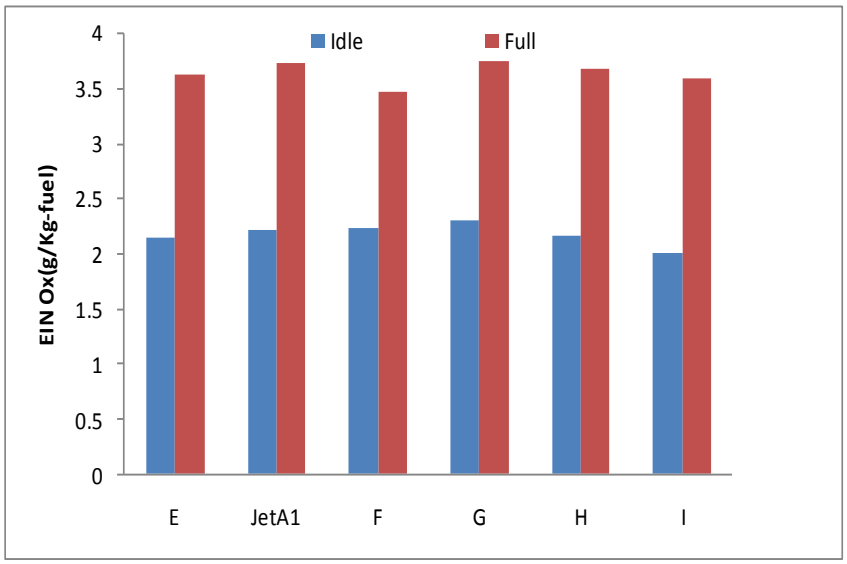

Figure 7.13: EINOx emissions (g/Kg-fuel) for different fuels at idle and full power.

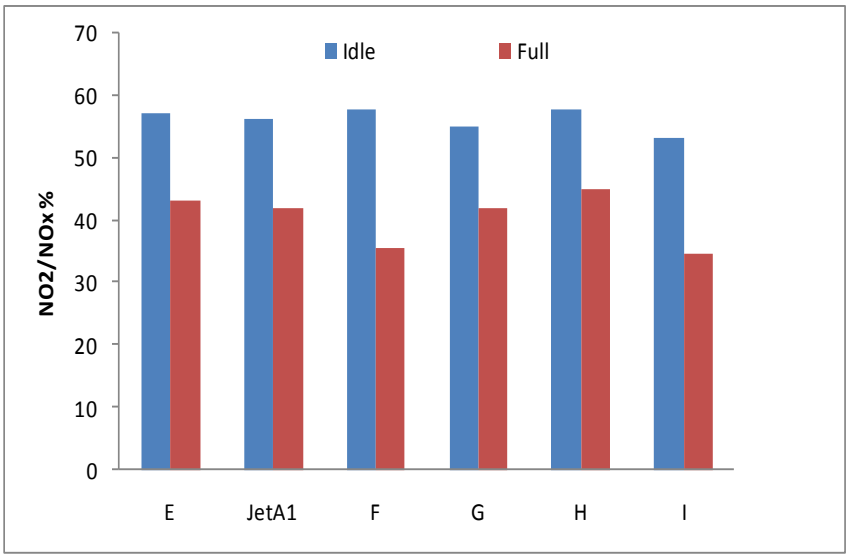

Figure 7.14: NO2/NOx (%) for different fuels at idle and full power.

Figs.7.15&7.16 displays the CO, CO_2, NOx and UHC emissions indices normalized to JetA1 data for all fuels at idle and full power engine settings. It is clearly shown that at idle the most notable changes were UHC and CO emissions. All fuels produced lower UHC and CO emissions than JetA1 with an extreme of 44% reduction of UHC by fuel E. There were no significant differences in NOx emissions between alternative fuel blends and JetA1 (within 5% except fuel I which was 9% reduction). For the full power condition, alternative fuels did not show the benefit of CO reductions as shown in the idle except fuel E. Fuel G and H in fact showed an increase in CO.

However, UHC emissions showed the similar trend to the idle, i.e. alternative fuel blends produced lower UHC emissions with a scale of up to 20% reductions except fuel G. For NOx emissions at full power, fuel E and F showed a reduction of 6% and 8% compared to JetA1 while the other fuel blends emitted the similar levels of NOx. CO_2 emissions were almost the same as expected but fuel E (GTL) had notably lower CO_2 due to its higher H/C ratio and thus lower carbon content in the fuel. As a result, fuel E produced more water in the exhaust as shown in Fig.7.10.

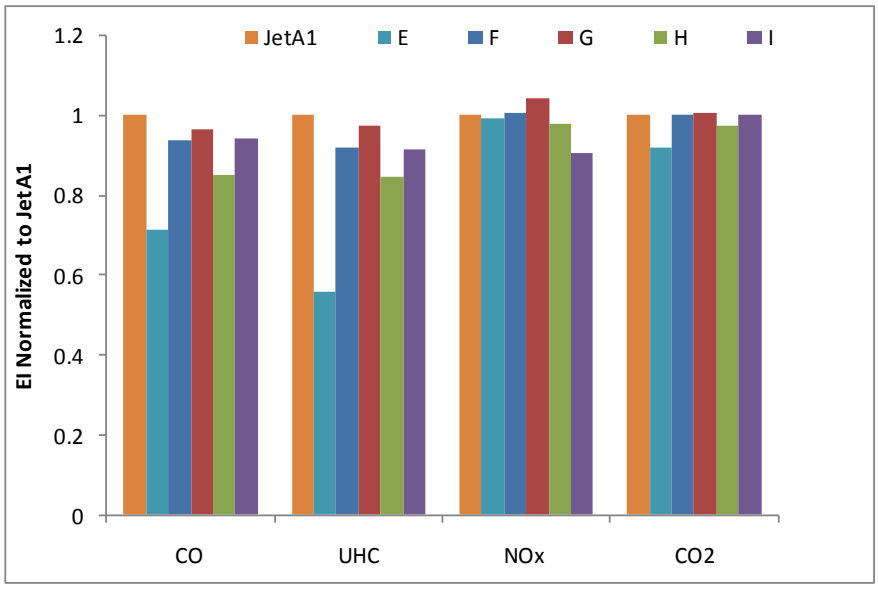

Figure 7.15: EI normalized to JetA1 at Idle condition.

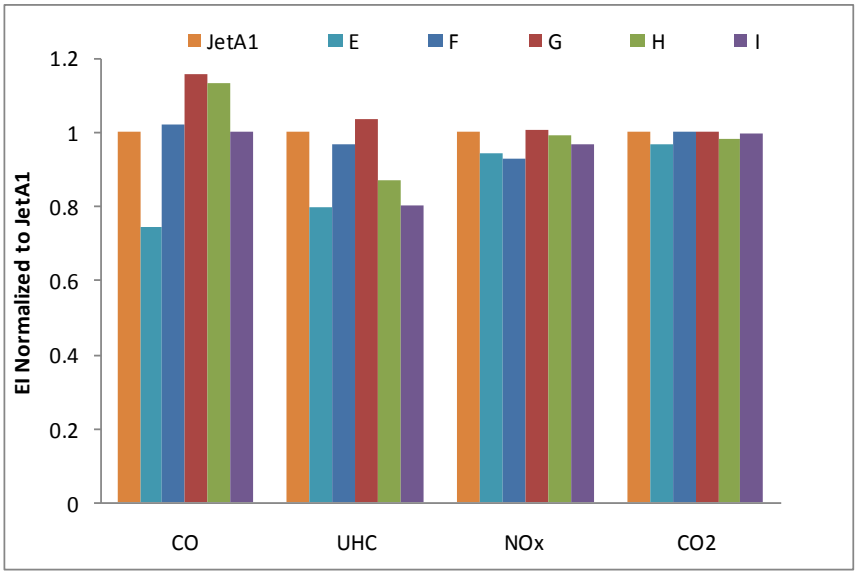

Figure 7.16: EI normalized to JetA1 at full condition.

7.2.2 Speciated HC Emissions

Common species emitted from engines during combustion such as NOx, CO, SOx, PM and UHC are regulated and considered as primary species in emission inventories. CO_2 is considered as a global concern rather than local issue. There is an increasing concern and need to include additional emission species which have potential health and environmental concerns in emission inventories. These species are often called HAPs (Hazardous Air Pollutants). ICAO reported some examples of HAPs that have been identified as representative pollutants from airport sources [190] including formaldehyde, acetaldehyde, acrolein,1, 3 butadiene, benzene, Naphthalene, toluene, xylene and propionaldehyde. Formaldehyde is the most dominant aldehyde in vehicle exhaust emissions and has a strong potential to form ozone and is classified as an active ozone formation precursor as mentioned in chapter 4.

The speciation of hydrocarbon pollutants will contribute to the understanding of the impact of air transport on global (cruise mode) and local air quality (airport) issues. There are several different techniques being used for the hydrocarbon speciation of aero engine exhaust: GC (Gas Chromatography), FTIR, Mass spectroscopy, and laser absorption. The GC technique has high accuracy and sensitivity but is only suitable for batch samples**.** Mass spectroscopy can provide accurate and transient measurement but it is expensive. FTIR technique with careful calibration is able to provide a reasonably accurate and transient measurement for multi-

compounds simultaneously with relatively low cost. In this research FTIR was used to measure and quantify speciated hydrocarbon emissions from APU engine at idle and full power conditions burning different alternative fuels beside base fuel (JetA1).

7.2.2.1 Review of previous work

The research for aviation activity related or sourced HAPs is still at early stages and knowledge on these HAPs emissions is very limited [190]. There are limited studies investigating the non-regulated emissions such as carbonyl compounds (CBCs) especially aldehydes. Knighton et al [191] measured 20+ VOCs including aldehydes and benzene using the tuneable infrared laser differential absorption spectroscopy for formaldehyde and the proton transfer reaction mass spectrometer for other VOCs from CMF56-2-C1 engines of a DC-8 aircraft during APEX program. They found that formaldehyde and benzene were hardly detectable at the higher engine thrust rating until the engine power was reduced 15% of rated thrust, where the concentrations of formaldehyde and benzene started to increase quickly as the engine power continued to reduce.

Yelvington et al[19] conducted chemical speciation of hydrocarbon emissions from a CMF56-2C1 high-bypass-ratio turbofan engine used to power the NASA DC-8 aircraft as part of the Aircraft Particle Emissions eXperiment (APEX)[19]. The species they analysed include formaldehyde, ethylene, acetaldehyde, benzene, toluene and several higher aromatics. The gas samples were taken at 1, 10, and 30m downstream of the engine-exit plane of the grounded aircraft. The engine power covered from ground idle up to take-off power. Three fuel types (a baseline JP-8, a high-aromatic fuel, and a high-sulphur fuel) were investigated. They found that at low power conditions such as idle, formaldehyde is the most abundant single species. As the engine power increased all the hydrocarbons decreased dramatically.

Mike-Lye et al[192] investigated effect of alternative fuels(standard JP8 and FT) on hydrocarbon and particle emissions from an aircraft gas turbine engine as part of the Aircraft Particle Emissions eXperiment (APEX[192]. They concluded that the hydrocarbon speciation profile depends on fuel type and power mode. Moreover, aromatics species emissions such as (benzene and toluene) are lower compared to formaldehydes and ethene.

Timko et al[103] concluded that HCHO emissions were reduced up to 43% for 100%FT and 32% for 40%FAME at the same operation condition.

Aldehydes emissions have been assessed under atmospheric pressure and 600K using a radial swirler industrial low NOx gas turbine combustor using biodiesel and its blend with kerosene as discussed in chapter 4. Aldehydes including formaldehyde, acetaldehyde and acrolein were measured by FTIR. The results showed that formaldehyde was the most prevalent aldehyde species for all fuels, accounted for up to 50%.The aldehydes decreased as equivalence ratio increased due to the increased flame temperatures.

7.2.2.2 Speciated Gas-Phase measured by FTIR

All speciated hydrocarbons were measured in ppm and converted to their emissions index (gram of HC per Kg of fuel) using CO_2 EI and the molecular weight of the species in the equation 24. In this study VOCs were divided into two categories: non methane volatile organic compounds (NMVOCs) (hydrocarbons and aromatics compounds) and carbonyls (oxygenated compounds). Effect of fuel compositions on VOCs from APU engine are presented in Figs.7.17 to 7.20. Fig.7.17&7.19 and table 24&27 illustrate the emissions indices of individual non methane volatile organic compounds (NMVOCs) from APU engine at both idle and full power conditions burning different alternative fuels beside base fuel (JetA1). EIs of Carbonyls are presented in Figs.7.18&7.20 for burning compositionally designed surrogate fuels and alternative aviation fuels respectively.

Overall, all fuels produced higher amount of speciated hydrocarbons at idle compared to full power. Table 24& Fig.7.17 show that JetA1 had emissions indices of 1300mg/Kg for NMVOCs and 7000 mg/Kg for carbonyls. These values are the highest among all the fuels tested, however fuel E produced the least amount of speciated HC with 5000 mg/Kg and 4000 mg/Kg for NMVOCs and carbonyls respectively.

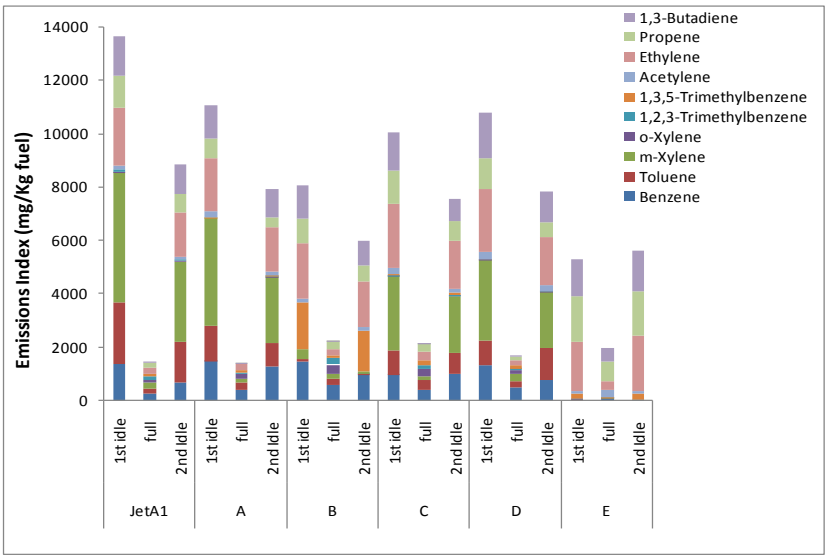

Figure 7.17: EI m of individual NMVOCs for compositionally designed surrogate fuels from APU at idle and full power.

Table 24 also shows the fractions of formaldehyde in total aldehydes in terms of EI and fractions of formaldehyde in total hydrocarbon which was detected by FID. All three aldehydes emissions are at the highest levels at cold idle and the lowest levels at full power, which were directly related to combustion temperatures. The results show that formaldehyde accounts for 55-70% of total aldehydes in terms of g/kg $_{fuel}$ and 13-20% of total hydrocarbons depend on the fuel type at both idle and full power conditions. There were no significant differences between idle and full power conditions.

Acrolein as the second dominant aldehyde has a share of around 30%. Acetaldehyde has around 10% of total aldehydes as in Fig.7.18. The dominance of formaldehyde could indicate that the breakup of hydrocarbon chains during partial oxidation of fuel is mainly α scissions of carbon chains. By comparison between the cold and hot idle formaldehyde emissions, it was observed that the engine produced higher emissions at cold idle than that at hot idle, indicating a lower combustion temperature at cold idle due to the cold engine components.

Table 24&25 show that all fuels have similar formaldehydes emissions except fuel E (GTL) where the lowest amount was found. However, GTL has strong effect on acetaldehyde and acrolein compared to formaldehyde emissions and reduced by 35% and 50% respectively compared to JetA1.

Table 24 shows that the addition of JetA1 to fuel x has no effect on aldehydes emissions.

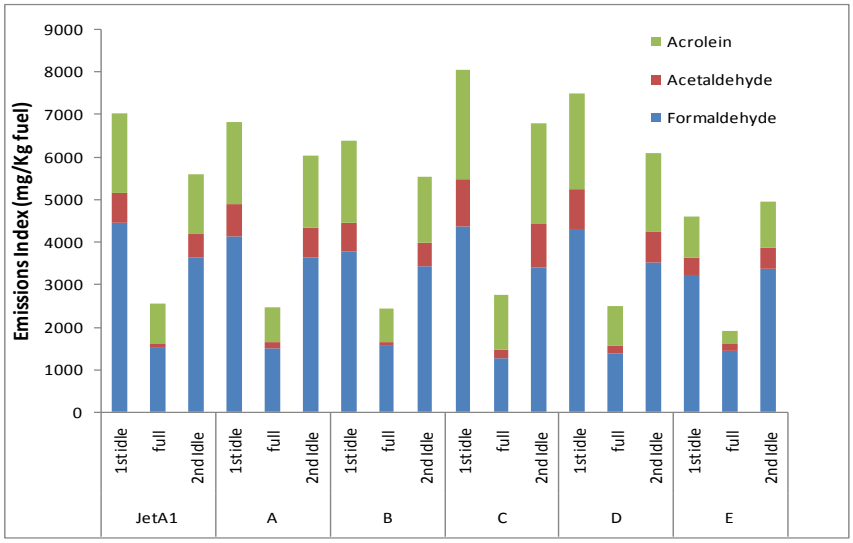

Figure 7.18: EI m of individual carbonyl compounds burning compositionally designed surrogate fuels from APU at idle and full power.

Table 25 and Figs.7.19&7.20 illustrate NMVOCs and carbonyls for alternative aviation fuels compared to JetA1 respectively. Similar observation has been seen, the highest EI of NMVOCs and carbonyls for JetA1 and the lowest amount for GTL fuel, whereas fuel F, H, I are in between. Fig.7.20 showed that fuels F and I showed the similar level of formaldehyde emissions at full engine power but fuel H had notably higher formaldehyde emissions, indicating more incomplete combustion at full engine power for fuel H. This could be attributed to 10% of fatty acid ester in fuel H, which has relatively high viscosity and low volatility and thus affect fuel vaporisation and atomisation in the combustion chamber. Interestingly, the fuel H had lower idle formaldehyde emissions. This may be due to that the fuel borne oxygen in the fatty acid ester assisted the combustion at the idle but this effect became limited as the amount of fuel is less compared to that at full power condition.

Table 28 provides EI of HC emissions from APU measured by FTIR relative to formaldehyde at both idle compared to Spicer et al [193] and Knighton et al [194]. The emission index of formaldehyde for JetA1 is ~4.5 g/kg-fuel and 3.6 mg/kg-fuel at cold and hot idles respectively, much higher than the values measured by Knighton et al[194] from CMF56-2-C1 engines

of a DC-8 aircraft during APEX program, in which they reported approximately 0.300~2.5 g/kg-fuel at 4% rated thrust (ground idle condition).

The large variations in Knighton's data were due to the change of ambient temperatures. The measurement in this research was taken via the indoor test and therefore the effect of ambient temperatures was minimal. Thus, Spicer et al [193] also measured formaldehyde from aircraft gas turbine engines and reported a value of 1.24 g/kg-fuel at 4% rated thrust, one third of the hot idle formaldehyde emissions of this research. Very high emissions from this research are due to the engine technology, as the engine used in this paper is 1950's design whereas the engine used by Knighton et al was modern engines.

Some of Speciated HC includes Benzene, toluene, propene, acetaldehyde and acrolein are compared with their results. It is difficult make any comparison between the results in present study with their finding due to different composition of used fuels. However, some of speciation falls within the range values determined by Knighton and Spicer[193, 194].

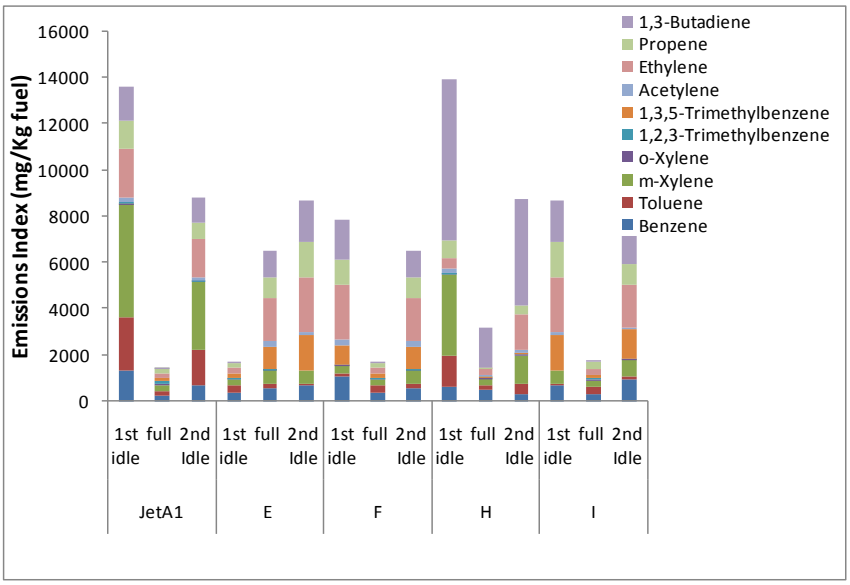

Figure 7.19: EI m of individual NMVOCs burning Alternative Aviation fuels from APU at idle and full power.

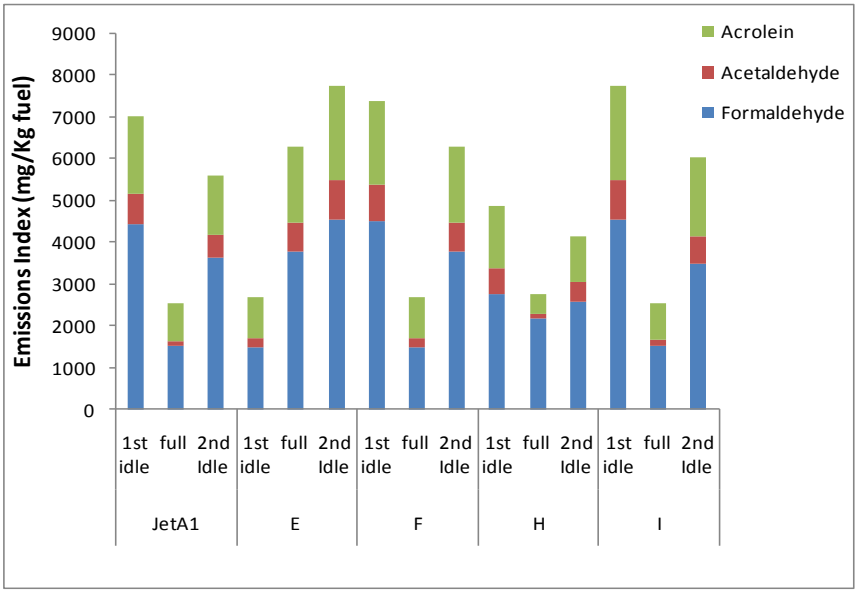

Figure 7.20: EI m of individual carbonyl compounds burning Alternative Aviation fuels from APU at idle and full power.

Comparison with JetA1

One of the criteria for assessing any aviation alternative fuels is their performance relative to conventional JetA1. It is hoped that alternative fuels provide improved performance including emissions or at least not worse than JetA1. Thus VOC emissions from compositional surrogate and aviation alternative/renewable fuels and their blends were normalised to JetA1 as shown in table 26 &27.

Table25 present VOC emissions of compositional surrogate fuels normalized to JetA1. Formaldehydes emissions were reduced for all fuels compared to JetA1 especially at idle conditions. There were no differences in acetaldehydes and acrolein emissions for all fuels; however, there was a noticeable reduction with GTL (fuel E).

Table 27 showed that at both cold and hot idle conditions, fuel H showed significant reductions in formaldehyde, which could be attributed to the fuel born oxygen in fatty acid ester (10% of FAE in fuel H) that helped the oxidation of fuels. Fatty acid ester has higher viscosity and low volatility than kerosene which could potentially affect fuel vaporisation and atomisation. At idle conditions, the fuel flow to the engine was low and the impact of viscosity and volatility is low. So the positive effect of fuel born oxygen became dominant. This effect is not present at full power condition, as the amount of fuel flow to the engine increased greatly, the impact of

inferior vaporisation and atomisation properties of FAE became significant and thus the combustion efficiency was deteriorated compared to JetA1. However, no clear differences between all fuel regarding to acetaldehydes and acrolein. Fuel H also had notable reductions in acrolein emissions at full power compared to JetA1.

The aromatic hydrocarbon emissions include benzene and toluenes are decreased for alternative fuels. The results in the table show that EIm of benzene decreased with deceasing JetA1 content. EIm for JetA1 was 1370g/Kg and reduced to 984 g/Kg for fuel C (40% JetA1) and to 47g/Kg with fuel E (0% JetA1). Similar observation with alternative aviation fuels, EIm for benzene reduced to 119g/Kg and 703 g/Kg fuel F(50% JetA1), and I (25% JetA1) respectively. These findings are in good agreements with Timko et al[103]. The effect of fuel composition on benzene emissions is much stronger than observed for formaldehydes, benzene was reduced by 96.5% with GTL compared to JetA1 at idle. The significant reduction is due to zero aromatic content in the fuel E. The tiny amount of benzene detected in the exhaust for the aromatics free fuel proved that aromatics could be formed by decomposition of fuel and recombination of smaller products of incomplete combustion. This finding is in consistent with related studies[192].

Toluene is reduced dramatically than benzene especially for zero aromatic fuel and their blends. Toluene was reduced by 99.9% with fuel E (0% aromatic) and 95% with fuel B (80% GTL) compared to JetA1. It also noticed by some authors that the aromatics is reduced as the size of the aromatic molecule increase[103].

Normalizing the HC emission data to formaldehyde is a way to provide relative distribution of hydrocarbon present in the exhaust used by Knighton et al[194]. They showed that normalizing VOC EIms to EIm of HCHO removes data variability caused by temperature and fuel flow fluctuations. HCHO was adopted for normalization as it is the most abundant VOC in the exhaust and represents about 20% of the total HC for all fuels.

Fig.7.21demonstrates emissions indices of selected HCs measured by FTIR relative to formaldehydes emissions indices for all fuels at both idle and full power. The graph reveals that HC components have similar liner relationship; this behaviour suggests that the scale of hydrocarbon

speciation is not significantly changed as a function of fuel composition and power. This finding is in good agreement with work done by Spicer et al, Herndon et al and Knighton et al [194-196].

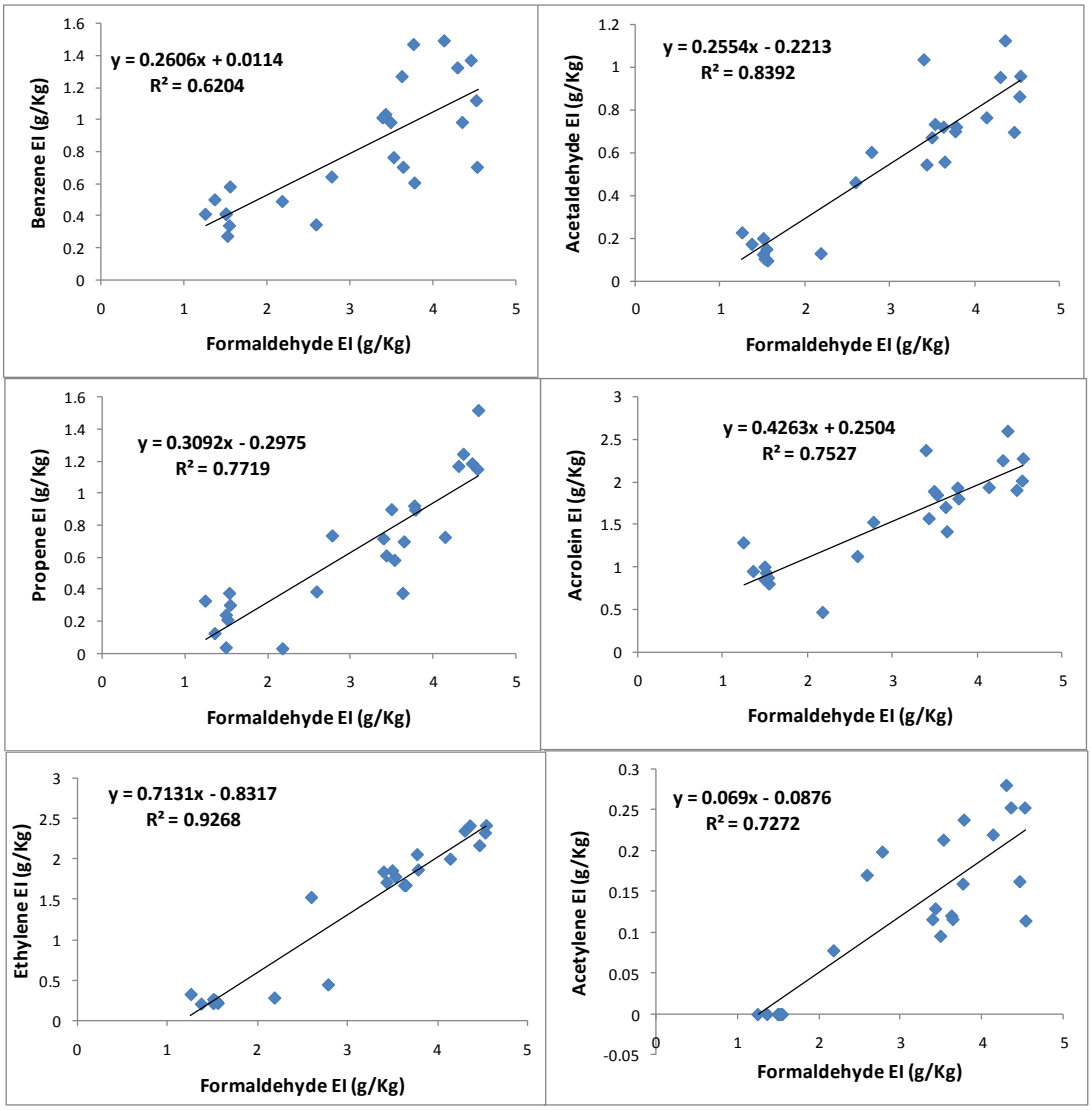

Figure 7.21: Representative plots of selected HC EI vs. HCHO EI at both idle and full power for all fuels.

Table 24: Emission Indices of Individual NMVOCs and Carbonyls for JetA1 and fuels (A-E) from APU at both idle and full power.

Fuel		JetA1			A			B			C			D			E	
	1st idle	Full Power	2nd Idle	1st idle	Full Power	2nd Idle	1st idle	Full Power	2nd Idle	1st idle	Full Power	2nd Idle	1st idle	Full Power	2nd Idle	1st idle	Full Power	2nd Idle
Gas Compound		mg/Kg			mg/Kg			mg/Kg			mg/Kg			mg/Kg			mg/Kg	
Methane	358.36	21.02	181.95	303.77	47.00	0.00	337.23	55.07	269.90	383.37	44.48	333.46	446.13	48.06	283.90	559.18	15.47	1265.04
NMVOC																		
Benzene	1371.34	272.11	703.51	1493.89	412.76	1270.42	1470.97	580.74	1033.49	984.12	409.97	1012.47	1325.09	500.33	764.19	47.62	121.61	35.56
Toluene	2304.86	192.91	1527.39	1318.56	299.55	896.93	95.40	265.78	0.13	895.80	395.40	767.84	946.07	253.59	1212.94	2.25	0.00	0.00
m-Xylene	4878.01	209.84	2951.41	4053.53	127.16	2499.83	382.56	178.80	62.67	2803.93	107.56	2116.28	3001.96	273.07	2119.77	31.06	0.23	0.00
o-Xylene	24.16	116.80	48.69	0.00	160.30	3.98	0.00	332.49	0.00	15.23	290.06	50.66	14.06	128.40	10.50	2.06	0.00	0.00
1,2,3-Trimethylbenzene	62.41	111.52	42.47	0.00	65.59	17.97	0.00	264.74	0.00	3.01	111.19	21.47	0.00	61.29	10.96	0.00	0.00	0.86
1,3,5-Trimethylbenzene	0.00	94.11	0.00	0.42	96.24	4.28	1719.31	102.01	1521.72	30.31	185.53	85.78	0.00	113.79	0.00	208.63	0.20	217.97
Acetylene	162.63	0.00	116.34	219.82	0.00	120.55	159.71	0.00	129.33	252.94	0.00	116.09	280.50	0.00	213.49	77.70	272.97	116.75
Ethylene	2158.81	245.49	1667.94	1992.83	211.93	1666.26	2048.39	214.24	1704.04	2402.39	323.31	1833.44	2338.43	204.46	1772.40	1820.92	333.46	2081.29
Propene	1180.24	207.25	693.73	721.62	34.06	372.86	917.04	298.48	606.39	1239.34	324.83	712.42	1164.04	122.38	578.32	1732.48	739.59	1660.77
1,3-Butadiene	1477.17	37.32	1104.08	1268.24	20.90	1061.24	1276.49	11.86	928.14	1397.83	1.90	851.69	1724.99	36.34	1157.03	1353.06	492.24	1496.22
ALDEHYDES																		
Formaldehyde	4462.36	1522.40	3642.99	4136.74	1503.27	3627.78	3767.87	1553.93	3431.24	4356.32	1254.06	3396.23	4299.07	1368.38	3529.22	3212.78	1449.07	3361.66
Acetaldehyde	694.88	103.45	556.19	762.93	124.33	719.17	698.38	95.09	543.14	1122.07	226.34	1033.67	951.29	172.58	732.13	436.11	172.06	518.52
Acrolein	1892.11	919.08	1404.44	1924.70	840.30	1691.04	1919.50	788.79	1559.18	2587.32	1273.96	2360.55	2240.61	937.57	1834.77	943.76	289.74	1062.39
NMVOCs (mg/Kg)	13619.64	1487.35	8855.56	11068.90	1428.51	7914.32	8069.87	2249.14	5985.89	10024.89	2149.75	7568.15	10795.12	1693.66	7839.59	5275.78	1960.30	5609.41
ALDEHYDES (mg/Kg)	7049.35	2544.93	5603.62	6824.37	2467.89	6037.99	6385.75	2437.81	5533.56	8065.71	2754.36	6790.44	7490.97	2478.53	6096.12	4592.64	1910.87	4942.57
NMVOCs (%)	65.89	36.89	61.25	61.86	36.66	56.72	55.83	47.99	51.96	55.41	43.84	52.71	59.03	40.59	56.26	53.46	50.64	53.16
Formaldehyde/Aldehydes (%)	63.30	59.82	65.01	60.62	60.91	60.08	59.00	63.74	62.01	54.01	45.53	50.01	57.39	55.21	57.89	69.95	75.83	68.01
Formaldehyde/ THC (%)	18.69	32.75	15.26	18.64	39.26	16.34	17.21	40.55	15.68	17.15	30.58	13.37	19.48	38.99	15.99	13.64	36.79	14.28

Table 25: Emission Indices of Individual NMVOCs and Carbonyls for JetA1 and fuels (E, F, H, I) from APU at both idle and full power.

Fuel		JetA1			E			F			H			I	
	1st idle	Full Power	2nd Idle	1st idle	Full Power	2nd Idle	1st idle	Full Power	2nd Idle	1st idle	Full Power	2nd Idle	1st idle	Full Power	2nd Idle
Gas Compound		mg/Kg			mg/Kg			mg/Kg			mg/Kg			mg/Kg	
Methane	358.3636	21.02436474	181.9479	44.83477	297.332163	361.5636	324.6062	44.8347717	297.3322	379.2306	23.8081578	0	361.5636	54.9026847	257.2288
NMVOC															
Benzene	1371.34	272.11	703.51	408.32	605.54	703.55	1119.76	408.32	605.54	642.81	489.69	343.71	703.55	337.93	983.35
Toluene	2304.86	192.91	1527.39	265.90	173.90	81.33	72.62	265.90	173.90	1342.56	194.93	411.81	81.33	301.41	128.70
m-Xylene	4878.01	209.84	2951.41	286.51	596.60	565.95	385.39	286.51	596.60	3534.16	341.75	1245.80	565.95	229.55	751.05
o-Xylene	24.16	116.80	48.69	80.26	19.72	0.00	11.48	80.26	19.72	32.81	24.02	62.50	0.00	87.50	20.13
1,2,3-Trimethylbenzene	62.41	111.52	42.47	13.29	5.84	0.00	0.00	13.29	5.84	29.31	17.82	28.57	0.00	49.58	0.00
1,3,5-Trimethylbenzene	0.00	94.11	0.00	133.51	954.46	1531.95	872.40	133.51	954.46	0.00	33.70	8.23	1531.95	145.31	1221.27
Acetylene	162.63	0.00	116.34	0.00	238.06	114.44	252.83	0.00	238.06	198.83	78.03	170.36	114.44	0.00	95.80
Ethylene	2158.81	245.49	1667.94	261.60	1858.80	2406.35	2314.58	261.60	1858.80	442.06	279.44	1520.11	2406.35	229.69	1848.74
Propene	1180.24	207.25	693.73	236.88	891.71	1511.90	1144.87	236.88	891.71	731.10	27.88	381.76	1511.90	373.11	894.14
1,3-Butadiene	1477.17	37.32	1104.08	25.93	1192.85	1777.45	1723.46	25.93	1192.85	6978.67	1735.37	4622.75	1777.45	16.46	1219.53
ALDEHYDES															
Formaldehyde	4462.36	1522.40	3642.99	1504.56	3780.22	4536.89	4525.87	1504.56	3780.22	2780.10	2182.70	2592.28	4536.89	1543.95	3493.04
Acetaldehyde	694.88	103.45	556.19	199.21	719.27	956.53	861.03	199.21	719.27	601.58	128.79	460.14	956.53	148.82	669.77
Acrolein	1892.11	919.08	1404.44	988.62	1790.62	2263.11	2001.79	988.62	1790.62	1515.78	454.82	1113.70	2263.11	861.40	1878.76
NMVOCs (mg/Kg)	13619.64	1487.35	8855.56	1712.20	6537.48	8692.93	7897.39	1712.20	6537.48	13932.31	3222.64	8795.60	8692.93	1770.55	7162.70
ALDEHYDES (mg/Kg)	7049.35	2544.93	5603.62	2692.39	6290.12	7756.53	7388.69	2692.39	6290.12	4897.47	2766.31	4166.12	7756.53	2554.17	6041.58
NMVOCs (%)	65.89	36.89	61.25	38.87	50.96	52.85	51.66	38.87	50.96	73.99	53.81	67.86	52.85	40.94	54.25
Formaldehyde/Aldehydes (%	63.30	59.82	65.01	55.88	60.10	58.49	61.25	55.88	60.10	56.77	78.90	62.22	58.49	60.45	57.82
Formaldehyde/ THC (%)	18.69	32.75	15.26	6.39	95.97	19.27	18.20	34.55	15.20	12.69	60.27	11.83	18.32	41.58	14.11

Table 26: Speciated HC normalized to JetA1 fuel

Fuel		JetA1			A			B			C			D			E	
Gas Compound	1st idle	Full Power	2nd Idle	1st idle	Full Power	2nd Idle	1st idle	Full Power	2nd Idle	1st idle	Full Power	2nd Idle	1st idle	Full Power	2nd Idle	1st idle	Full Power	2nd Idle
Benzene	1.00	1.00	1.00	1.09	1.52	1.81	1.07	2.13	1.47	0.72	1.51	1.44	0.97	1.84	1.09	0.03	0.45	0.05
Toluene	1.00	1.00	1.00	0.57	1.55	0.59	0.04	1.38	0.00	0.39	2.05	0.50	0.41	1.31	0.79	0.00	0.00	0.00
m-Xylene	1.00	1.00	1.00	0.83	0.61	0.85	0.08	0.85	0.02	0.57	0.51	0.72	0.62	1.30	0.72	0.01	0.00	0.00
o-Xylene	1.00	1.00	1.00	0.00	1.37	0.08	0.00	2.85	0.00	0.63	2.48	1.04	0.58	1.10	0.22	0.09	0.00	0.00
1,2,3-Trimethylbenzene	1.00	1.00	1.00	0.00	0.59	0.42	0.00	2.37	0.00	0.05	1.00	0.51	0.00	0.55	0.26	0.00	0.00	0.02
1,3,5-Trimethylbenzene	1.00	1.00	0.00	0.00	1.02	0.00	0.00	1.08	0.00	0.00	1.97	0.00	0.00	1.21	0.00	0.00	0.00	0.00
Acetylene	1.00	0.00	1.00	1.35	0.00	1.04	0.98	0.00	1.11	1.56	0.00	1.00	1.72	0.00	1.84	0.48	0.00	1.00
Ethylene	1.00	1.00	1.00	0.92	0.86	1.00	0.95	0.87	1.02	1.11	1.32	1.10	1.08	0.83	1.06	0.84	1.36	1.25
Propene	1.00	1.00	1.00	0.61	0.16	0.54	0.78	1.44	0.87	1.05	1.57	1.03	0.99	0.59	0.83	1.47	3.57	2.39
1,3-Butadiene	1.00	1.00	1.00	0.86	0.56	0.96	0.86	0.32	0.84	0.95	0.05	0.77	1.17	0.97	1.05	0.92	13.19	1.36
Formaldehyde	1.00	1.00	1.00	0.93	0.99	1.00	0.84	1.02	0.94	0.98	0.82	0.93	0.96	0.90	0.97	0.72	0.95	0.92
Acetaldehyde	1.00	1.00	1.00	1.10	1.20	1.29	1.01	0.92	0.98	1.61	2.19	1.86	1.37	1.67	1.32	0.63	1.66	0.93
Acrolein	1.00	1.00	1.00	1.02	0.91	1.20	1.01	0.86	1.11	1.37	1.39	1.68	1.18	1.02	1.31	0.50	0.32	0.76

Table 27: Speciated HC normalized to JetA1 fuel

Fuel		JetA1			E			F			H			I	
Gas Compound	1st idle	Full Power	2nd Idle	1st idle	Full Power	2nd Idle	1st idle	Full Power	2nd Idle	1st idle	Full Power	2nd Idle	1st idle	Full Power	2nd Idle
Benzene	1.00	1.00	1.00	0.30	2.23	1.00	0.82	1.50	0.86	0.47	1.80	0.49	0.51	1.24	1.40
Toluene	1.00	1.00	1.00	0.12	0.90	0.05	0.03	1.38	0.11	0.58	1.01	0.27	0.04	1.56	0.08
m-Xylene	1.00	1.00	1.00	0.06	2.84	0.19	0.08	1.37	0.20	0.72	1.63	0.42	0.12	1.09	0.25
o-Xylene	1.00	1.00	1.00	3.32	0.17	0.00	0.48	0.69	0.40	1.36	0.21	1.28	0.00	0.75	0.41
1,2,3-Trimethylbenzene	1.00	1.00	1.00	0.21	0.05	0.00	0.00	0.12	0.14	0.47	0.16	0.67	0.00	0.44	0.00
1,3,5-Trimethylbenzene	1.00	1.00	1.00	0.00	10.14	0.00	0.00	1.42	0.00	0.00	0.36	0.00	0.00	1.54	0.00
Acetylene	1.00	0.00	1.00	0.00	0.00	0.98	1.55	0.00	2.05	1.22	0.00	1.46	0.70	0.00	0.82
Ethylene	1.00	1.00	1.00	0.12	7.57	1.44	1.07	1.07	1.11	0.20	1.14	0.91	1.11	0.94	1.11
Propene	1.00	1.00	1.00	0.20	4.30	2.18	0.97	1.14	1.29	0.62	0.13	0.55	1.28	1.80	1.29
1,3-Butadiene	1.00	1.00	1.00	0.02	31.96	1.61	1.17	0.69	1.08	4.72	46.49	4.19	1.20	0.44	1.10
Formaldehyde	1.00	1.00	1.00	0.34	2.48	1.25	1.01	0.99	1.04	0.62	1.43	0.71	1.02	1.01	0.96
Acetaldehyde	1.00	1.00	1.00	0.29	6.95	1.72	1.24	1.93	1.29	0.87	1.24	0.83	1.38	1.44	1.20
Acrolein	1.00	1.00	1.00	0.52	1.95	1.61	1.06	1.08	1.27	0.80	0.49	0.79	1.20	0.94	1.34

Table 28: Comparison of FTIR Speciated HC measurements normalized to HCHO with Spicer et al and Knighton et al.

Fuel	JetA1		A		B		C		D		E		F		H		I		Spicer et al	Knighton et al
Gas Compound	1st idle	2nd Idle	1st idle	2nd Idle	1st idle	2nd Idle	1st idle	2nd Idle	1st idle	2nd Idle	1st idle	2nd Idle	1st idle	2nd Idle	1st idle	2nd Idle	1st idle	2nd Idle	4% Idle	
Benzene	0.31	0.19	0.36	0.35	0.39	0.30	0.23	0.30	0.31	0.22	0.01	0.01	0.25	0.16	0.23	0.13	0.16	0.28	0.053	0.06
Toluene	0.52	0.42	0.32	0.25	0.03	0.00	0.21	0.23	0.22	0.34	0.00	0.00	0.02	0.05	0.48	0.16	0.02	0.04	0.017	0.02
m-Xylene	1.09	0.81	0.98	0.69	0.10	0.02	0.64	0.62	0.70	0.60	0.01	0.00	0.09	0.16	1.27	0.48	0.12	0.22	N/A	N/A
o-Xylene	0.01	0.01	0.00	0.00	0.00	0.00	0.00	0.01	0.00	0.00	0.00	0.00	0.00	0.01	0.01	0.02	0.00	0.01	N/A	N/A
1,2,3-Trimethylbenzene	0.01	0.01	0.00	0.00	0.00	0.00	0.00	0.01	0.00	0.00	0.00	0.00	0.00	0.00	0.01	0.01	0.00	0.00	N/A	N/A
1,3,5-Trimethylbenzene	0.00	0.00	0.00	0.00	0.46	0.44	0.01	0.03	0.00	0.00	0.06	0.06	0.19	0.25	0.00	0.00	0.34	0.35	N/A	N/A
Acetylene	0.04	0.03	0.05	0.03	0.04	0.04	0.06	0.03	0.07	0.06	0.02	0.03	0.06	0.06	0.07	0.07	0.03	0.03	N/A	N/A
Ethylene	0.48	0.46	0.48	0.46	0.54	0.50	0.55	0.54	0.54	0.50	0.57	0.62	0.51	0.49	0.16	0.59	0.53	0.53	N/A	N/A
Propene	0.26	0.19	0.17	0.10	0.24	0.18	0.28	0.21	0.27	0.16	0.54	0.49	0.25	0.24	0.26	0.15	0.33	0.26	0.26	0.31
1,3-Butadiene	0.33	0.30	0.31	0.29	0.34	0.27	0.32	0.25	0.40	0.33	0.42	0.45	0.38	0.32	2.51	1.78	0.39	0.35	N/A	N/A
Acetaldehyde	0.16	0.15	0.18	0.20	0.19	0.16	0.26	0.30	0.22	0.21	0.14	0.15	0.19	0.19	0.22	0.18	0.21	0.19	0.24	0.18
Acrolein	0.42	0.39	0.47	0.47	0.51	0.45	0.59	0.70	0.52	0.52	0.29	0.32	0.44	0.47	0.55	0.43	0.50	0.54	0.19	0.18

7.2.2.3 Effect of properties of compositionally designed surrogate fuels on aldehydes emissions

7.2.2.3.1 Impact of fuel density on aldehyde emissions

Fuel density is a function of fuel chemical compositions and related to hydrocarbon types, length of carbon chains and ratio of H/C etc. Fig.7.22 shows the formaldehyde emissions as a function of fuel density for cold idle and full power engine running conditions respectively. The GTL fuel (fuel E) has the lightest density while the cycloalkane based fuels (A and C) have the heaviest density similar to conventional kerosene fuel. The emissions of formaldehyde increased as the fuel density increased at the cold idle engine condition. A good linear correlation was shown. Thus high H/C will have low soot and this is shown in the results. Aromatics also have a higher density than paraffins and so high H/C fuels are low density**.** However, there was no correlation between formaldehyde emissions and fuel density at the full power condition. This is due to that at the full power condition the flame temperatures were higher and thus resulted in more complete combustion.

Acetaldehyde emissions detected were not significant (lower than 5 ppm) and thus not presented. Acrolein emissions showed a weak correlation with fuel density at both idle and full power conditions as shown in Fig.7.23.

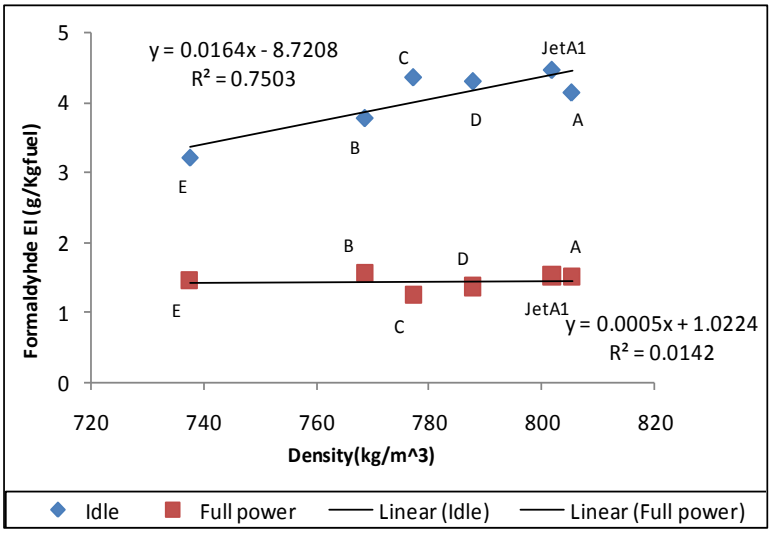

Figure 7.22: Formaldehyde emissions as a function of fuel density.

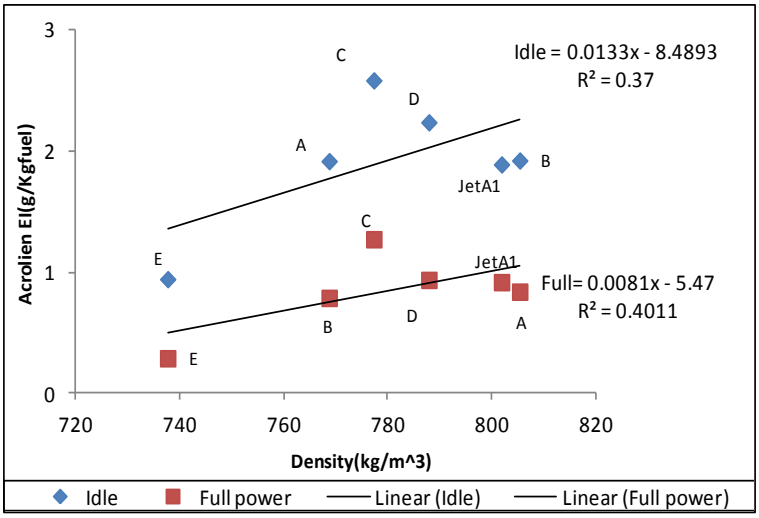

Figure 7.23: Acrolein emissions as a function of fuel density.

7.2.2.3.2 Influence of hydrogen to carbon ratio of fuels on aldehyde emissions

All the testing fuels' hydrogen to carbon elemental ratio was determined. The influence of H/C ratio on emissions was investigated. Fig.7.24 shows the correlation of formaldehyde emission and fuel H/C ratio for cold idle and full power conditions respectively. An inverse correlation between formaldehyde and H/C ratio was observed at the idle condition with a reasonable coefficient (R^2 = 0.56). The formaldehyde emissions were reduced as the H/C ratio increased. There were no correlations observed at the full power condition, which was related to the higher flame temperatures. Fig.7.25 shows that there was no clear correlation between acrolein emissions and fuels' H/C ratio. Acetaldehyde emissions detected were not significant (lower than 5 ppm) and thus not reported.

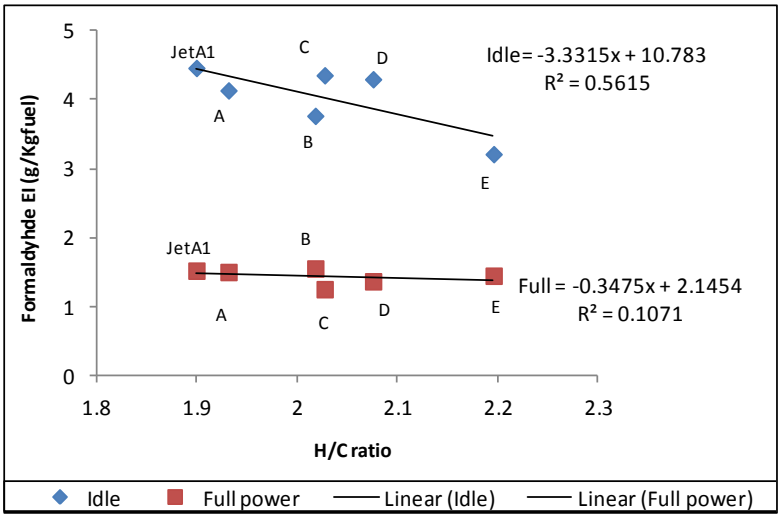

Figure 7.24: Formaldehyde emission index as a function of fuel H/C ratio.

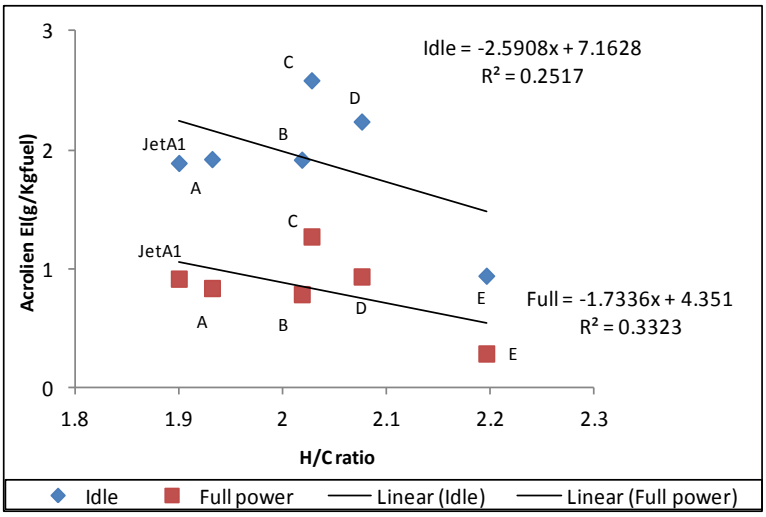

Figure 7.25: Acrolein emissions as a function of fuel H/C ratio.

7.2.2.3.3 Correlation between alkane fraction and aldehyde emissions

The influence of fractions of alkane components in the fuel on aldehyde emissions was determined by comparison of four fuels with different GTL fractions, i.e. the GTL(E) fuel was used as a blending component to represent pure alkanes. Fig.7.26 shows the formaldehyde emissions in g/kgfuel as a function of alkane fractions (by mass) at the idle and full power conditions. The results showed that the increase of alkane fractions in fuels caused a decrease in formaldehyde emissions at the idle condition but reductions were not linear. The most significant decrease occurred between 80% and 100% alkane fractions, which acounted for 28% reduction in formaldehyde emissions. There was no influence of alkane fractions on

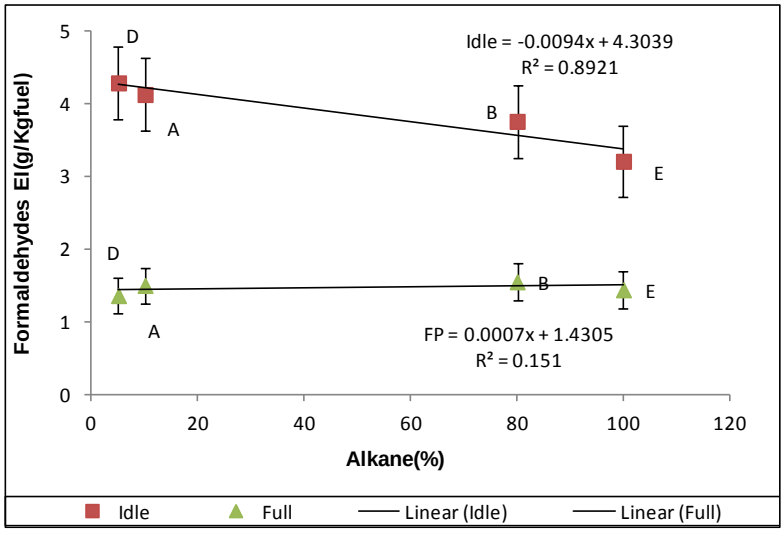

Figure 7.26: Formaldehyde EI as a function of alkane fractions.

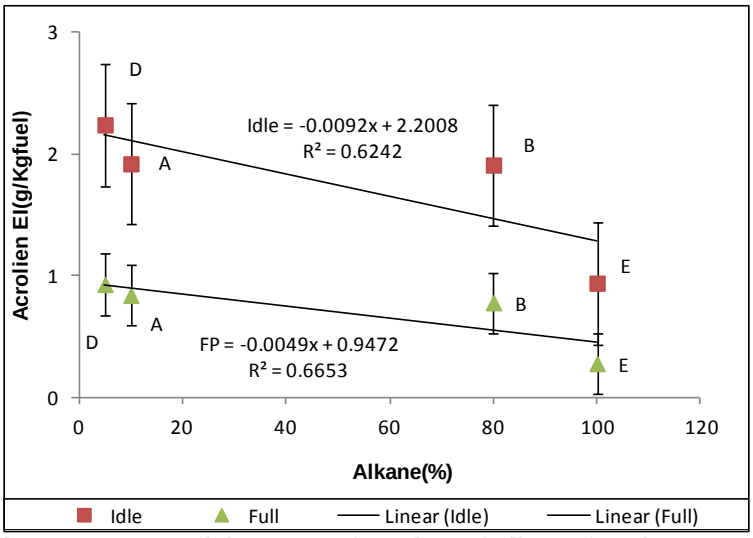

Figure 7.27: Acrolein EI as a function of alkane fractions.

formaldehyde emissions at the full power condition. Fig.7.27 shows acrolein emissions as a function of alkane fractions. A similar trend was observed for the idle condition with the exception of more obvious reduction between 80% and 100% alkane fractions.

7.2.2.3.4 Correlation between cycloalkane and aldehyde emissions

Fig.7.28 shows the formaldehyde emissions as a function of cycloalkane fractions. The addition of cycloalkanes caused an increase in formaldehyde emissions at the idle condition but no influence at the full power condition. Fig.7.29 shows the acrolein emissions as a function of cycloalkane fractions. A clear trend of positive correlation between the fraction of cycloalkane and acrolein emissions was shown at both idle and

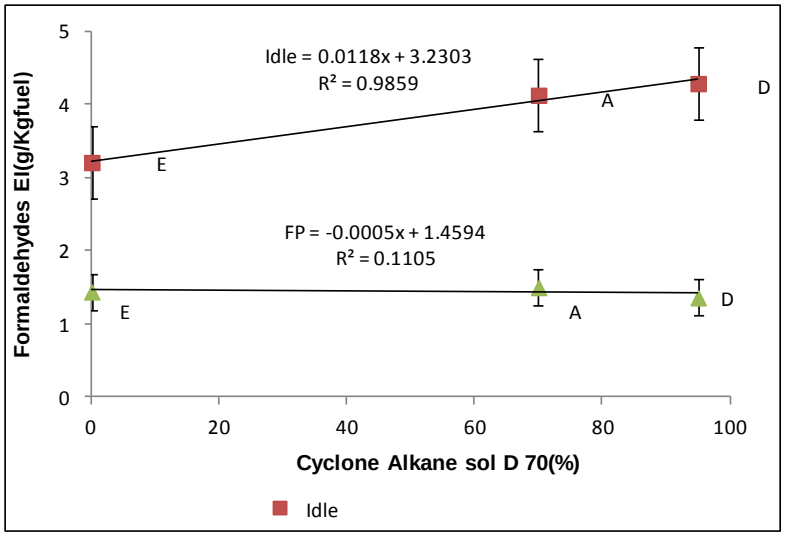

Figure 7.28: Formaldehyde emissions as a function of cycloalkane fraction

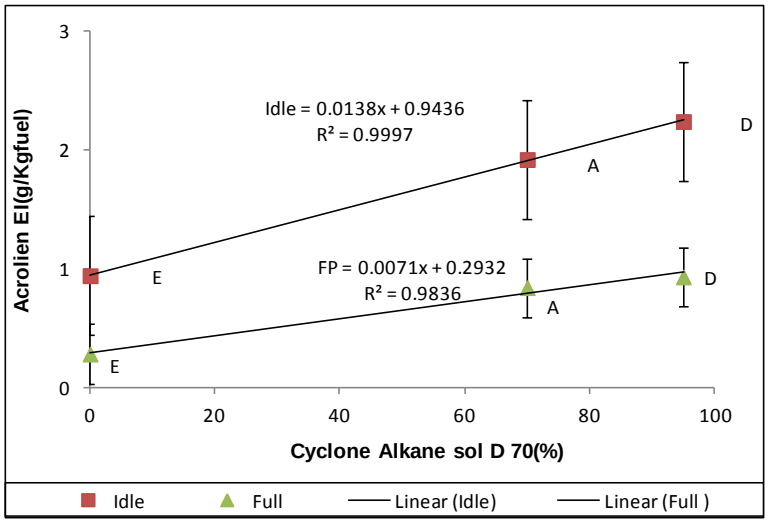

Figure 7.29: Acrolein emissions as a function of cycloalkane.

full power conditions. Formaldehyde emissions increased by ~80 at idle and ~100% at full power.

7.2.2.3.5 Correlation between aromatics fraction and aldehyde emissions

Aromatic hydrocarbons exist naturally in conventional petroleum derived fuels. The influence of aromatics on formaldehyde emissions was determined by a comparison of JetA1, E and B fuels. The former has no aromatics and the latter has 20% aromatics. Fig.7.30 shows the comparison results. It shows that aromatics fractions intended to increase formaldehyde emissions at the idle condition but no impact at the full power condition. However, the difference is not significant and within the error band.

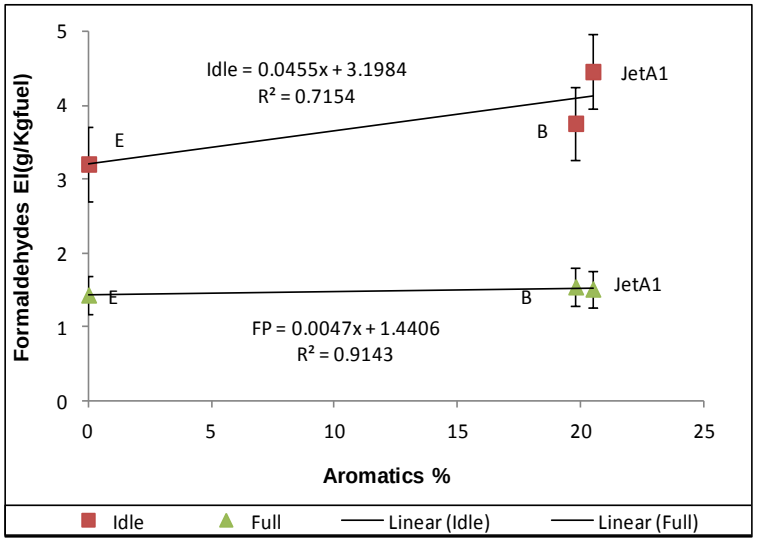

Figure 7.30: Influence of aromatics fraction on formaldehyde emissions.

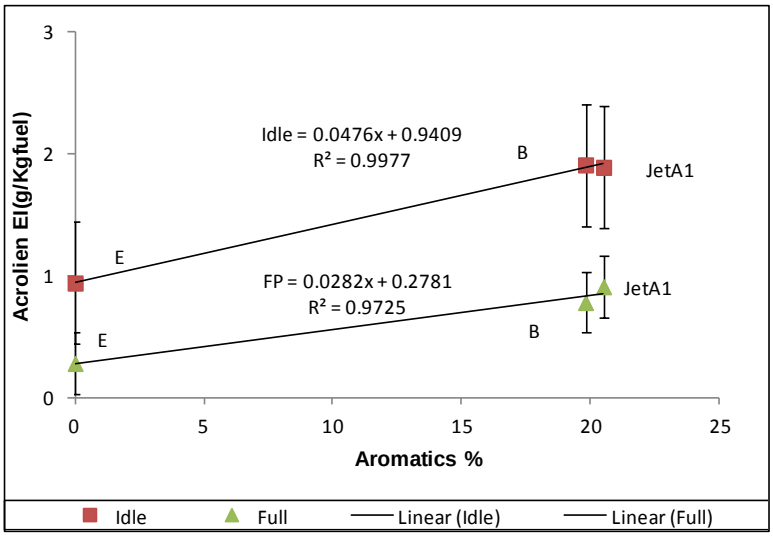

Figure 7.31: Influence of aromatics fraction on Acrolein emissions.

The increase of fractions of aromatics increased acrolein emissions as shown in Fig.7.31 at both idle and full power conditions.

7.3 Conclusions

Five compositionally designed surrogate fuels were tested for gaseous emissions, VOCs and smoke numbers using a re-commissioned gas turbine Artouste Mk113 APU engine. The engine was operated at two power settings and three operational modes: cold and hot idle and full power. Also a matrix of fuels comprised of conventional JetA1, GTL, HVO, HRJ and FAE etc were tested using the same engine. The results show that:

1. The CO emissions index ranges from 69-97g/Kg depending on fuel type. The higher the fuel energy content, the lower CO emissions. At idle CO were reduced by 18% for fuel A, B and D and 12% for fuel C relative to JetA1, whereas 28% reduction for the GTL fuel (E).

2. At idle, fuels A-D registered a 17% reduction of UHC relative to JetA1, whereas a 44% reduction for the GTL (E). This demonstrated that the greatest reduction in CO and UHC emissions were achieved by removing aromatics in fuel.

3. The result showed that there are no significant differences in NOx emissions were observed for all fuels at both conditions, indicating the flame temperature are close.

4. JetA1 produced the highest amount of CO_2 and lowest amount of water vapour due to its lowest H/C ratio.

5. For all fuels at both the idle and full power engine operation conditions, formaldehyde is the dominant aldehydes species with a fraction of 45~75% of total measured aldehydes in terms of g/kgfuel.
6. Formaldehyde emissions showed a clear positive linear correlation with fuel density at the idle engine condition. The trend for acrolein emissions was less clear. There was no correlation between formaldehyde, acrolein and fuel density at the full power engine condition.
7. Formaldehyde emissions were inversely correlated to the fuel H/C ratio at the idle engine condition. There was no clear correlation between the fuel H/C ratio and acrolein emissions at both engine power conditions.
8. The increased fractions of alkanes in the fuel could reduce aldehydes emissions at the idle engine condition but the reduction was not linear.
9. The increase of cycloalkane fractions in the fuel could increase aldehydes emissions at the idle engine condition.
10. The comparison between 0% and 20% aromatics fractions showed that aromatic components could increase idle formaldehyde emissions slightly. The impact of aromatics is more obvious for acrolein emissions.
11. Aldehydes emissions from conventional JetA1 fuel could be reduced by the addition of alkanes (<40% alkanes).

12. The results show that at the idle condition, CO and UHC emissions were reduced by all five alternative fuels compared to JetA1 whereas at the full power condition both reductions and increases in CO were observed by alternative fuels.

13. In general, alternative fuels showed similar or lower level of NOx at both power conditions. NO_2/NOx fraction for all fuels was around ~40% and 55% at full and idle conditions respectively.

14. Fuel E produced the lowest CO_2 emissions due to its highest H/C ratio but it also produced the highest amount of water vapour, which may be of concern for aviation as water vapour at altitude could contribute to the formation of contrails.

Chapter 8 : Particulate matter emissions of alternative aviation fuels form Auxiliary Power Unit (APU).

8.1 Introduction

Particles from combustion processes in aero gas turbine engines are small in size but large in number with diameters ranging from 15 to 40nm in fresh exhaust [140, 142]. Nanoparticles are typically hydrocarbons or sulphate and formed by nucleation during dilution and cooling of the exhaust, whereas ultrafine particles (accumulation mode particles) are mainly carbonaceous soot agglomerates formed directly by combustion [175, 189]. Volatile particles may grow significantly in terms of mass and number in the engine plume depending relative humidity and temperature. Currently probe measurement and ICAO methodology are being adopted in the measurement of gaseous and smoke emissions from aircraft engines and its Auxiliary power unit (APU) [6, 8]. The PM emission can be then determined by smoke number (SN) using FAO method.

8.2 Review of previous work

Lack of information on particulate number concentration and size distribution made the evaluation of the impacts of aviation on environment difficult. Timko et al [184]measured particulate emissions of 16 separate gas turbine engines and investigated the effect of fuel composition at engine exit and 15-50 meter downwind. Their main findings are that a greater amount of soot generated at climb out and takeoff compared to idle and approach. Also the total number of the particulates increased by one or two orders of magnitude at 50m compared at the engine exit. The main reason behind this is nucleation of the volatile particles which consist of sulphate and organic materials. Corporan et al observed significant reductions in non-volatile PM from an older military engine and from a research combustor using FT fuels[179]. The effect of alternative fuels on particle emissions from a NASA DC-8 aircraft with GE CFM56-2C1 and APU burning JP8, FT and blend of both were investigated by Bulzan. Significant reductions in particulates emissions were observed with FT and blends at all power levels. The reduction was a function of power level and fuel composition[181].

This work investigated the impact of fuel compositions on particulate number and mass concentrations and size distributions from an APU gas turbine engine. The fuels tested for gaseous emissions and VOCs in the previous chapter will be tested here for PM. Two engine power settings were used: idle and full power conditions. Particle number concentration and size distribution as a function of fuel H/C ratio and fuel compositions (blending ratio) at each operating condition was determined and compared to reference fuel JetA1. Details about the engine, fuel properties and experimental set up were described in section 3.1.2. Line losses were measured using JetA1 fuel as discussed in chapter 6 and particle sizes were plotted against penetration factors as shown in Fig. 6.3. The corrections of line losses applied for all fuels at idle and full power and there was no fuel effect. This was done by divided the particulate number by penetration factor at each diameter.

8.3 Particulates from Compositionally designed surrogate fuels

8.3.1 The number and mass particle size distributions (PSD)

8.3.1.1 Effect of engine power on Particulate size distributions

The number and mass size distributions recorded during the study at cold and hot idle and full power for all fuels and were converted to EIn and EIm size distributions. Fig.8.1 shows EIn(P/Kg-fuel) and EIm(g/Kg-fuel) for JetA1 and fuels A, B, C, D and E respectively. The EIn from all conditions displayed unimodal, nearly lognormal distributions. The peak size (mode size) was at around 35 nm, shifting towards the larger size as the power changed from idle to full power for all fuels probably due to coagulations. Comparing particle concentrations between cold and hot idles and full power, it is observed that the full power condition produced the highest number of particles, followed by the cold idle and then the hot idle. This was similar to the results reported by other people that the particulate numbers were sensitive to engine power settings [181, 184].

The distribution of particles for both idles were similar but the hot idle produced lower peak numbers of particles compared to cold idle for all fuels. Between different fuels, the peak concentrations at full power showed a

similar level for fuel A, B and C at around $2.43x10^{16}$ N/cm^3, and started to reduce for fuel D and were approximately halved for fuel E. The same trends were observed for idles, with an extreme case that fuel E had very low particle concentrations at both idle conditions where the peak concentrations were $7.06x10^{14}$ $P/_{Kg}$ and $9.6x10^{14}$ P/cm^3 at cold and hot idle respectively whereas the peak concentrations for JetA1 were $1.53x10^{16}$ $P/_{Kg}$ and $1.18x10^{16}P/_{Kg}$ at cold and hot idle respectively. All these indicated that as the H/C ratio of fuels increased the particle numbers decreased at the idle and full power conditions but the largest reduction was achieved by the neat GTL fuel (the highest H/C ratio) at the idle conditions.

Fig.8.1 also shows that particle mass distributions for all fuels in the range from 40nm to 100nm emitted at both idles and full power. This finding is consistent with Lobo et al and Mazaheri et al results[197, 198].Thus, lower mass particles size disruptions at idle compared to full power were observed. Fuel A has higher particle mass compared to JetA1, whereas fuels B, C, D and E produced lower mass emissions at all power conditions. The presence of 70% of cycloalkanes and 20% aromatics in fuel A made the EIm higher than base fuel.

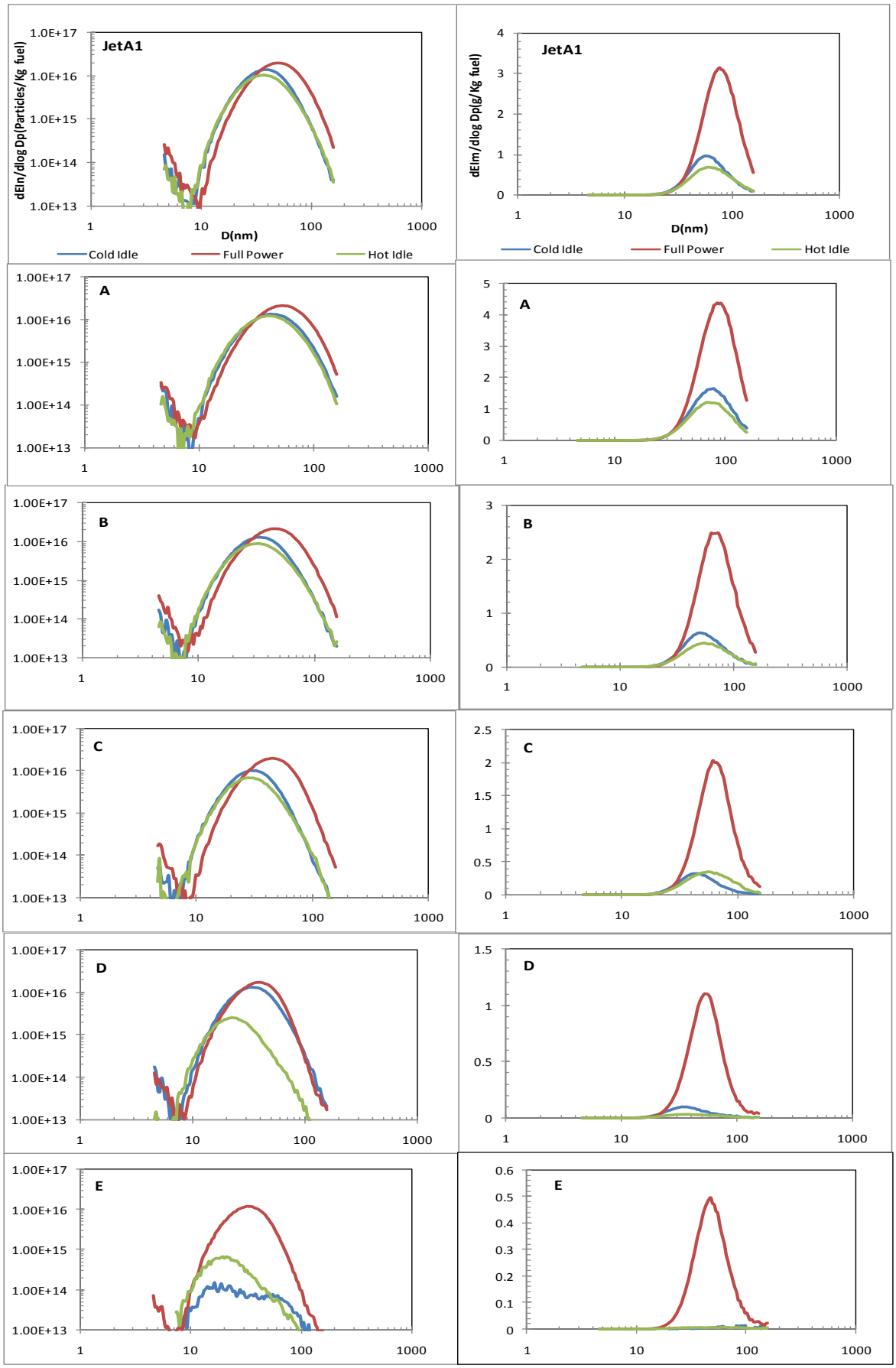

Figure 8.1: Comparison of particulate number and mass size distributions of all fuels at cold idle, hot idle and full power condition.

8.3.1.2 Effect of fuel H/C elemental ratio on particle number and size distribution

The number and mass of particle size distributions as a function of fuel H/C ratio at cold idle, full power and hot idle respectively are presented in Fig.8. 2. Particulate number concentrations decreased as the fuel H/C ratio increased for all three engine operation conditions. For EIn, the peak size (mode size) was at around (20-40 nm) for both idles and shifting towards the larger size (30-60 nm) at full power. The highest peak particle concentrations were found at full power conditions. Again as mentioned earlier, the hot idle produced lower peak particle concentrations compared to the cold idle for all fuels for the same reason explained previously. A general trend was observed for all three operation conditions, i.e. as the H/C ratio increased the particle peak concentrations reduced and the mode sizes were also reduced. The results also showed that particle peak concentrations were more sensitive to fuel H/C ratio at idles than the full power condition. This could be due to the lower combustion temperature at idles.

The shift of the mode size towards smaller diameter particles with the higher H/C ratio was primarily due to reductions in soot nuclei formation with non-aromatic fuel, therefore, reducing the pond of growing particles available for coagulation and surface growth. Fuel E has the highest H/C ratio (2.19) and zero aromatics while JetA1 has the lowest H/C ratio (1.89) and highest aromatics. Consequently, the mode size for fuel E is the smallest. The smaller mode size at idle was due to the higher unburned hydrocarbon emissions produced at idle than full power, which promoted the formation of nanoparticles. No aromatics and higher (H/C) ratio were the major factors in the reduction of particles for fuel D and E at both idle and full power conditions. However, particle size distributions of fuel A shifted slightly to the right to bigger diameter particles with the same peak concentration compared to base fuel (JetA1) at cold idle and higher peak at hot idle. This is in good agreement with other people's work[181].

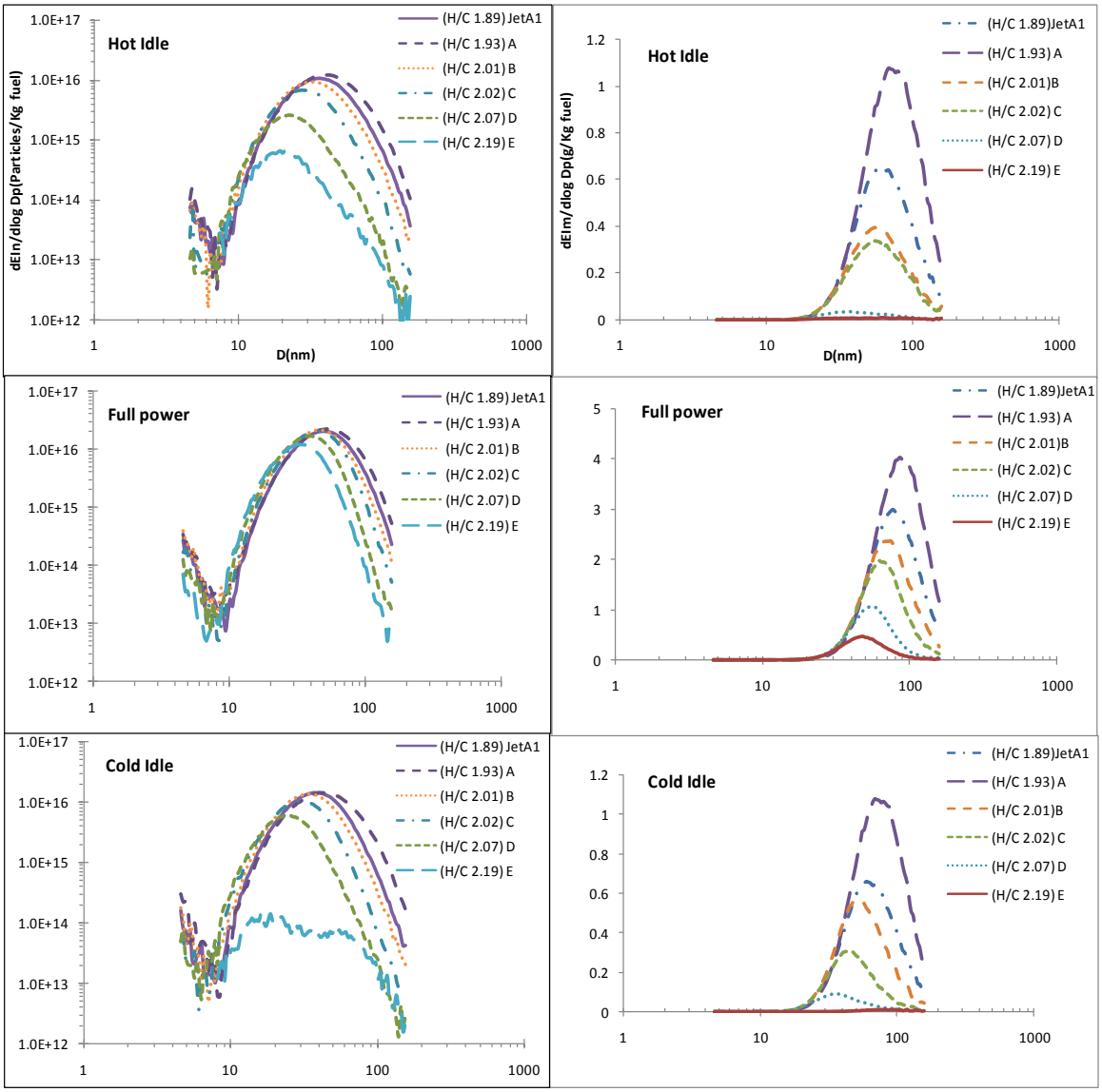

Figure 8.2: Particle size number and mass distributions (Eln& Elm) for the fuels with different H/C ratio.

For all the fuels, the peak particle concentrations at full power were between $1.18x10^{16}$ and $2.43x10^{16}$ $P/_{Kg}$ and the peak size range was 30-60nm, significantly higher than that observed at idle. The fuel E produced the lowest peak particle number and mass concentrations for all the three operation conditions. At the full power condition, fuels A, B, C and JetA1 produced the similar peak concentrations of particle number because all of them contained aromatics. At the idle condition, fuel C produced slightly lower peak concentration of particles than fuels A, B and JetA1 but in general, fuels A, B, C and JetA1 had higher peak concentrations than fuels D and E. Comparing fuel A with fuel D, both fuels contained large fractions of cycloalkanes but fuel D has no aromatics. Therefore fuel D produced lower

peak particle number concentrations and smaller mode size of particles. All of these are clearly showing that aromatics have a significant impact on particle concentrations. By comparison of fuel D (95% of cycloalkanes) and E (100% alkanes), Fuel D produced obviously higher peak particle number concentrations. This is because cycloalkanes can raise soot emission due to that they are known to dehydrogenate and produce aromatics which can lead to the production of polycyclic aromatics that are thought to be inception sites for soot growth.

Similar trend was observed with EIm, Particulate mass concentrations decreased as the fuel H/C ratio increased for all three engine operation conditions. The peak size for EIm, was larger than that observed with EIn, (20-50 nm) for both idles and shifting towards the larger size (50-100 nm) at full power. Moreover, as mentioned earlier as the H/C ratio increased the particle mass peak concentrations reduced and the mode sizes were also reduced for all fuels except fuel A which is due to cycloalkanes. For EIm at idle dramatic reductions of 86% were observed for GTL, 34% for fuel B and C and 83% for fuel D. At full power Elm was reduced by 83% for the GTL fuel, 16% with fuel B, 33% for fuel C and 66% with fuel D relative to JetA1. However, fuel composition such aromatics and carbon to hydrogen ratio has great impact on particle mass concentration.

8.3.1.3 Effects of Cold and Warm Engine Conditions

The PM emissions were measured under both cold and hot idle engine conditions. The particle size distributions were compared between the cold and hot starts for total number concentrations (dW/dlogDp), total EIn, number based GMD and GSD (Geometric Standard Deviation) as shown in Fig.8.3 and the same comparison for the mass based distributions also shown in the same figure. Slight differences were observed in particle number distributions between cold and warm engine conditions for all fuels except for fuel D and E, where cold idle has particle number concentration higher than warm idle. Particle number concentration, GMD and GSD obtained at cold engine conditions were plotted against the corresponding data under warm engine conditions in Fig.8.3 to investigate the magnitude of these differences. The figure shows that the particle number concentration data obtained from cold engines were linearly correlated with the data

obtained from warm engines. The straight line had a slope of 0.95, indicating that the particle number concentrations were ~5% lower with warm engine than they were with cold engine. Also, the GMD and GSD, the correlation lines between cold and warm engine conditions have slope equal to 0.93 for GMD and 0.95 for GSD. Engine warm-up results in fewer particles being emitted, but does not markedly change the particle size distribution.

Similar trends were observed for particle mass distributions for all fuels at both cold and warm idle. The particle mass concentrations were about 2% lower with warm engine (hot idle) compared to cold idle, whereas, GMD of cold idle is 3% bigger than warm idle, whereas the GSD slope equal to 0.8.

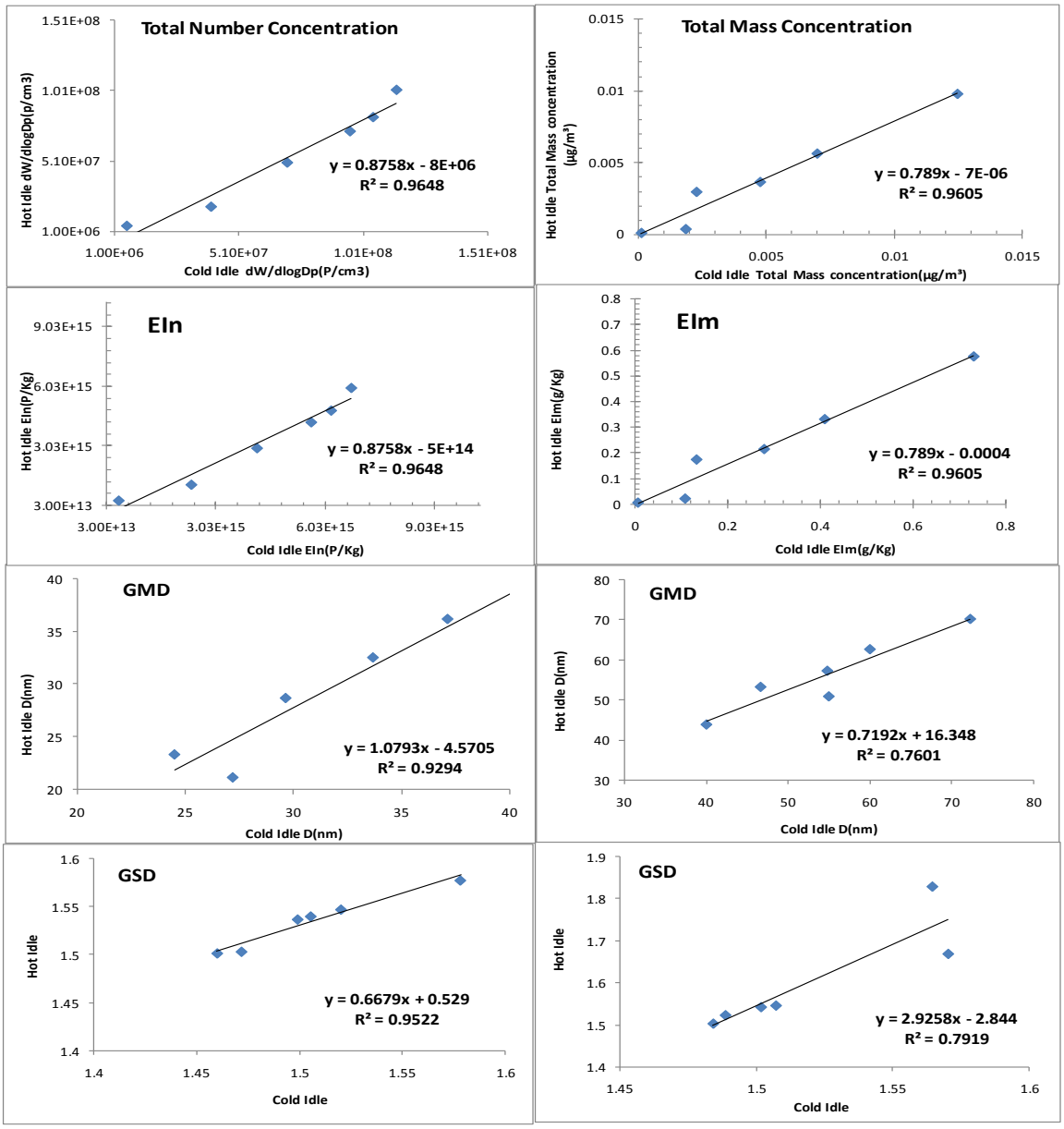

Figure 8.3: Comparisons of particle number, mass, EIn, EIm, GMD and GSD at both Idle.

8.3.2 Geometric Mean Diameter (GMD) and Standard Deviation (GSD)

The Geometric Mean Diameter (GMD) of particulate is a substitute for arithmetic mean diameter when incorporating logarithms of numbers. The value of the mean size is related to all particulates and thus sensitive to the quantities of particulate matter at the lower and upper ends of the distribution. Fig.8.4 presented number and mass based particles geometric mean diameter as a function of H/C ratio respectively. The results in Fig.8.4 (a & b) shows that the geometric mean diameter increased as the engine power increased.

Fig.8.4a showed that there are good linear negative correlations between the fuel H/C ratio and the GMD, especially at the full engine power condition. The number based geometric mean diameter (GMD) of particulates from this APU engine was in the range of 20~40 at nm at idle and 35-60 nm at full power. The higher GMD at high power (high fuel and exhaust flow rate) is due to short residence time in the plume and higher exhaust gas temperature which tend to suppress nucleation process.

Fig.8-4b presented mass based geometric mean diameter for all fuels at both idle and full power. The results illustrated that there were more scatter at both idles especially cold idle compared to full power data which have little scatter. The GMDm at both idle are small due to effect of nucleation, whereas at full power the size is larger. This finding is consistent with published work carried by Lobo et al[121]. The mass based geometric mean diameter (GMD) of particulates from for all fuels using APU engine was in the range of 40~70 at nm at idle and 50-80 nm at full power.

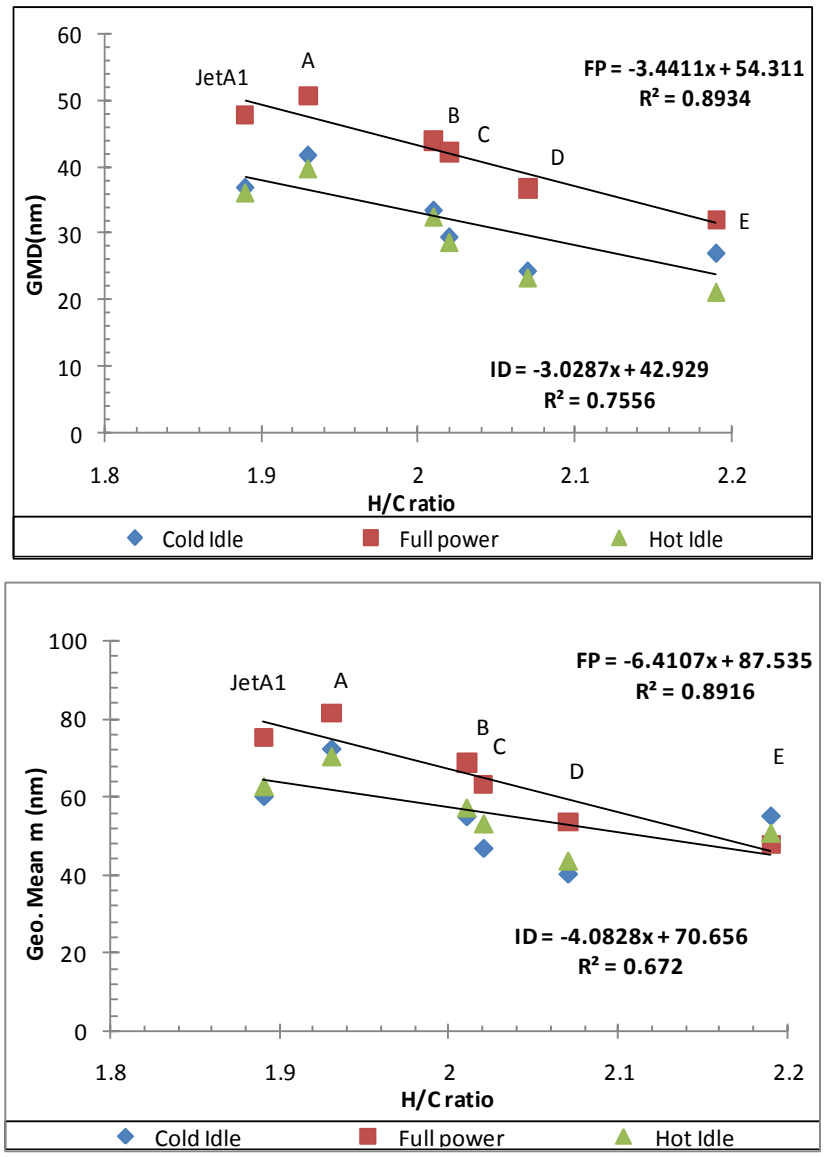

Figure 8.4: Geometric mean diameter of particulates as a function of fuels and engine mode, a) number, b) mass.

The geometric standard deviation (GSD), as a measure to assess the width of distribution curves. The geometric standard deviation for all fuels is displayed in Fig.8.5. There were no significant differences between different fuels, indicating very similar distribution characteristics. The results show that the GSDs for all fuels and conditions were close with a value of about 1.5~1.6 except the fuel (E) at cold idle, indicating very similar distribution characteristics for all fuels and conditions. The higher GSD value for the fuel (E) at cold idle was due to its significantly lower peak concentrations but similar distribution width.

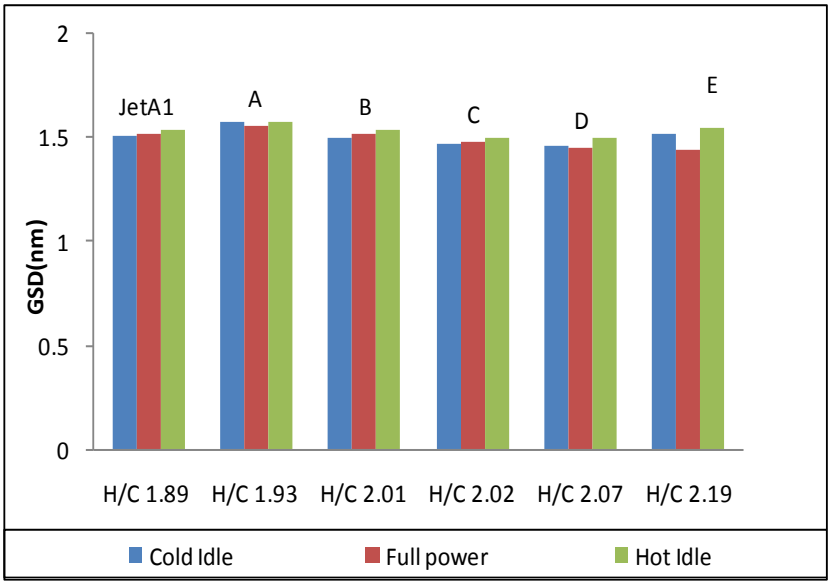

Figure 8.5: Geometric Standard Division of Particulates as a function of fuels and engine mode.

8.3.3 Effect of fuel Chemical compositions on total particle number concentrations

Fig.8.6 shows the total particle number concentrations (particles/cm^3) as a function of fuel H/C ratio at cold and hot idles and full power. There was a significant increase in total particle concentrations at full power for all fuels. This demonstrated that the engine produced a significantly higher number of particulates at full power condition. A clear trend for all power conditions was shown that total particle concentrations were decreased as the H/C ratio increased. A good linear relationship between total particle concentrations and fuel H/C ratio was observed.

A key objective of this research is to assess the influence of fuel blending components such as aromatics, cycloalkanes and alkenes on emissions. Fig.8.7 shows the total particle concentrations as a function of aromatics fractions. Good linear correlations between the fraction of aromatics in fuels and total particle concentrations are shown.

Fig.8.8&8.9 show the total particle concentration as a function of cycloalkanes fractions and alkenes fraction respectively. The results showed that total particle concentration independent of cycloalkanes fractions and alkenes fraction

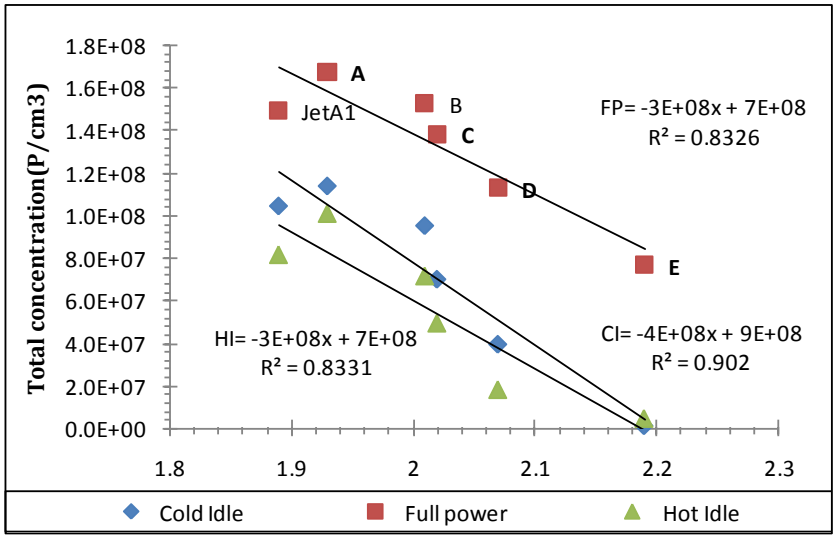

Figure 8.6: Total particulate number concentrations as a function of fuel H/C ratio at various fuels and engine mode.

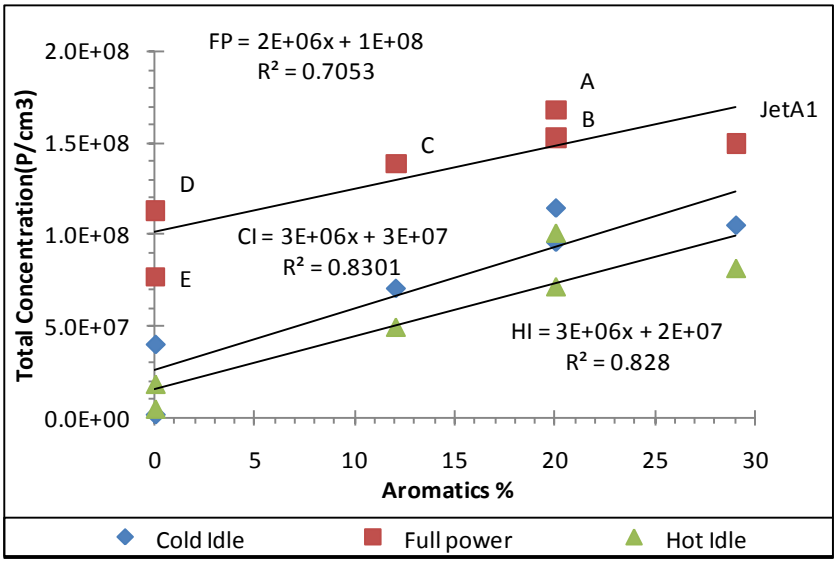

Figure 8.7: Total particle number as a function of Aromatics %.

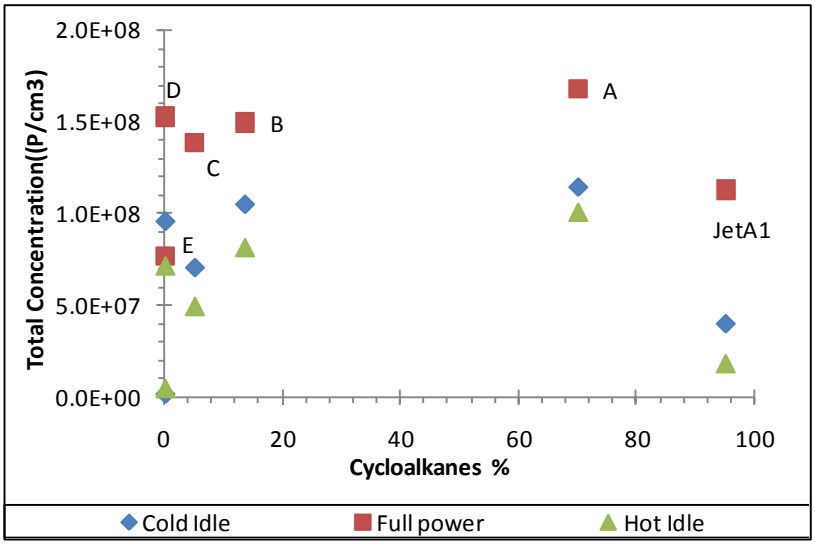

Figure 8.8: Total particle number as a function of Cycloalkanes %

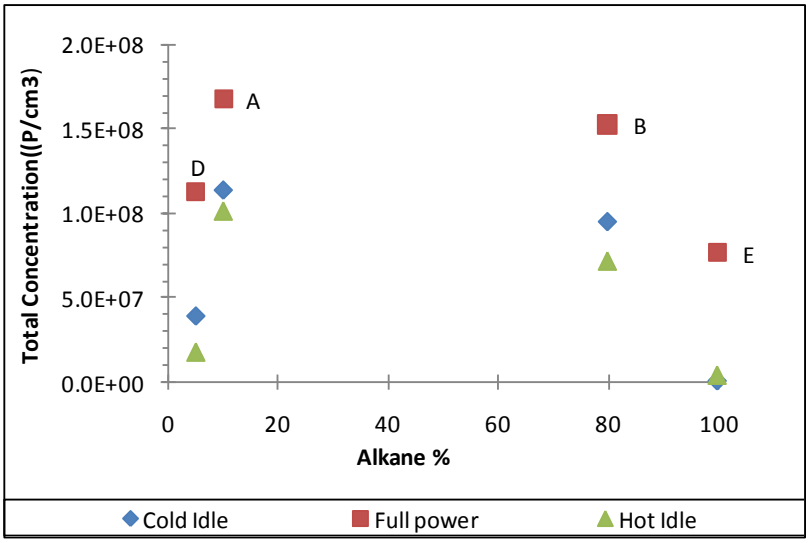

Figure 8.9: Total particle number as a function of Alkane content.

8.3.4 Emissions index (EI)

Beside the above parameters, it is convenient to discuss the influence of operating conditions (fuel type and fuel rate) on emissions index EI both number and mass based. Equation 24 was used to calculate both number and mass emissions index (EI).

Figs.8.10&8.11 represent number and mass based emissions index as a function of fuel type and power. EI n did not show a correlation with fuel H/C ratio while EIm had a reasonably good correlation with H/C ratio. Therefore, fuels properties have effect on EIm, these findings are in good agreements with other authors [13].

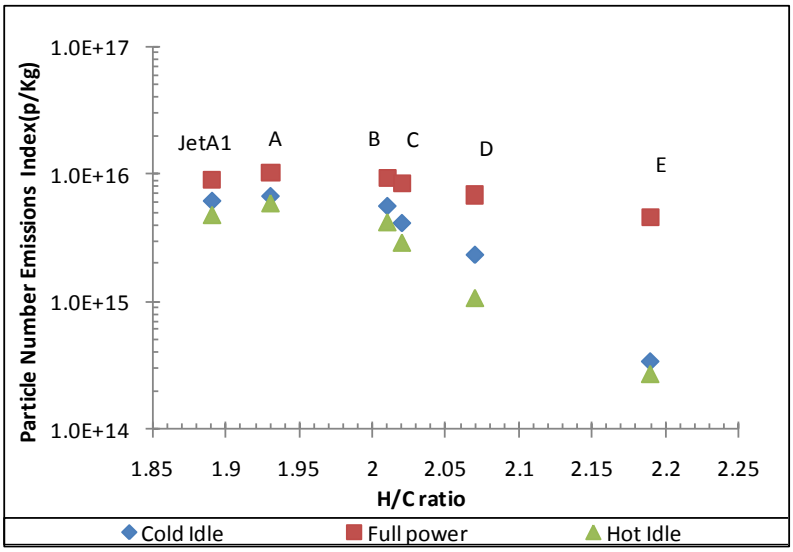

Figure 8.10: Number based emissions index EI n (N/kg fuel) as a function of fuels and engine mode.

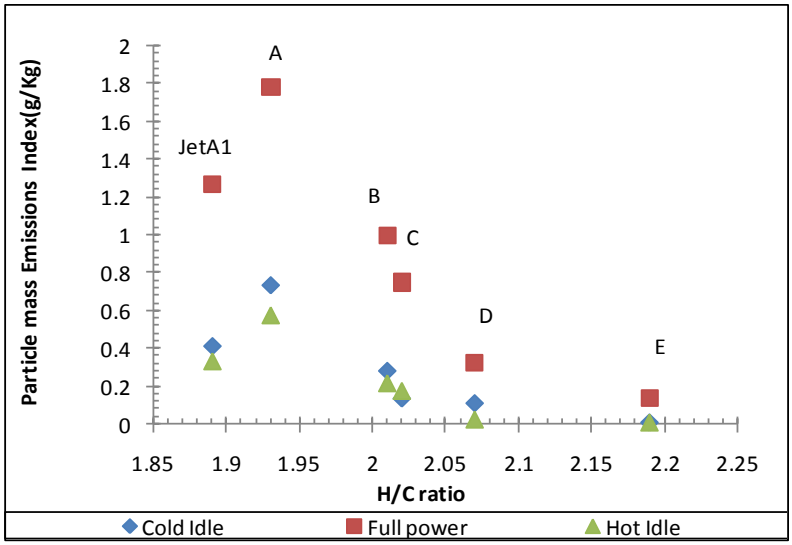

Figure 8.11: Number based emissions index EI m (g/kg fuel) as a function of fuels and engine mode.

8.3.5 Smoke Number

Engine exhaust smoke numbers (SNs) for different fuels were measured and are shown in Fig.8.12 as a function of fuel H/C ratio. The results showed that significant reductions in engine smoke numbers were observed as the fuel H/C ratio increased. The high smoke numbers for A and B were due to aromatics contents in fuels. The reduction of smoke number from A to B was due to replacement of cycloalkanes by alkanes (GTL) in B, indicating a stronger smoke tendency of cycloalkanes compared to alkanes.

The significant reductions in smoke numbers for D, C and E clearly demonstrated the role of aromatics in exhaust smoke, where all these three fuels had no aromatics and thus resulted in significant reductions in smoke numbers. The smoke number of A is higher than JetA1, indicating the combined contribution from aromatics and cycloalkanes. Aromatics on its own would not lead to a higher smoke number than JetA1, which was supported by the smoke number of B in which aromatics content was the same but has no cycloalkanes and thus resulted in a lower smoke number than JetA1.

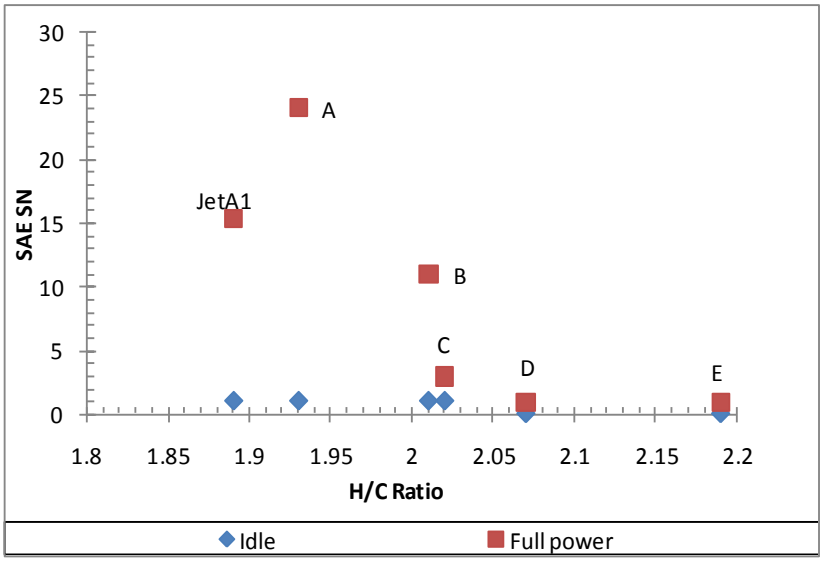

Figure 8.12: Smoke number measurements for various fuels at idle and full power operating conditions.

8.4 Particulates from Aviation Alternative fuels

The impact of fuel compositions (H/C elemental ratio), engine power (idle and full power) and operation mode (cold ad hot idle) on particulate number and mass concentrations and size distributions from an APU gas turbine engine will be investigated in this section. Four alternative fuels, including GTL (Gas To Liquid), HRJ (Hydrogenated Renewable Jet), HVO (Hydrogenated Vegetable oil) and FAE (Fatty Acid Ester), along with naphthenic cut were blended with convention Jet A1 and tested for engine exhaust particle number and mass size distributions. Two engine power settings and three operational modes were used: cold and hot idle and full power. The results will be compared to reference fuel JetA1.

8.4.1 The number and mass particle size distributions (PSD)

8.4.1.1 Effect of engine power on Particulate size distributions

The particle number and mass size distributions at cold and hot idle and full power for all fuels in terms of EIn (Particles/kg-fuel) and EIm (g/kg-fuel) are shown in Fig.8.13. The EIn from all conditions displayed bimodal distributions with a small peak at particle size of around 5 nm. The dominant particles are distributed around 10-100 nm. The mode size was at around 20-30 nm at idle and shifting towards 30-40 nm when the engine power changed from the idle to full power, which was probably due to the coagulation effects at full power. Comparing particle numbers between cold,

hot idles and full power, it is observed that the full power condition produced the higher number of particles than the cold and hot idles. This is similar to the results reported by other people that the particulate numbers were sensitive to engine power settings [19, 184]. Particle numbers were in a magnitude of 10^{15} to 10^{16} P/kg-fuel at the full power condition whereas 10^{14} to 10^{16} P/kg-fuel in the idle modes.

The influence of engine power on particle numbers varied depending on fuels. JetA1 showed minimal differences in particle numbers between full power and idle conditions while the fuel E had the most significant difference with a order of magnitude of 2 in particle numbers between the full power and idles. The fuel E demonstrated the lowest particle mass at idle conditions with the peak concentrations of $7.06x10^{14}$ P/kg and $9.6x10^{14}$ P/cm3 at cold and hot idles respectively whereas the peak concentrations for JetA1 were $1.53x10^{16}$ P/kg and $1.18x10^{16}$P/kg at cold and hot idle respectively. The significant lower particle numbers at idles for fuel E indicated the good combustion performance of GTL fuels at the low engine power condition due to its chemical characteristics. GTL fuels are paraffinic hydrocarbons and require lower flame temperatures to break and to be oxidized.

The mass size distribution of particles as shown in Fig 8.13 showed more variations between fuels. The peak particle mass was in a range of 0.06 to 1 g/kg-fuel at both idles 0.15-3.8 g/kg-fuel for full power. JetA1 had the highest mass particle emissions at all three engine operation modes. The fuel H had the lowest particle mass emissions at the full engine power due to its lowest number emissions. Fuel E produced the lowest mass emissions at the idle conditions. The difference in peak EIm between JetA1 and fuel H is ~25 times. The much high mass emission from JetA1 was due to the double effects: higher particle numbers and larger particle sizes (wider distributions). Comparing the fuels JetA1, E, F and H, the peak of EIn were similar for all fuels (10^{16}), but the peak of EIm were significantly different due to the different size distribution characteristics, i.e. the greater tail of the distribution curve (more larger particles) in JetA1 resulted in remarkably higher particle mass. Comparing to number distributions, the peak size (mode) of the mass distributions was increased and the distribution was narrower. The particle

mass distributions for all fuels were in the range of 20nm to 160nm for idles and full engine power conditions. This finding is consistent with Herndon et al and Mazaheri et al [197, 198].

The number and mass particle size distributions discussed above reflected the importance of fuel chemical compositions. Among three major hydrocarbon groups in fuels: paraffinic, cyclo-paraffinic and aromatic, paraffinic are the easiest to break down and to be oxidized while the aromatics are very stable and the most difficult to break down into small molecules. Aromatics in fuels tend to form carbonaceous particles and also could be a source for particulate PAH. This is why JetA1 showed the highest mass emissions and the fuel E had the lowest particle emissions at idle. The fuel born oxygen could reduce particle mass as shown in fuel H at full power but the high viscosity of FAE could cause adverse effect in fuel atomization if the blending ratio is to increase (in this case it is 10%) and thus deteriorate the combustion and emissions. Also the low energy density of FAE could lead to higher fuel consumption.

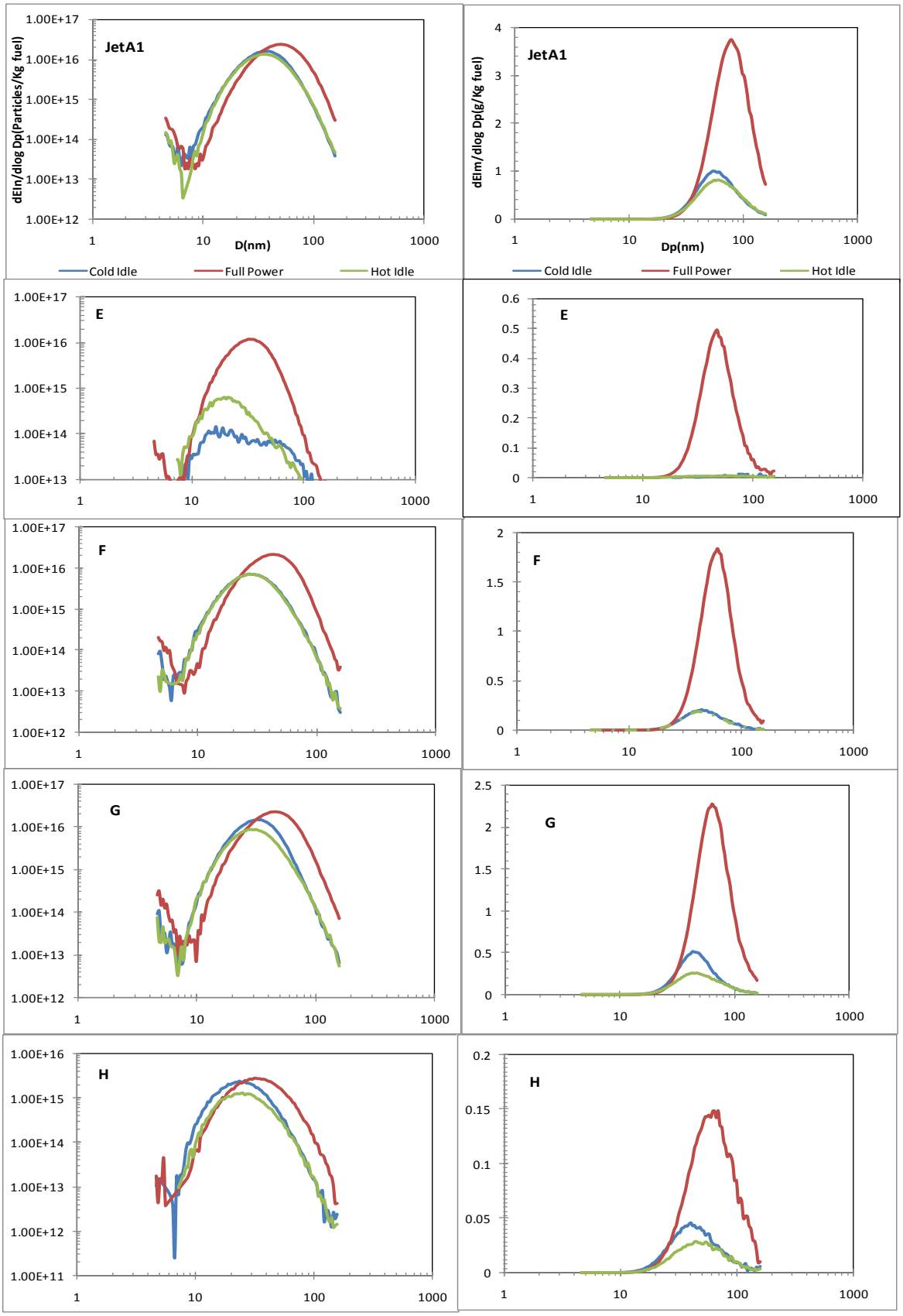

Figure 8.13: Comparison of particulate number and mass size distributions of all fuels at cold idle, hot idle and full power condition.

8.4.1.2 Effect of fuel H/C elemental ratio on particle number and size distribution

Fig.8.14 presents the particle size number and mass distributions in terms of EIn & EIm as a function of fuel H/C ratio for three engine operational modes. The peak number concentrations were mainly in the scale of 10^7~10^8 and EIn was mainly in the range of 10^{15}~10^{16} P/kg-fuel. A general trend of decreasing particle concentrations with increasing fuel H/C ratio is demonstrated, i.e. an inversely proportional correlation between fuel H/C ratio and particle numbers is present. Such correlations were the strongest at cold and hot idle and the weakest at full engine power condition.

The fuel H/C ratio is related to the fuel hydrocarbon compositions. As the fractions of alkanes increase the fuel H/C ratio would increase and thus the temperatures for complete combustions would be lower. The fuel E showed a clearly lower peak particle numbers at cold and hot idles but no such trend was shown at the full power. As the fuel E is GTL fuel (100% alkanes) the advantages of pure alkanes in reducing particle number emissions at low engine power conditions are demonstrated. The particle mass size distributions in Fig.8.14 followed the same trend of number, but JetA1 showed clearly higher EIm values than other fuels. This was due to that particle number distribution from JetA1 showed higher number of larger particles than other fuels.

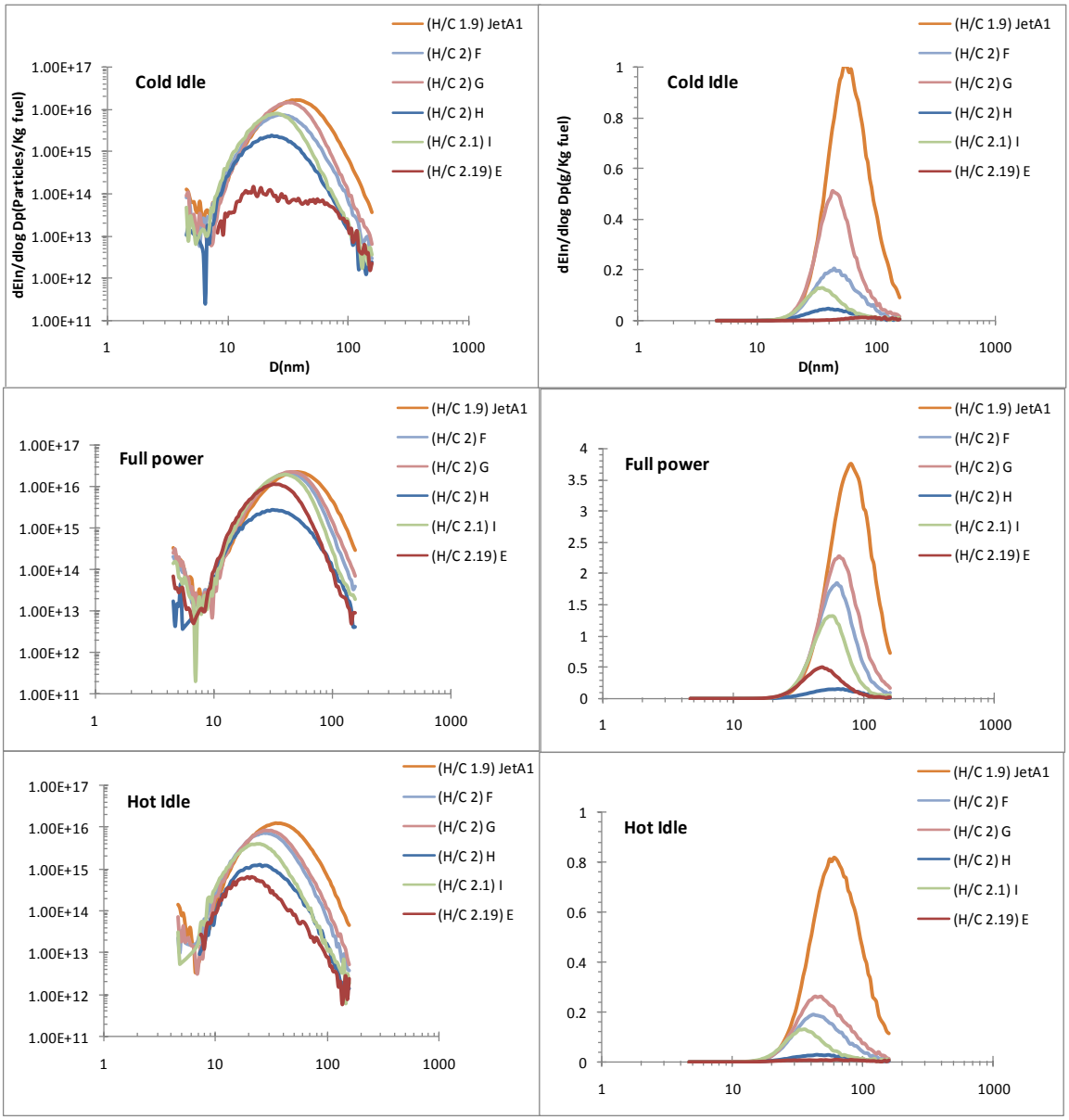

Figure 8.14: Particle size number and mass distributions (EIn& EIm) for the fuels with different H/C ratio.

8.4.1.3 Effects of Cold and Warm Engine Conditions

The engine was stared from a cold start (idle), followed by a full power mode and then reduced power to a hot idle mode before stop. The particle size distributions were compared between the cold and hot idles for total number concentrations (dW/dlogDp), total EIn, number based GMD and GSD (Geometric Standard Deviation) as shown in Fig.8.15 and the same comparison for the mass based distributions also shown in the same figure. The total number and mass concentrations from the hot idle were about 20% lower than that for the cold idle. The GMD for number distributions was 25~35 nm and increased to 40~50 nm for mass distributions, indicating an increase in particle sizes when converted the mass distributions. There were

little differences in the particle mean diameters between the hot and cold idles for both number and mass distributions. GSD, as a measure of width of the distribution curves, showed that the particle numbers had narrow distributions than the mass distributions. The wider mass distributions were due to the greater contributions to particle mass from relatively larger particles. The hot idle had narrower number and mass distributions than that of the cold idle. Good linear correlations between the hot and cold idles were observed for all these parameters, particularly for total particle concentrations and GMDs.

It needs to be stated that the cold idle measurements were started after the engine was stabilized which may take a few minutes. The transient emissions during the initial startup stages of the engine were not reported here, which would be higher.

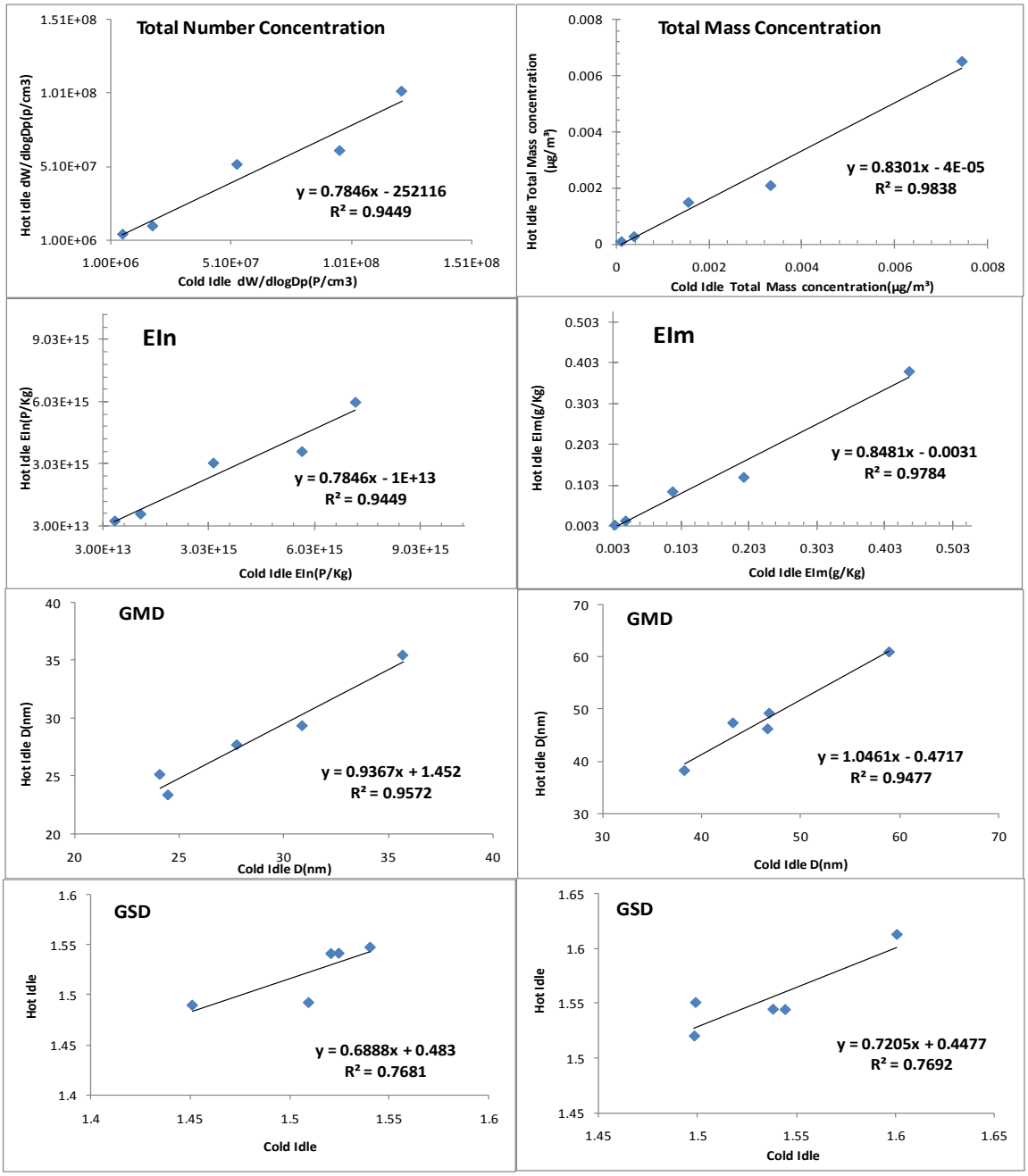

Figure 8.15: Comparisons of particle number, mass, EIn, EIm, GMD and GSD at both Idle.

8.4.2 Geometric Mean Diameter (GMD) and Standard Deviation (GSD)

Geometric Mean Diameter (GMD) of particle number and mass distributions was plotted against the fuel H/C ratio for all three engine operating conditions as shown in Fig.8.16 (a, b). For the number size distributions, there was a good inverse linear relationship between fuel H/C ratio and GMD for full power condition (R^2= 0.9) and reasonably good linear correlation for the idle condition (R^2=0.76). For the mass size distributions, a

fairly good inverse linear correlation between fuel H/C ratio and GMD was observed at the full power condition and idle conditions. The shift of particle mean diameters towards smaller sizes with the increase of fuel H/C ratio was related to aromatics contents in fuels. The increased fuel H/C ratio here was due to reduced aromatics in fuels, i.e. the aromatics would increase the mean particle sizes.

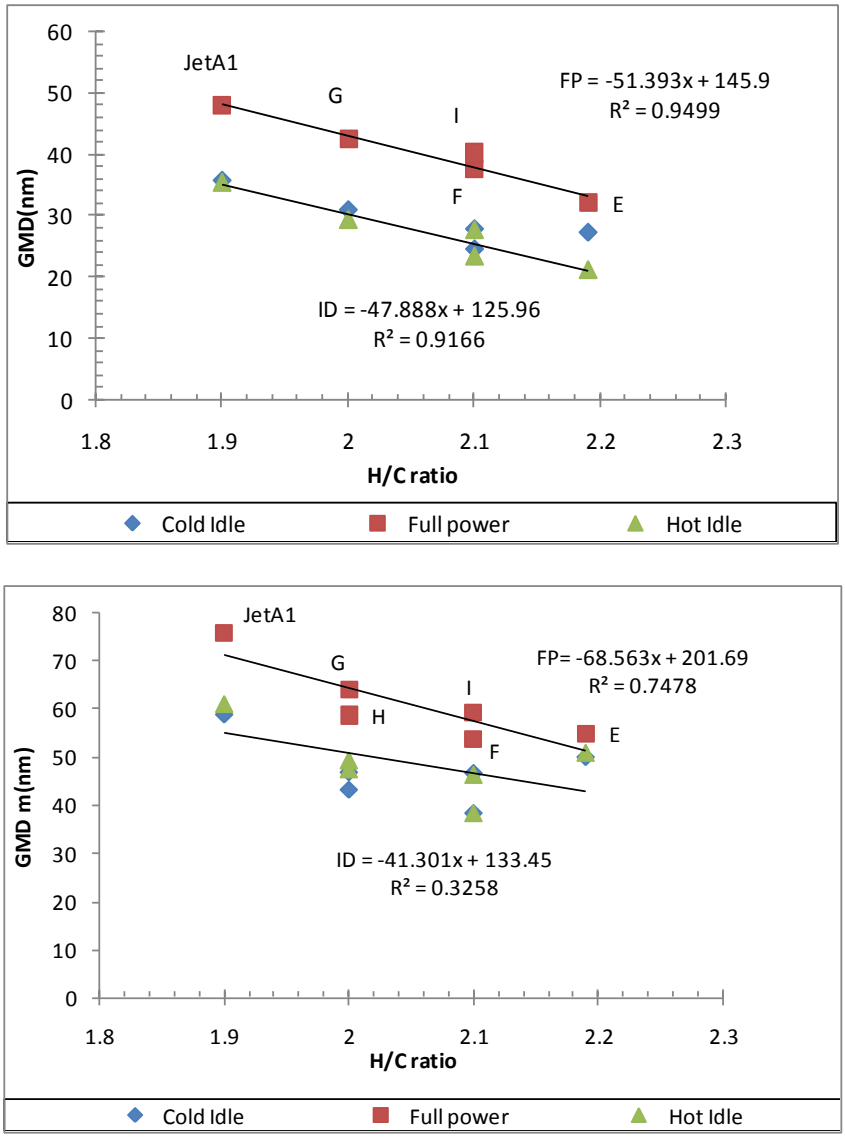

Figure 8.16: Geometric mean diameter of particulates as a function of fuels and engine mode, a) number, b) mass.

The geometric standard deviation for all fuels is presented in Fig.8.17. The results show that the GSDs for all fuels JetA1, E and H were close with a value of about 1.52~1.55 and fuel F, G and I have lower value between 1.44~ 1.5. The higher GSD value for the fuel (H) at cold idle was due to its significantly lower peak concentrations but similar distribution width.

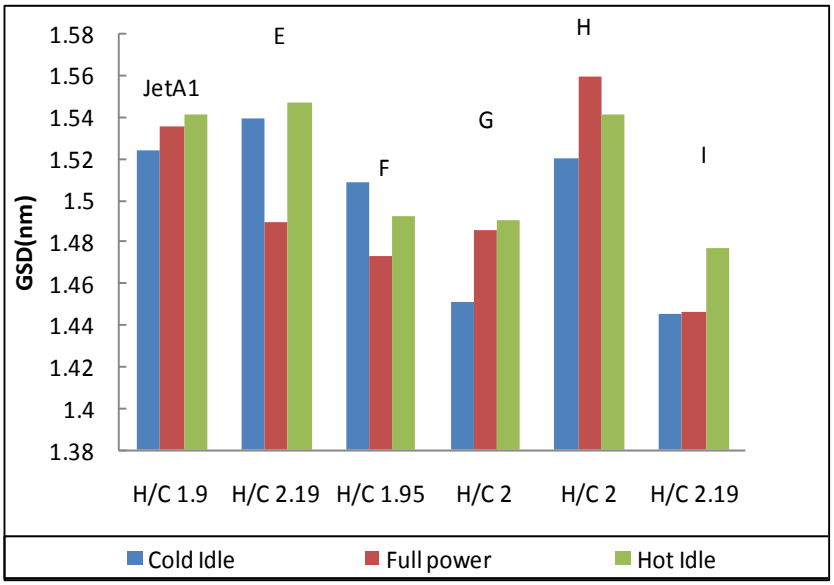

Figure 8.17: GSD for alternative aviation fuels.

8.4.3 Emissions index (EI)

Number and mass based emissions index as a function of fuel type and power are presented in Figs.8.18&8.19 respectively. EI was calculated using equation 24. Fig.8.18 showed that at full power, EIn and EIm did not show a correlation with fuel H/C. Therefore, fuels properties have no effect on EI.

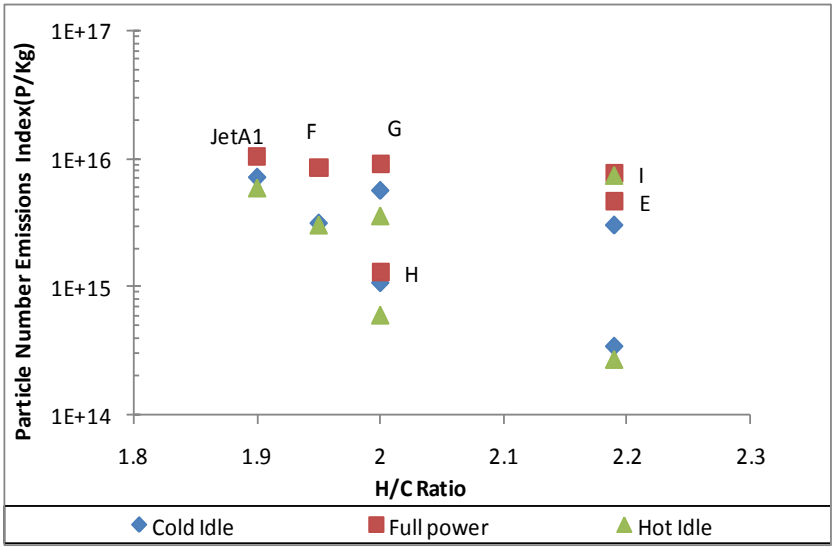

Figure 8.18: Particle number emissions index (P/Kg).

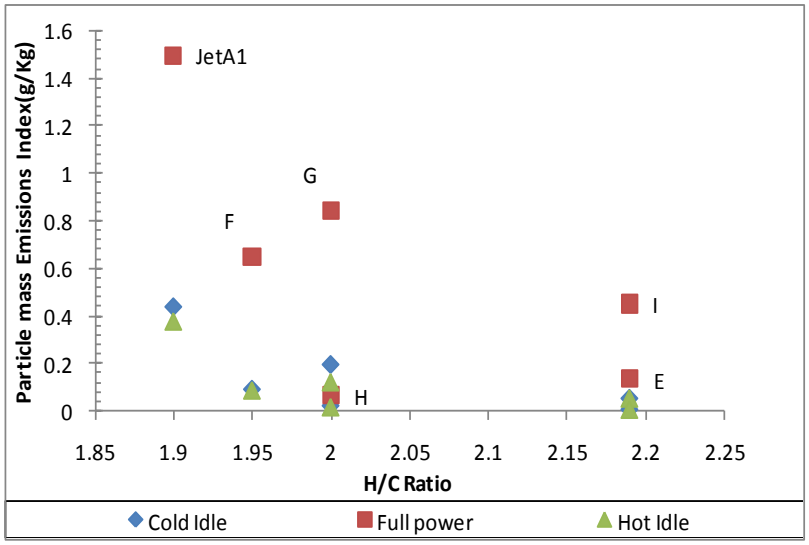

Figure 8.19: Particle mass emissions index (P/Kg)

8.4.4 Smoke Number

Engine exhaust smoke numbers (SNs) as a function of fuel H/C ratio for different fuels were measured and are shown in Fig.8.20. Significant reductions in engine smoke numbers were observed as the fuel H/C ratio increased. The high smoke numbers for H fuel was due to sulphur contents in fuels. The smoke number is also plotted as a function of fuel aromatics contents as shown in Fig.8.21. The significant reductions in smoke numbers for F, E and I fuels clearly demonstrated the role of aromatics in exhaust smoke, where fuels F and E had no aromatics and fuel I had low aromatics. However, aromatic hydrocarbons are not the only source to cause high smoke. The aromatic in Fuel H is similar to fuel I and yet the fuel H had significantly high smoke number due to FAE components in the blend. This is because of the poor vaporisation and atomisation of FAE due to its high viscosity and low volatility.

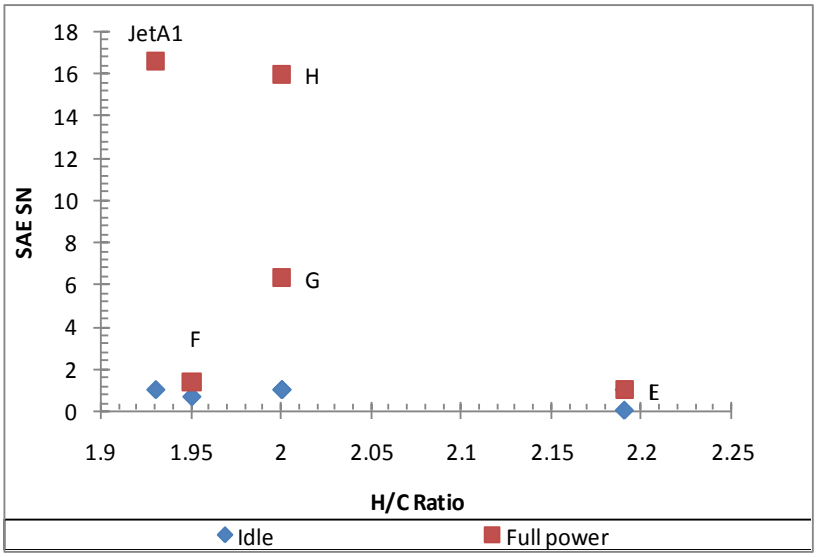

Figure 8.20: Smoke number measurements for all fuels at idle and full power operating conditions.

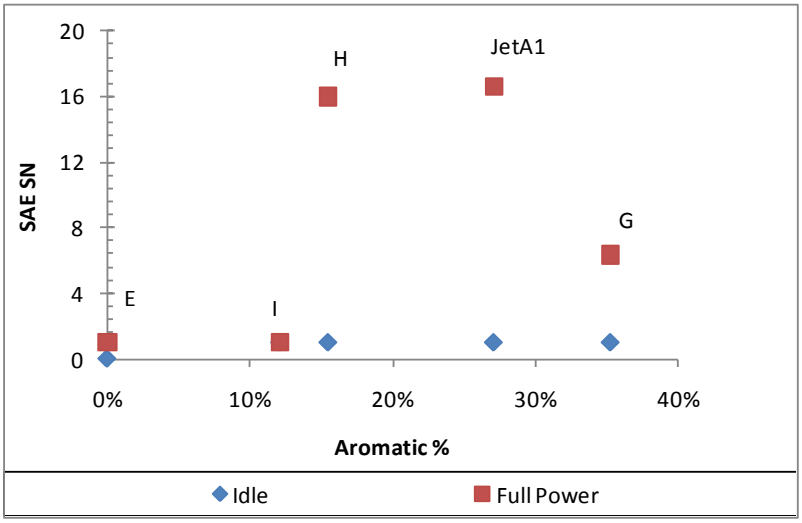

Figure 8.21: Smoke number as a function of aromatics for all fuels at idle and full power operating conditions.

8.5 Conclusions

Two groups of fuels were tested for PM and smoke numbers using a re-commissioned gas turbine Artouste Mk113 APU engine. The first group was five compositionally designed surrogate fuels. The second group was a matrix of fuels comprised of conventional JetA1, GTL, HVO, HRJ and FAE The engine was operated at two power settings and three operational modes: cold and hot idle and full power. The influence of fuel H/C ratio, engine power, cold and hot idle on the particle number and mass size distributions were investigated. The results show that:

1. For compositionally designed surrogate fuels, Particulate number concentrations decreased as the fuel H/C ratio increased at all power

conditions. A negative linear correlation between total particle concentration and fuel H/C ratio was observed.

2. The particulates from all fuels displayed a unimodal, nearly lognormal distribution. The standard deviation analysis indicated that the distribution characteristics were very similar for all fuels. The peak size was at around (20-40 nm) for both idles and shifting towards the larger size (30-60 nm) at full power condition. The geometric mean size of particles was reduced as the fuel H/C ratio increased.

3. Hot idle produced lower number of particles compared to cold idle for all fuels, the sharp increase at cold idle is due to particle nucleation in the sampling lines found during the colder ambient temperatures. A very low particle number concentration for pure alkanes GTL fuel (8115) at idle was observed and demonstrated a good low temperature combustion property of the alkane fuel. The differences in particle number concentrations between different fuels were more significant at idle power conditions due to its relatively low combustion temperature.

4. Aromatics were the most important component to contribute to the increase of particle number concentrations and engine smoke numbers. Cycloalkanes were the second important contributors. Alkanes showed the lowest particle concentrations and smoke numbers.

5. For alternative aviation fuels, the Peak of particle numbers were in a magnitude of 10^{15} to 10^{16} P/kg-fuel at the full power condition and 10^{14} to 10^{16} P/kg-fuel at the idle modes for all the fuels. The peak particle mass was in a range of 0.15 to 3.8 g/kg-fuel at idle modes and 0.06 to 1 g/kg-fuel at full power condition.

6. JetA1 produced the highest number and mass peak particle emissions, especially for mass size distributions. The GTL fuel produced the much lower number and mass peak particle emissions at the cold and hot idle, indicating an excellent low engine power combustion performance.

7. There were clear correlations between fuel H/C ratio and particle number and mass emission distributions in terms of particle number concentration, emission index EIn and EIm and particle diameter GMD. As the fuel H/C ratio increased, particle number concentration, EIn and EIm and GMD were decreased.

8. By comparison of particle total concentration, GMD and GSD for both number and mass size distributions between hot and cold idles, it was observed that the engine produced ~20% less particles at the hot idle mode than that at the cold idle mode. The GMDs were similar. The hot idle had narrow size distributions.

9. The smoke number measurement showed that all alternative fuels had lower smoke numbers than JetA1 at both power conditions. The differences were the greatest at the full power. The results also showed that smoke number increased as the aromatics and sulphur contents increased.

Chapter 9 : Hydrogen Combustion using an Impinging Jet Flame Stabilizer

9.1 Introduction

Hydrogen is gradually more being used as fuel for industrial gas turbine as it can be burned without CO, CO_2 and UHC emissions. However, NOx emissions are the main concern with hydrogen combustion[199, 200]. Hydrogen is a carbon free fuel and hence is the ideal energy source in a carbon free world. Hydrogen combustion is thus one route to meet future CO_2 targets that potentially can use existing gas turbine plant with only modifications to the fuel supply system. However, if the NOx regulations are also to be met it is likely that some redesign of low NOx combustion system will be necessary. The alternative low carbon solution is to use carbon capture and storage which is unproven and relatively costly.

Hydrogen can be produced without associated CO_2 using water as the source and electrolysis using nuclear electricity, wind or solar power[199, 200]. The impetus for the present work was the possibility of large scale solar hydrogen plants in desert countries. Unfortunately at present none of these CO_2 free hydrogen sources exist and most hydrogen is generated from natural gas with the production of CO_2 [201, 202] which could be captured using conventional amine scrubbers to give a CO_2 free source of hydrogen [203, 204] but this is not done at present. There is also current interest in the gasification of coal with conversion of CO and hydrocarbons to CO_2 followed by CO_2 capture using amine solvent extraction, leaving pure hydrogen as the resultant gas[205]. This is promoted as a preferable technology to post combustion capture of CO_2 [206].

9.2 Pros and cons of Hydrogen fuel

Hydrogen has a major advantage as a gas turbine fuel in that it has an extremely wide flammability range and its lean limit is Ø= 0.13 at 300K [207] and leaner at industrial gas turbine operating conditions. Its critical flame temperature for lean flammability, which should be the same as for weak extinction in a well-designed low NOx system[174], is 700K. Hence, with gas turbine compressor air temperatures close to this a hydrogen flame should be stable at all gas turbine powers from start up to full load and should be

capable of sustaining all transient loads. This ability to deal with the complete power range of an industrial gas turbine without any need for air or fuel staging means that much of current gas turbine low NOx design would be unnecessary, apart from the need for dual fuelling. Also, hydrogen does not need the large central recirculation zone that occurs in swirl based flame stabilisation, as it has very good stability characteristics without the need for high internal EGR that comes with the central recirculating flow of swirlers.

Hydrogen is potentially a difficult fuel to burn in low NOx gas turbine combustors. Its high burning velocity makes flashback into premixing ducts much more of a problem than for natural gas. The relative burning velocity ratios of hydrogen to natural gas are of the order of 7-8[199, 200, 208] so that a premixed hydrogen/air passage would be 7-8 times more likely to flash back than the natural gas equivalent condition if they were operated at the same equivalence ratio. However, hydrogen has a higher peak flame temperature than natural gas [209] so a leaner mixture would be operated for the same combustion temperature and this would reduce the burning velocity ratio a little to say five. The normal solution to flashback, apart from fitting a flame trap at the end of the duct [210], is to increase the duct velocity at the outlet by contracting the area [211, 212] or to operate the whole duct at a higher velocity [213], However, it is impossible to increase the duct velocity by a factor of five to counteract the burning velocity changes due to pressure loss considerations. Thus an increase in flashback risk is inevitable.

Increased flashback tendency with hydrogen added to methane has been demonstrated [214] and the critical equivalence ratio for flashback for hydrogen/methane mixtures has been found to be reduced from Ø=0.8 to Ø=0.4 as hydrogen was increased in methane [215]. As Ø=0.4 is leaner than is used for low NOx primary zones, this means that there is no low NOx operation in premixed mode due to flashback. Even when a premixed duct design that is very resistant to flashback [213] is used with a fuel that contains hydrogen, such as gasified coal gases, the manufacturer has used a different fuel injection location through the wall of the swirler outlet duct[216]. This is a fuel injection position that was developed by Alkabie and Andrews [69] for radial swirler duct outlets and applied to axial swirler low

NOx combustion as well [115]. As this is a non-premixed type of fuel injection it would have been a possible fuel injection system to investigate with hydrogen. This was not done as there were concerns that the dump expansion plane from the swirler outlet would be too hot as this was only backside cooled. The issue of overheated flame stabilisers was a serious problem in the present work.

9.3 Review of previous work

Several workers have shown that if hydrogen is fully premixed, whether as 100% hydrogen or as a blend with natural gas, then for the same primary zone temperature there is no increase in NOx [199, 200, 217-220]. However, if there are any imperfections in mixing then the higher flame temperatures with hydrogen can lead to increased NOx. Also, it is doubtful, for the flashback reasons discussed above, that practical existing low NOx systems could be operated premixed with hydrogen. All the above data [217-220] for no effect of hydrogen on NOx were for laboratory demonstrators not practical engines. For a practical low NOx combustors operated at full power the increase in NOx has been measured at a factor of 3.5 for pure hydrogen and an increase by a factor of 1.6 for a 50/50 hydrogen natural gas mixture[221].

A low NOx FLOX burner [222] operated at gas turbine engine pressures with 40% hydrogen and 60% natural gas had NOx increased at 1800K from 25ppm for 100% natural gas to 55ppm for methane, this is a similar finding as that for a practical low NOx gas turbine. This illustrates that the issue of fuel and air mixing quality is crucial if low NOx is to be achieved without using conventional premixing ducts. In the present work a rapid fuel and air mixing system was investigated that has demonstrated good mixing and low NOx with natural gas and propane[52, 129].

As hydrogen will not need any air staging to cope with power variation, there will be no need for any dilution air if the lowest NOx is to be achieved. All the air will then pass through the hydrogen flame stabiliser. Studies of hydrogen combustion at this condition have not been done previously to the authors' knowledge.

This work was carried out close to the M=0.05 reference Mach number condition used in most aero derived combustor designs. This produces the lowest combustor primary zone residence time. M_1 ($=U_1/(\gamma RT)^{0.5}$) is based on the inlet temperature and the air velocity in the combustor at the maximum combustor internal cross sectional area. The highest M_1 produces the lowest combustor primary zone residence time. The high reactivity of hydrogen makes the residence time for complete combustion to be much less than for hydrocarbon fuels and hence the combustor could be shorter. A 330mm length was used in the present work which is short relative to many industrial gas turbines. Although the present work was carried out on one flame stabiliser, a practical combustor would use several of these [135] in the same way several axial swirlers are used in many current low NOx designs.

The objectives of the present work were to evaluate NOx emissions and combustion efficiency of direct hydrogen injection at constant pressure loss and compare it with premixed and direct propane injection. All test carried out at actual Mach number of 0.047, 4.3% pressure loss and 600k inlet air temperature.

9.4 Results and discussion

9.4.1 Hydrogen fuel

9.4.1.1 Effect of inlet Temperature

NOx emissions corrected to 15% oxygen as a function of flame temperature for hydrogen at different inlet temperature (300, 400 &600K) and 20% inline Jet Mix radial flow are shown in Fig.9.1. The results showed that the three different inlet temperature produce similar level of NOx <5ppm at ~950K. However, at 1000K and higher, lower air inlet temperature produce higher NOx emissions compared to high inlet air temperature. At 1250K, NOx emissions are 13, 10 and 5ppm at 300, 400 and 600K inlet air temperature respectively.

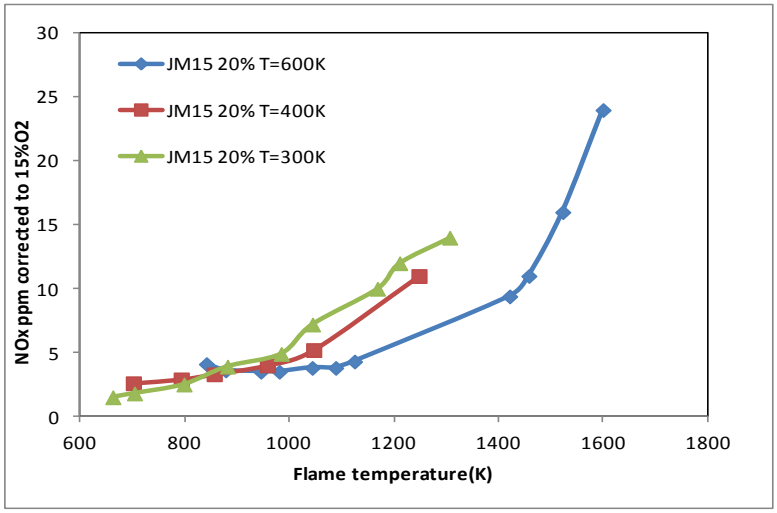

Figure 9.1: Hydrogen NOx emissions corrected to 15% oxygen as a function of flame temperature for 20% inline Jet mix at and Tin=600, 400& 300K.

9.4.1.2 Effect of inlet radial air

Fig.9.2 shows hydrogen NOx emissions corrected to 15% oxygen as a function of flame temperature for both proportions of the Jet Mix radial flow (6.5% &20%) at different inlet air temperatures. Hydrogen in the 6.5% radial jet air flame stabilise shows that the NOx was increased relative to the 20% radial jet hydrogen results at 600K inlet air temperature and at all flame temperatures investigated up to 1600K. However, similar trend has been seen by 300K at all flame temperature up to 1100K where same levels of NOx were produced by both radial jets. After 1100k, 20% radial jet has higher NOx than 6.5% at the same inlet temperature. Generally, 20% and Tin=600K generate the lowest level of NOx and this results will be compared later with premixed and direct propane.

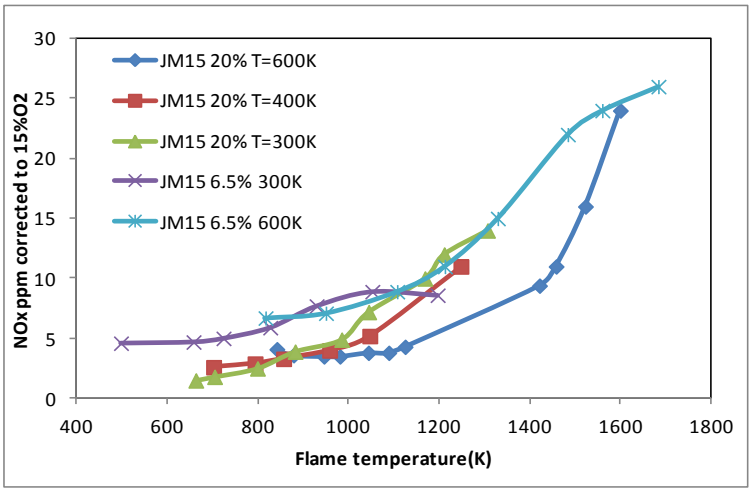

Figure 9.2: Hydrogen NOx emissions corrected to 15% oxygen as a function of Flame Temperature for inline Jet mix at Tin=600, 400 and 300K and 20% & 6.5%..

9.4.1.3 Comparison with other micro mix 100% Hydrogen Combustors.

Most industrial GT manufacturers have work in progress on premixed hydrogen combustion but operating systems are diffusion flame based [223]. One 100% hydrogen system under development by one manufacturer is the Micromix combustor [224]. This is a non-premixed design due to the problem of flashback. Rapid mixing of hydrogen and air was achieved by injecting hydrogen directly at 90^o to a cross flow air jet. In principle it was the same as the present Jet Mix system without the radial jet air flow to assist initial mixing and to give the radial hydrogen jet better penetration of the axial air jet. The micromix design[225] avoids the problem of the Jet Mix design of a large central hub as it uses a large number of hydrogen jets in an annular ring with an axial air jet for each hydrogen jet. The latest version of this design used 1600 hydrogen holes and associated axial air jets.

This micromix design[224] was tested at 1 bar and 560K, similar to the present test conditions. Three flow conditions were tested with 5, 10 and 15 MW/(m^2bar) using the equation below

$$\mathbf{MW/(PA_1) = [(Ø/S)M_1CV(\gamma/RT)^{0.5}]\ MW/(barm^2)} \qquad \mathbf{(26)}$$

Where S is the stoichiometric A/F by mass
CV is the calorific value of the fuel, MJ/kg

The reference Mach number, M_1, is related to the heat release (MW) per combustor cross sectional area, A_1, per bar. For natural gas at 600K and M_1 = 0.05 the combustion heat release rate is 19.2 MW/(m^2bar) and at 700K it is 20 MW/m^2bar. This was the combustion heat release condition used in the present work and this is the only work on 100% hydrogen combustion that has been carried out at the heat release rate and reference Mach number that would occur with 100% hydrogen combustion. However, as mentioned earlier, only the highest heat release is relevant to hydrogen gas turbine combustors and most of the work on this design was carried out at the 5 MW/(m^2bar) condition. At this low value of heat release the NOx was very low in the 1-3ppm range with Ø 0.15 – 0.5 in the range. However, for 15 MW/(m^2bar)[224], the NOx was much higher and these NOx are compared

with the present results in Figs.9.3&9.4. NOx emissions corrected to 15% oxygen are shown as a function of both the equivalence ratio in Fig.9.3 and flame temperature in Fig.9.4 for hydrogen fuel at 20% inline jet mix and micro mix burner.

These micromix results are similar to the present Jet Mix results. Below 1300K the NOx was slightly lower and above1300K the Jet Mix results were lower than those for the micromix design. A disadvantage of the Micromix design[224] was that it had a hydrogen combustion efficiency problem for all flame temperatures below 1400K. For temperature below 1100K this hydrogen combustion inefficiency problem was greater than 5% this would prevent all the power turndown requirements being met without fuel or air staging. In contrast the present Jet Mix design could operate to at least 850K without measurable hydrogen in the exhaust.

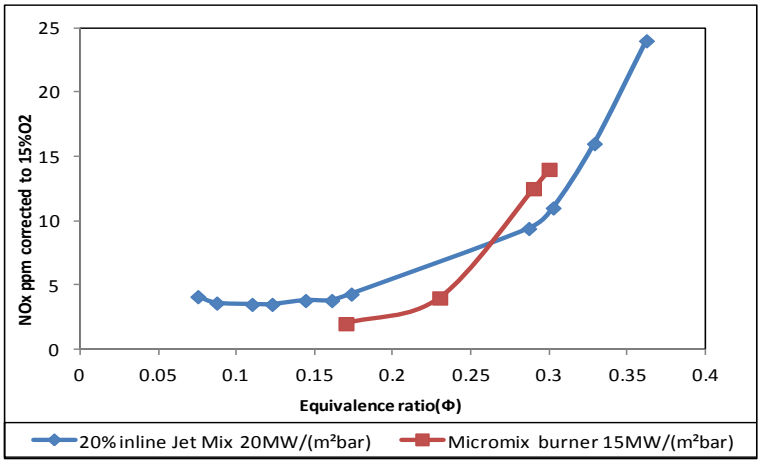

Figure 9.3: Hydrogen NOx emissions corrected to 15% oxygen as a equivalence ratio for 20% inline Jet mix and micro jet burner at Tin=600.

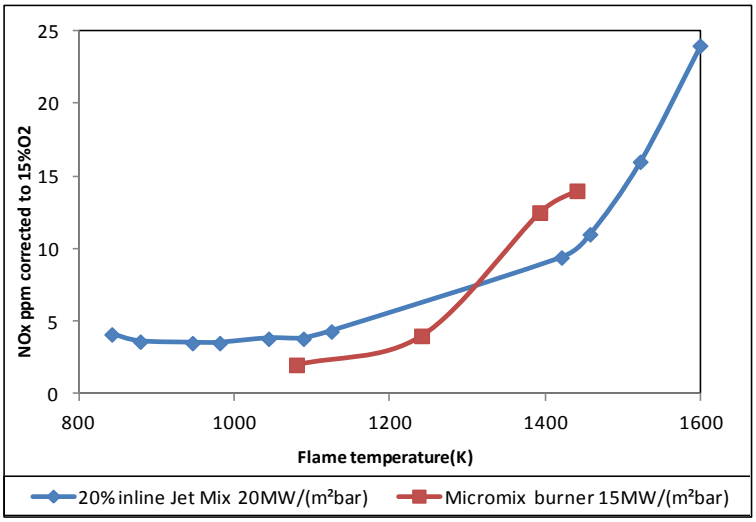

Figure 9.4: Hydrogen NOx emissions corrected to 15% oxygen as a function of Flame Temperature for 20% inline Jet mix and micro jet burner at Tin=600.

9.4.2 Comparison of Hydrogen Fuel with Propane and Premixed.

9.4.2.1 Wall Temperature Axial Development

Fig.9.5 shows the Jet Mix recirculation zone length of approximately 100mm as measured using wall static pressure profile prior to ignition and confirmed by flow visualisation using a water modelling facility [128]. The wall static pressure results also showed that there was a little change in the recirculation zone size during all combustion tests. The axial wall temperature profiles show that the main heat release of the flame was developed. The temperature is not important as this is a balance between heat gained from combustion and heat lost by radiation and natural convection from the uncooled combustor. However, the temperature profile is related to the gas side temperature in the wall region and hence reflects where heat release occurs.

Fig.9.5 shows the wall temperature profiles for propane and hydrogen combustion for the two radial flow air jet proportions investigated of 6.5 and 20%. The temperature profiles were taken for an equivalence ratio where the maximum efficiency occurred for propane at Ø=0.62 at 600K. The propane adiabatic flame temperature at Ø=0.62 was 1850K. It was intended to operate hydrogen at an equivalent adiabatic flame temperature condition, but this proved impossible as the stabiliser was in danger of melting and the highest operating temperature with hydrogen was 1600K at a hydrogen equivalence ratio of 0.36. For this temperature the equivalent propane Ø was 0.44. This is the main reason that the final wall temperatures are lower for hydrogen combustion in Fig.9.5. The flame temperature was 250^{o}C lower and the wall temperature was also about 250^{o}C lower.

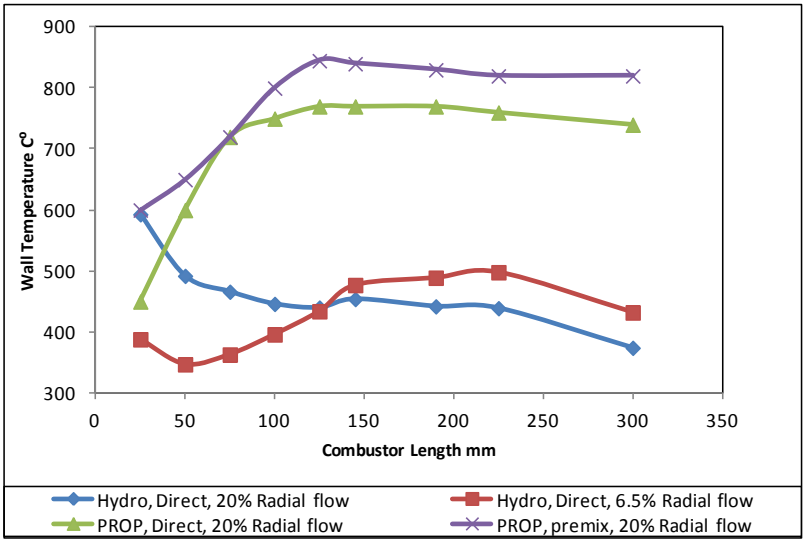

Figure 9.5: Wall axial temperature profiles

The propane results showed for premixed combustion with 20% radial jet flow a peak wall temperature of 850^{o}C at 125mm from the flame stabiliser. This indicates complete heat release at the end of the large central recirculation zone and the main combustion development zone upstream of this in the eight jet shear layers. With direct propane injection into the radial jet and no fuel in the axial jet that the peak wall temperature occurred in the same place at 125mm from the flame stabiliser, however, close to the stabiliser the wall temperature was nearly 200^{o}C lower and this indicated that the radial and axial jet mixing process had delayed the onset of reaction. For propane the radial jet with 20% of the air had a local equivalence ratio of 3.1 for an overall equivalence ratio of 0.62. This was too rich to be flammable and mixing of some axial jet air had to occur before there was locally a flammable mixture. This delayed the onset of heat release, as shown in Fig.9.8. The peak wall temperature with direct radial jet fuelling was lower than for premixed combustion, which possibly indicates that combustion heat release was not complete at the end of the recirculation zone and needed more time to burn out CO and UHC.

For hydrogen direct fuelling into the radial jet the situation was quite different. Firstly the peak temperatures were at the flame stabiliser outlet where no wall thermocouple was located. Fig.9.5 shows the wall temperature was rising rapidly closer to the stabiliser outlet, which is the complete opposite of the propane trends. Visually from the observation window it could be seen that the stabiliser back wall and central hub were all

red hot. This was of such concern that the overall operating temperature was limited to 1600K as melting of the stabiliser was likely if more hydrogen was added. It is likely in these circumstances that the radial jet was flammable and the action of the axial jet was to act as dilution air. The radial jet equivalence ratio for the overall Ø of 0.36 was 1.8 and unfortunately hydrogen-air has a peak adiabatic flame temperature at Ø=1.3 and hence direct combustion of the radial jet was most likely occurring in this work.

The dilution of this by the axial jet air prevented complete melt down of the flame stabiliser and combustor head, but operation beyond 1600K overall would have resulted in flame stabiliser melt down. This is just one illustration of the problem of 100% hydrogen combustion without premixing.

To control this problem operating with more radial jet air was unwise as this would move the radial jet closer to the maximum adiabatic flame temperature. Thus it was decided to make the radial jet richer and reduce the radial jet air flow from 20% to 6.5% of the total using a new flame stabiliser with appropriate changes in the radial and axial hole sizes. The radial jet equivalence ratio for the same overall Ø of 0.36 was now Ø= 5.5 and this was considered to be sufficiently rich that hydrogen could not burn in the radial jet. Combustion would then occur in the mixing with the axial air jet and this would result in lower flame stabiliser temperatures. This did produce lower flame stabiliser temperatures and Fig.9.5 shows a quite different axial variation of temperature for 6.5% radial jet air. The profile is now closer to that of propane with lower temperatures close to the injector and the peak temperature at the end of the recirculation zone. However, this flame stabiliser was not operated at temperatures higher than 1700K as a conservative measure to prevent any risk of flame stabiliser melts down.

9.4.2.2 Weak Extinction Results

At constant mean velocity and inlet temperature the fuel flow was gradually reduced until visual observation through the 100mm window in the exhaust showed the flame go out. This process was repeated at each condition. Table 29 shows weak extinction results for 600K inlet temperature with the inline jet configuration, The Mach number was 0.047 and the pressure loss was 4.3%. Direct hydrogen fuel injection was compared with direct propane and premixed propane at 20% and 6.5% radial flow.

Table 29: weak extinction results at 600K inlet temp, inline jet configuration, and M number 0.047 and 4.3% pressure loss

Fuel injection method	Radial Jet Air (%)	Weak extinction (Ø)
Direct Hydrogen	20%	0.0286
Direct Hydrogen	6.5%	0.0167
Direct propane	20%	0.33
Direct propane	6%	0.15
Premixed propane	20%	0.4

Table 29 shows that the premixed propane weak extinction results were close to the fundamental flammability limits, which are Ø=0.37 for a 1500K critical flame temperature for lean flammability at 600K. However, they are no particularly good as premixed weak extinction and leaner mixtures can be achieved, but it is the very high reference velocity here that probably makes flame stabilisation difficult[174]. The addition of direct propane injection for the 20% radial jets reduces the weak extinction from premixed to Ø=0.33, which indicates some unmixedness in the jet shear layer. Reducing the radial air to 6.5% further increases the propane and air unmixedness but extends the weak extinction to Ø=0.15. For hydrogen the weak extinction was incredibly low and difficult to determine due to flow measurement problems at less than 10% of the hydrogen flow in the high temperature operating region. The Stoichiometric A/F by mass for hydrogen is 30/1 A/F so the lean limit in A/F terms is 1050/1 for the 20% radial jet and 1800/1 for the 6.5% radial jet air. No hydrocarbon based combustion system with diffusion combustion and stage air can come anywhere near this stability, especially at the high M of the present work.

If it is assumed that the lean limit is controlled by combustion in the radial jet then the radial jet Ø was 0.143 for 20% radial air flow and 0.257 for 6.5% radial air flow. The lean flammability limit for hydrogen is Ø=0.133 at 300K. Hence it can be concluded that the weak extinction is so good with hydrogen because the flame can stabilise in the radial jet air as a near premixed radial jet. This superb level of flame stability for hydrogen has not been reported in other work on hydrogen combustion for gas turbines. It will be shown in the NOx emissions results that flames were measured down to flame temperatures of 800K for hydrogen and the lean flammability limit for hydrogen at 300K is equivalent to an adiabatic flame temperature of 700K.

To stabilise such lean flames at reference Mach number conditions of 0.047 shows incredible flame stability with hydrogen relative to propane. This demonstrates that a gas turbine designed for hydrogen operations needs none of the flame stability enhancing features used for hydrocarbon fuels such as IGVs, fuel or air staging and the basic flame stabiliser can cope with all operating powers.

9.4.2.3 Inline Jet NOx Results

Fig.9.6 shows the NOx emissions (ppm) as a function of the equivalence ratio for hydrogen and propane for both proportions of the Jet Mix radial flow. Fig.9.7 shows the same results as a function of the flame temperature and Fig.9.8 shows the NOx emissions corrected to 15% oxygen as a function of the adiabatic flame temperature. The results are mainly discussed in terms of the NOx corrected to 15% oxygen, which is the legislated form of NOx emissions. For premixed combustion the NOx had a very steep dependence on flame temperature, but 2ppm NOx at 15% oxygen was achieved at 1800K. For the 20% radial jets the direct propane injection has higher NOx for the same flame temperature, due to the addition of mixing between the radial fuel rich jet and the non-fuelled axial jet. At 1800K the NOx was 30ppm, but reduced to 10 ppm at 1600K and 5ppm at 1400K. At 1800K the Ø was 0.52 and the radial jet Ø was 2.6. Thus in mixing out this local rich region some NOx will have reacted in a local near Stoichiometric high NOx production region and increased the NOx emissions.

The hydrogen NOx results for 20% radial flow show a large increase in NOx relative to propane with 24ppm at 1600K and increasing rapidly with temperature. However, this result does show that NOx <25ppm can be achieved up to combustor outlet temperatures of 1600K, which covers quite a range of practical gas turbine applications. The hydrogen NOx is 2.4 times that for propane. At 1400K the NOx was 10ppm which was 2.0 times that for propane and at 1200K the NOx was 5ppm, with propane unable to sustain a flame at this condition.

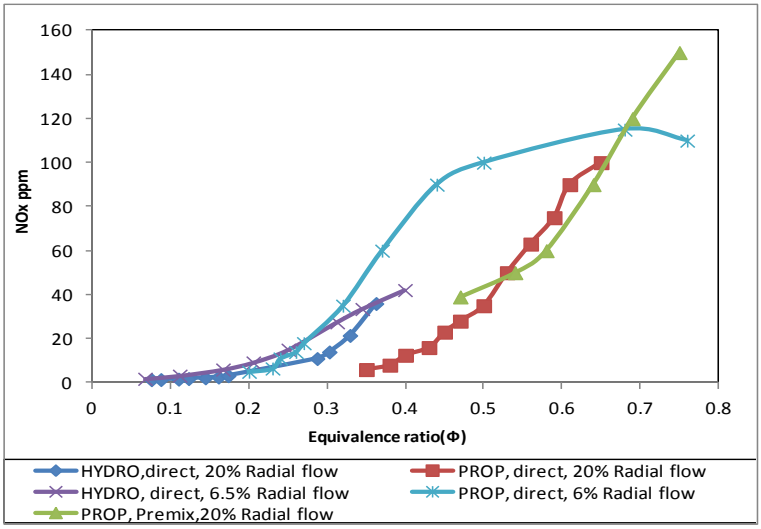

Figure 9.6: NOx emissions as a function of equivalence ratio for inline Jet mix, Tin=600K for all fuels.

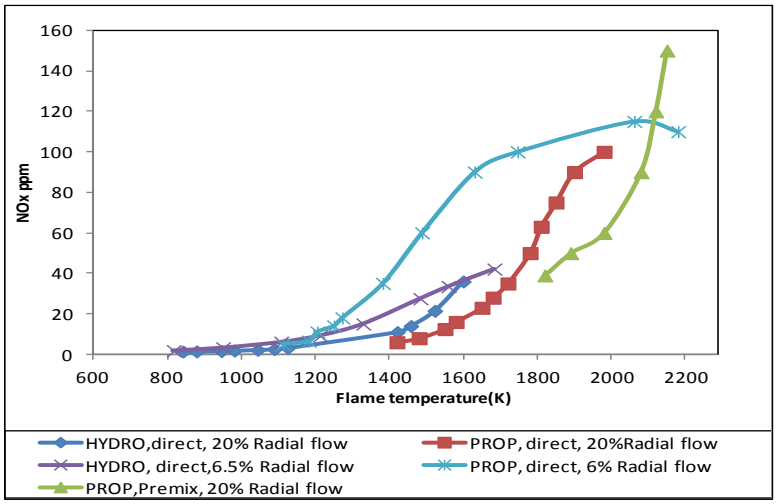

Figure 9.7: NOx emissions as a function of Flame Temperature for inline Jet mix, Tin=600K for all fuels.

These NOx increases were lower than the 3.4 factor found for a production low NOx gas turbine combustion system [221]. However, they show that hydrogen has a greater sensitivity to unmixedness as the flammable range is much wider and very locally rich zones that cannot burn with hydrocarbons will burn with hydrogen.

The weak extinction results showed that the flame was burning in the radial jet for lean reason that the stabiliser was extremely hot in the tests. At 1600K overall temperature the hydrogen equivalence ratio was 0.36 and the radial jet equivalence ratio was 1.8. With some mixing with the axial air it is likely that a near Stoichiometric flame was burning close to the radial hole outlet, the residence time would be very short as the rest of the axial air mixed in but this is likely to be the source of the enhance NOx.

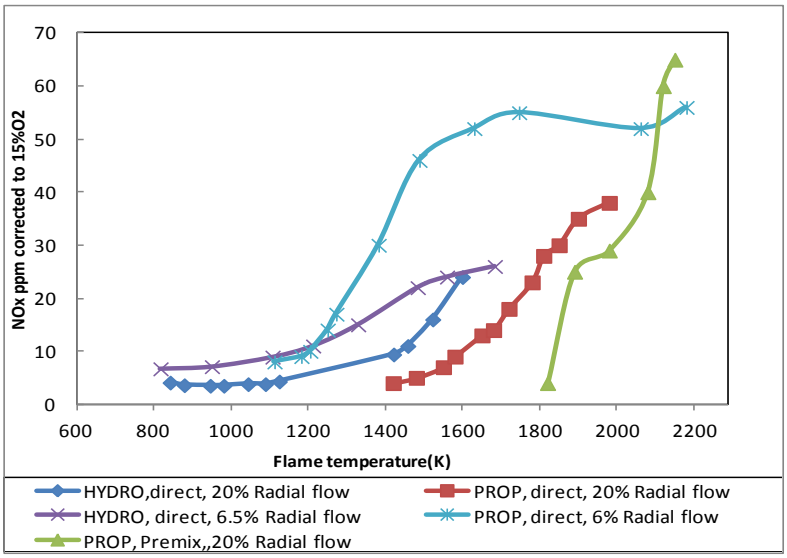

Figure 9.8: NOx corrected to 15% oxygen as a function of Flame Temperature for inline Jet mix, Tin=600K for all fuels.

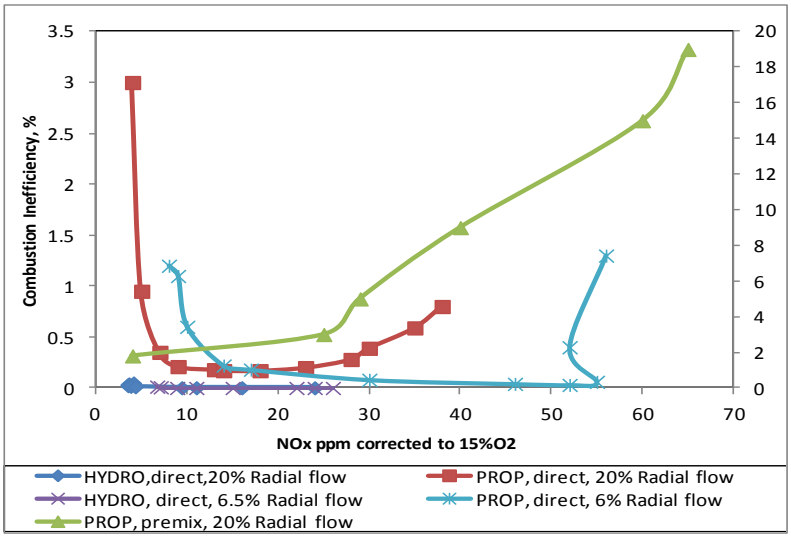

Figure 9.9: Combustion inefficiency as a function of NOx corrected to 15% oxygen for inline Jet mix, Tin=600K for all fuels.

The action on NOx of reducing the radial air flow proportion to 6.5% for propane was to greatly increase the NOx emissions. At 1600K the NOx was 52ppm in Fig.9.8 and the overall equivalence ratio was 0.42 which gives a radial jet equivalence ratio of 6.5. This cannot burn in the radial jet but is likely to have the characteristics of micro scale rich/lean combustion in the mixing zone with the axial air jets. Fig.9.8 indicates that the NOx peaks at 1800K and then start to decline, which is a feature of rich lean combustion. However, the flame stability of this design is excellent as this rich zone maintains stable combustion at flame temperatures where the 20% radial jet

has extinguished. At 1200K the NOx was 8ppm and very close to the hydrogen results for this stabiliser at this temperature. For propane the Ø at 1200K was 0.23 and the radial jet Ø was 3.5. However, the rapid mixing with axial jet air has probably created lean local mixture at the point of flame stabilisation which then gives the observed low NOx.

For hydrogen in the 6.5% radial jet air flame stabiliser Fig.9.8 shows that the NOx was increased relative to the 20% radial jet hydrogen results at all flame temperatures investigated up to 1600K. However, the figure shows that as 1600K is approached the 20% radial jet air NOx is increasing rapidly and the 6.5% radial jet air has peaked in a similar way that the propane results peaked. However, this peak NOx with hydrogen is roughly 50% of that with propane. This contrasts with the 20% radial jet results where the hydrogen NOx was 2.4 times higher than propane at 1600K. Again the reason is the local radial jet equivalence ratio. At 20% radial air and 1600K the radial jet was Ø=1.8 and very close to the maximum flame temperature condition, At the same condition the 6.5% radial jet was at Ø=5.5 and at a locally low temperature condition. The radial jet then produces no NOx directly but does produce NOx in the mixing region with the axial jet and continuous to produce this NOx for very lean mixtures.

The combustion inefficiency was always 100% for hydrogen but for propane it decreased near the weak extinction condition as shown in Fig.9.9. This effect would limit the propane lowest NOx condition that was usable to 16ppm for 6.5% radial jet air and 8ppm for 20% radial jet air. Hydrogen in contrast would have no combustion efficiency limit at any operational condition.

9.4.2.4 Comparison of inline and offline Jets

Operation with offset jets delays the axial jet mixing with the radial jet and promotes the micro rich/lean combustion mode. Thus the radial jet local equivalence ratios discussed above are more likely to give local combustion when the mixing with the axial air is delayed. This would normally increase the NOx and extend the lean flammability. This effect was only investigated for 20% radial jets and the inline and offset jets NOx are compared in Fig.9.10 as a function of the adiabatic flame temperature. The propane results showed higher NOx for offset jets for flame temperatures <~1600K

and similar NOx above this. As shown above at 1800K the radial jet equivalence ratio was 2.6 and hence with offset jets local rich zone burning was promoted which produced slightly lower NOx than for inline jet mixing. However, at leaner mixtures the mixing between the rich zone and the axial air jet would produce local Stoichiometric burning and increase the NOx. At 1400K the overall Ø was 0.34 and the radial jet Ø was 1.7. Thus as the overall mixture was reduced the radial jet was moving toward stoichiometric and a higher local NOx production. This caused the NOx to be high relative to inline jets for low temperature mixtures.

For operation on hydrogen the radial jets were now free to burn alone as the axial jet air mixing was delayed. It was shown above that at 1600K the radial jet was at Ø=1.8. However, at 1200K the overall Ø was 0.2 and the radial jet was Stoichiometric. This caused near catastrophe on the test rig, as the radial jets were impinging directly on the combustor wall and creating local white hot spots and this condition was close to melting the combustor liner. Further experiments on hydrogen on the offset jet configuration were abandoned. The few NOx results that were obtained at low temperatures are shown in Fig.9-10 to be similar to the same results for inline jets, but they had a steeper dependence on flame temperature. All the NOx in this low temperature region was about 5ppm or lower. It may be possible that if richer operation overall had been attempted that as the radial jet became richer local jet combustion would have ceased and NOx would have decreased in

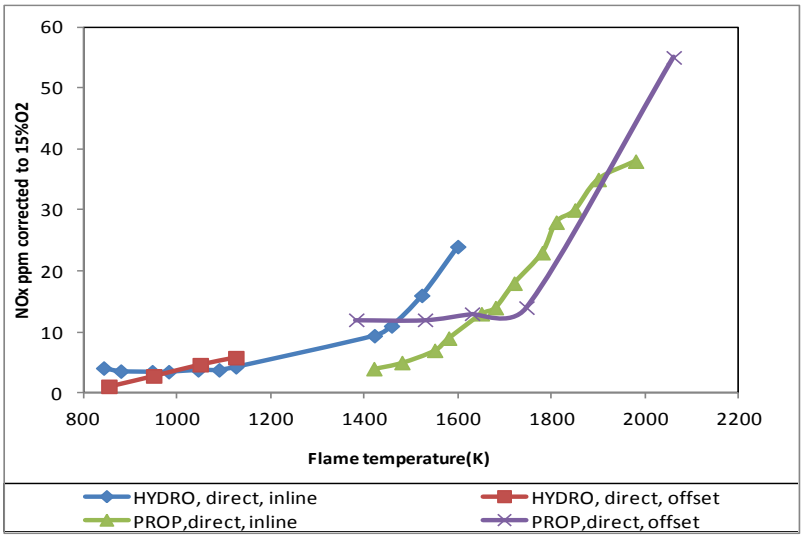

Figure 9.10: NOx emissions at 15% oxygen for offset jets with 20% radial air flow.

classic rich/lean combustion mode. However, these experiments were considered to be too dangerous to attempt.

9.5 Conclusions

Combustion and emissions of direct hydrogen fuel using impinging Jet mix flame stabilizer were conducted. The test was carried out at Mach number of 0.047, 4.3% pressure lose and 600K inlet temperature. The results were compared with premixed and direct propane injection and the main findings have been drawn:

1. Hydrogen is potentially an excellent gas turbine fuel and its very wide flame stability makes it possible to achieve all engine power levels without air or fuel staging.

2. Hydrogen stability can be exploited fully only if all the combustion air passes though the flame stabiliser and this entails development of low NOx hydrogen combustion at reference Mach number of 0.05. This is a very arduous test condition for hydrocarbon fuels to make but easy for hydrogen due to its high reactivity.

3. Hydrogen cannot be used in any premixed flame stabiliser as flashback will always occur due to the high burning velocity of hydrogen. This requires a flame stabiliser for hydrogen with direct fuel injection and rapid fuel and air mixing.

4. The Jet Mix flame stabiliser with impinging radial and axial air jets and the fuel injected into the radial jet was shown to be a suitable flame stabiliser for hydrogen provided the inline jet configuration was used. Flame stability was outstanding and weak extinction was equivalent to 800K critical flame temperature.

5. Hydrogen heat release close to the flame stabiliser was a major problem. The flame development was quite different to that with propane as propane could not burn in the high velocity regions close to the flame stabiliser, but hydrogen could.

6. At the same adiabatic flame temperature of 1600K the hydrogen NOx was 2.4 times that for propane. At 1400K the NOx was 10ppm which

was 2.0 times that for propane. Hydrogen was more sensitive to unmixedness due to its much wider flammable range. These are lower increases in NOx that has been reported by others for low NOx gas turbines.

7. For 20% radial air jets and adiabatic flame temperatures <1600K the NOx corrected to 15% oxygen was <24ppm on hydrogen and hence the Jet Mix design is one potential design that can achieve low NOx for 100% hydrogen combustion.

8. Reducing the proportion of radial jet air to 6.5% was only beneficial in terms of NOx if operation at adiabatic flame temperatures >1600K was desired. This is because this flame stabiliser had a micro rich/lean combustion operation. The main advantage of reducing the radial jet air was to move the flame away from the flame stabiliser and hence prevent the overheating that was occurring with the 20% radial air jet proportion. The NOx emissions were still <24ppm for all adiabatic flame temperatures <1600K and hence this was a viable design and may be more practical in terms of flame stabiliser durability.

Chapter 10: General Conclusions and recommendations for Future Work

10.1 General conclusions

Due to environmental concerns and supply security, alternative fuels derived from various sources including renewable resources have attracted ever increasing interests. These fuels vary significantly in their compositions, which could affect engine combustion and emissions. So there is a need to improve the understanding of the influence of fuel composition and properties on engine performance in order to promote the utilization of alternative fuels without causing adverse effect. Combustion and emissions of alternative fuels were tested in low NOx combustors and APU engines and the general conclusions drawn from present work are as follows:

10.1.1 Biodiesel in low NOx combustor

Pure WME (B100) and its blends with kerosene (B20 and B50) and pure kerosene were tested on a radial swirler industrial low NOx gas turbine combustor under atmospheric pressure and 600K. The fuels were tested for weak extinction, gaseous emissions and particulate matter (PM) as a function of equivalence ratio at a reference Mach number of 0.017& 0.023. The following conclusions have been drawn:

1) WME and its blends (B50, B20) had lower CO, UHC emissions and higher NOx emissions than the kerosene.
2) As the Mach number or residence time decreased, the NOx emissions decreased for all fuels.
3) CO and UHC emissions decreased as the Mach number increased due to the shorter residence time.
4) Biodiesel has larger droplet sizes than kerosene at the same conditions. The big difference in the droplet size of both fuels is due to dynamic viscosity. The effect of Mach number was to significantly reduce the SMD at the higher M and this was responsible for the improved mixing at the higher M.
5) The NOx emissions were below 10ppm with kerosene co-fired with NG for $\Phi<0.6$. With the addition of NG for the same Φ there was a

reduction in NOx compared with the liquid fuel alone, for the same Φ. This was greatest for B50 with NG when NOx was reduced from 34ppm to 9 ppm when premixed NG was present. This reduction in NOx was due to the improvement in overall mixing of fuel and air by injecting liquid fuel into a near premixed main flame.

6) The presence of premixed NG flames strongly reduced the CO emissions at the same Φ, particularly for B50 and B20/NG flames.
7) UHC emissions were relatively low for B100 indicating that fuel vaporization was not a major problem. This indicates that the central fuel injection of liquid fuels is vaporized by the recirculation of burnt gases on the centerline of the radial swirler. This process is not strongly dependent on the atomization of the fuel.
8) The lean extinction limit has been tested and is related to the fraction of biodiesel. The more the fraction of biodiesel, the lower the lean extinction limits.
9) The reduced emissions (CO&UHC) and lower extinction limit with biodiesel is considered due to the oxygen content in the fuel, which assisted the combustion process.
10) Formaldehyde is the dominant aldehyde in the exhaust and represents about 50% of the total hydrocarbon emissions for B20 at low equivalence ratios.
11) The results also show that there was no increase in aldehyde emissions with the biofuels and that the aldehydes correlated with flame temperature and increased as flame temperature was reduced.
12) The OFP of formaldehyde emissions showed a strong correlation with equivalence ratio and flame temperature regardless of fuel types.

10.1.2 Combustion and emissions of alternative fuels from APU

A matrix of fuels comprised of conventional JetA1, GTL, HEFA and FAE etc were tested using an APU engine. The influence of fuel H/C ratio, engine power, cold and hot idle on the particle number and mass size distributions and gaseous emissions were investigated. The results show that:

1) Most of the fuels had very close hydrogen/ Carbon ratios (~2), the amounts of CO_2 emissions are similar. However, CO_2 decreased as hydrogen to carbon ratio increased and GTL had the lowest CO_2 about (3000 g/Kg) with H/C ratio about 2.2 compared all fuels.

2) At idle condition, there are slight reductions in CO and UHC emissions for all fuels compared to JetA1. However, a significant reduction in CO (~28%) and UHC (~44%) was observed with GTL fuel

3) All fuels produce similar level of NOx emissions and fuel properties have little impact on NOx emissions at both conditions. NO_2/NOx fraction for all fuels was about 55% and ~40% at idle full conditions respectively.

4) GTL has strong effect on acetaldehyde, acrolein and benzene emissions and reduced by 35%, 50% and 96.5% respectively compared to JetA1.

5) Peak particle numbers were in a magnitude of 10^{15} to 10^{16} P/kg-fuel at the full power condition and 10^{14} to 10^{16} P/kg-fuel at the idle modes for all the fuels. The peak particle mass was in a range of 0.15 to 3.8 g/kg-fuel at idle modes and 0.06 to 1 g/kg-fuel at full power condition.
6) JetA1 produced the highest number and mass peak particle emissions whereas, GTL fuel produced the much lower number and mass peak particle emissions at both idles.
7) As the fuel H/C ratio increased, particle concentration, EIn and EIm and GMD were decreased.
8) The engine produced ~20% less particles at the hot idle mode compared to cold idle. The GMDs were similar. The hot idle had narrow size distributions.

10.1.3 Hydrogen combustion in impinging jet mix flame stabilizer

Combustion and emissions of direct hydrogen fuel using impinging Jet mix flame stabilizer were conducted. The test was carried out at Mach number of 0.47, 4.3% pressure lose and 600K inlet temperature. The main findings are:

1) Hydrogen is an excellent gas turbine fuel and its very wide flame stability makes it possible to achieve all engine power levels without air or fuel staging. It can be only injected directly due to high burning velocity and cannot be premixed due to flashback problem.

2) The Jet Mix flame stabiliser with impinging radial and axial air jets and the fuel injected into the radial jet was shown to be a suitable flame stabiliser for hydrogen provided the inline jet configuration was used.

3) Hydrogen heat release close to the flame stabiliser was a major problem and reducing the proportion of radial jet air from 20% to 6.5% to move the flame away from the flame stabilizer.

4) Both 20% and 6.5% radial air jets produce < 24ppm NOx emissions corrected to 15% oxygen at flame temperature < 1600K for 100% hydrogen combustion.

10.2 Recommendations for Future Work

Combustion and emissions of alternative fuels from low NOx burner have been measured and compared to base fuel. Many suggestions and ideas could be made for forthcoming research, and can be summarised as follows:

10.2.1 Effect of pressure on regulated and non-regulated emissions from low emissions gas turbines.

The combustor inlet temperature and residence time have influences on the flame temperatures; the later one has small effect on thermal NOx formation for lean mixtures. The inlet air temperature is a major factor in determining NOx level, as an increase to the inlet temperature of 100 K can be lead to increase the flame temperature by about 50 K. The results in this work showed that the aldehydes decreased as equivalence ratio increased due to the increased flame temperatures**.** It is worth noting that industrial gas turbines for electrical power operate at high pressure around 20bar and aero gas turbines at take-off could reach up to 60bar. The influence of pressure on emissions should be considered. However, no literature or report on the

influence of pressure on aldehydes emissions has been found. It would be interested to investigate the effect of pressure on gaseous emissions and hydrocarbon species including aldehydes emissions in the future work. The work on radial swirlers should be repeated on a lower NOx configuration with a higher pressure loss and the use of central injection with no swirler outlet throat should be investigated, as previous work has shown that this gives low NOx with liquid fuels. More work should be undertaken on NG/biofuel co-firing and vane passage injection for NG with no outlet throat might be a better configuration.

10.2.2 Combustion instabilities in lean premixed combustion at high pressures

Environmental constraint drives gas turbine manufacturers to develop new design for combustion chamber, in order to decrease pollutant emissions. The technological emerging ways consist of lean premixed combustion for reduction of NOx emissions. Unfortunately, lean premixed combustion is limited by the apparition of combustion instabilities, which induce high pressure fluctuations, which can produce turbine damage, flame extinction, and CO emissions. The mechanisms of combustion instabilities have been extensively studied in the past, especially in industrial burners and pulse combustors, but little work can be found relevant to modern gas turbines. The noise is generated by combustion process (direct combustion noise) or by flow of hot combustion products (indirect). However, it is worth to understand the mechanisms governing instabilities in lean premixed gas turbine. More attention need to be paid to influence of flame stability, fuel volatility on oscillating of combustion, combustion time, operating conditions (inlet air temperature, combustion pressure) and ambient conditions (air temperature and humidity).

10.2.3 Effect of incomplete fuel and air mixing on NOx Emissions and Stability.

One of the more promising ultra-low NOx gas turbine combustor concepts is the lean, premixed combustor that has demonstrated the potential for significant reductions in NOx emissions over what can be achieved by current designs. Studies have shown that incomplete fuel-air

mixing can have a significant effect on NOx emissions. Premixed combustors are more susceptible to combustion instabilities, so it is also important to understand the effect of incomplete fuel-air mixing on combustion stability. In the future it is worth to investigate the effects of incomplete fuel-air mixing on both NOx emissions and flame stability both in terms of the level of combustion-generated noise during combustion oscillations and the lean blowout limit in lean premixed combustors.

10.2.4 Apply CFD code to the experimental geometry that has been investigated.

Computational fluid dynamics (CFD) is one of the branches of fluid mechanics that uses numerical methods and algorithms to solve and analyze problems that involve fluid flows. Computers are used to perform the millions of calculations required to simulate the interaction of liquids and gases with surfaces defined by boundary conditions. CFD has been widely used in recent years as a design tool for gas turbine combustors due to its low cost compared with experimental testing. There are number of models have been used and successfully implemented into CFD such as eddy-dissipation, eddy –break up model and so on. King el al investigated the aerodynamic, air/fuel mixing, flame temperature and NOx emissions for similar deign of radial swirl as in the present work used CFD. He found that experimental combustion results could be predicted well using fluent based CFD model with the K-e turbulence and flamelet combustion model burning natural gas, kerosene, gas oil and propane. In the future, the similar code will be applied experimental geometries using biodiesel and its blends and compared to kerosene fuel. Moreover, Comparisons among experimental results with simulated work will be investigated at the same conditions.

References

[1] Saravanamuttoo, H., G. Rogers, and H. Cohen.Gas Turbine Theory Longman imprint, 2001.

[2] Lefebvre, A. H.Gas Turbine combustion, second edition. United states of America: edwards brothers, 1998.

[3] Ltd, R.-R.The Jet Engine/Rolls-Royce, 6th London Rolls-Royce 2005.

[4] Andrews, G. E., "Ultra-low nitrogen oxides (NOx) emissions combustion in gas turbine systems," in Modern Gas Turbine Systems: High Efficiency, Low Emission, Fuel Flexible Power Generation, P. Jansohn and S. Institute, P, Eds. Switzerland: Woodhead Publishing 2013.

[5] Willis, J. D., I. J. Toon, T. Schweiger, and D. A. Owen. Industrial RB211 dry low emission combustor. Proceedings of ASME Turbo Expo, 1993, 93-GT-391.

[6] Huang, Y. and V. Yang. Dynamics and stability of lean-premixed swirl-stabilized combustion. Progress in Energy and Combustion Science, 2009, 35, pp. 293-364.

[7] Hashimoto, N., Y. Ozawa, N. Mori, I. Yuri, and T. Hisamatsu. Fundamental combustion characteristics of palm methyl ester (PME) as alternative fuel for gas turbines. Fuel, 2008, 87, pp. 3373-3378.

[8] Basha, S. A., K. R. Gopal, and S. Jebaraj. A review on biodiesel production, combustion, emissions and performance. Renewable and Sustainable Energy Reviews, 13, pp. 1628-1634.

[9] Blakey, S., L. Rye, and C. W. Wilson. Aviation gas turbine alternative fuels: A review. Proceedings of the Combustion Institute, 2011, 33, pp. 2863-2885.

[10] Dagget, D. L., R. C. Hendricks, R. Walther, and E. Corporan, "Alternate Fuels for use in Commercial Aircraft ": The Boing Company 2007.

[11] Lefebvre, A. H. and D. R. Ballal. Gas Turbine combustion Alternative fuels and emissions USA: CRC Press Taylor&Francis Group, 2010.

[12] Goodger, E. and R. Vere. Aviation Fuels Technology Sheridan House Inc 1985.

[13] Phan, A. N. and T. M. Phan. Biodiesel production from waste cooking oils.Fuel, 2008, 87, pp. 3490-3496.

[14] Jha, S. K., S. Fernando, and S. D. F. To. Flame temperature analysis of biodiesel blends and components. Fuel, 2008, 87, pp. 1982-1988.

[15] Kinsey, J. S., Y. Dong, D. C. Williams, and R. Logan. Physical characterization of the fine particle emissions from commercial aircraft engines during the Aircraft Particle Emissions eXperiment (APEX) 1-3.Atmospheric Environment, 2010, 44, pp. 2147-2156.

[16] Billingsley, M., T. Edwards, and L. M. Shafer. Extent and Impacts of Hydrocarbon Fuel Compositional Variability for Aerospace Propulsion Systems American Institute of Aeronautics and Astronautics (AIAA), 2010, 10331, p. 16.

[17] Lee, S., J. G. Speight, and S. K. Loyalka. Handbook of Alternative Fuel Technologies: CRC Press, Boca Raton, 2007.

[18] Fyffe, D., M. John, k. Kumaran, R. Sadr, and A. AL-sharshani. Effect of GTL-like Jet Fuel Composition on GT Engine Altitude Ignition Performance-Part I: Combustor operability Proceedings of ASME Turbo Expo 2011: Power for Land, Sea, and Air (GT2011) 2011.

[19] Bulzan, D., B. Anderson, C. Wey, R. Howard, E. Winstead, and A. Beyersdorf. Gaseous and Particulate Emissions Results of the NASA Alternative Aviation Fuel Experiment (AAFEX).Proceeding of ASME Turbo Expo 2010: Power for Land, Sea, and Air (GT2010) 2010.

[20] Beyersdorf, A. and B. Anderson. An Overview of the NASA Alternative Aviation Fuel Experiment (AAFEX).TAC-2 Proceedings, June 22nd to 25th, 2009, Aachen and Maastricht, 2009.

[21] Kowkabi, M., "Swirl Combustors for Low Emission Gas Turbines," Department of fuel and energy. ph.D Leeds: leeds university, 1987, p. 214.

[22] Kurniawan, J. S. and S. Khardi. Comparison of methodologies estimating emissions of aircraft pollutants, environmental impact assessment around airports. Environmental Impact Assessment Review, 2011, 31, pp. 240-252.

[23] Sgouridis, S., P. A. Bonnefoy, and R. J. Hansman. Air transportation in a carbon constrained world: Long-term dynamics of policies and

strategies for mitigating the carbon footprint of commercial aviation. Transportation Research Part A: Policy and Practice, 45, pp. 1077-1091.

[24] Andrews, G. E., "Short course, Ultra Low NOx Gas Turbine Combustion," Leeds: Energy and Resources Research Institute, Leeds University,, 2009.

[25] Kim, M. N., "Design of Low NOx Gas Turbine Combustion Chamber," Department of Fuel and Energy Leeds: Leeds University, 1995, p. 181.

[26] Pavri, R. and G. Moore, D, "Gas Turbine Emissions and Control," Atlanta, GA: GE power Systems, GER-4211-03/01, 2003.

[27] McDoneli, V. and S. Samuelsen. Evaluation of the Level of Gaseous Fuel-Bound Sulfur on Fine Particulate Emissions from a Low Emission Gas Turbine Engine. Proceedings of ASME Turbo Expo Copenhagen, Denmark 2012, GT2012-69352.

[28] Dockery, D. and A. Pope.“Epidemiology of acute health effects: Summary of time-series studies”. Om: ‘Particles in Our Air - Concentrations and Health Effects Wilson, R. and Spengler J. (Eds.). Harvard University Press 1996, pp. 123-147.

[29] Seaton, A., W. MacNee, K. Donaldson, and D. Godden. Particulate air pollution and cut health effects. The Lancet 1995, 345, pp. 176-178.

[30] Wey, C. C., B. E. Anderson, C. Hudgins, C. Wey, A. Li-Jones, E. Winstead, L. K. Thornhill, P. Labo, D. Hagen, P. Whitefield, P. E. Yelvington, T. B. Herndon, R. C. Onasch, R. C. Miake-Lye, J. Wormhoudt, W. B. Knighton, R. Howard, D. Bryant, E. Corporan, C. Moses, D. Holve, and W. Dodds. Aircraft Particle Emissions eXperiment (APEX).2006.

[31] Han, H. S., D. R. Chen, and D. Y. H. Pui. A Fast Response Nano-meter Aerosol Size Analyser (nASA): Measurement and Data Inversion. NASA Report2002.

[32] Ai, T., C. Koeneke, H. Arimura, and Y. Hyakuake. Development of an Air Cooled G Class Gas Turbine(The M501 GAC).Proceeding of ASME Turbo Expo: Power for Land, Sea and Air Orlando, Florida, USA, 2009, GT2009-60321.

[33] Ito, E., I. Pkada, K. Tsukagoshi, A. Muyama, and J. Masada. Development of Key Technologies for the Next Generation 1700C-Class Gas Turbine. Proceeding of ASME Turbo Expo: Power for Land, Sea and Air Glasgow, UK 2009, GT2009-59783.

[34] Andrews, G. E., N. T. Ahmed, and R. Phylaktou "Weak Extinction in Low NOx Gas Turbine Combustion," Proceedings ASME Turbo Expo. GT2009-59830 Orland, Florida, USA, 2009.

[35] Escott, N. H., G. E. Andrews, U. S. Alkabie, A. F. A. AlShaikhly, and B. George.Large Airflow Capacity Radial Swirlers for Ultra Low NOx at High Inlet Temperatures. Proceedings og IGTI Seventh Congress and Exposition on Gas Turbines in Cogeneration, Utility, Industrial and Independent Power Generation, 1993, 8, pp. 241-243.

[36] Andrews, G. E, "ultra low NOX gas turbine combustion," Leeds: Leeds university, Energy and Resources Research Institute, 2009.

[37] Andrews, G. E., H. Li, and S. Wright. Particulate mass emissions from aircraft: A first order Approximation method based on experience from diesel particulate mass emissions measurement. Proceeding of ASME Turbo Expo 2009: Power for Land, Sea, and Air (GT2009), Orlando, Florida, USA, 2009, GT2009-59572.

[38] Andrews, G. E., I. Andrews, D, D. Dixon-Hardy, B. Gibbs, M, H. Li, and S. Wright. Airport PM10 Emissions: Development of a first order approximation (FOA) methodology for aircraft and airport particulate mass emissions. Proceeding of ASME Turbo Expo 2010: Power for Land, Sea, and Air (GT2010), 2010.

[39] Harrison, R. M., J. P. Shi, S. Xi, A. Khan, D. Mark, R. Kinnersley, and J. Yin.Measurement of number, mass and size distribution of particles in the atmosphere. Phil. Trans. R. Soc. Lond. A, 2000, 358, pp. 2567-2580.

[40] Lighty, J. S., J. M. Veranth, and A. F. Sarofim. Combustion Aerosols: Factors Governing Their Size and Composition and Implications to Human Health. Air & Waste Management Association, 2000, 50, pp. 1565-1618.

[41] Lavoie, G. A., J. B. Heywood, and J. C. Keck. Experimental and Theoretical Study of Nitric Oxide Formation in Internal Combustion

Engines. Combustion Science and Technology, 1970, 1, pp. 313-326.

[42] Fenimore, C. P. Formation of Nitric Oxide in Premixed Hydrocarbon Flames. Thirteenth Symposium (Int.) on Combustion, 1971 pp. 373-380.

[43] Lefebvre, A. H., "The Role of Fuel Preparation in Low Emissions Combustion," ASME GT-465-1995, 1995.

[44] Nicol, D. G., P. C. Malte, J. Lai, N. N. Marinov, and D. T. Pratt, "NOx Sensitivities for Gas Turbine Engines Operated on Lean Premixed Combustion and Conventional Diffusion Flames," ASME GT-115-1992, 1992.

[45] Bozzelli, J. W. and M. Antony.NNH: Possible new route for NOx Formation in Flames. Chem Kinetics, 1995, 27, pp. 1097-1109.

[46] Kyne, A. G., A. Williams, C. W. Wilson, and M. Pourkashanian. Modelling NO-NO2 Conversion in Counter-Flow Diffusion Flames. Proceedings of ASME Turbo Expo 2003, GT2003-38017.

[47] Schorr, M. M. and J. Chalfin, "Gas Turbine NOx Emissions Approaching Zero-Is it worth the price?," G. E. p. s. (GE), Ed. Schenectady, New york: GE Power Generation, 1999, p. 9.

[48] P.Schmittel, B.Gunther, B.Lenze, W.Leuckel, and H.Bockhorn. turbulent swirling flames: experimental investigation of the flow filed and formation of nitrogen oxide. combustion institute, 2000, 28, pp. 303-309.

[49] Al-Dabagh, N. A. and G. E. Andrews. The influence of flame stabiliser pressure loss on mixing combustion performance and flame stability Sixth International Symposium on air Breathing Engines, Paris, AIAA, 1983, pp. 172-181.

[50] Al-Dabbagh, N. A. and G. E. Andrews. Influence of flame stabiliser geometry on premixed combustion flame stability and emissions. Transactions of the ASME, Journal of Engineering for Power, 1981, 103, pp. 749-758.

[51] Andrews, G. E. and S. A. R. Ahmad, "Noncircular Jet Shear Layer Turbulent Diffusion Flames for Ultra Low NOx Gas Turbine Primary Zones," ASME Cogen-Turbo Portland, 1994, pp. 411-417.

[52] Abdul Hussian, U. S. and G. E. Andrews. Low NOx Primary Zones Using Jet Mixing Shear Layer Combustion. Proceedings ASME Turbo Expo, 1988, 88-GT-308.

[53] Ashrul ishak, M. S. and M. N. Jaafar. The effect of swirl number on discharge coefficient for various orifice sizes in a burner system. Mekanikal Journal, 2004, 17, p. 10.

[54] Andrews, G. E., N. Escott, and M. C. Mkpadi, "Radial swirler designs for ultra low NOx gas turbine combustion," Proceedings ASME Turbo Expo. 50406 Berlin, Germany, 2008.

[55] Andrews, G. E., M. N. Kim, M. C. Mkpadi, and S. A. Akande. Liquid fuelled low NOx radial swirlers with central pilot combustion. Proceeding of ASME Turbo Expo Montreal, Canada, 2007, GT2007-27415.

[56] Escott, N. H., G. E. Andrews, A. F. A. Al-Shaikhly, and H. S. Alkabie, "Counter-rotating Radial Swirlers for low NOx Emissions with air Staging " Yokohama, Japan II International Gas Turbine Conference IGTC 1995, pp. 333-346.

[57] Andrews, G. E. and M. C. Mkpadi. High turndown ratio, low NOx gas turbine combustion Proceedings of ASME Turbo Expo 2001, 2001-GT-59.

[58] Andrews, G. E., E. Z. Delgadillo, M. C. Mkpadi, and G. Hayes, "Hydrogen as a pilot gas to improve power turndown in simulated ultra low NOx gas turbine combustion," Proceedings ASME Turbo Expo. GT2007-27414

Montreal, Canada, 2007.

[59] Andrews, G. E., N. H. Escott, and A. F. A. Al-shaikly. Counter-rotating radial swirlers for low NOx emissions with passage fuel injection.12th Int. Symp. on Air Breathing Engines., AIAA: Melbourne., 1995.

[60] Abdulsada, M., N. Syred, A. Griffiths, P. Bowen, and S. Morris. Effect of swirl number and fuel type upon the combustion limits in swirl combustors .Proceeding of ASME Turbo Expo 2010: Power for Land, Sea, and Air 2011, GT2011-45544.

[61] Andrews, G. E. and N. T. Ahmad. Axial Swirler Design Influences on NOx Emissions for Premixed Combustion in Gas Turbine Combustors

with All the Combustor air Flow Passing through the Swirler Proceedings of ASME Turbo Expo: Power for Land, Sea and Air, Vancouver, British Columbia, Canada, 2011, GT2011-45418.

[62] Beer, J. M. and N. A. Chigier. Combustion Aerodynamics Applied Science Publishers Ltd 1972.

[63] Alkabie, H. S. and G. E. Andrews. The aerodynamics of radial swirlers in lean gas turbine primary zones. Proceedings of the Second IMechE International Conference on 'Computers in Engine Technology', 1991, C430, pp. 91-100

[64] King, P. T., N. Escott, G. E. Andrews, M. Pourkashanian, and A. C. McIntosh, "CFD Predictions of Low NOx Radial Swirlers with Vane Passage Fuel Injection with Comparison with Internal Gas Analysis Flame Composition " Proceedings of ASME Turbo Expo. 51138 Berlin, Germany, 2008, p. 14.

[65] Andrews, G. E., T. B. Matt Lazim, and M. C. Mkpadi. Low NOx Axial swiler with fuel injection into the downstream dump expansion shear layer. Energy institute, 2005, p. 25.

[66] Alkabie, H. S., R. McMillan, R. Noden, and C. Morris. Dual Fuel Dry Low Emissions (DLE) Combustion System for the ABB Alstom Power 13.4 MW Cyclone Gas Turbine. Proceedings of ASME Turbo Expo, Munich, Germany, 2000, 2000-GT-111.

[67] Lee, J., J. Armstrong, and D. Santavicca. Experiments on Lean Blowout and NOx Emissions of a Premixed Trapped Vortex Combustor with High G-Loading Proceedings of ASME Turbo Expo Glasgow, UK, 2010, GT2011-46396.

[68] Alkabie, H. S. and G. E. Andrews. Ultra-low NOx Emissions for Gas and Liquid Fuels using Radial Swirlers. Proceedings of ASME Turbo Expo Tornto, Ontario, 1989, 89-GT-322.

[69] Alkabie, H. S. and G. E. Andrews. Radial swirlers with peripheral fuel injection for ultra-low NOx emissions. ASME IGTI International Gas Turbine Congress, Brussels, Belgium, 1990, 90-GT-102

[70] Alkabie, H. S., G. E. Andrews, and N. T. Ahmad, "Lean low NOx Primary Zonez using Radial Swirlers " ASME 88-GT-245, 1988.

[71] Willis, J. D., I. J. Toon, T. Schweiger, and D. A. Owen, "Industrial RB211 Dry Low Emissions Combustor " ASME 93-GT-391, 1993.

[72] Scarinci, T. and J. L. Halpin, "Industrial Trent Combustor-Combustion Noise Characteristics " ASME 99-GT-9, 1999.

[73] Andrews, G. E., H. S. Alkabie, U. S. Abdul Hussain, and M. Abdul Aziz. Ultra low NOx ultra lean gas turbine primary zones with liquid fuels. .AGARD 81st Symposium of the Propulsion and Energetics Panel of Fuels and Combustion Technology for Advanced Aircraft Engines. , 1993 pp. 24.1-24.14

[74] King, P. T., H. S. Al Kabie, G. E. Andrews, M. Pourkashanian, and A. C. McIntosh.CFD Predictions of Low NOx Radial Swirlers with Central Fuel Injection.gas turbine, 2009, 60106, p. 8.

[75] King, P. T., G. E. Andrews, M. N. Kim, M. Pourkashanian, and A. C. McIntosh, "CFD Prediction and Design of Low NOx Radial Swirler Systems," Proceedings of ASME Turbo Expo. GT2009-60107 Orlando, Florida, USA, 2009.

[76] Ahmad, N. T., G. E. Andrews, M. Kowkabi, and S. Sharif. Centrifugal mixing in lean swirl stabilised primary zones, ASME International Gas Turbine Symposium, Beijing, China 1985, 85-IGT-103.

[77] Ahmad, N. T., G. E. Andrews, M. Kowkabi, and S. F. Sharif. Centrifugal Mixing Forces in Enclosed Swirling Flow Proceedings of 20th Symposium Combustion: Combustion Institute, 1984, pp. 259-267.

[78] Gordon E.Andrew, M. N. K., Mike C.Mkpadi and Sheriff A.Akande.Liquid fuelled low NOx radial swirlers with central pilot combustion.gas turbine, 2007, 27415, p. 11.

[79] Burtscher, J. R., C. Hirsch, and T. Sattlemeyer.Operation Characteristics of a Premixed Sub-ppm NOx Burner with Periodical Recircuation of Combustion Products Poroceedings of ASME Turbo Expo: Power for Land, Sea and Air 2006, GT2006-90072.

[80] Davis, L. B. and R. M. Washam, "Development of a Dry Low NOx Combustor " ASME paper 89-GT-255, 1989.

[81] Davis, L. B. and S. H. Black.Dry Low NOx Combustion Systems for GE Heavy-Duty Gas Turbines GE Power Systems Schenectady, NY 2000.

[82] Feigl, M., F. Setzer, R. Feigl-Varela, G. Myers, and B. Sweet.Field Test Validation of the DLN2.5H Combustion System on the 9H Gas Turbine at Baglan Bay Power Station Proceedings of ASME Turbo Expo: Power for Land, Sea and Air Reno-Tahoe, Nevada, USA 2005, GT2005-68843

[83] Doebbeling, K., J. Hellat, and H. Koch.25Years of BBC/ABB/ALSTOM Lean Premix Combustion Technologies Proceedings of ASME Turbo Expo: Power for Land, Sea and Air Reno, USA, 2005, GT2005-68296.

[84] Zajadatz, M., S. Bernero, R. Lancher, C. Motz, and P. Flohr. Development and Design of Alstom's Staged Fuel Gas Injection EV Burner for NOx Reduction Proceedings of ASME Turbo Expo: Power for Land, Sea and Air Montreal, Canada 2007, GT2007-27730

[85] Magni, F., D. Hudgins, W. Geng, and F. Grimm. Reduction of NOX Emissions in ALSTOM GT11NM Engines: Development, Validation and Engine Operation Experience of the EV-ALPHA Burner. Proceedings of ASME Turbo Expo: Power for Land, Sea and Air Copenhagen, Denmark GT2012-68345.

[86] Guyot, D., T. Meeuwissen, and D. Rebhan. Staged Premix EV Combustion in Alstom's GT25 Gas Turbine Engine Proceedings of ASME Turbo Expo: Power for Land, Sea and Air Copenhagen, Denmark 2012, GT2012-70102

[87] Kokanovic, S., G. Guidati, S. Torchalla, and B. Schuermans. Active Combustion Control System for Reduction of NOx and Pulsation Levels in Gas Turbines. Proceedings of ASME Turbo Expo: Power for Land, Sea and Air, 2006, GT2006-90895.

[88] Zajadatz, M., D. Pennell, S. Bernero, B. Paikert, R. Zoli, and K. Döbbeling. Devopment and Implementation of the AEV Burner for the Alstom GT13E2.Journal of Engineering for Gas Turbines and Power, 2013, 135, pp. 1-11.

[89] Jansohn, P., T. Ruck, C. Steinbach, H. P. Knöpfel, and T. Sattelmayer. Development of the Advanced EV (AEV) Burner for the ABB GTX100 Gas Turbine. ASME Turbo Asia Singapore, 1997, 97-AA-139.

[90] Willis, J. D., I. J. Toon, T. Schweiger, and D. A. Owen, "Industrial RB211 Dry Low Emission Combustion System," ASME Paper 93-GT-391, 1993.

[91] Willis, J. D. and A. J. Moran, "Industrial RB211 DLE Gas Turbine Combustion Update " ASME paper 2000-GT-109, 2000.

[92] Rokke, P. E., J. E. Hustad, N. A. Rokke, and O. B. Svendsgaard. Technology Update on Gas Turbine Dual Fuel, Dry Low Emissions Combustion System Proceedings of ASME Turbo Expo: Power for Land, Sea and Air Atlanta, 2003, GT-2003-38112.

[93] Scarinci, T. and J. L. Halpin. Industrial Trent Combustor- Combustion Noise Characteristics Journal of Engineering for Gas Turbines and Power, 2000, 122, pp. 280-286.

[94] Rodriguez, J., S. Tanimura, M. Nose, S. Takiguchi, and K. Ishizaka. Advanced Dry Low Nox Combustor for Mitsubishi G Class Gas Turbines. Proceedings of ASME Turbo Expo: Power for Land, Sea and Air 2008, GT2008-50819.

[95] Saltou, T., H. Inoui, K. Miura, N. Kobayashi, and S. Suzuki. Performance Demonstration of the Full Size Multi Cluster Combustor for DME under Real Engine Conditions. Proceedings of ASME Turbo Expo: Power for Land, Sea and Air 2005, GT2005-68647.

[96] Fleuti, E. and P. Hofmann, "Aircraft APU Emissions at Zurich Airport ": Unique(Flughafen Zurich AG) 2005.

[97] Watterson, J., C. Walker, and S. Eggleston. Revision to the Method of Estimating Emissions from Aircraft in the UK Greenhouse Gas Inventory. London 2004.

[98] Lin, Y., Y. Lin, C. Zhang, and Q. Xu, "Evaluation of Combustion Performance of a Coal-Derived Synthetic Jet Fuel," Proceedings of ASME Turbo Expo. GT2012-68604 Copenhagen, Denmark, 2012.

[99] Gökalp, I. and E. Lebas. Alternative fuels for industrial gas turbines (AFTUR).Applied Thermal Engineering, 2004, 24, pp. 1655-1663.

[100]Lefebvre, A. H., "Airblast atomization," Progress in Energy and Combustion Science. 6, 1980, pp. 233-261.

[101]Semião, V., P. Andrade, and M. d. G. Carvalho. Spray characterization: Numerical prediction of Sauter mean diameter and droplet size distribution. Fuel, 1996, 75, pp. 1707-1714.

[102]Corporan, E., "Comparisons of Emissions Charactristics of Several Turbine Engines Burning Fischer-Tropsch and Hydroprocessed Esters and Fatty Acids Alternative Jet Fuels," Proceedings of ASME Turbo Expo. GT2012-68656 Copenhagen, Denmark, 2012.

[103]Timko, M. T., S. C. Herndon, E. R. Blanco, E. C. Wood, Z. Yu, R. C. Miake-Ly, W. B. Knighton, M. DeWitt, and E. Corporan. Combustion Products of Petroleum Jet Fuel, A Fischer-Tropsch Synthetic Fuel, and a Biomass Fatty Acid Methyl Ester Fuel for a Gas Turbine Engine Combustion Science and Technology 2011, 183, pp. 1039-1068.

[104]Suder, J. L., "Effect of Aromatic Concentration of a Fischer-Tropsch fuel on Thermal stability " Proceedings of ASME Turbo Expo. GT2012-68626 Copenhagen, Denmark, 2012.

[105]Mckibben, G. P. B. Biodiesel Growing a New Energy Economy, frst edition. Chelsea Green, 2005.

[106]Canakci, M., "Performance and emissions characteristics of biodiesel from soybean oil." 41380: Faculty of Technical Education, Kocaeli University, 2005, pp. 915-922.

[107]Souza, G. R., A. M. Santos, S. L. Ferreira, K. C. R. Martins, and D. L. Módolo.Evaluation of the performance of biodiesel from waste vegetable oil in a flame tube furnace.Applied Thermal Engineering, 2009, 29, pp. 2562-2566.

[108]Gupta, K. K., A. Rehman, and R. M. Sarviya.Bio-fuels for the gas turbine: A review. Renewable and Sustainable Energy Reviews, 14, pp. 2946-2955.

[109]Lue, Y. F., Y. Yeh, and C. Wu.The Emission Characteristics of a Small D.I.Diesel Engine using Biodiesel Blended Fuel. Environmental Science and Health, 2001, A36(5), pp. 845-859.

[110]Liu, K., J. P. Wood, E. R. Buchana, P. Martin, and V. E. Sanderson. Biodiesel as an alternative fuel in Siemens DLE

combustors:atmosheric and high pressure rig testing. Proceedings of ASME turbo Expo Orlando, Florida, USA, 2009, GT2009-59065.

[111] Lapuerta, M., J. Rodríguez-Fernández, and J. R. Agudelo. Diesel particulate emissions from used cooking oil biodiesel. Bioresource Technology, 2008, 99, pp. 731-740.

[112] Zhang, Y., M. A. Dubé, D. D. McLean, and M. Kates. Biodiesel production from waste cooking oil: 2. Economic assessment and sensitivity analysis. Bioresource Technology, 2003, 90, pp. 229-240.

[113] Ma, F. and M. A.Hanna. Biodiesel production: a review. Bioresource Technology, 1999, 70, pp. 1-15.

[114] SABC, "Alternative Aviation Fuels " SABC Aviation and Environment Briefing Papers

[115] Andrews, G. E., T. B. Matt Lazim, and M. C. Mkpadi. Low NOx Axial Swirler with Fuel Injection into the Downstream Dump Expansion Shear Layer. Proceedings of the Energy Institute, 2005.

[116] Escott, N. H., G. E. Andrews, H. S. Alkabie, A. F. A. AlShaikhly, and B. George.Large Airflow Capacity Radial Swirlers for Ultra Low NOx at High Inlet Temperatures.ASME COGEN Turbo Power Meeting, Bournemouth, England., 1993.

[117] "GASMETTM CR-Series FT-IR GAS Analyzer IN-LAB Series Instruction& operating Manual " Temet Instrument oy. Helsinki, Finland, 2002.

[118] Leong, C. C., R. Lucas, S. Blakey, and C. W. Wilson, "Reverse Engineering Gas Turbine Emissions Performance: Applied to an Aircraft Auxilary Power Unit " Proceedings of ASME Turbo Expo. GT2010-22478 Glasgow, UK, 2010.

[119] Crayford, A., M. Johnson, R. Marsh, Y. Sevcenco, D. Walters, P. Williams, S. Christie, W. W Chung, A. Petzold, A. Ibrahim, D. Delhaye, P. Quincey, P. Bowen, H. Coe, D. Raper, and C. Wilson. Studying, sampling and measurement of aircraft particulate emissions III (SAMPLE III) - Final Report European Aviation Safety Agency 2011.

[120] Swanson, J. and D. Kittelson. Evaluation of thermal denuder and catalytic stripper methods for solid particle measurements. Journal of Aerosol Science, 41, pp. 1113-1122.

[121]Lobo, P., D. Hagen, E, P. Whitefield, D, and D. Alofs, J. Physical Characterization of Aerosol Emissions from a Commercial Gas Turbine Engine. Propulsion and Power 2007, 23, pp. 919-982.

[122]Lobo, P., L. Rye, P. I. Williams, S. Christie, I. Uryga-Bugajska, C. W. Wilson, D. E. Hagen, P. D. Whitefield, S. Blakey, H. Coe, D. Raper, and M. Pourkashanian. Impact of Alternative Fuels on Emissions Characteristics of a Gas Turbine Engine â€“ Part 1: Gaseous and Particulate Matter Emissions. ENVIRONMENTAL SCIENCE & TECHNOLOGY, 46, pp. 10805-10811.

[123]Abdul Aziz, M. M., U. S. Abdul Hussian, N. A. Al-Dabbagh, G. E. Andrews, and A. R. Shahabadi. Lean Primary Zone: Pressure Loss and Residence Time Influences on Combustion Performance and NOx Emissions. Tokyo International Gas Turbine Congress, 1987, Vol.III, pp. 89-96.

[124]Abdul Aziz, M. M. and G. E. Andrews. Jet Mixing Shear Layers for the Lean Combustion of Liquid fuels with Low NOx at Gas Turbine Primary Zone Conditions.Yokohama International Gas Turbine Congress, Japan, 1991, Vol.1, pp. 179-189.

[125]Andrews, G. E., M. M. Abdul Aziz, and N. A. Al-Dabbagh. Mixing and Fuel Atomisation Effects on Premixed Combustion Performance. Proceedings ASME Turbo Expo, Arizona, USA, 1983.

[126]Abdul Hussian, U. S. and G. E. Andrews. Air Blast Atomization as a Function of Pressure Loss for Large Air Flow Rates. Proceedings of ASME Turbo Expo, Brussels, Belgium 1990, 90-GT-277.

[127]Andrews, G. E. and U. S. Abdul Hussian. Concentration Fluctuations in Turbulent Cross Jet Mixing. Proceedings of ASME Turbo Expo, Cologne, Germany 1992.

[128]Andrews, G. E., M. M. Abdul Aziz, and N. A. AlDabagh. Mixing fuel Atomisation effects on premixed combustion performance.International Journal of Turbo and Jet Engines, 1984, 1, pp. 363-374.

[129]Abdul Hussian, U. S. A., G. E. Jet mixing Shear layer combustion: an ultra-low NOx system for natural-gas-fired gas turbine. IMech. E, 1988,

[130]Abdul-Aziz, M. M. and G. E. Andrews. Smoke emissions from lean well mixed gas turbine primary zones. The ASME, International Gas Turbine Symposium, Beijing, Chaina 1985, 85-IGT-l 17.

[131]Al-Dabbagh, N. A., G. E. Andrews, and A. R. Shahabadi. Combustion and emissions performance of a rapid fuel and air mixing combustor. Proceedings of the Seventh International Symposium on Air Breathing Engines, , Bejing, China, 1985, AIAA, pp. 804-812

[132]Mustafa, A. and G. E. Andrews. Isothermal modelling study of concentration fluctuation in multi-jet turbulent mixing. Journal Teknologi, 2005, 42, pp. 75-88, ISSN 0127-9696.

[133]Tacina, R. R. Low NOx Potential of Gas Turbine Engines. AIAA-90-0550 and NASA TM102452,1990.

[134]Andrews, G. E. and M. N. Kim, "The influence of film cooling on emissions for a low radial swirler gas turbine combustor," Proceedings ASME Turbo Expo New Orleans, 2001.

[135]Antos, R. J., S. E. Mumford, and J. Winter. A Dual Fuel Dry Low NOx Combustion System for Industrial Combustion Turbines. Proc. of American Power Conf. 53rd Annual Meeting, Chicago, USA, 1991.

[136]Abdul Hussian, U. S., G. E. Andrews, W. G. Cheung, and A. R. Shahabadi. Jet mixing Shear layer combustion: an ultra-low NOx system for natural-gas-fired gas turbine.IMech.E, 1988.

[137]Daham, B., B. E. Anderson, and H. Li. Application of a portable FTIR for measuring on road emissions SAE, 2005, 2005-01-0676.

[138]Peck, J., M. T. Timko, Z. Yu, H.-W. Wong, S. S. Herndon, P. E. yelvington, and R. C. Miake-Ly. Measurement of Volatile Particulate Matter Emissions from Aircraft Engines Using Simulated Plume Aging System Proceeding of ASME Turbo Expo 2010: Power for Land, Sea, and Air (GT2011), 2011, GT2011-46626.

[139]Wong, H.-W., Z. Yu, M. T. Timko, S. S. Herndon, E. R. Blanco, and R. C. Miake-Ly. Design Parameters for an Aircraft Engine Exit Plane Particle Sampling System. Engineering for Gas Turbine and Power, 2011, 133.

[140]Sevcenco, Y., A. Crayford, R. March, P. Bown, and M. Johnson. Evaluation of a particulate sampling methodology from a gas turbine

exhaust using real-time size and number analysis at simulated aircraft conditions. Proceedings of ASME Turbo Expo 2010: Power for Land, Sea, and Air (GT2010) 2010.

[141]Cheng, M., E. Corporan, M. J. DeWitt, and B. Landgraf. Emissions of Volatile Components from Turboshaft Engines Operated with JP-8 and Fischer-Trosch Fuels. Aerosol and Air Quality Research, 2009, 9, pp. 237-256.

[142]Bhargava, A., D. Liscinsky, R. McKinney, B. E. Anderson, A. Petzold, and R. C. Miake-Lye. Characterising Particulate Matter Emissions from Aircraft Engines. Proceedings of ASME Turbo Expo Copenhagen, Denmark, 2012, GT2012-69598.

[143]Wayson, R. L., G. G. Fleming, and R. Iovinelli. Methodology to Estimate Particulate Matter Emissions from Certified Commercial Aircraft Engines. Air & Waste Management Association, 2009, 59, pp. 91-100.

[144]Wayson, R. L., G. G. Fleming, B. Kim, and J. Draper. Derivation of A First Order Approximation of Particulate Matter From Aircraft.96th Annual Meeting of the Air& Waste Management Association; A&WMA, Pittsburgh. PA, 2003.

[145]Tan, P., Z. Hu, D. Lou, and B. Li. Particle Number and Size Distribution from a Diesel Engine with Jatropha Biodiesel Fuel.SAE, 2009, 2009-01-2726.

[146]TSI.Model 3936 SMPS (Scanning Mobility Particle Sizer), Instruction Manual P/N 1933796, Revision H, 2003.

[147]Morley, C., " Gaseq, Chemical equilibria in perfect gases,v0.79." Feb 2010, pp. http://www.gaseq.co.uk,.

[148]Carter, W. P. L. Development of ozone reactivity scales for volatile organic compounds Air and Waste Management Association, 1994, 44, p. 881.

[149]Carter, W. P. L. Additions and Corrections to the Saprc-99 Maximum Incremental Reactivity (MIR) Scale. Air Pollution Research Centre and College of Engineering Centre for Environmental Research and Technology, University of California: California., 2000, 97-314. 2000.

[150]Duxbury, R. M. C. and S. G. C. Morton. Measurements of Ozone Precursor Substances. Environmental Law. Oxford University Press., 2004, Fifth Edition.

[151]Panchasara, H. V., B. M. Simmons, A. K. Agrawal, S. K. Spear, and D. T. Daly, "Combustion Performance of Biodiesel and Diesel-Vegetable Oil Blends in a Simulated Gas Turbine Burner," Proceedings of ASME Turbo Expo. 131 Orlando, Florida, USA, 2009.

[152]Li, H., G. E. Andrews, and J. L. Balsevich-Prieto. Study of Emissions and Combustion Characteristics of RME B100 Biodiesel from a Heavy Duty DI Diesel Engine.SAE Fuels and Emissions Conference, Cape Town, 2007, 2007-01-0074.

[153]Verhaeven, E., L. G. Pelkmans, R. Lamers, and F. Theuissen, "Results of demonstration and evaluation projects of biodiesel from rapeseed and used frying oil on light and heavy duty vehicles," SAE Technical Paper. 2005-01-2201, 2005.

[154]Lupandin, V., R. Thamburaj, and A. Nikolayev. Test results of the OGT2500 gas turbine engine running on alternative fuels: biooil, ethanol, biodiesel and crude oil. Proceeding of ASME Turbo Expo, Reno, Nevada, USA, 2005, GT2005-68488.

[155]Bolszo, C., V. McDonell, and S. Samuelsen. Impact of biodiesel on fuel preparation and emissions for a liquid fired gas turbine engine. Proceedings of ASME Turbo Expo Montreal, Canada, 2007, GT2007-27652.

[156]Chiang, H. W. D., I. C. Chiang, and H. L. Li. Performance testing of mircoturbine generator system fuelled by biodiesel. Proceedings of ASME Turbo Expo, Montreal, Canada, 2007, GT2007-28075.

[157]Molière, M., M. Panarotto, M. Aboujaib, J. M. Bisseayd, A. Campbell, J. Citeno, P. A. Mire, and L. Ducrest. Gas turbines in alternative fuel applications: biodiesel field test. Proceedings of ASME Turbo Expo, Montreal, Canada, 2007 GT2007-27212.

[158]Campbell, A., G. J., H. T., W. R., M. M., and C. J. Heavy duty gas turbines fuel flexibility. Proceedings of ASME Turbo Expo, Berlin, Germany, 2008, GT2008-51368.

[159]Park, S. H., H. J. Kim, H. K. Suh, and C. S. Lee. A study on the fuel injection and atomization characteristics of soybean oil methyl ester (SME).International Journal of Heat and Fluid Flow, 2009, 30, pp. 108-116.

[160]Li, H., G. E. Andrews, and S. Wright. Application of the FTIR Technique in the Hydrocarbon Speciation of Exhaust Gases for a micro gas Turbine Jet Engine. American Institute of Aeronautics and Astronautics Inc 2009, 1303.

[161]He, C., Y. Ge, J. Tan, K. You, X. Han, J. Wang, Q. You, and A. Shah. Comparison of carbonyl compounds emissions from diesel engine fuelled with biodiesel and diesel. Atmospheric Environment, 2009, 43, pp. 3657-3661.

[162]Pang, X., X. Shi, Y. Mu, H. He, S. Shuai, H. Chen, and R. Li. Characteristics of carbonyl compounds emission from a diesel-engine using biodiesel-ethanol-diesel as fuel. Atmospheric Environment, 2006, 40, pp. 7057-7065.

[163]Lea-Langton, A., H. Li, and G. E. Andrews. Investigation of Aldehyde and VOC Emissions during Cold Start and Hot Engine Operations using 100% Biofuels for a DI Engine.SAE 2009, 2009-01-1515.

[164]Salooja, K. C. The role of aldehydes in combustion: Studies of the combustion characteristics of aldehydes and of their influence on hydrocarbon combustion processes. Combustion and Flame, 1965, 9, pp. 373-382.

[165]Wei, Y., S. Liu, F. Liu, L. Liu, Z. Zhu, and G. Li. Aldehydes and Methanol Emission Mechanisms and Characteristics from a Methanol/Gasoline-Fuelled Spark-Ignition (SI) Engine. Energy Fuels, 2009, 23, pp. 6222–6230.

[166]Lingard, J. J., E. L. Agus, D. T. Young, and G. E. Andrews. Observations of urban airborne particle number concentrations during rush-hour conditions: analysis of the number based size distributions and modal parameters. Journal of Environmental Monitoring, 2006, 8, pp. 1203-1218.

[167]Kittelson, D. B., W. F. Watts, G. R. Johnson, M. I. Remerowski, E. E. ISche, G. Obernberger, R. M. Gelein, A. C. Elder, and P. K.

Hopke.On-road exposure to highway aerosols. 1. Aerosol and gas measurements. Inhalation Toxicology, 2004, 16, pp. 31-39.

[168]Klippel, N., T. J. Wood, R. E. Pearce, K. Begtsson, M. Kasper, and T. Mosimann, "On-line Measurements of Ultrafine particle Emissions from Gas Turbines," Power Gen Europe Dusseldorf, Germany, 2003.

[169]Herndon, S. C., J. T. Jayne, P. Lobo, T. B. Onasch, G. Fleming, D. E. Hagen, P. D. Whitefield, and R. C. Minke-Lye. Commercial Aircraft Engine Emissions Characteristics of in-Use Aircraft at Hartfield-Jackson Atlanta International Airport. Environ. Sci. Techno, 2008, 42, pp. 1877-1883.

[170]Kittelson, D. B., J. P. Watts, D. Johnson, A. Zarling, U. Kasper, H. Baltensperger, J. Burtscher, and S. Schiller. Gasoline vehicle exhaust particle sampling study. Contract final report U.S Department of Energy Cooperative Agreement DE-FC04-01A166910.2003

[171]Johnson, J., D. Kittelson, and W. Watts .Source Apportionment of Diesel and Spark Ignition Exhausts Aerosol using on-road Data from the Minneapolis Metropolitan area. Atmospheric Environment, 2005, 39, pp. 2111-2121.

[172]Li, H., A. Lea-Langton, G. E. Andrews, M. Thompson, and C. Musungo. Comparison of Exhaust Emissions and Particulate Size Distribution for Diesel, Biodiesel and Cooking oil from a Heavy Duty DI Diesel Engine.SAE 2008, 2008-01-0076.

[173]Lea-Langton, A., H. Li, G. E. Andrews, and P. Biller. The Influence of Fuel Pre-Heating on Combustion and Emissions with 100% Rapeseed oil for a DI Diesel Engine.SAE international 2009, p. 12.

[174]Andrews, G. E., N. T. Ahmed, R. Phylaktou , and P. T. King.Weak extinction in low NOx gas turbine combustion. Proceedings of ASME Turbo Expo, Orlando, USA, 2009, GT2009-59830.

[175]Kittelson, D. B.Engines and nanoparticles: a review. Journal of Aerosol Science, 1998, 29, pp. 575-588.

[176]Karcher, B. and D. W. Fahey.The role of sulphur emission in volatile particle formation in jet aircraft exhaust plumes Geophysical research letters, 1997, 24, pp. 389-392

[177]Johnson, M. Aero Gas Turbine Emissions Measurements-State of the art review.Workshop: In Plume Imaging of Gas Turbine Exhust Species IET, UK, 2013.

[178]Johnson, M. P., M. Hilton, R. Burrows, and P. Madden. Characterisation of particulates emitted from gas turbine exhausts.Journal of Aerosol Science, 2000, 31, pp. 618-619.

[179]Timko, M. T., T. B. Onasch, M. J. Northway, J. T. Jayne, M. R. Canagaratna, S. C. Herndon, E. C. Wood, and R. C. Miake-Ly. Gas Turbine Engine Emissions—Part II: Chemical Properties of Particulate Matter.Journal of Engineering for Gas Turbines and Power, 2010, 132.

[180]Marsh, R., A. Crayford, A. A Petzold, M. Johnson, P. Williams, A. Ibrahim, P. Kay, S. Morris, D. Delhaye, D. Lottin, X. Vancassel, D. Raper, S. Christie, M. Bennett, M. Miller, Y. Sevcenco, C. Rojo, H. Coe, and P. Bowen. Studying, sampling and measurement of aircraft particulate emissions II (SAMPLE II) – Final Report. European Aviation Safety Agency 2010.

[181]Bulzan, D., B. Anderson, C. Wey, R. Howard, E. Winstead, and A. Beyersdorf, " Gaseous and particulate emissions results of the NASA alternative aviation fuel experiment(AAFEX)," Proceedings of ASME Turbo Expo. GT2010-23524 Glasgow, UK, 2010.

[182]Islin, M. J. A., M. Cerza, and P. E. Jenkins. An experimental study on the effects of Fisher-Tropsch(FT) blends with diesel#2 and JP5 on the performance of a Rolls-Royse model 250-C20B gas turbine engine. Proceedings of ASME Turbo Expo, Glasgow, UK, 2010, GT2010-22436.

[183]Pucher, G., W. Allan, and P. Poitras, "Emissions from gas turbine sector rig operated with synthetic aviation and biodiesel fuel " Proceedings of ASME Turbo Expo. GT2010-22494 Glasgow, UK, 2010.

[184]Timko, M. T., Z. Yu, T. B. Onasch, H.-W. Wong, R. C. Miake-Lye, A. J. Beyersdorf, B. E. Anderson, K. L. Thornhill, E. L. Winstead, E. Corporan, M. J. DeWitt, and C. D. Klingshirn.Particulate Emissions of

Gas Turbine Engine Combustion of a Fischer-Tropsch Synthetic Fuel.Energy Fuels, 2010, 24, pp. 5883-5896.

[185]Anderson, B. E., A. J. Beyersdorf, C. H. Hudgins, P. Lobo, P. D. Whitefield, D. E. Hagen, and K. L. Thornhill. Alternative Aviation Fuel Experiment (AAFEX).NASA Centre for Aerospace Information, Hanover2011.

[186]Wood, E. C., S. C. Herndon, M. T. Timko, P. E. Yelvington, and R. C. Miake-Lye.Speciation and Chemical Evolution of Nitrogen Oxides in Aircraft Exhaust near Airports. ENVIRONMENTAL SCIENCE & TECHNOLOGY, 2008, 42, pp. 1884-1891.

[187]Chishty, W. A., C. R. Davison, J. Bird, T. Chan, K. Cuddihy, M. McCurdy, P. Barton, A. Krasteva, and P. Poitras. Emissions Assessment of Alternative Aviation Fuel at Simulated Altitudes.Proceedings of ASME Turbo Expo, Vancouver, British Columbia, Canada 2011, GT2011-45133.

[188]Lobo, P., L. Rye, P. I. Williams, S. Christie, I. Uryga-Bugajska, C. W. Wilson, D. E. Hagen, P. D. Whitefield, S. S Blakey, H. Coe, D. Raper, and M. Pourkashanian. Impact of Alternative Fuels on Emissions Characteristics of a Gas Turbine Engine – Part 1: Gaseous and Particulate Matter Emissions. Environmental Science & Technology 2011, 46 (19), pp. 10805-10811

[189]Corporan, E., M. J. DeWitt, V. Belovich, Robert Pawlik, A. C. Lynch, J. R. Gord, and T. R. Meyer. Emissions Characteristics of a Turbine Engine and Research Combustor Burning a Fischer−Tropsch Jet Fuel.Energy & Fuels 2007, 21 (5), 2615-2626

[190]ICAO. Airport Air Quality Guidance Manual.2007.

[191]Knighton, W. B., T. Rogers, C. C. Wey, B. E. Anderson, S. C. Herndon, P. E. Yelvington, and R. C. Miake-Lye. Quantification of Aircraft Engine Hydrocarbon Emissions Using Proton Transfer Reaction Mass Spectromety.J. Propulsion Power, 2007, 23, pp. 949-957.

[192]Miake-Lye, R. C., E. C. Wood, M. T. Timko, z. Yu, and S. S. Herndon. Effects of Alternative fuels on Hydrocarbon and particle Emissions

from Aircraft Engines.TAC-2 Proceedings of Aachen and Maastricht, 2009.

[193]Spicer, C. W., M. W. Holdren, R. M. Riggin, and T. F. Lyon. Chemical Composition and Phtochemical Reactivety of Exhaust from Aircraft Turbine Engines. Annales Geophysicae: Atmospheres, Hydrospheres and space Sciences, 1994, 12, pp. 944-955.

[194]Knighton, W. B. Quantification of Aircraft Engine Hydrocarbon Emissions Using Proton Transfer Reaction Mass Spectrometry Propulsion and Power, 2007, 23, pp. 949-958.

[195]Herndon, S. S., T. Rogers, E. J. Dunlea, J. T. Jayne, R. C. Miake-Ly, and B. Knighton. Hydrocarbon Emissions From In-use Commercial Aircraft during Airport Operation. Environ. Sci. Techno, 2006, 40, pp. 4406-4413.

[196]Herndon, S. S., E. C. Wood, M. J. Northway, R. C. Miake-Ly, K. L. Thornhill, A. J. Beyersdorf, B. E. Anderson, R. Dowlin, W. Dodds, and B. Knighton. Aircraft Hydrocarbon Emissions at Oakland International Airport Environ. Sci. Techno, 2009, 43, pp. 1730-1736.

[197]Lobo, P., D. E. Hagen, and P. D. Whitefield. Measurement and analysis of aircraft engine PM emissions downwind of an active runway at the Oakland International Airport. Atmospheric Environment, 61, pp. 114-123.

[198]Mazaheri, M., G. R. Johnson, and L. Morawska. Particle and Gaseous Emissions from Commercial Aircraft at Each Stage of the Landing and Takeoff Cycle. ENVIRONMENTAL SCIENCE & TECHNOLOGY, 2008, 43, pp. 441-446.

[199]York, W. D. and W. S. Ziminsky. Development and Testing of a Low NOx Hydrogen Combustion System for Heavy Duty Gas Turbines.Proceedings of ASME Turbo Expo Copenhagen, Denmark, 2012, GT2012-69913.

[200]Lin, Y. C., S. Daniele, and P. Jansohn. Combustion Characteristics and NOx Emissions of Hydrogen-Rich Fuel Gases at Gas Turbine relvant Conditions Proceeding of ASME Turbo Expo, Copenhagen, Denmark, 2012, GT2012-69080.

[201]Corradetti, A. and U. Desideri, "A Techno-Economic Analysis of Different Options for Cogenerating Power in Hydrogen Plants Based on Natural Gas Reforming," Proceedings of ASME Turbo Expo. GT2006-90360 Barcelona, Spain, 2006, pp. 343-357

[202]Lin, S., M. Harada, Y. Suzuki, and H. Hatano. Hydrogen production from coal by separating CO2 during gasification. Fuel 2002, 81, pp. 2079-2085.

[203]Kakaras, E., A. Koumanakos, and P. LKimantos, "Novel Solid Fuel Gasification Power Plant for In Situ CO2 Capture," Proceedings of ASME Turbo Expo. GT2007-27868 Montreal, Canada, 2007, pp. 969-976

[204]Nord, L. and O. Bolland, "HRSG Design for Integrated Reforming Combined Cycle With CO2 Capture," Proceedings of ASME Turbo Expo. GT2010-22389 Glasgow, UK, 2010, pp. 559-568.

[205]Chang, S., T. Liou, and W. Yeh, "Heat Transfer in a Radially Rotating Square-Sectioned Duct With Two Opposite Walls Roughened by 45° Staggered Ribs," Proceedings of ASME Turbo Expo. GT2006-90153 Barcelona, Spain, 2006, pp. 117-126

[206]Zachary, J., "Design Challenges for Combined Cycles With Post-Combustion CO2 Capture," Proceedings of ASME Turbo Expo. GT2009-59381 Orlando, Florida, USA, 2009, pp. 881-890

[207]Zabetakis, M. G.Flammability characteristics of combustible gases and vapors U.S. Department of the Interior, Bureau of Mines, , Washington, USA1995.

[208]Andrews, G. E. and D. Bradley. Determination of burning velocity.Combustion and Flame, 1972, 18, p. 133.

[209]Alavandi, S. and A. K. Agrawal. Lean Premixed Combustion of Carbon-Monoxide-Hydrogen-Methane Fuel Mixtures Using Porous Inert Media.Proceedings ASME Turbo Expo, Reno, Nevada, USA, 2005, GT2005-68586

[210]Palomba, C., P. Puddu, and F. Nurzia, "3D Flow Field Measurement Around a Rotating Stall Cell," Proceedings of ASME Turbo Expo. 98-GT-596 Stockholm, Canada, 1998.

[211] Mcleroy, J. and W. Weaver, "Retrofittable. Dry Low Emissions Combustor for 50l-K Industrial Gas. Turbine Engines," Proceedings of ASME Turbo Expo. 94-GT-439, 1994.

[212] Meleroy, J. T., D. A. Smith, and M. K. Razdan, "Development and Engine Testing of a Dry Low Emissions Combustor for Allison 501 -K Industrial Gas Turbine Engines," Proceedings of ASME Turbo Expo. 95-GT-335, 1995.

[213] Pilidis, P., A. Tourlidakis, and K. Kumar, "Analysis of 115MW, 3-Shaft Helium Brayton Cycle Using Nuclear Heat Source," Proceedings of ASME Turbo Expo. 2001-GT-53, 2001.

[214] Song, Q., A. Fang, and G. Xu. Dynamic and Flashback Characteristics of the Syngas Premixed Swirling Combustors. Proceedings of ASME Turbo Expo, Berlin, Germany, 2008, GT2008-50752 pp. 515-525

[215] Kishida, H. and R. Singh. Influence of Hydrogen Enriched Fuel on Power Generation Gas Turbine. International Gas Turbine congress, Tokyo, Japan, 2007, IGTC 2007-TS-135.

[216] Wu, J., P. Brown, and I. Diakunchak, "Advanced Gas Turbine Combustion System Development for High Hydrogen Fuels," Proceedings of ASME Turbo Expo. GT2007-28337 Montreal, Canada, 2007 pp. 1085-1091

[217] Hernandez, S. R., Q. Wang, and V. MecDonell, "Micro Mixing Fuel Injectors for Low Emissions Hydrogen Combustion," Proceedings of ASME Turbo Expo. GT2008-50854 Berlin, Germany, 2008, pp. 675-685.

[218] Lee, H., S. R. Hernandez, and V. McDonell, "Development of Flashback Resistant Low-Emission Micro-Mixing Fuel Injector for 100% Hydrogen and Syngas Fuels," Proceedings of ASME Turbo Expo. GT2009-59502 Orlando, Florida, USA, 2009.

[219] Alavandi, S. and A. K. Agrawal. Lean Premixed Combustion of Methane and Hydrogen-Enriched Methane Using Porous Inert Media. Proceedings ASME Turbo Expo, Vienna, Austria, 2004, GT2004-53231.

[220]Littlejohn, D., R. K. Cheng, D. Noble, and T. Lieuwen, "Laboratory Investigations of Low-Swirl Injectors Operating with Syngases," Proceedings of ASME Turbo Expo. GT2008-51298 Berlin, Germany, 2008.

[221]Balestri, M., D. Cecchini, and V. Cinti, "Unconventional Fuels Experimental Campaigns in Gas Turbine Combustor at ENEL Sesta Facility," Proceedings of ASME Turbo Expo. GT2004-53274 Vienna, Austria, 2004, pp. 121-128

[222]Luckerath, R., W. Meier, and M. Aigner, "FLOX® Combustion at High Pressure With Different Fuel Compositions," Proceedings of ASME Turbo Expo. GT2007-27337 Montereal, Canada, 2007.

[223]Scholz, M.Gas Turbines for Syngas and Hydrogen Apllication.CPD course on Ultra Low NOx Gas Turbines, 2012.

[224]Funke, H. H.-W., S. Boerner, W. Krebs, and E. Wolf. Experimental Characterisation of Low NOx Micromix prototype combustion for industrial Gas Turbine Application Proceeding of ASME Turbo Expo 2010: Power for Land, Sea, and Air (GT2011), 2011, GT2011-45305.

[225]Funke, H. H.-W., S. Boerner, J. Keinz, K. Kusterer, D. Kroniger, J. Kitajima, M. Kazari, and A. Horikawa. Numerical and Experimental Characterization of Low NOx Micromix Combustion Principle for Industrial Hydrogen Gas Turbine Applications Proceedings of ASME Turbo Expo Power for Land, Sea and air Copenhagen, Denmark 2012, GT2012-69421.